



**HAL**  
open science

# Hydroisomerization and hydrocracking of naphthenes

Larissa Brito Sousa

► **To cite this version:**

Larissa Brito Sousa. Hydroisomerization and hydrocracking of naphthenes. Catalysis. Université de Lyon, 2020. English. NNT: 2020LYSE1013 . tel-04071002

**HAL Id: tel-04071002**

**<https://theses.hal.science/tel-04071002>**

Submitted on 17 Apr 2023

**HAL** is a multi-disciplinary open access archive for the deposit and dissemination of scientific research documents, whether they are published or not. The documents may come from teaching and research institutions in France or abroad, or from public or private research centers.

L'archive ouverte pluridisciplinaire **HAL**, est destinée au dépôt et à la diffusion de documents scientifiques de niveau recherche, publiés ou non, émanant des établissements d'enseignement et de recherche français ou étrangers, des laboratoires publics ou privés.



N°d'ordre NNT: 2020LYSE1013

## **THESE de DOCTORAT DE L'UNIVERSITE DE LYON**

opérée au sein de  
**l'Université Claude Bernard Lyon 1**

**Ecole Doctorale 206**  
**Ecole Doctorale de Chimie de Lyon**

**Spécialité de doctorat** : Matériaux et Catalyse  
**Discipline** : Chimie

Soutenue publiquement le 15/01/2020, par :  
**Larissa Brito Sousa**

---

# **Hydroisomerization and hydrocracking of naphthenes**

---

Devant le jury composé de :

Tayakout-Fayolle, Melaz	Professeur, Université Lyon 1, LAGEPP	Présidente
Ribeiro, Filipa	Professeur, Université de Lisbonne, CQE	Rapporteuse
Thybaut, Joris	Professeur, Université de Gand, LCT	Rapporteur
Glaeser, Roger	Professeur, Université de Leipzig, ITC	Examinateur
Guillon, Emmanuelle	Ingénieur de Recherche, IFPEN	Examinatrice
Laurenti, Dorothée	Chargée de Recherche CNRS, IRCELYON	Examinatrice
Martens, Johan	Professeur, KU Leuven, COK	Examinateur
Pirngruber, Gerhard	Ingénieur de Recherche, IFPEN	Directeur de thèse
Albrieux, Florian	Ingénieur de Recherche, Owens Corning	Invité

## **Université Claude Bernard – LYON 1**

Président de l'Université	M. Frédéric FLEURY
Président du Conseil Académique	M. Hamda BEN HADID
Vice-Président du Conseil d'Administration	M. Didier REVEL
Vice-Président du Conseil des Etudes et de la Vie Universitaire	M. Philippe CHEVALLIER
Vice-Président de la Commission de Recherche	
Directeur Général des Services	M. Damien VERHAEGHE

### **COMPOSANTES SANTE**

Faculté de Médecine Lyon-Est – Claude Bernard	Doyen : M. Gilles RODE
Faculté de Médecine et Maïeutique Lyon Sud Charles. Mérieux	Doyenne : Mme Carole BURILLON
UFR d'Odontologie	Doyenne : Mme Dominique SEUX
Institut des Sciences Pharmaceutiques et Biologiques	Directrice : Mme Christine VINCIGUERRA
Institut des Sciences et Techniques de la Réadaptation	Directeur : M. Xavier PERROT
Département de Formation et Centre de Recherche en Biologie Humaine	Directrice : Mme Anne-Marie SCHOTT

### **COMPOSANTES & DEPARTEMENTS DE SCIENCES & TECHNOLOGIE**

UFR Biosciences	Directrice : Mme Kathrin GIESELER
Département Génie Electrique et des Procédés (GEP)	Directrice : Mme Rosaria FERRIGNO
Département Informatique	Directeur : M. Behzad SHARIAT
Département Mécanique	Directeur M. Marc BUFFAT
UFR - Faculté des Sciences	Administrateur provisoire : M. Bruno ANDRIOLETTI
UFR (STAPS)	Directeur : M. Yannick VANPOULLE
Observatoire de Lyon	Directrice : Mme Isabelle DANIEL
Ecole Polytechnique Universitaire Lyon 1	Directeur : Emmanuel PERRIN
Ecole Supérieure de Chimie, Physique, Electronique (CPE Lyon)	Directeur : Gérard PIGNAULT
Institut Universitaire de Technologie de Lyon 1	Directeur : M. Christophe VITON
Institut de Science Financière et d'Assurances	Directeur : M. Nicolas LEBOISNE
ESPE	Administrateur Provisoire : M. Pierre CHAREYRON

Aos meus avós e ao meu padrinho (*in memoriam*)  
que sempre me quiseram ver doutora. Amo vocês.



*O que será que será*  
*Que dá dentro da gente e que não devia*  
*Que desacata a gente, que é revelia*  
*Que é feito uma aguardente que não sacia*  
*Que é feito estar doente de uma folia*  
*Que nem dez mandamentos vão conciliar*  
*Nem todos os unguentos vão aliviar*  
*Nem todos os quebrantos, toda alquimia*  
*Que nem todos os santos, será que será*  
*O que não tem descanso, nem nunca terá*  
*O que não tem cansaço, nem nunca terá*  
*O que não tem limite*  
O que será (à flor da pele) – Chico Buarque  
Chanteur et compositeur brésilien

*Il y a toujours quelque chose d'absent qui me tourmente.*

Camille Claudel, sculptrice française, dans une lettre à Rodin en 1886.

## REMERCIEMENTS

---

Chers lecteurs,

On m'a dit une fois (Esther, je te fais un clin d'œil virtuel) « Il y a des thèses et des thèses... » et puis, c'est vrai, ni toutes les thèses sont les mêmes. Mais ce qui est commun à tous les doctorants, c'est ça : nous y mettons tous notre cœur, nos pensées les plus raisonnables (parfois) et nous croyons qu'un jour ça va finir. Et je vous assure, c'est bien comme cela, puisque maintenant ça y est, je vois le bout du tunnel, et je peux enfin vous écrire les remerciements pour ces travaux. Si cette thèse a pu voir le jour, c'est parce que j'ai compté sur le soutien d'un bon nombre de personnes qui s'y sont engagées. Superviseurs, ingénieurs, techniciens, collègues, famille, amis... le bilan est non-exhaustif. J'espère vous rendre honneur dans les lignes qui suivent.

Ces travaux de thèse ont été réalisés à l'IFP Energies Nouvelles au sein de la Direction Catalyse, Biocatalyse et Séparation, en profonde synergie avec la Direction Physique et Analyse. Je tiens à remercier les directeurs Luc Nougier et Nathalie Schildknecht, ainsi que les chefs de département Tivadar Cseri puis Emmanuelle Guillon (Catalyse par les Métaux et Solides Acido-Basiques), Magalie Roy-Auberger (Catalyse par les Sulfures) et Jérémie Ponthus (Analyse Chimique) pour les moyens mis à disposition pour le bon déroulement de la thèse.

Je ne serai pas sur le point de vous écrire ces remerciements si ces travaux n'auraient pas été minutieusement analysés et puis validés par le jury de thèse. Je remercie chaleureusement les rapporteurs, les professeurs Filipa Ribeiro (IST, Lisbonne) et Joris Thybaut (LCT, Ghent) pour leur avis positif et leur évaluation de ce manuscrit; les examinateurs représentés par les professeurs Roger Glaeser (ITC, Leipzig) et Johan Martens (COK, KU Leuven), et M. Dorothée Laurenti, chercheuse à l'IRCELYON ; et la présidente du jury, professeur Melaz Tayakout-Fayolle (Université de Lyon). Merci pour vos commentaires, suggestions et la riche discussion scientifique que nous avons tenue lors de la soutenance et le pot de thèse (et oui, parce que c'est possible de parler Science entre deux bières).

Pendant ces 3 années (et un peu plus) de travail, j'ai énormément embêté pas mal de gens (on a tous survécu !), mais personne d'autre comme mon « chef », Gerhard Pirngruber. Il a

---

suivi de près toutes les galères que j'ai dû surmonter pour croiser la dernière ligne droite et n'a jamais été trop occupé pour parler de la biblio (même après le déjeuner), des tests qui ne marchaient pas et des résultats quelques fois pas trop motivants. Et avec la même motivation, nous avons célébré toutes les victoires, surtout au volley en jeudi de l'ALSIP (une revanche, Etienne ?). Merci, chef, d'avoir mené ces travaux en tant que directeur, et surtout merci pour la confiance que tu as fait à mon travail. Est-ce qu'on peut encore travailler ensemble ? Bis bald !

J'ai eu également la chance de compter sur l'expertise scientifique d'Emmanuelle Guillon, Johan Martens et Florian Albrieux. Un grand merci à « Manue » qui m'a fait monter en compétences sur les zéolithes, ce vaste monde poreux, mais aussi sur la conduite du projet et la valorisation de nos résultats. Merci pour le temps que tu m'as accordée et pour toujours me pousser vers un niveau plus élevé; à Johan, la « bible de la catalyse hétérogène », merci pour toutes les discussions enrichissantes (et les blagues belges), ton envie de m'apprendre à bien rapporter nos résultats, ta disponibilité et calme malgré ton emploi du temps chargé. Merci à toi et au personnel du COK de KU Leuven de m'avoir accueillie au sein du labo pour quelques semaines, séjour qui a abouti dans nos premières publications; et puis merci à toi, « Floflo », pour cette introduction au monde analytique, ton dynamisme et bonne humeur toujours au rendez-vous. Aujourd'hui je peux te dire que je sais comment placer le montage 2D après que plusieurs PONAs ont retrouvé leur cruel destin au fond du four du GC (désolée, Vincent et Nadège).

Vous vous en doutez, mais une thèse expérimentale s'appuie beaucoup sur l'expertise technique. Dans mon cas, je n'aurais pas pu réussir ce travail sans la coopération et connaissances de Denis Suida (je t'ai promis un chapitre de remerciements, on y est presque !), Pascal Galguen « Pascalou », Charles Leroux « Charlux », Eugénie Rabeyrin, Sophie Bailly, Cédrik Popelin, Clara Voisin, George Fernandes « Jorginho », Denis Barrallon « Denilou », Julie Marin « Juliette », Gracinda Ribeiro « Grace », Nathalie Lett « Nathalette », Laetitia Jacquet, Marie-Paule Finot, Amaury Donnette « Amaurette », Véronique Delattre, Anne Boffo, Vanessa Regamey, Florence Del-Toso, Nadège Cellier, Stéphane Clavel « Hello Kitty », Yoham Mouillet, Lyes Assam, Laurent Lemaître, le bureau d'études, et tant d'autres que j'ai côtoyé en stage et en thèse. Merci pour vos conseils, le partage de connaissances et de pièces détachées, les formations sur les unités, mais aussi les

---

blagues et les chants au labo (Aznavour te manque déjà, Pascalou ? Et ta guitariste, Jorginho ?), les pause-café, les repas en bonne compagnie. Vous avez été essentiels pour cette réussite.

Pendant cette période, j'ai été en contact avec pas mal de gens, soit pour demander un conseil technique, soit pour partager des passions similaires. Ainsi, je veux laisser mon petit mot chaleureux à Antoine Daudin, Céline Chizallet, Christophe Bouchy, Elodie Devers, Audrey Bonduelle, Pascal Raybaud, Sylvie Maury, Jacques Lavy, Céline Pagis, Philippe Beard, Patrick Mathieu, Romain Rousset, Sylvain Ravo, Etienne Girel, Pierre-Louis Carrette, Charlie Blons, Bertrand Guichard, Mathieu Vidalie, Vincent Souchon, Christophe Roulet, Laurent Simon, Michel Thomas, Fabrice Diehl, Marie-Claude Beaufiles et Nathalie Farrenq; merci à François Payan pour l'opportunité d'encadrer son stage de Master 2 et pour les tests catalytiques effectués; merci à Javier Perez-Pellitero pour le travail de simulation moléculaire, merci aux équipes de badminton et volley de l'ALSIP pour tous ces matchs conviviaux et les soirées de compétition; merci à la chorale de l'IFPEN pour l'opportunité de chanter des si beaux morceaux avec un groupe très sympathique (Nkosi Sikelel' iAfrika !).

Ces dernières années à l'IFPEN et en France ont été aussi synonyme d'amitié. Merci Pedro, Fafa Caron, Rickinho, Greg, Pierre-Yves, Pauline, Maloche, Juan, Jérôme, mes voisins de bureau ou co-bureaux, d'avoir rendu les journées plus légères et moins stressantes ; merci Damien (Rice), Julie, Elsy, Ana Teresa, Ana Sofia, Esther, Laurèline, Amit, Farah, July Carolina, Maroua, Clément, Leonor, Audrey, Paul, Angélique, Adrien, Phuong, Luc, Matthieu, Sanaz, Sharmin, pour les histoires inoubliables partagées lors de nos covoiturages, votre soutien dans les moments compliqués, les repas et soirées ensemble; Mayara, Marisa, Ana Rita, Izabel, Edwyin, merci pour cette petite famille portugaise/brésilienne que nous avons créé et que j'y tiens à cœur (oui, Damien, tu peux t'y compter aussi); merci à Nastenka, Flavio, Robson, Geovani, Rosangela, Rafaela, Germán, Oscar, Eva, Pauline, Mélanie, John, Claire Simon et famille, Florian, Sophie, mes chers amis de l'INSA de Toulouse et UFC Brésil, qui ne m'ont pas abandonnée malgré tous mes refus d'invitation en période de rédaction du manuscrit. Vous êtes ma famille en France.

Et en parlant de famille, j'ai été énormément gâtée de compter sur la présence de mes parents lors de la soutenance de thèse, après 3 longues années sans les avoir vus (merci

---

encore à mes chefs d'avoir rendu cela possible). Obrigada, mamãe e papai, por terem atravessado o Oceano para estarem comigo nesse dia especial e por tudo o que fazem por mim. Obrigada, Karinne, por toda a ajuda com os nossos pais e os preparativos da viagem; obrigada, Azinha, por todos estes anos de amizade e por toda a ajuda com a tese; aos meus tios e tias, primos e primas, obrigada por toda a torcida e por investirem na minha formação. Devo tudo a vocês.

En somme, chers lecteurs, je suis très reconnaissante d'avoir fini ce chapitre à côté des professionnels et d'amis que j'admire autant. Ce fût un privilège et ça me manque déjà (sauf les heures réduites de sommeil). J'espère qu'on se croisera un jour, soit pour travailler ensemble, soit pour partager un bon moment à l'exemple de ces dernières années. Merci à vous et à la prochaine !

Bonne lecture

Larissa/Larusso/Larousette/Laricouette

---

Hydrocracking is a versatile process used for the conversion of heavy oil cuts into lighter fractions, for instance, the processing of Vacuum Gas Oil into middle distillates. Vacuum Gas Oil is in large majority composed of cyclic molecules (aromatics and naphthenes), and the mechanisms involved in the hydroconversion of polycyclic naphthenes are not yet well understood, in contrast to alkanes, which were largely reported in literature. This work aims to study the hydrocracking of polycyclic naphthenes over Pt- and NiMoS-modified zeolites shaped with alumina and amorphous silica-alumina bifunctional catalysts.

Catalytic tests were performed in a continuous fixed bed reactor, under high hydrogen pressure, by using perhydrophenanthrene ( $C_{14}H_{24}$ ) or octylcyclohexane ( $C_{14}H_{28}$ ) as model feedstocks. The saturated molecule was obtained after *in situ* hydrogenation of the parent aromatic compound, phenanthrene ( $C_{14}H_{10}$ ) or phenyloctane ( $C_{14}H_{22}$ ). Large-pore commercial zeolite catalysts, USY (CBV720) and Beta (CP814e), and an amorphous silica-alumina catalyst (Siralox 30), whose hydrogenating function was provided by Pt or NiMoS, were compared in the hydrocracking of perhydrophenanthrene and octylcyclohexane. The reaction generated hundreds of products and their thorough identification was essential to constitute the reaction pathways involved in these complex networks. This was achieved thanks to an analytic method specially conceived for this application, based on coupling GCxGC to FID and MS detectors.

The reaction products were then lumped into groups according to carbon number and chemical family. The evolution of the families and of reaction products within these subgroups were investigated in order to propose hydroisomerization and hydrocracking pathways, according to the chemistry of carbocations. Shape selectivity effects were evidenced experimentally and investigated with Molecular Simulation in hydrocracking of perhydrophenanthrene. The influence of the number of naphthenic cycles, in addition to the presence of a long substituent alkyl-chain, in hydrocracking reactions were tackled through analysis of results acquired on hydroconversion of both model molecules over the bifunctional catalysts. Finally, the activity of Pt-supported catalysts was evaluated in

---

hydroisomerization of n-hexadecane ( $C_{16}H_{34}$ ), a long-chain alkane, and compared to results obtained with the naphthenic model molecules.

**Keywords** : *hydroisomerization, hydrocracking, bifunctional catalysis, naphthenes, zeolites, perhydrophenanthrene, octylcyclohexane, GCxGC*

---

L'hydrocraquage est un procédé flexible utilisé pour la conversion de charges lourdes de pétrole vers des coupes plus légères, par exemple, lors de l'hydroconversion des Distillats sous Vide (DSV) dans des distillats moyens. Le DSV est majoritairement composé par des molécules cycliques (aromatiques et naphthènes), mais les mécanismes qui régissent la transformation de composés polycycliques ne sont pas encore bien maîtrisés, contrairement aux alcanes, qui sont vastement rapportés dans la littérature. Ce travail a pour but d'étudier l'isomérisation et le craquage de naphthènes, en présence de l'hydrogène, sur des catalyseur Pt ou NiMoS supportés sur des zéolithes mises en forme ou sur des silices alumines amorphes.

Des tests catalytiques ont été réalisés dans un réacteur lit-fixe, sous haute pression d'hydrogène, en utilisant perhydrophénanthrène ( $C_{14}H_{24}$ ) ou octylcyclohexane ( $C_{14}H_{28}$ ) comme des charges modèle. La molécule saturée a été obtenue après hydrogénation *in situ* du composé aromatique correspondant, soit phénanthrène ( $C_{14}H_{10}$ ) ou phényloctane ( $C_{14}H_{22}$ ). Des zéolithes à large pore, USY (CBV720) et Beta (CP814e), et une silice-alumine amorphe (Siralox 30), dont la fonction hydrogénante a été représentée par Pt ou sulfures de molybdène promues par du Ni, ont été évaluées dans l'hydroconversion du perhydrophénanthrène et de l'octylcyclohexane. La réaction a produit quelques centaines de composés et leur identification minutieuse a été essentielle pour constituer les schémas réactionnels impliqués dans ces réseaux complexes. Cela a été réussi grâce à une méthodologie analytique spécialement conçue pour cette application, basée sur un couplage GCxGC aux détecteurs à ionisation de flamme et de masse.

Les produits de réaction ont été groupés selon leur nombre d'atomes de carbone et famille chimique. L'évolution des familles et des produits de réaction au sein de ces groupes a été étudiée avec l'objectif de proposer des schémas réactionnels concernant l'hydroisomérisation et l'hydrocraquage des molécules modèle. Des effets de sélectivité de forme ont été mis en évidence expérimentalement en hydrocraquage du perhydrophénanthrène et investigués à l'aide de simulations moléculaires utilisant la méthode de Monte Carlo. L'influence du nombre de cycles naphthéniques, ainsi que la présence d'une longue chaîne alkyle attaché au cycle, sur les réactions d'hydroisomérisation et d'hydrocraquage a été abordée à travers de

---



l'analyse de résultats obtenus lors de l'hydroconversion de ces molécules modèle sur les catalyseurs bifonctionnels. Enfin, l'activité de catalyseurs Pt a été évaluée dans l'hydroisomérisation du n-hexadecane ( $C_{16}H_{34}$ ), un alcane à chaîne longue, et comparée aux résultats obtenus sur les molécules naphthéniques.

**Mots-clés :** *hydroisomérisation, hydrocraquage, catalyse bifonctionnelle, naphthènes, zéolithes, perhydrophénanthrène, octylcyclohexane, GCxGC*

---

## RESUME SUBSTANTIEL

---

L'objectif principal de ce travail a été de comprendre les mécanismes impliqués dans l'hydroconversion de naphthènes polycycliques et substitués, les composants majoritaires des fractions lourdes du pétrole, comme les Distillats Sous Vide (DSV). Les catalyseurs bifonctionnels étudiés, caractérisés par une phase hydrogénante (Pt ou NiMoS) supportée sur des phases acides mises en forme, représentées par des zéolithes à large pore (USY ou Beta) ou une silice-alumine (ASA), ont été employés dans l'hydroisomérisation et l'hydrocraquage de deux molécules cycliques à 14 atomes de carbone. Le perhydrophénanthrène, un naphtène polycyclique, et l'octylcyclohexane, un naphtène monocyclique substitué par une chaîne alkyle, ont été choisis en tant que molécules modèles pour évaluer la réactivité de différentes structures cycliques en mécanismes bifonctionnels. L'hydroconversion de ces composés a suivi les principes de la chimie de carbocations et a généré quelques centaines de produits, lesquels ont été exhaustivement identifiés et quantifiés par GCxGC-FID/MS. La caractérisation détaillée des produits de réaction a permis d'établir une étude approfondie de schémas réactionnels et l'identification de familles de composés qui sont rarement rapportées dans la littérature.

L'hydroisomérisation et l'hydrocraquage du perhydrophénanthrène (PHP,  $C_{14}H_{24}$ ) ont été réalisés sur les catalyseurs bifonctionnels Pt/H-USY, Pt/H-Beta et Pt/ASA. Un schéma global à tous les catalyseurs passe par l'isomérisation du naphtène tricyclique, suivie par une étape d'ouverture du cycle central de PHP, en amont du craquage. La formation des isomères de PHP et produits d'ouverture de cycle a été contrôlée par la sélectivité de forme, conduisant à différentes distributions en nombre d'atomes de carbone. Ainsi, les catalyseurs supportés contenant de la zéolite USY ont donné une large distribution de produits de craquage, alors que les catalyseurs bifonctionnels à base de Beta et ASA ont privilégié le craquage central de la molécule modèle à naphthènes ayant 7 atomes de carbone. Une autre route d'isomérisation du perhydrophénanthrène a résulté dans la production d'adamantanes substitués à 14 atomes de carbone. Ces molécules sont très stables du point de vue thermodynamique et ne subissent pas facilement le craquage. Les alkyladamantanes ne sont pas souvent rapportés dans la littérature en catalyse bifonctionnelle, probablement à cause des difficultés liées à leur séparation et identification parmi d'autres produits de réaction. Dans notre travail, la formation des alkyladamantanes a été attribuée à la catalyse en

---

bouche de pore et a été favorisée à haute conversion de perhydrophénanthrène sur le catalyseur Pt/H-USY. Les effets de sélectivité de forme et plus spécifiquement de la catalyse en bouche de pore ont été rationalisés à l'aide de techniques de simulation moléculaire, en prenant en compte des importants intermédiaires de réaction comme molécules cible. Les zéolithes USY ont été plus actives en hydroconversion de perhydrophénanthrène, suivies par la zéolithe Beta et, à un degré plus faible, par la silice-alumine. L'activité plus importante de Pt/H-USY dans la conversion de naphhtènes polycycliques est liée à l'adsorption favorisée du perhydrophénanthrène dans la topologie de FAU, comme les simulations le démontrent.

L'hydroconversion de l'octylcyclohexane ( $C_{14}H_{28}$ ) a été effectuée sur des catalyseurs supportés Pt et NiMoS, sous les mêmes conditions opératoires que les tests catalytiques menés sur le perhydrophénanthrène. Le schéma réactionnel, valide tant pour les catalyseurs Pt que pour les catalyseurs NiMoS, commence par l'isomérisation de la molécule modèle, avant que les isomères arrivent à une conformation qui permet la beta-scission rapide. Dans ce cas, l'ouverture de cycle a été une réaction minoritaire, ce qui est attendu en hydroconversion de naphhtènes monocycliques. La distribution des isomères a été équivalente sur des catalyseurs zéolithiques, tandis que l'ASA a formé préférentiellement des structures multibranchées, ce qui est lié à une faible activité de craquage de la phase silice-alumine. En accord avec la littérature, le branchement consécutif des isomères s'est initié au niveau du cycle, avec migration du branchement créé vers la chaîne alkyle substituant le naphhtène. Les catalyseurs Pt ont donné une distribution similaire en nombre d'atomes de carbone, avec un craquage préférentiel vers la formation de composés à 7 atomes de carbone et une distribution plate autour des atomes de carbone restants. Les catalyseurs bifonctionnels NiMoS étaient moins équilibrés que les catalyseurs Pt, ce qui a résulté dans la formation de produits de craquage plus légers, à cause du sur-craquage. Nous avons essayé de rationaliser la compétition entre isomérisation et craquage en comparant le degré de branchement des molécules représentatives de ces deux familles. Malgré un nombre inférieur de carbones tertiaires, les isomères di- ou tribranchés ont craqué préférentiellement, en comparaison avec les isomères multibranchés. En effet, ces derniers nécessitent un nombre supérieur d'étapes lentes d'isomérisation type B pour les produire. L'ordre d'activité en hydroconversion de l'octylcyclohexane a été l'opposé de celui obtenu sur les essais avec le perhydrophénanthrène. Les zéolithes Beta ont été plus actives que les zéolithes USY, et l'ASA a été le solide le

---

moins actif parmi ceux testés, quelle qu'en soit la phase métallique présente sur le catalyseur bifonctionnel.

Les catalyseurs Pt ont également été évalués en hydroconversion d'une longue chaîne alkyle, le n-hexadécane (n-C<sub>16</sub>H<sub>34</sub>). Comme pour l'octylcyclohexane, les catalyseurs Beta ont été plus efficaces dans la conversion de l'alcane, suivis par les zéolithes USY. Encore une fois, le catalyseur ASA a été le moins actif parmi les solides testés. Ces résultats, en consonance avec les effets de sélectivité de forme observés en hydroisomérisation du perhydrophénanthrène, peuvent confirmer la conversion préférentielle de structures linéaires sur les zéolithes Beta. Nous pouvons aussi inférer que l'octylcyclohexane, un naphène monocyclique substitué par une longue chaîne alkyle, a réagi d'une façon similaire que le n-hexadécane, et le cycle a fourni les branchements nécessaires à la beta-scission.

Ce travail offre une caractérisation approfondie des intermédiaires de réaction et de schémas réactionnels qui sont utiles pour la compréhension de la distribution de produits de craquage sur des catalyseurs Pt et NiMoS. Il est clair que naphènes mono- et polycycliques réagissent d'une façon différente, et la complexité de schémas réactionnels augmente avec le nombre de cycles de la molécule. Les données disponibles dans cette étude peuvent aider à comprendre le comportement de charges plus complexes d'un point de vue moléculaire, et à adapter les propriétés texturales et l'acidité de catalyseurs bifonctionnels par conséquent.

En perspective pour des travaux futurs, ce serait particulièrement intéressant de tester des intermédiaires de réaction qui peuvent résulter de l'isomérisation ou de l'ouverture de cycle du perhydrophénanthrène ou de l'octylcyclohexane, de façon à construire un schéma réactionnel encore plus complet. Une autre possibilité serait de convertir différents types de molécules qui sont en général présents dans la fraction de Distillats Sous Vide, i.e. alcanes, naphènes et aromatiques, pour analyser la réactivité de ces composés dans une charge plus réaliste. En outre, une étude cinétique pourrait être envisagée pour calculer les vitesses d'isomérisation, ouverture de cycle et craquage, et ainsi éclaircir la compétition entre les différentes voies réactionnelles.

Par manque de temps, l'hydroconversion du perhydrophénanthrène n'a pas été étudié sur les catalyseurs supportés NiMoS. L'objectif dans ce cas était de vérifier l'impact de la balance entre la phase métallique et la phase acide en hydroisomérisation et hydrocraquage

---

du naphène tricyclique. Comme mentionné précédemment, la conversion de cette molécule a généré un large nombre de produits de réaction, et des effets de sélectivité de forme ont joué un rôle important dans la distribution d'atomes de carbone, ce qui rend le perhydrophénanthrène un composé très intéressant à étudier d'un point de vue mécanistique. Par ailleurs, les catalyseurs NiMoS sont largement appliqués dans les opérations industrielles, ainsi ils peuvent être évalués sous des conditions opératoires plus sévères, renforçant les connaissances en hydroconversion de molécules cycliques dans ce type d'environnement.

---

## TABLE OF CONTENTS

---

INTRODUCTION.....	1
CHAPTER I: LITERATURE REVIEW .....	6
<b>1. Hydrocracking catalysts.....</b>	<b>6</b>
<b>2. Mechanisms of hydrocracking of naphthenes .....</b>	<b>8</b>
<i>2.1. Metal-catalyzed reactions .....</i>	<i>8</i>
<i>2.2. Acid-catalyzed reactions.....</i>	<i>10</i>
<b>3. Bifunctionality .....</b>	<b>18</b>
<b>4. Analysis of effluents .....</b>	<b>23</b>
<i>4.1. Principles of two-dimensional gas chromatography .....</i>	<i>24</i>
<i>4.2. Principles of mass spectrometry.....</i>	<i>26</i>
<b>5. Conclusions .....</b>	<b>28</b>
<b>References .....</b>	<b>29</b>
CHAPTER II: HYDROCONVERSION OF PERHYDROPHENANTHRENE OVER BIFUNCTIONAL PT/H-USY ZEOLITE CATALYST.....	42
<b>1. Introduction .....</b>	<b>43</b>
<b>2. Materials and methods.....</b>	<b>45</b>
<i>2.1. Preparation and characterization of catalysts.....</i>	<i>45</i>
<i>2.2. Catalytic tests .....</i>	<i>47</i>
<b>3. Results .....</b>	<b>50</b>
<i>3.1. Identification and quantification of reaction products with GCxGC-FID/MS ....</i>	<i>50</i>
<i>3.2. Hydroconversion of perhydrophenanthrene.....</i>	<i>53</i>
<b>4. Discussion.....</b>	<b>64</b>
<i>4.1. Hydroisomerization and hydrocracking reaction pathways .....</i>	<i>64</i>
<i>4.2. Detailed analysis of the hydrocracking pathways.....</i>	<i>67</i>
<i>4.3. Attempts to rationalize the yield of cracked products .....</i>	<i>75</i>
<b>5. Conclusions .....</b>	<b>77</b>
<b>References .....</b>	<b>77</b>

---

## TABLE OF CONTENTS

---

CHAPTER III: HYDROCONVERSION OF PERHYDROPHENANTHRENE OVER BIFUNCTIONAL CATALYSTS - A COMPARISON BETWEEN PT/H-USY, PT/H-BETA AND PT/SILICA-ALUMINA .....	86
<b>1. Introduction .....</b>	<b>87</b>
<b>2. Materials and methods.....</b>	<b>88</b>
2.1. Preparation and characterization of catalysts.....	88
2.2. Catalytic tests .....	89
2.3. Molecular simulation with Grand Canonical Monte Carlo (GCMC).....	90
<b>3. Results .....</b>	<b>91</b>
3.1. Identification and quantification of reaction products with GCxGC-FID/MS....	91
3.2. Hydroconversion of perhydrophenanthrene.....	94
3.3. Molecular simulation .....	104
<b>4. Discussion.....</b>	<b>108</b>
4.1. Attempts to rationalize hydrocracking pathways .....	108
<b>5. Conclusions .....</b>	<b>116</b>
<b>References .....</b>	<b>117</b>
CHAPTER IV: HYDROCONVERSION OF OCTYLCYCLOHEXANE OVER BIFUNCTIONAL PT/H-USY ZEOLITE CATALYST.....	125
<b>1. Introduction .....</b>	<b>126</b>
<b>2. Materials and methods.....</b>	<b>128</b>
2.1. Preparation and characterization of catalysts.....	128
2.2. Catalytic tests .....	129
2.3. Methodology of analysis of liquid reaction products .....	131
<b>3. Results .....</b>	<b>132</b>
3.1. Identification and quantification of reaction products with GCxGC-FID/MS ...	132
3.2. Hydroconversion of octylcyclohexane.....	134
<b>4. Discussion.....</b>	<b>145</b>
4.1. Attempts to rationalize isomerization pathways .....	145
4.2. Attempts to rationalize hydrocracking pathways .....	150
4.3. Rationalization of the products distribution.....	156
<b>5. Conclusions .....</b>	<b>157</b>
<b>References .....</b>	<b>158</b>

---

## TABLE OF CONTENTS

CHAPTER V: HYDROCONVERSION OF OCTYLCYCLOHEXANE OVER BIFUNCTIONAL CATALYSTS: USY VS. BETA VS. SILICA-ALUMINA AND PT VS. MOS <sub>2</sub> .....	165
<b>1. Introduction</b> .....	<b>166</b>
<b>2. Materials and methods</b> .....	<b>167</b>
<i>2.1. Preparation and characterization of catalysts</i> .....	<i>167</i>
<i>2.2. Catalytic tests</i> .....	<i>169</i>
<i>2.3. Methodology of analysis of reaction products</i> .....	<i>172</i>
<b>3. Results</b> .....	<b>172</b>
<i>3.1. Identification and quantification of reaction products with GCxGC-FID/MS</i> ...	<i>172</i>
<i>3.2. Hydroconversion of octylcyclohexane</i> .....	<i>175</i>
<b>4. Discussion</b> .....	<b>186</b>
<i>4.1. Comparison of isomerization and cracked products</i> .....	<i>186</i>
<i>4.2. Pt vs. NiMoS catalysts</i> .....	<i>187</i>
<i>4.3. Comparison of the hydroconversion of perhydrophenanthrene vs. octylcyclohexane and n-hexadecane</i> .....	<i>190</i>
<b>5. Conclusions</b> .....	<b>192</b>
<b>References</b> .....	<b>193</b>
CHAPTER VI: GENERAL DISCUSSION .....	202
<b>References</b> .....	<b>212</b>
CONCLUSIONS.....	217

---



The worldwide demand in oil fuels is still expected to increase in the next years. Transport sectors will therefore require great capacities of diesel and jet fuel that should be supplied from the processing of heavy oil fractions, e.g. Vacuum Gas Oil (VGO). VGO is obtained from straight run distillation of crude oil, with temperature boiling range around 350-600°C (C<sub>20</sub>-C<sub>60</sub>). In refineries, VGO is often upgraded via hydrocracking, a versatile catalytic process that may provide a great variety of good quality products. In the context of energy transition, it is essential to obtain such oil derivatives in an efficient way, in order to increase the selectivity towards desirable compounds. For this reason, an expertise in reaction mechanisms and catalyst design is necessary to improve the performance of hydrocracking units.

Hydrocracking is performed over bifunctional catalysts in the presence of hydrogen. Catalysts are constituted of a (de)hydrogenating metallic function supported on an acid cracking phase. In an industrial environment, catalysts should be resistant to impurities, such as nitrogen, sulfides, oxygen and water. The metallic phase is mostly constituted of molybdenum sulfides promoted by nickel, cobalt or tungsten because of their nitrogen and sulfur resistance. Platinum may also be used as a stronger hydrogenating agent for sulfur-free feedstocks. The acid phase is brought by zeolites shaped with an alumina binder and amorphous silica-alumina (ASA). These solids present different porosity and acidity tuned to reach targeted cracking products.

VGO is mainly composed of cyclic compounds, i.e. naphthenes and aromatics, in addition to alkanes. Hydroconversion of long-chain alkanes has been widely reported in literature and follow a well described bifunctional mechanism based on carbocation chemistry. In contrast, reaction routes of hydroisomerization and hydrocracking of (poly)cyclic molecules have been less discussed in previous works and are more difficult to predict. Indeed, different reaction possibilities rely on the number of cycles and alkylation degree of the studied molecule. Thus, the objective of this work is to understand the reactivity of polycyclic and substituted naphthenes and rationalize reaction pathways leading to their hydroconversion. Our attempt is to improve scientific foundations regarding these less explored areas.

In this work, perhydrophenanthrene ( $C_{14}H_{24}$ ), a 3-cycle naphthene, and octylcyclohexane ( $C_{14}H_{28}$ ), a substituted monocyclic naphthene, were chosen as  $C_{14}$  model molecules. They were obtained after *in situ* hydrogenation of the parent aromatic, respectively phenanthrene ( $C_{14}H_{10}$ ) and phenyloctane ( $C_{14}H_{22}$ ). Octylcyclohexane was assigned as model molecule because it could be a reaction intermediate formed during hydrocracking of perhydrophenanthrene. By doing so, we aim to address the reactivity of both compounds in respect to the number of cycles of the model molecule, and the presence of a long alkyl-chain attached to the cycle.  $C_{14}$  molecules are not truly representative of a VGO feedstock ( $C_{20}$ - $C_{60}$ ). Nevertheless, for heavier compounds, the complexity of the reaction mechanisms would increase the difficulties in analyzing reaction products, leading to a poor comprehension of hydroconversion pathways. Both molecules were proceeded for catalytic testing in a fixed-bed reactor, employing the same operating conditions. Different families of bifunctional catalysts were tested. Reaction products were extensively characterized by two-dimensional gas chromatography coupled to flame ionization and mass detectors.

The impact of the acid phase on hydroconversion reaction pathways was tackled by comparing commercial large-pore zeolites (ultrastable Y and Beta) to amorphous silica-alumina (Siralox 30). We aimed to evaluate the role of acidity and porosity on naphthenes reactivity. Both zeolites were chosen given their similar concentration of BAS, and higher concentration of strong acid sites compared to silica-alumina. Ultrastable Y zeolites possess larger porosity (supercages) that may accommodate large molecules compared to Beta zeolite. ASA catalysts have the largest pore opening among the solids tested. The evaluation of bifunctional catalysts with distinct pore size enabled to verify the occurrence of shape selectivity effects and their influence on the carbon atoms distribution.

The bifunctionality of the catalysts was assessed by changing their metallic phase. The shaped acidic supports were impregnated with either platinum or molybdenum sulfide precursors. The impact of this balance between (de)hydrogenation and isomerization/cracking reactions on the distribution of carbon atoms was carried out by taking octylcyclohexane ( $C_{14}H_{28}$ ) as model molecule.

This work is divided into four parts. The first part (Chapter 1) consists in a brief literature review, to highlight the main previous studies and to facilitate the understanding on mechanisms of hydroconversion of polycyclic naphthenes. Following chapters are organized

as scientific publications, where specific literature is provided as an introduction to the approached theme. Details on experimental methodology are also furnished in each chapter.

The second part of this work emphasizes results obtained in hydroisomerization and hydrocracking of perhydrophenanthrene (PHP), in Chapters 2 and 3. Chapter 2 deals with hydrocracking of PHP over Pt/H-USY zeolite catalyst. Reaction pathways were proposed based on a comprehensive description of reaction intermediates. Chapter 3 compares reaction pathways for hydroconversion of PHP over Pt/H-USY, Pt/H-Beta and Pt/ASA bifunctional catalysts. Pore size effects are discussed, helped by Molecular Simulation with Grand Canonical Monte Carlo (GCMC).

Reaction pathways on hydroisomerization and hydrocracking of octylcyclohexane (OCC6) were described in the third part of this work, also divided into two chapters. Chapter 4 discusses hydroconversion of OCC6 over Pt/H-USY zeolite catalyst. Chapter 5 compares noble metal (Pt) and base metal (NiMoS) bifunctional catalysts on hydroconversion of OCC6. The objective is to shed light on reaction pathways obtained over bifunctional catalysts containing different metallic phases, widely employed in industrial applications, and compare the reactivity of octylcyclohexane on Pt- and sulfide-based catalysts. A brief comparison with hydroconversion of a long-chain alkane is also provided.

The fourth part (Chapter 6) of this study promotes an overall discussion which connects key results obtained throughout this work. A comparison between perhydrophenanthrene and octylcyclohexane in terms of reactivity, reaction intermediates and distribution of carbon atoms is presented.

Final conclusions and perspectives for future work are addressed in the last part of this report.



---

## TABLE OF FIGURES – CHAPTER I

---

<b>Figure 1.</b> Organization of Si and Al tetrahedra in zeolites network [13]. Si, Al, O and Na+ atoms are indicated in the figure. ....	7
<b>Figure 2.</b> Hydrogenation mechanism over a Ni catalyst according to Horiuti <i>et al.</i> [27]. A, B and C correspond to initial, half hydrogenated and final hydrogenated transition states, respectively. ....	9
<b>Figure 3.</b> Dicarbene mechanism: A) $\pi$ -adsorbed olefin perpendicular to the metal surface; B) formation of the complex with a metal particle [32,33]. ....	10
<b>Figure 4.</b> Types of isomerization and comparison between alkanes and naphthenes. Adapted from references [13,41]. ....	11
<b>Figure 5.</b> Isomerization pathways of 1-cyclohexyloctane adapted from Souverijns <i>et al.</i> [40]. ....	12
<b>Figure 6.</b> Effect of orbital overlap on beta-scission of C-C bonds according to Brouwer and coworkers [45]. ....	13
<b>Figure 7.</b> Beta-scission types and comparison between alkanes and naphthenes. Adapted from references [43,48]. ....	14
<b>Figure 8.</b> Reaction pathway of exocyclic beta-scission (“paring”) of 1,2,3,4-tetramethylcyclohexane towards formation of methylcyclopentane and isobutane (adapted from Egan <i>et al.</i> [23]). ....	15
<b>Figure 9.</b> Carbon number distribution curves of a n-alkane (left, bell-type) and a naphthene (right, M- type) [50]. ....	16
<b>Figure 10.</b> Comparison between ring-opening and cracking rates according to references [13,52]. $V_o$ stands for ring-opening rate, $V_c$ corresponds to rate of beta-scission of opening products (or of the corresponding alkanes). ....	17
<b>Figure 11.</b> Overall conversion and product yields as a function of Pt loading on catalysts at 50 bar, 553 K, contact time= 3.8 h-1,H2/decalin (molar)=260. RC, RO and CK correspond to ring-contraction, ring-opening and cracking reactions. ....	20
<b>Figure 12.</b> Steps of hydrocracking of perhydrophenanthrene highlighting isomerization and cracking as competing pathways. ....	22
<b>Figure 13.</b> Yield of ring-opening products produced from 1-methylnaphthalene in function of temperature for Pt-Beta and Pt-USY catalysts. ....	23
<b>Figure 14.</b> Schematic representation of a separation by GCxGC [121]. ....	25
<b>Figure 15.</b> Normal and reverse column sets for separation of components of VGO. Courtesy of Jeol. ....	26
<b>Figure 16.</b> Fragmentation pathway of radical cations in EI [125]. ....	27
<b>Figure 17.</b> Spectra of different C <sub>8</sub> H <sub>16</sub> isomers according to NIST mass spectra database. ....	28

---

### 1. Hydrocracking catalysts

Hydrocracking catalysts are bifunctional solids constituted of a metal and an acid phase. The metal function enables (de)hydrogenation reactions, while the acid one catalyzes isomerization and cracking mechanisms. The choice of metal and acid functions relies on the type of process, as well as on the selectivity to the desired product [1]. This section aims to make an overview of hydrocracking catalysts that are used in hydroconversion of heavy oil fractions, as Vacuum Gas Oil.

The metal function must assure high activities of (de)hydrogenation reactions in order to prevent over-cracking [2]. Noble metals as Pt and Pd can be used for this purpose, but only when the feedstock is free of nitrogen and sulfur impurities [3]. Otherwise, metal sulfides promoted by other non-noble metals are used in hydrocracking, due to their greater resistance to the impurities found in standard oil feedstock [4]. Therefore, Mo and W promoted by Ni and Co, respectively, are preferentially used in industrial applications. According to literature, (de)hydrogenation activities increases in the following order: sulfide metals  $\ll$  Pd  $<$  Pt [5].

Amorphous silica-alumina and, more recently, zeolites are the main solids which are used to perform the role of acid function in hydrocracking catalysts [6]. There are several works dealing with the performance of zeolites in bifunctional catalysis [7–10]. In effect, their crystalline structure and resistance to tough operating conditions make of them a suitable choice in hydrocracking processes. Zeolites are constituted of tetrahedral blocks connected by oxygen atoms. The channels produced by these blocks enables the classification of zeolites in ultra-large ( $> 12$  membered-ring), large (12 membered-ring), medium (10 membered-ring) and small (8 membered-ring) ones. Besides, their pore system can be uni-, di- or tridimensional, with diameters varying from 0.5 to 2 nm [11].

Aluminum or silicon atoms are placed in the center of each tetrahedron, as illustrated in Figure 1. It is interesting to notice that all tetrahedra centered in aluminum ( $\text{AlO}_4^-$ ) are separated from each other by at least one silicon tetrahedron ( $\text{SiO}_4$ ), according to Loewenstein's rule [12]. Another particularity of zeolites structure is the presence of compensation cations, as it can be seen in Figure 1, exemplified by sodium metal cations.

Given that aluminum tetrahedra possess a negative charge, these cations can neutralize the overall charge of the structure. This is an important feature because these compensation metals can be easily exchanged by other cations, creating Brønsted acid sites (BAS) when they are replaced by a proton  $H^+$ . This means that each tetrahedron centered in aluminum corresponds potentially to a BAS. Therefore, the general formula for a zeolite framework is given by  $M^+[AlO_2, nSiO_2] \cdot xH_2O$ , where the coefficient  $x$  depends on the content of aluminum in the framework. Water can be easily removed from the structure by thermal treatments as drying and calcination.

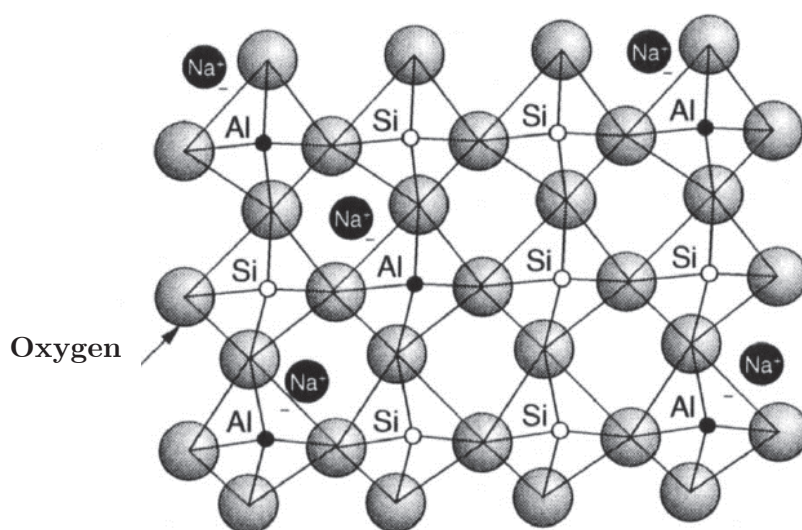


Figure 1. Organization of Si and Al tetrahedra in zeolites network [13]. Si, Al, O and  $Na^+$  atoms are indicated in the figure.

Activity and selectivity of bifunctional catalysts can be mainly influenced by the acidity and porosity of zeolites. The acidity of zeolites is intrinsically related to the density of BAS and their strength. The concentration of BAS increases inversely with Si/Al ratio of the zeolite framework, given that it is associated to the aluminum content. The strength of the sites is associated to their tendency to donate a proton and it depends on the interaction between proton and zeolite framework, on the length of the tetrahedron bonds (Si-OH-Al) and on the structure of the zeolites, as well as their chemical nature [14]. On the other hand, the porosity of the zeolites can lead to confinement and shape selective effects [15–23]. The latter parameter will be discussed in the section dedicated to bifunctionality.

Silica-aluminas are disordered structures composed of tetrahedral and octahedral building

blocks. These materials have large surface area, and are difficult to characterize due to their amorphous character. Their porous structure is linked to their composition and synthesis conditions [24].

In a general way, amorphous silica-aluminas present a lower activity than zeolites. This is related to the strength, concentration and accessibility of the acid sites [25–27]. Regarding the strength of the acid sites, the interaction of oxygen atoms with the proton leads to stress in the structure, but silica-aluminas have a greater potential of relaxation than zeolites. This effect yields more covalent O-H bonds, reducing the acidity of the hydroxyl groups. In respect to the concentration of acid sites, silica-aluminas are more susceptible of producing small alumina clusters, which are situated in non-tetrahedral sites. When thermal treatments take place, these clusters can be removed from the structure, creating Lewis acid sites (LAS). Therefore, while zeolites are normally considered as BAS, the silica-aluminas are potentially linked to LAS. The last aspect regards the porous system of these structures: in comparison with zeolites, amorphous silica-aluminas do not have the same degree of crystallinity and density of acid sites.

## 2. Mechanisms of hydrocracking of naphthenes

This section aims to present the main mechanisms involved in hydrocracking of naphthenic compounds, according to a bifunctional approach, i.e. catalysts presenting metal and acid functions, and following the chemistry of carbocations.

### 2.1. *Metal-catalyzed reactions*

Hydrogenation mechanism was established by Horiuti *et al.* [28], who worked on the exchange of hydrogen between water and ethylene, water and benzene, and among benzene and ethylene over a series of Ni and Pt catalysts. They proposed that chemisorption of one molecule of hydrogen over two metallic sites is followed by the chemisorption of an unsaturated compound on two other metallic sites. Then, a half hydrogenated state is formed by the transfer of one hydrogen atom to the adsorbed hydrocarbon, which is progressively changed in a final hydrogenated state by the shift of the remaining hydrogen atom, as shown



in Figure 2.

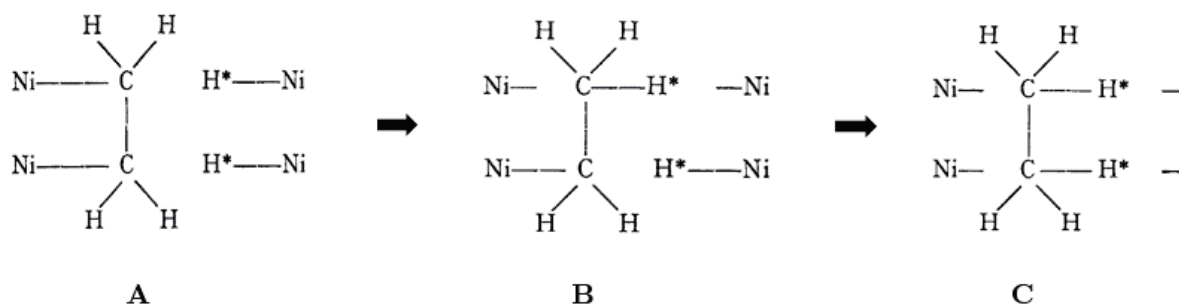


Figure 2. Hydrogenation mechanism over a Ni catalyst according to Horiuti *et al.* [27]. A, B and C correspond to initial, half hydrogenated and final hydrogenated transition states, respectively.

In addition to (de)hydrogenation reactions, the metal phase can also be associated to ring-opening through C-C bond cleavage [29,30]. Ring-opening is an essential tool to increase the cetane number of fuels, avoiding the formation of light compounds [31].

Ring opening on metal surface can take place mainly by two pathways: the multiplet and the dicarbene mechanisms [32–34]. Multiplet mechanism, on the other hand, can be divided into doublet and sextet-doublet mechanism, both competitive during the reaction. The former is catalyzed by small metal particles, favoring the selective ring-opening (non-statistical C-C bonds scission) of secondary carbons, once bonds between tertiary carbons cannot undergo ring-opening in this condition due to steric hindrance. This pathway involves the participation of only two metal atoms in the physical adsorption. Sextet-doublet mechanism allows flat adsorption of the naphthenic compound, with participation of several metal atoms and cleavage of tertiary-secondary or tertiary-tertiary carbon bonds.

The dicarbene mechanism goes through the formation of olefins after the cleavage of C-H bonds. In a non-selective ring-opening scenario, only one metal atom participates in the reaction and the olefin is adsorbed parallel to the metallic surface (Figure 3A). Selective ring-opening of cyclic compounds, which involves the participation of several metal atoms, may occur, however, in a perpendicular direction to the metal particles. In a way that compensates the steric hindrance of tertiary carbons, an alkyl side-chain can form a complex with the metal particles, allowing tertiary-secondary or tertiary-tertiary C-C bonds to be catalyzed (Figure 3B).

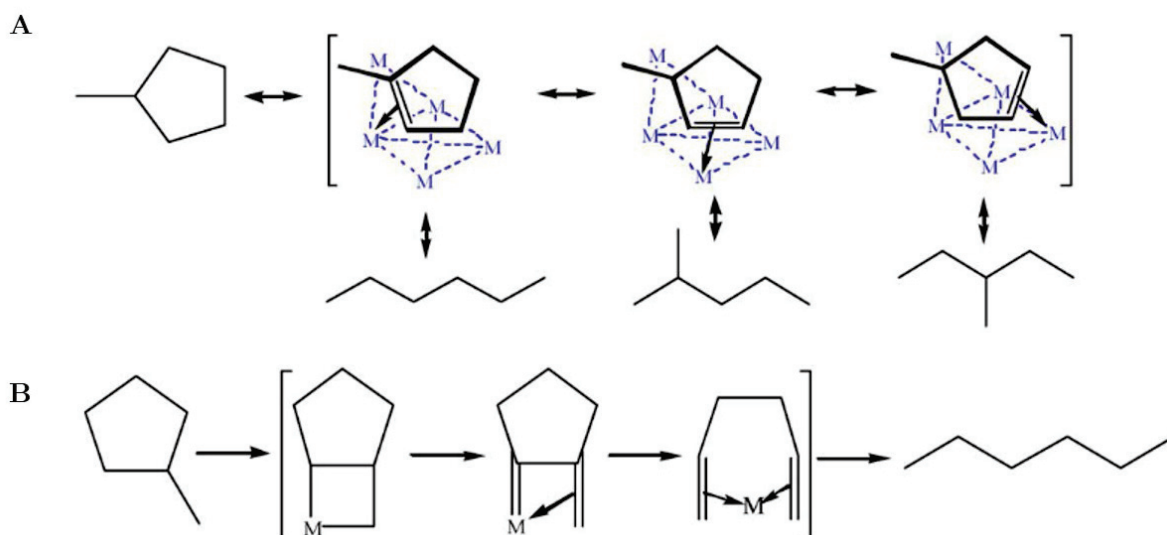


Figure 3. Dicarbene mechanism: A)  $\pi$ -adsorbed olefin perpendicular to the metal surface; B) formation of the complex with a metal particle [32,33].

It should be noted that ring-opening of six-membered rings occurs in a more sluggish way than five-membered ones. McVicker *et al.* verified that ring-opening of methylcyclohexane and n-butylcyclohexane over iridium, ruthenium, nickel and platinum proceeds slower than five-membered rings for all the metals tested [35]. Therefore, in order to increase the rate of opening C<sub>6</sub>-rings and avoid loss of carbon atoms, an acidic function must be used in order to isomerize C<sub>6</sub>-cycles into C<sub>5</sub>-rings (see section below).

## 2.2. Acid-catalyzed reactions

Similar to alkanes, alicyclic compounds go through different types of isomerization and C-C bonds scission, which are favored by the formation of the most stable carbocation. Among the pathways that should be considered in hydroconversion of naphthenic molecules, intramolecular, represented by isomerization and  $\beta$ -scission, and intermolecular mechanisms, as proton and hydride transfer, are some examples of rearrangements observed [36–39].

In superacidic media, two types of isomerization might be distinguished, considering the degree of branching of the final compound. For naphthenic molecules, each tertiary carbon atom corresponds to 1 branching, while quaternary carbon atoms contribute with two branchings [40]. If the degree of branching does not change during the rearrangement, the

isomerization is called of type A. Otherwise, it is named type B. Both of them proceed via formation of protonated cyclopropanes (PCP) intermediates [41,42], as shown in Figure 4 for alkanes and cyclic molecules. Type A isomerization is faster than type B one because the latter involves a corner to corner proton jump, which is considered a slow step of the reaction, with respect to hydride shifts observed on the former.

Martens *et al.* estimated isomerization rates of cycloalkanes on bifunctional noble catalysts (Pt/Y zeolites) [43]. According to the authors, composite activation energies of external and internal alkyl shifts (Figure 4, II and IV) are in the range of 21-25 kJ/mol, whereas cyclic PCP branchings energies are higher (Figure 4, VI), within the interval of 27-40 kJ/mol. Moreover, internal alkyl shifts (cyclohexane to cyclopentane interconversions) are slower than external alkyl shifts (10-16 kJ/mol), while PCP branchings (type B isomerization) and corresponding acyclic rearrangements are energetically comparable (30-42 kJ/mol for alkanes).

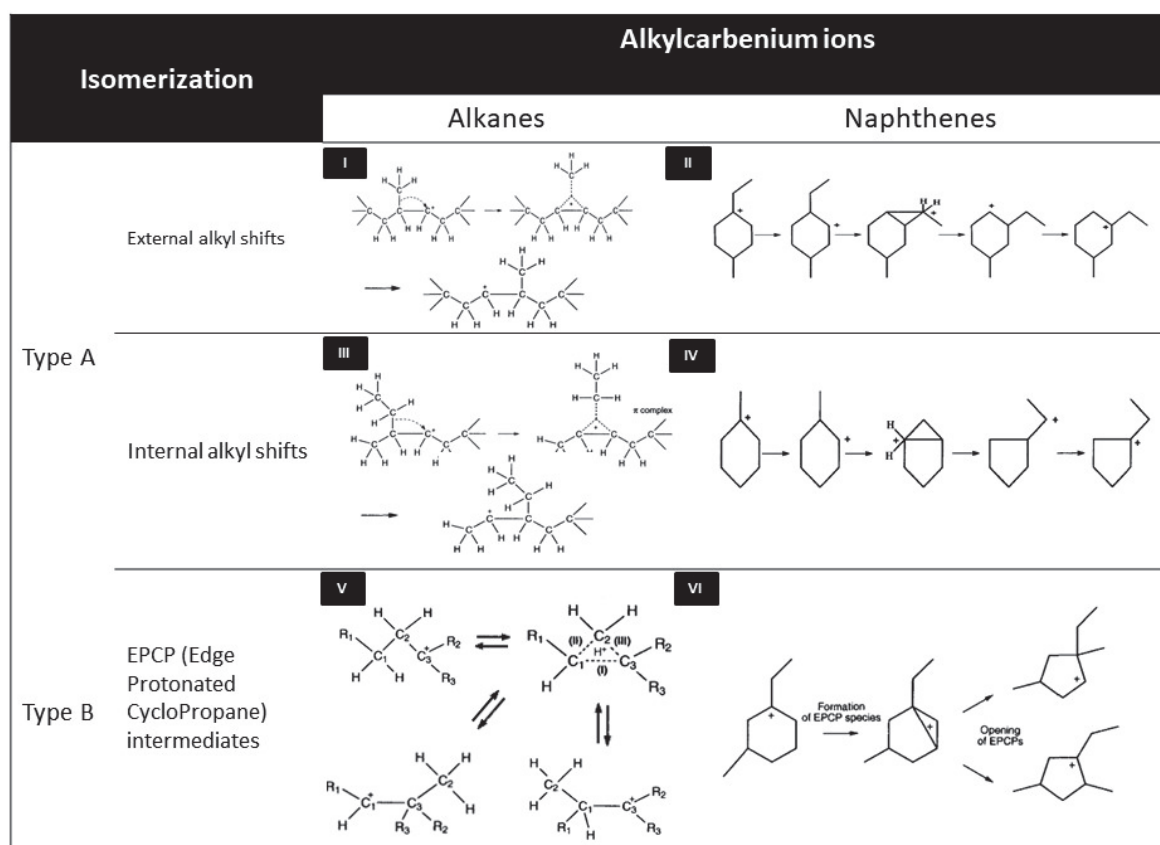


Figure 4. Types of isomerization and comparison between alkanes and naphthenes. Adapted from references [13,41].

Souvereinjs *et al.* [40], working on the hydroconversion of 1-cyclohexyloctane over Pt/H-Y

zeolite, identified numerous isomers resulting mainly from type A isomerization, besides a first step of ring branching initiated by type B rearrangement (Figure 5). Type A and B isomerization in the ring were faster than chain branching, and methyl-shifts were favored from the cycle towards the alkyl substituent. Moreover, the most preferred positions for branching were near the cycle.

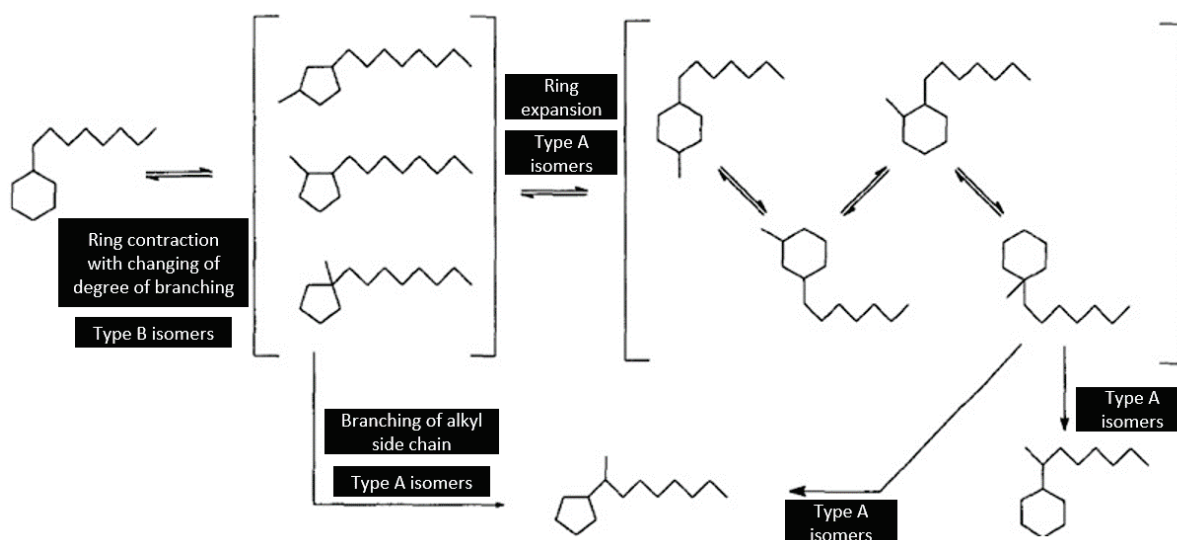


Figure 5. Isomerization pathways of 1-cyclohexyloctane adapted from Souverijns et al. [40].

Beta-scission occurs after skeletal rearrangement [44] and it is most favored when the p orbital from the positive carbon and the one from the beta bond are in a coplanar orientation. This configuration is well attained in aliphatic carbenium ions, because the alpha bond can rotate without hindrance. The same conclusion cannot be afforded to C-C bonds which form a ring, because  $\beta$ -bonds and p-orbitals are linked in a perpendicular position, avoiding the orbitals overlap.

This effect was observed by Brouwer and Hogeveen, who studied the rates of hydride and alkyl shifts and cleavage of  $\beta$  C-C bonds in superacid media ( $\text{FSO}_3\text{H-SbF}_5\text{-SO}_2\text{ClF}$ ) [45]. The authors compared the conversion of a branched alkane (2,4,4-trimethylpentyl cation) and a cyclic compound with the same degree of branching (1,3,3-trimethylcyclopentyl cation). Although the former was easily cracked at  $-73^\circ\text{C}$ , the latter did not undergo the same reaction even for temperatures up to  $0^\circ\text{C}$ , as seen in Figure 6.

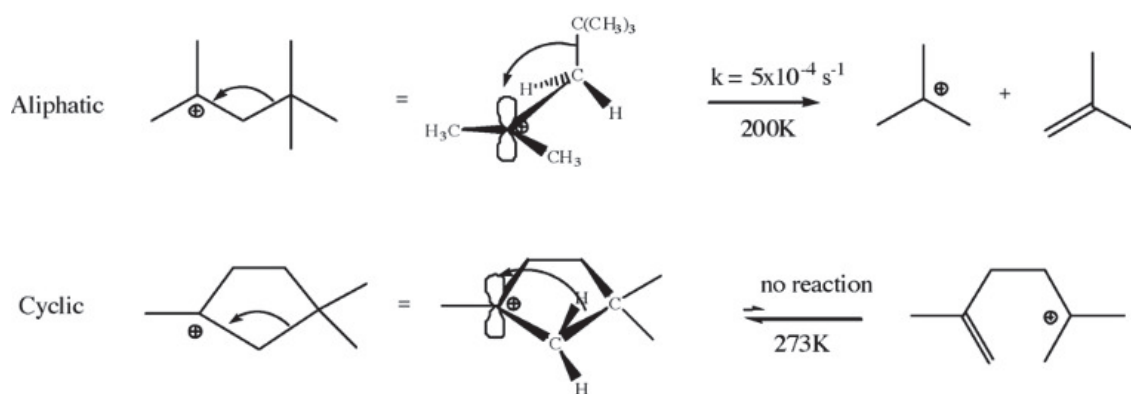


Figure 6. Effect of orbital overlap on beta-scission of C-C bonds according to Brouwer and coworkers [45].

Thus, endocyclic cracking of naphthenes is a very difficult reaction and exocyclic cracking is usually preferred. In general, alicyclic alkylcarbenium ions go through the same  $\beta$ -scission mechanisms as aliphatic alkylcarbenium ions, and one may classify the different pathways with respect to the types of substituted carbons (primary, secondary, tertiary) involved before and after the cleavage [46].

Figure 7 shows examples of hydroconversion of  $C_{10}$ -naphthenes. It can be noticed that C-C bond scission of these different cyclic structures occurs at the alkyl-chain (exocyclic C-C cleavage) and all of them result exclusively in  $C_6$  and  $C_4$  products. Preferential exocyclic scission of naphthenes occurs due to orbital effects described above, and the selectivity to  $C_6$  and  $C_4$  products is explained through “paring reactions”, as this type of pathway was first named by Chevron researchers, in the beginning of the 1960s. Egan et al studied hydrocracking of  $C_9$  to  $C_{12}$ -naphthenes over nickel sulfide (5.3% Ni) catalysts supported on silica-alumina (10% alumina) [47]. Conversion of  $C_{10}$  to  $C_{12}$ -naphthenes showed high selectivity to isobutane and to n-4 cyclic hydrocarbons, where n is the number of carbons. Among the naphthenes formed, methylcyclopentane was the major product.

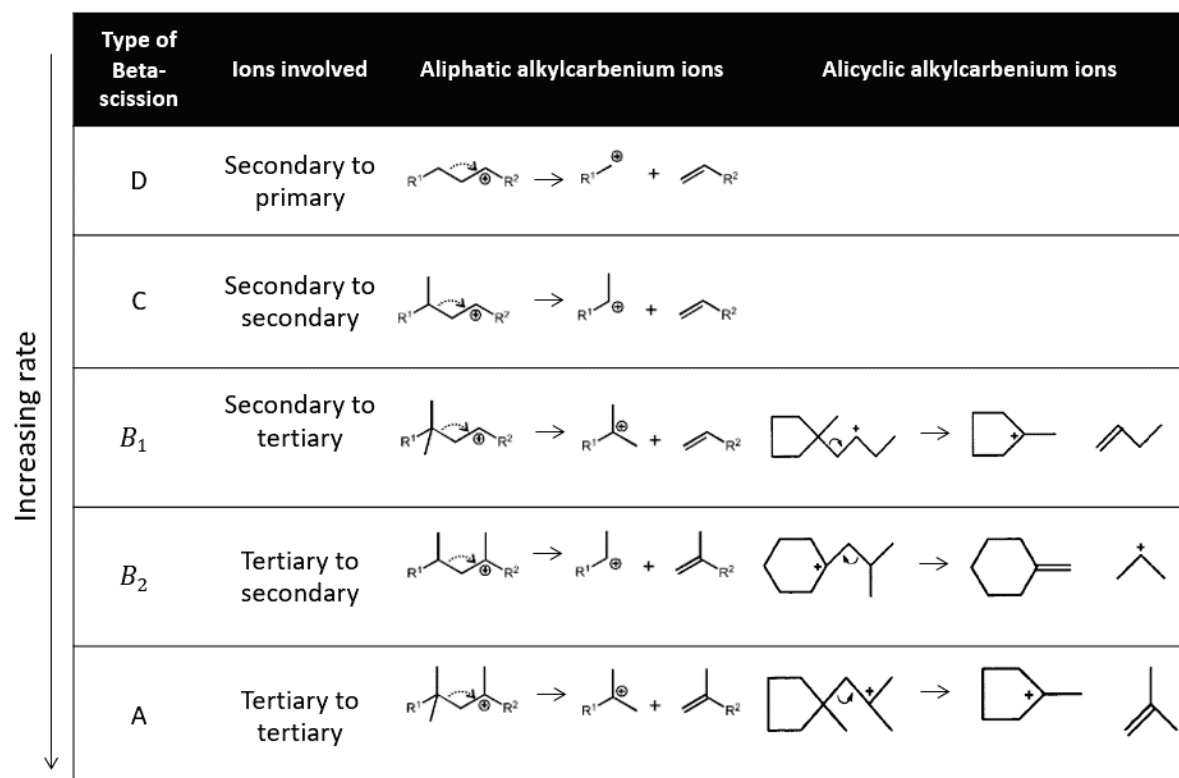


Figure 7. Types of beta-scission and comparison between alkanes and naphthenes. Adapted from references [43,48].

Paraffin reaction mechanism is shown in Figure 8. First reaction steps are dehydrogenation on metallic sites and protonation of the double bond or hydride transfer on acidic sites of the catalyst. Then, a series of rearrangements can take place in order to get the most favorable configuration which enables exocyclic cracking by type A beta-scission (tertiary-tertiary). In the case of C<sub>10</sub> to C<sub>14</sub>-naphthenes, this effect allows fast isomerization of the ring with contraction of the cycle. In effect, the methyl groups seem to leave from the ring, being eliminated as branched alkanes (e.g. isobutanes), conserving the ring.

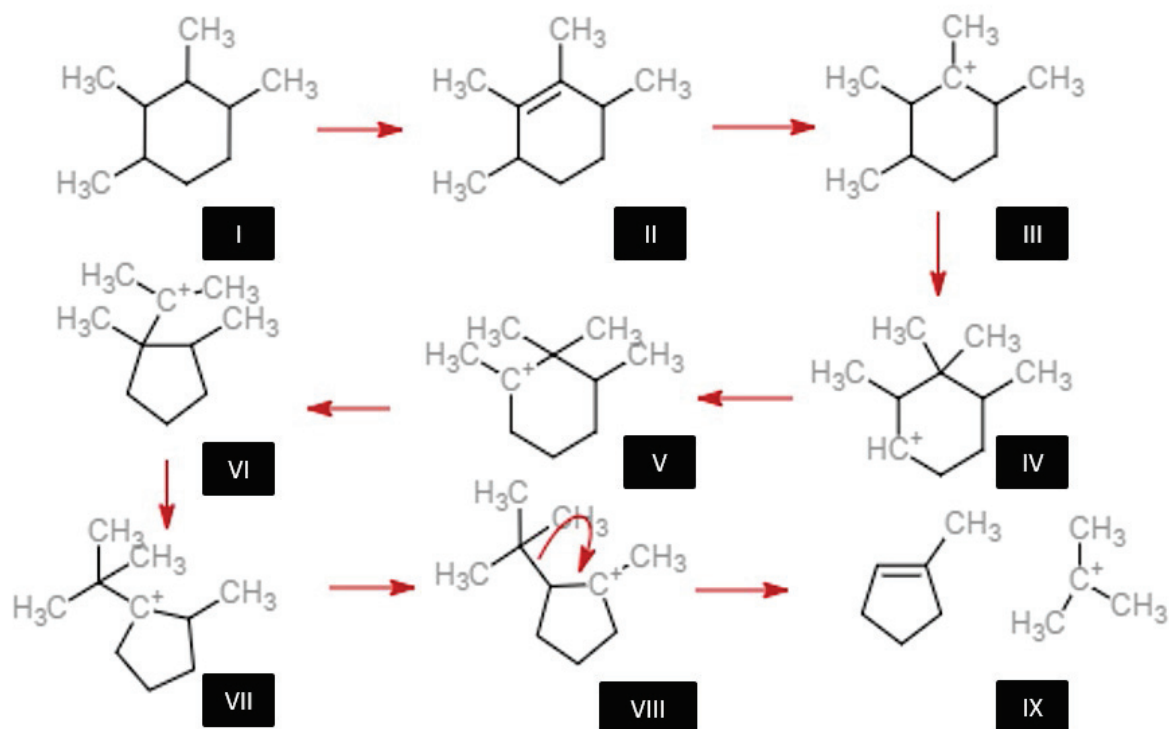


Figure 8. Reaction pathway of exocyclic beta-scission (“paring”) of 1,2,3,4-tetramethylcyclohexane towards formation of methylcyclopentane and isobutane (adapted from Egan *et al.* [23]).

Moreover, naphthenes with less than 10 carbon atoms do not crack in the same way as  $C_{10}$  to  $C_{14}$ -naphthenes. In effect, they do not have an enough number of carbons to ensure the formation of tertiary carbon atoms that can produce tertiary ions by beta-scission, as structure VII (Figure 8). Differences on distribution of reaction products can also be observed in respect to n-alkanes: their cracking profiles present a “bell”-shape, whereas  $C_{10}$  to  $C_{12}$ -naphthenes ones correspond to a M-shape (Figure 9) [49]. The major difference between these two profiles is the distribution around  $C_5$  products, which highlights the occurrence of paring reactions.

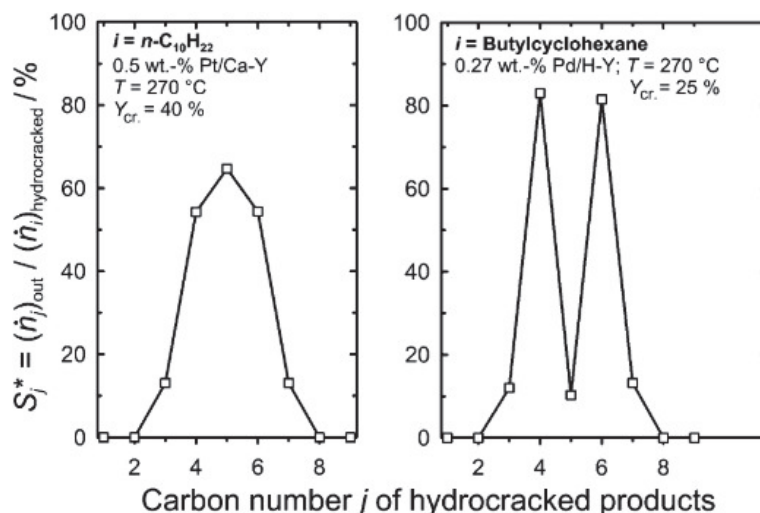


Figure 9. Carbon number distribution curves of a n-alkane (left, bell-type) and a naphthene (right, M- type) [50].

Preferential isomerization over ring-opening reactions (beta-scission mechanisms) was evidenced by Weitkamp *et al.*, on the hydroconversion of ethylcyclohexane on Pd/LaY catalyst. The authors verified that, at high conversion of the C<sub>6</sub>-cycle compound, the formation of tribranched C<sub>5</sub>-cycles, specially 1,1,3-trimethylcyclopentane was favored over the production of n-octane, formed after ring-opening of the six-membered ring. In fact, the latter represents a yield of only 2% at 87.6% conversion [51].

This result suggests that ring isomerization is the fastest reaction with respect to ring-opening by beta-scission. In contrast, by comparing, in similar conditions, the hydroconversion of 2-methylheptane (acyclic molecule corresponding to ethylcyclohexane), the isomerization into 2,2,4-trimethylpentane (corresponding alkane of 1,1,3-trimethylcyclopentane) was not verified, due to the fast type A beta-scission that can occur in this case. In this context, Figure 10 attempts to compare ring-opening rates with rates of Beta-scission of the opening products (or corresponding acyclic compounds).



Mode	$m \geq$	Reactants (methylnaphthenes)	Ring opening products	Ions involved	Rate classification
A	8		$\begin{array}{c} \text{C} \quad \text{C} \\   \quad   \\ \text{C}=\text{C}-\text{C}-\text{C}-\text{C}_+-\text{C} \end{array}$	T $\rightarrow$ T	$V_o < V_c$
B1	7		$\begin{array}{c} \text{C} \\   \\ \text{C}=\text{C}-\text{C}-\text{C}-\text{C}_+-\text{C} \end{array}$	S $\rightarrow$ T	$V_o \approx V_c$
B2	7		$\begin{array}{c} \text{C} \\   \\ \text{C}=\text{C}-\text{C}-\text{C}-\text{C}_+-\text{C} \end{array}$	T $\rightarrow$ S	$V_o \approx V_c$
C	6		$\text{C}=\text{C}-\text{C}-\text{C}-\text{C}_+-\text{C}$	S $\rightarrow$ S	$V_o > V_c$
D	5		$\text{C}=\text{C}-\text{C}-\text{C}-\text{C}_+$	S $\rightarrow$ P	(No data)

Figure 10. Comparison between ring-opening and cracking rates according to references [13,52].  $V_o$  stands for ring-opening rate,  $V_c$  corresponds to rate of beta-scission of opening products (or of the corresponding alkanes).

As explained previously, ring-opening may take place through acid-catalyzed mechanisms. In acidic sites of bifunctional catalysts, beta-scission is the main pathway that enables the formation of ring-opening products, i.e. compounds having the same number of carbons of the parent naphthene, but containing an inferior number of cycles.

In a general way, the reactivity of the cycle is determined by the number of tertiary carbons attained to the ring, as well as their placement, the number of isomers of the cyclic compound and the total number of carbon atoms of the molecule [53]. For instance, six-membered rings are unlikely to open directly by hydrogenolysis or beta-scission, on the other hand, ring-contraction into five-membered rings and consequently formation of a tertiary carbon atom increases ring-opening rates.

Regarding polycyclic naphthenes, it is expected that ring-opening of the first cycle will be

faster than opening of the subsequent cycles, due to a decrease in the number of tertiary carbons [54]. Therefore, one cannot expect to obtain high yields of long-chain alkanes starting from polycyclic naphthenes. Considering bifunctional mechanisms in ring-opening of cyclic molecules, several works [35,55–60] used monocyclic compounds as model molecules. In recent years, other works took into consideration bicyclic molecules [53,61–69] (tetralin, indan, decalin), in order to represent in a more faithful way real feedstocks of heavier oil cuts. The hydrogenating function plays an essential role together with the acidic function of the catalyst [70]. Kubicka *et al.* [53,71–73] studied the hydroconversion of decalin using Pt-supported catalysts (BEA, Y and MOR as supports) at temperatures varying from 200 to 270°C. Isomerization of decalin and ring-opening reactions were favored by the contribution of the metal, as compared to proton-form zeolites. Isomerization and ring-opening rates increased about three and five times, respectively, in the presence of Pt. Furthermore, the addition of Pt prevented the cracking activity of the parent zeolites, reducing the yield in light compounds (C<sub>1</sub>-C<sub>4</sub>).

In conclusion, according to Egan and coworkers [47,74,75], the main reactions on hydroisomerization and hydrocracking of alkylnaphthenes, performed from 250 to 350°C, may be arranged in terms of rates as it follows: type A Beta-scission > Type A isomerization of the ring > Type A isomerization of the alkyl chain ≥ exocyclic cracking ≥ Type B isomerization of the ring > Type B isomerization of the alkyl chain > Type B Beta-scission of the alkyl chain ≥ opening of the last ring.

### 3. Bifunctionality

According to what was exposed previously, bifunctional mechanisms are governed by metallic and acidic reactions according to the chemistry of carbocations. In a general way, this mechanism is initiated by the dehydrogenation of the cycle on the metal site, creating a cyclic olefin which diffuses into the acidic phase, where these species undergo isomerization and cracking. Then, these intermediates diffuse towards the metallic phase, where hydrogenation takes place. Therefore, the mechanism of hydroconversion processes will be driven by the rate limiting step of the reaction, i.e. metal- or acid-catalyzed reactions, which may, consequently, change the activity and selectivity of the catalyst [76].

The term “ideal” catalyst was first used by Weitkamp [77] and it is related to the balance between metal and acid functions in a bifunctional catalyst. For instance, if the (de)hydrogenating function is more active than the acidic one, the reactions performed on the latter represent then the rate limiting step of the process and the catalyst is considered to be “well balanced” or “ideal”. Conversely, if the metal function is weaker than the acidic one, then (de)hydrogenating reactions become the rate limiting steps in the overall process, characterizing a “poorly balanced” catalyst [78]. Moreover, the diffusion between metal and acidic functions cannot create transport limitations and should obey the Weisz intimacy criterion [79,80].

Other factors can influence the behavior (ideal or non-ideal) of the catalyst, as the strength of the metal and acidic functions, operating conditions (temperature, total pressure, molar hydrogen to feedstock ratio) and number of carbons of the reactant [64]. Therefore, a catalyst can behave ideally in certain conditions, and, in contrast, be considered poorly balanced in a different application. It is necessary to verify the equilibrium of phases for each system studied.

Metal-acid balance of bifunctional catalysts has been widely studied for small and long-chain alkanes [81–88], but few studies reported the influence of the acid-metal balance on hydrocracking of polycyclic naphthenes, specially tricyclic ones. Most model molecules are mono- or bicyclic naphthenes [64,65,67,89,90] and the analysis is restricted to the effect of the metal loading on the selectivity of the catalyst.

In this context, Monteiro *et al.* studied the hydroconversion of decalin, a bicyclic naphthene, over a series of Pt-modified Beta catalysts containing different Pt loadings, in order to evaluate the effect of the acid-metal balance in conversion and products distribution [64]. They verified that the yield of ring-contraction and ring-opening products increased with the metal/acid ratio until the concentration of Pt achieved 1 wt.% (Figure 11). The overall conversion of decalin did not change when the concentration of Pt increased, which may indicate that the (de)hydrogenation step was not the limiting one, even for low concentrations of Pt. The authors claimed that protolytic dehydrogenation could be the first step in hydroconversion of decalin when small contents of metallic phase are in use.

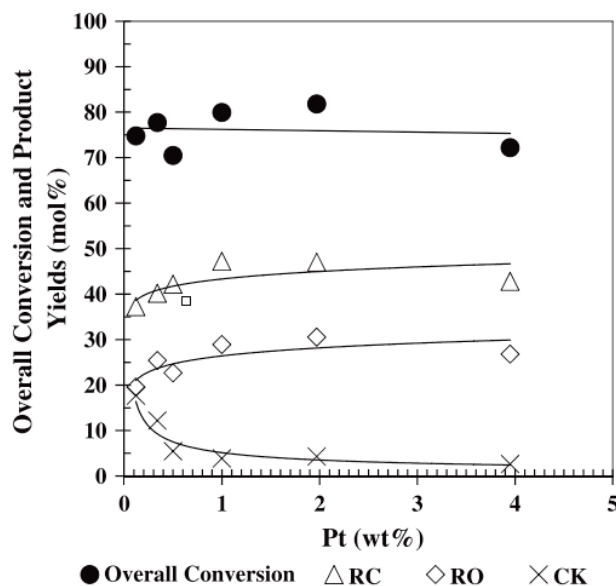


Figure 11. Overall conversion and yield of reaction products as a function of Pt loading on catalysts at 50 bar, 553 K, contact time= 3.8 h-1, H<sub>2</sub>/decalin (molar)=260. RC, RO and CK correspond to ring-contraction, ring-opening and cracking reactions, respectively [64].

Arribas and coworkers [91] verified the effect of metal content in hydroconversion of tetralin. They varied the Pt loading from 0.25 wt % to 4.0 wt % and the metal was directly impregnated onto USY zeolite. In this case, conversion of tetralin was up to 94% even for the least metal-charged catalyst. High metal loading favored the ring contraction of decalin (the hydrogenated product of tetralin) into five-membered rings, enhancing formation of ring-opening products. The same tendency was observed for selectivity to ring-opening and cracking products. This means that dehydrogenation of the cycle in the metal sites was the rate-determining step in those conditions.

In the same work, Arribas *et al.* analyzed the distance between metallic and acid phases and its effect on selectivity in tetralin hydroconversion. First, the authors performed catalytic tests by using three different catalyst configurations, where the two phases were put in different distances. The first configuration contained two layers of catalysts (Pt/Al<sub>2</sub>O<sub>3</sub> in one layer and USY in another), the second one was composed of a mechanical mixture of Pt/Al<sub>2</sub>O<sub>3</sub> and USY zeolite, and the third one was constituted of Pt impregnated directly onto the zeolite (Pt/USY), which represented the configuration with the smallest distance between the two functions. In addition, the number of metallic and Brønsted acid sites were

almost equivalent. The third configuration presented the greatest yield of decalin isomers and ring-opening products, which was about five times higher with Pt/USY compared to USY alone.

The morphology of the acid function may also influence the activity and selectivity of bifunctional catalysts on hydrocracking of naphthenes. When hydrocracking of heavy cyclic molecules takes place, e.g. hydrocracking of Vacuum Gas Oil, the acid function must assure that the free diffusion path can accommodate such compounds, in order to avoid transport limitations and shape selectivity effects. Weitkamp *et al.* used ethylcyclohexane and methylcyclohexane as model feedstocks and compared selectivity to type B isomers over Pd/LaY, Pd/H-Mordenite and Pd/HZSM-5, having different Si/Al ratios (2.5, 6.7 and 40, respectively) [92].

Besides the fact that Mordenite supported catalysts were the most active ones, presenting the same conversion as the others at lower temperatures, the formers did not produce any type of A isomers at low conversion, differently from the other solids. In this case, type A isomers were represented by propylcyclopentane and methylcycloheptane, considering ethylcyclohexane as model molecule; and ethylcyclopentane, when using methylcyclohexane as model feedstock. This effect was granted to a transition state shape selectivity, where the geometry of Mordenite pores intrinsically favored type B isomers formation.

Other structural effects were evidenced by Leite and co-workers [93,94]. The authors used Pt-supported catalysts in hydrocracking of phenanthrene and varied Si/Al ratio of the supports (Y, Beta zeolites and silica-alumina) in order to investigate the effects of acidity in the hydroconversion of the polycyclic compound. For beta zeolites and silica- alumina, the activity varied as a function of the acidity. Nevertheless, the selectivity to isomers and cracked products was not affected when the acidity varied. These competing pathways are illustrated in Figure 12. With respect to Y zeolites, dealumination process led to a higher microporous volume, therefore different selectivities to isomerization and cracked products could not be associated only to different acidities. Molecular simulation results showed that this difference could be related to the adsorption energy of the model molecule (perhydrophenanthrene isomers) and its intermediate products on the pores of the zeolites. Given that this energy was smaller for Y zeolites (compared to Beta ones), the selectivity to isomers products increased.

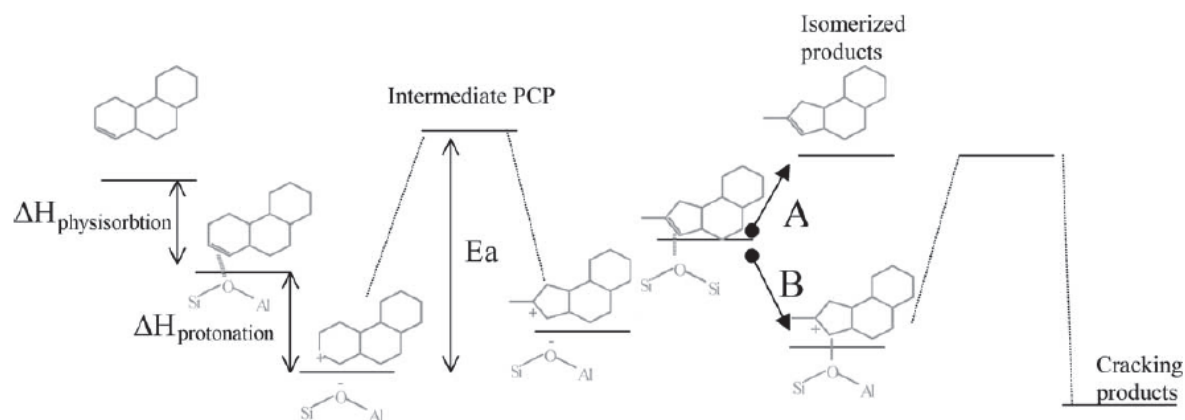


Figure 12. Steps of hydrocracking of perhydrophenanthrene highlighting isomerization and cracking as competing pathways according to references [93,94].

The influence of zeolites structure on ring-opening of bicyclic naphthenes was also reported in literature [91]. Taking tetralin as model molecule, the authors noticed that ring-opening products were favored on large-pore (12MR) zeolites, especially on Beta and USY zeolites, compared to the other acidic supports having similar Si/Al ratio and different pore topology. Experimental results showed that Pt/Beta catalysts led to a maximum yield of ring-opening products, followed by Pt/USY.

Arribas and coauthors [91] compared Beta and Y zeolites in ring-opening of 1-methylnaphthalene, in order to verify the effect of the reactant size in the selectivity of the catalysts. Figure 13 shows a better performance of Y zeolites in terms of selectivity, in contrast to results obtained in ring-opening of tetralin. Attempting to understand this behavior, they performed a molecular simulation by using propyl-ethyl-cyclohexane (PECH) as model feedstock. The authors found out that Beta zeolites may interact with PECH through van der Waals forces, which can hinder diffusion and turn the opening of the second cycle difficult. Conversely, no interactions were observed with respect to Y zeolites.

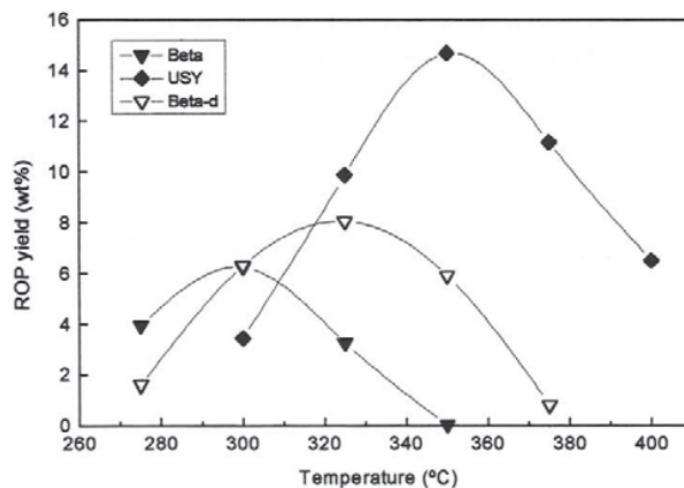


Figure 13. Yield of ring-opening products produced from 1-methylnaphthalene as a function of temperature for Pt-Beta and Pt-USY catalysts [91].

#### 4. Analysis of effluents

Molecular identification of effluents is crucial to determine coherent pathways in hydroconversion processes. This could be, however, a challenging task, given that heavier oil fractions will be more difficult to characterize. For instance, Vacuum gas oil cut, whose total number of carbons varies from 20 to 60 atoms, presents boiling points comprised between 350 and 600°C, which limits its identification by standard methods [95]. In this case, other strategies must be employed in order to define the families of compounds that constitute heavy oil fractions [96–98]. Table 1 makes an overview of the techniques applied in the identification of complex mixtures of hydrocarbons, classifying them in families.

Table 1. Separation methods for petroleum matrix [99–101].

Method	Main characteristics
Distillation [102,103]	Representation of the distillation curve of a given cut as a function of its boiling point
Liquid chromatography (LC) [104,105]	Great range of selectivity, poor separation efficiency, difficulty on molecular identification.
Supercritical fluid chromatography (SFC)[106,107]	Separation of complex mixtures, no volatile and temperature sensitive
Gas chromatography (GC)[108,109]	Total separation of light compounds (until C <sub>35</sub> -C <sub>40</sub> ), but olefins and naphthenes not well separated due to coelution. Great variety of specific and universal detectors.

Among these techniques, despite its limitations, gas chromatography (GC) is still widely used in works dealing with separation of complex mixtures, given that it is compatible with several oil derivatives [110–114]. GC is usually coupled to identification methods, especially mass spectrometry (MS) [115]. In recent years, with the evolution of analysis techniques (frequency, resolution, and mass accuracy for MS and modulator, stationary phase for GC), other methods started to be used as essential tools for the characterization of liquid effluents. Consequently, multidimensional chromatography coupled to MS has been applied in the treatment of trace compounds [116–119]. From now on, the focus of this chapter will be directed towards some principles of two-dimensional chromatography and mass spectrometry.

#### *4.1. Principles of two-dimensional gas chromatography*

In two-dimensional gas chromatography, two columns are connected, allowing the separation of the mixture in a high resolution column (first dimension) and a fast, isothermal separation of the effluents in a short column (second dimension). The two columns are connected by a device, e.g. a thermal or fluidic modulator [120], that allows pulses of effluents separated in the first column to be sent towards the second one.

Figure 14 illustrates the principle of a comprehensive GCxGC separation. In the 2D color plot, the first dimension is usually represented in minutes, corresponding to the retention time of the first column, while the second one is represented in narrow intervals of time (seconds). Occasionally, the resulting chromatogram can be represented in 3D plots, where the third dimension corresponds to the signal intensity.



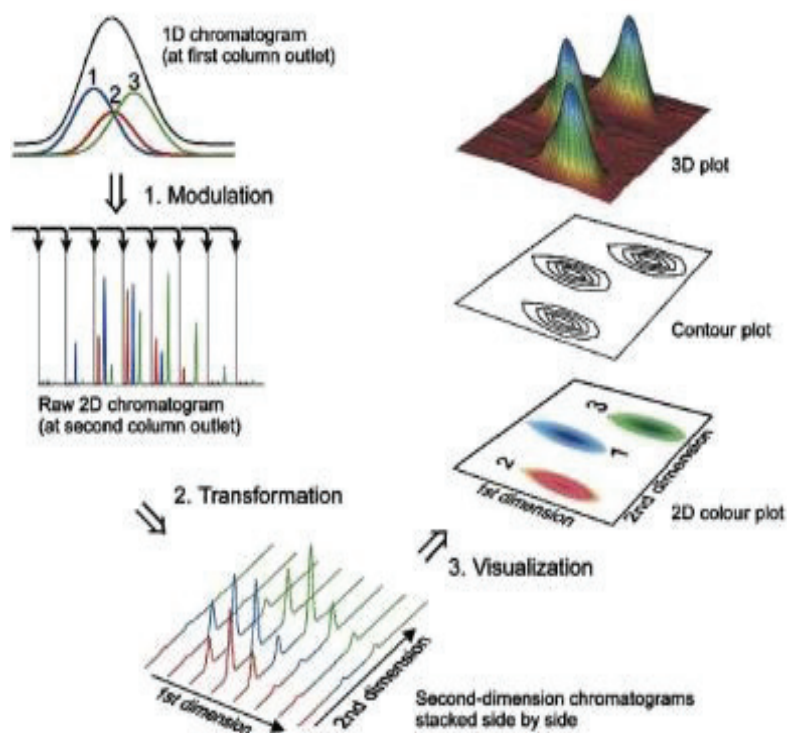


Figure 14. Schematic representation of a separation by GCxGC [121].

Regarding the choice of the column set, the possible configurations are related to temperature and polarity of the mixture to be characterized. Usually, the first dimension separates the compounds by boiling point and the second one by polarity, which is called a normal setup, contrary to a reverse setup [122]. The efficiency of such setups in the separation of complex mixtures has been studied by Jeol and coworkers (Figure 15). According to the profiles shown below, a normal column setup would be suitable to separate aromatic fractions, due to a higher chromatographic space, whereas a reverse column setup would fit the conditions to well separate naphthenic compounds.

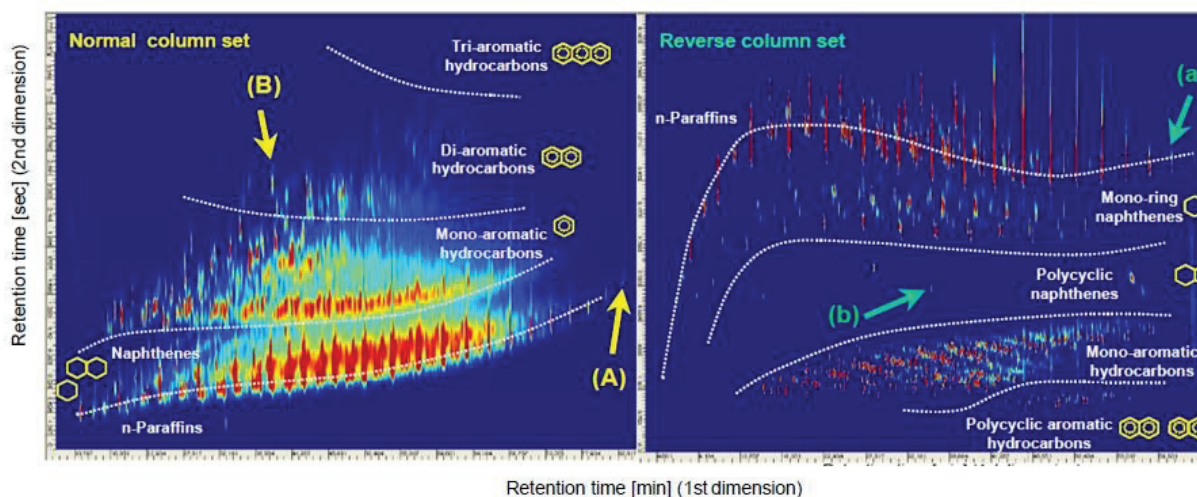


Figure 15. Normal and reverse column sets for separation of components of VGO. Courtesy of Jeol.

Main advantages of two-dimensional gas-chromatography are an improving on the separation of complex mixtures, besides the possibility of grouping the compounds in families, when they elute as ordered structures as in petroleum cuts which are composed of a continuum of molecules.

#### 4.2. Principles of mass spectrometry

Mass spectrometry allows the identification of a compound by taking into account the molecular ion and fragments mass/electrical charge (notated  $m/z$ ) generated throughout the contact of the molecule with a source of electrons to produce ions. These fragments and molecular ion are analyzed and detected, producing a spectrum with all the fragments yielded during this process. The interpretation of this spectrum can give information about the former molecule, i.e. its molecular mass, which can be converted to its molecular formula [123].

There are several ionization techniques available in hyphenation with gas chromatography and their choice depends on the type of molecule to be identified [124]. The most used and most informative is the electron ionization (EI), which produces molecular ion and fragment ions. It is also possible to use softer ion sources such as chemical ionization (CI) and field ionization (FI) to have access to the molecular ion and molecular formula of a given compound. NIST mass spectrometry database lists the spectrum of more than 100,000

molecules recording with electron ionization ion source, thus herein this will be the technique discussed.

Regarding EI, the first step in the fragmentation mechanism is represented in Figure 16. When energetic electrons (i.e. 70eV) interact with neutral molecules in the gas phase, ions (radical cations) are produced. The radical cations follow different fragmentation pathways and the produced fragments give the structural information of the starting molecule. From a radical cation, it is possible to produce a radical and a cation or a neutral molecule and a radical cation [125].

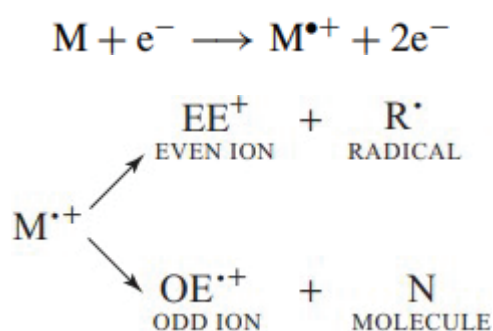


Figure 16. Fragmentation pathway of radical cations in EI [125].

The fragmentation process in EI may give structural information related to a specific molecule. In the case of naphthenic molecules, it is possible to identify different isomers, as exemplified in Figure 17 with respect to  $\text{C}_8\text{H}_{16}$  cyclic compounds.

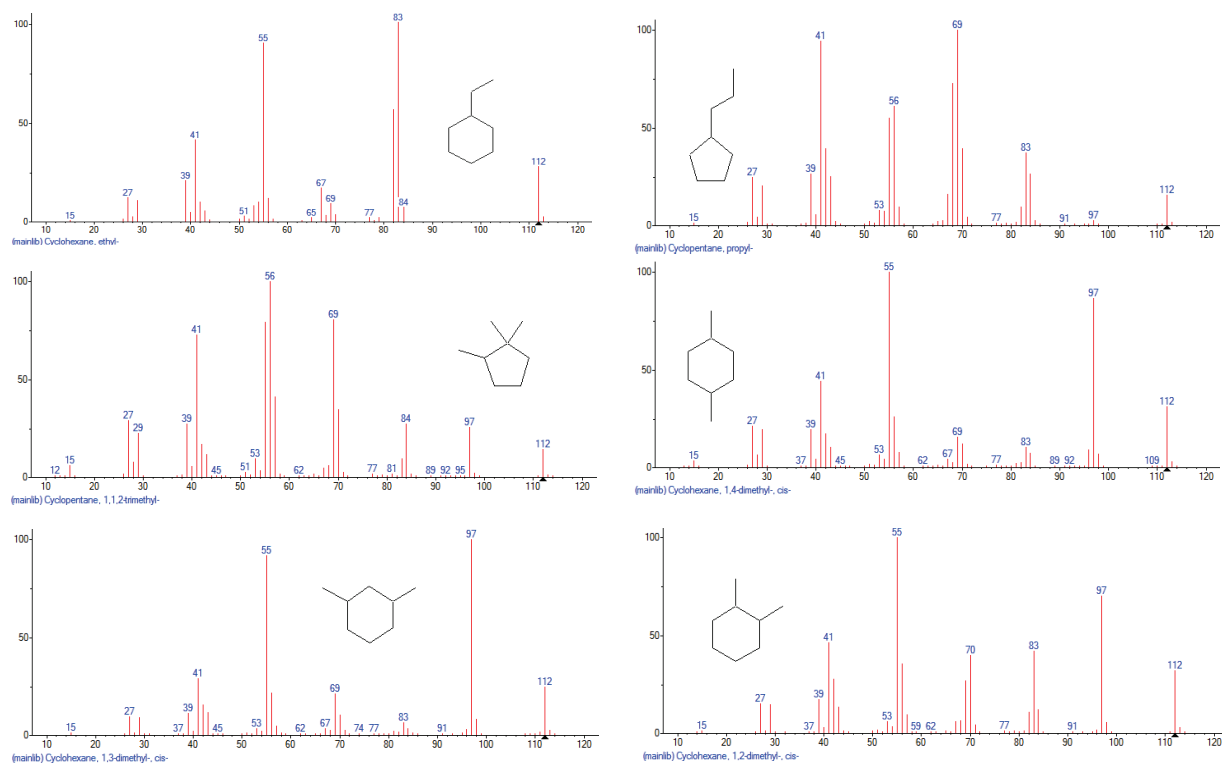


Figure 17. Spectra of different  $C_8H_{16}$  isomers according to NIST mass spectra database.

## 5. Conclusions

Oil industry faces restricted environmental regulations and, at the same time, an increasing demand in middle distillates, especially diesel and kerosene, as indicated by market trends. Therefore, new technologies should be developed in order to reach a better selectivity to such products. However, from what has been exposed in this chapter, the mechanisms governing the conversion of heavy oil cuts (VGO) into middle distillates are still poorly understood. In fact, most works from literature deal with bicyclic compounds, which not represent properly the real feedstocks found in industry. Besides, these works are particularly interested in selective ring-opening of naphthenic compounds, which does not take into account cracking steps seen in hydrocracking pathways.

Another point is that none of the works considered the comparison between different cyclic molecules having the same number of carbon atoms, at the same operating conditions. The comparison was limited to molecules having the same number of cycles and different saturation degrees, as in the comparison between tetralin and decalin. The same is valid for

the study of bifunctionality regarding polycyclic hydrocarbons: scarce literature is provided for 3-cycle naphthenes or heavier alkyl-substituted naphthenes, i.e. naphthenes having more than 12 carbon atoms.

Taking into account what has been discussed so far, this thesis proposes the study of hydrocracking of polycyclic hydrocarbons in order to understand the mechanisms involved in the hydroconversion of (poly)cyclic molecules. The reaction pathways shown in this chapter will be useful for the proposal of a mechanism in hydroisomerization and hydrocracking of polycyclic and substituted naphthenes, as it will be discussed in the following chapters.

## REFERENCES

- [1] Arunas T. Lapinas, Michael T. Klein and Bruce C. Gates, Catalytic Hydrogenation and Hydrocracking of Fluorene: Reaction Pathways, Kinetics, and Mechanisms, *Ind. Eng. Chem. Res.* 30 (1991) 42–50.
- [2] J.W. Ward, *Applied Industrial Catalysis*, Academic Press, San Diego, 1984.
- [3] J.W. Ward, Design And Preparation Of Hydrocracking Catalysts, in: G. Poncelet, P. Grange, P.A. Jacobs (Eds.), *Preparation of Catalysts III*, Elsevier, 1983, pp. 587–618.
- [4] K.H. Kang, G.T. Kim, S. Park, P.W. Seo, H. Seo, C.W. Lee, A review on the Mo-precursors for catalytic hydroconversion of heavy oil, *Journal of Industrial and Engineering Chemistry* 76 (2019) 1–16.
- [5] J.W. Ward, Hydrocracking Processes And Catalysts, *Fuel Process. Technol.* 35 (1993) 55–85.
- [6] M.A. Ali, T. Tatsumi, T. Masuda, Development of heavy oil hydrocracking catalysts using amorphous silica-alumina and zeolites as catalyst supports, *Appl Catal a-Gen* 233 (2002) 77–90.
- [7] A. Primo, H. Garcia, Zeolites as catalysts in oil refining, *Chem. Soc. Rev.* 43 (2014) 7548–7561.
- [8] M. Guisnet, F.R. Ribeiro, *Les zéolithes: un nanomonde au service de la catalyse*, EDP Sciences, 2006.
- [9] A. Martínez, M.A. Arribas, S.B.C. Pergher, Bifunctional noble metal/zeolite catalysts for upgrading low-quality diesel fractions via selective opening of naphthenic rings, *Catal. Sci. Technol.* 6 (2016) 2528–2542.
- [10] Vogt, Eelco T. C., G.T. Whiting, A. Dutta Chowdhury, B.M. Weckhuysen, Chapter Two - Zeolites and Zeotypes for Oil and Gas Conversion, in: Friederike C. Jentoft (Ed.), *Advances in Catalysis*, Academic Press, 2015, pp. 143–314.

- 
- [11] C. Baerlocher, L.B. McCusker, D.H. Olson, Atlas of Zeolite Framework Types, 6th ed., 2007.
- [12] A.G. Pelmenschikov, E.A. Paukshtis, M.O. Edisherashvili, G.M. Zhidomirov, On the Loewenstein rule and mechanism of zeolite dealumination, *The Journal of Physical Chemistry* 96 (1992) 7051–7055.
- [13] C. Marcilly, D. Decroocq, T. Jones, Acido-basic catalysis, Ed. Technip, Paris, 20052006.
- [14] J.L. Agudelo, Hensen, E. J. M., S.A. Giraldo, L.J. Hoyos, Influence of steam-calcination and acid leaching treatment on the VGO hydrocracking performance of faujasite zeolite, *Fuel Process. Technol.* 133 (2015) 89–96.
- [15] T.F. Degnan, The implications of the fundamentals of shape selectivity for the development of catalysts for the petroleum and petrochemical industries, *J. Catal.* 216 (2003) 32–46.
- [16] H. Toulhoat, P. Raybaud, E. Benazzi, Effect of confinement on the selectivity of hydrocracking, *Journal of Catalysis* 221 (2004) 500–509.
- [17] S.M. Csicsery, Shape-selective catalysis in zeolites, *Zeolites* 4 (1984) 202–213.
- [18] C.R. Marcilly, Where and how shape selectivity of molecular sieves operates in refining and petrochemistry catalytic processes, *Top Catal* 13 (2000) 357–366.
- [19] E. Verheyen, C. Jo, M. Kurttepel, G. Vanbutsele, E. Gobechiya, T.I. Korányi, S. Bals, G. van Tendeloo, R. Ryoo, Kirschhock, Christine E. A., J.A. Martens, Molecular shape-selectivity of MFI zeolite nanosheets in n-decane isomerization and hydrocracking, *J. Catal.* 300 (2013) 70–80.
- [20] M. Zhang, Y. Chen, L. Wang, Q. Zhang, C.-W. Tsang, C. Liang, Shape Selectivity in Hydroisomerization of Hexadecane over Pt Supported on 10-Ring Zeolites: ZSM-22, ZSM-23, ZSM-35, and ZSM-48, *Ind. Eng. Chem. Res.* 55 (2016) 6069–6078.
- [21] H.B. Mostad, T.U. Riis, O.H. Ellestad, Shape selectivity in Y-zeolites, *Applied Catalysis* 58 (1990) 105–117.
- [22] A. Patrigeon, E. Benazzi, C. Travers, J.Y. Bernhard, Influence of the zeolite structure and acidity on the hydroisomerization of n-heptane, *Catalysis Today* 65 (2001) 149–155.
- [23] G. Noh, Z. Shi, S.I. Zones, E. Iglesia, Isomerization and  $\beta$ -scission reactions of alkanes on bifunctional metal-acid catalysts, *Journal of Catalysis* 368 (2018) 389–410.
- [24] J. Kijenski, Baiker A, Acidic sites on catalyst surfaces and their determination, *Catalysis Today* 5 (1989) 1–120.
- [25] G. Crépeau, V. Montouillout, A. Vimont, L. Mariey, T. Cseri, F. Maugé, Nature, structure and strength of the acidic sites of amorphous silica alumina: an IR and NMR study, *The journal of physical chemistry. B* 110 (2006) 15172–15185.
- [26] E.J.M. Hensen, D.G. Poduval, P.C.M.M. Magusin, A.E. Coumans, J.A.R. van Veen, Formation of acid sites in amorphous silica-alumina, *Journal of Catalysis* 269 (2010) 201–218.
-

- [27] I.S. Pieta, M. Ishaq, R.P.K. Wells, J.A. Anderson, Quantitative determination of acid sites on silica–alumina, *Applied Catalysis A: General* 390 (2010) 127–134.
- [28] I. Horiuti, M. Polanyi, Exchange reactions of hydrogen on metallic catalysts, *Trans. Faraday Soc.* 30 (1934) 1164–1172.
- [29] A. Haas, Ring Opening of Mono- and Bicyclic Naphthenes via Hydrogenolysis on Noble Metal Catalysts, 2012.
- [30] S. Yanatake, Y. Nakaji, M. Betchaku, Y. Nakagawa, M. Tamura, K. Tomishige, Selective C–C Hydrogenolysis of Alkylbenzenes to Methylbenzenes with Suppression of Ring Hydrogenation, *ChemCatChem* 10 (2018) 4172–4181.
- [31] A. Galadima, O. Muraza, Ring opening of hydrocarbons for diesel and aromatics production, *Fuel* 181 (2016) 618–629.
- [32] F.G. Gault, Mechanisms of Skeletal Isomerization of Hydrocarbons on Metals, in: D.D. Eley, H. Pines, P.B. Weisz (Eds.), *Academic Press*, 1981, pp. 1–95.
- [33] H. Du, C. Fairbridge, H. Yang, Z. Ring, The chemistry of selective ring-opening catalysts, *Applied Catalysis A: General* 294 (2005) 1–21.
- [34] K. Hayek, R. Kramer, Z. Paál, Metal-support boundary sites in catalysis, *Applied Catalysis A: General* 162 (1997) 1–15.
- [35] G. McVicker, Selective Ring Opening of Naphthenic Molecules, *Journal of Catalysis* 210 (2002) 137–148.
- [36] J. Weitkamp, S. Ernst, Comparison Of The Reactions Of Ethylcyclohexane And 2-Methylheptane On Pd/Lay Zeolite, in: B. Imelik, C. Naccache, G. Coudurier, Y. Ben Taarit, J.C. Vedrine (Eds.), *Catalysis by Acids and Bases*, Elsevier, 1985, pp. 419–426.
- [37] H. Abrevaya, Unique Aspects of Mechanisms and Requirements for Zeolite Catalysis in Refining and Petrochemicals, in: *Zeolites in Industrial Separation and Catalysis*, Wiley-VCH Verlag GmbH & Co. KGaA, 2010, pp. 403–478.
- [38] H.L. Coonradt, W.E. Garwood, Mechanism of hydrocracking - reactions of paraffins + olefins, *Ind Eng Chem Proc Dd* 3 (1964) p. 38.
- [39] A.T. Lapinas, M.T. Klein, B.C. Gates, A. Macris, J.E. Lyons, Catalytic Hydrogenation and Hydrocracking of Fluorene: Reaction Pathways, Kinetics, and Mechanisms, *Ind. Eng. Chem. Res.* 30 (1991) 42–50.
- [40] W. Souverijns, R. Parton, J.A. Martens, G.F. Froment, P.A. Jacobs, Mechanism of the paring reaction of naphthenes, *Catal Lett* 37 (1996) 207–212.
- [41] P.A. Jacobs, J.A. Martens, Chapter 12 Introduction to Acid Catalysis with Zeolites in Hydrocarbon Reactions, in: H. van Bekkum, E.M. Flanigen, J.C. Jansen (Eds.), *Introduction to zeolite science and practice*, Elsevier, Amsterdam, New York, 1991, pp. 445–496.



- 
- [42] J.A. Martens, P.A. Jacobs, Evidence for branching of long-chain n-alkanes via protonated cycloalkanes larger than cyclopropane, *Journal of Catalysis* 124 (1990) 357–366.
- [43] G.G. Martens, J.W. Thybaut, G.B. Marin, Single-Event Rate Parameters for the Hydrocracking of Cycloalkanes on Pt/US-Y Zeolites, *Ind. Eng. Chem. Res.* 40 (2001) 1832–1844.
- [44] J. Weitkamp, S. Ernst, R. Kumar, The spaciousness index: A novel test reaction for characterizing the effective pore width of bifunctional zeolite catalysts, *Applied Catalysis* 27 (1986) 207–210.
- [45] D.M. Brouwer, H. Hogeveen, *Recl. Trav. Chim. Pays-Bas* 89 (1970) 211–224.
- [46] J. Weitkamp, P.A. Jacobs, J.A. Martens, Isomerization and hydrocracking of C<sub>9</sub> through C<sub>16</sub> n-alkanes on Pt/HZSM-5 zeolite, *Appl Catal* 8 (1983) 123–141.
- [47] C.J. Egan, G.E. Langlois, R.J. White, Selective Hydrocracking of C<sub>9</sub> - to C<sub>12</sub> - Alkylcyclohexanes on Acidic Catalysts. Evidence for the Paring Reaction, *J. Am. Chem. Soc.* 84 (1962) 1204–1212.
- [48] J. Weitkamp, S. Ernst, H.G. Karge, Peculiarities in the Conversion of Naphthenes on Bifunctional Catalysts, *Erdol und Kohle - Erdgas* 37 (1984) 457.
- [49] J.W. S. Ernst (Ed.), *Proceedings of the International Symposium on Zeolite Catalysis*, Hungary, 1985.
- [50] J. Weitkamp, Catalytic Hydrocracking-Mechanisms and Versatility of the Process, *ChemCatChem* 4 (2012) 292–306.
- [51] J. Weitkamp, P.A. Jacobs, S. Ernst, Shape Selective Isomerization and Hydrocracking of Naphthenes Over Pt/HZSM-5 Zeolite, in: P.A. Jacobs, N.I. Jaeger, P. Jírů, V.B. Kazansky, G. Schulz-Ekloff (Eds.), *Structure and Reactivity of Modified Zeolites*, Elsevier, 1984, pp. 279–290.
- [52] H.F. Schulz, J. Weitkamp, Eberth H (Eds.), *Proceed 5th Intern Congr on Catalysis*, Amsterdam, NorthHolland Publ Co, Amsterdam, 1972.
- [53] M. Kangas, D. Kubička, T. Salmi, D.Y. Murzin, Reaction Routes in Selective Ring Opening of Naphthenes, *Top Catal* 53 (2010) 1172–1175.
- [54] V.A. Filimonov, Popov A.A., Khavkin V.A., Perezhigina I.Y., L.N. Osipov, S.P. Rogov, A.V. Agafonov, *Int Chem Eng* 12 (1972).
- [55] L.M. Kustov, Opening of the Rings of Aromatic and Naphthene Hydrocarbons: A new way of improving the quality of fuels, *Catal. Ind.* 3 (2011) 358–369.
- [56] P. Samoila, F. Epron, P. Marécot, C. Especel, Influence of chlorine on the catalytic properties of supported rhodium, iridium and platinum in ring opening of naphthenes, *Applied Catalysis A: General* 462-463 (2013) 207–219.
-



- [57] H. Ziaei-Azad, A. Sayari, Bifunctional MCM-41 aluminosilicate supported Ir with adjusted metal and acid functionality for catalytic ring opening of 1,2-dimethylcyclohexane, *Journal of Catalysis* 344 (2016) 729–740.
- [58] S.A. D’Ippolito, C. Especel, L. Vivier, S. Pronier, F. Epron, C.L. Pieck, Influence of the support on the selective ring opening of methylcyclohexane and decalin catalyzed by Rh–Pd catalysts, *Journal of Molecular Catalysis A: Chemical* 398 (2015) 203–214.
- [59] S.A. D’Ippolito, C. Especel, L. Vivier, F. Epron, C.L. Pieck, Influence of the Brønsted acidity, SiO<sub>2</sub>/Al<sub>2</sub>O<sub>3</sub> ratio and Rh–Pd content on the ring opening. Part II. Selective ring opening of methylcyclohexane, *Applied Catalysis A: General* 469 (2014) 541–549.
- [60] R. Nageswara Rao, N. You, S. Yoon, D.P. Upare, Y.-K. Park, C.W. Lee, Selective Ring Opening of Methylcyclopentane and Methylcyclohexane Over Iridium Bifunctional Catalysts Supported on Surface Modified  $\gamma$ -Al<sub>2</sub>O<sub>3</sub>, SiO<sub>2</sub> and Ultra Stable Y Zeolites, *Catal Lett* 141 (2011) 1047–1055.
- [61] K. Sato, Y. Iwata, T. Yoneda, A. Nishijima, Y. Miki, H. Shimada, Hydrocracking of diphenylmethane and tetralin over bifunctional NiW sulfide catalysts supported on three kinds of zeolites, *Catalysis Today* 45 (1998) 367–374.
- [62] S.G.A. Ferraz, B.M. Santos, F.M.Z. Zotin, L.R.R. Araujo, J.L. Zotin, Influence of Support Acidity of NiMo Sulfide Catalysts for Hydrogenation and Hydrocracking of Tetralin and Its Reaction Intermediates, *Ind. Eng. Chem. Res.* 54 (2015) 2646–2656.
- [63] Tobias Holl, Competitive Hydroconversion of Decalin and n-Decane on Noble-Metal Catalysts and the Evaluation of Molybdenum Carbide as Ring-Opening Catalyst.
- [64] C.A.A. Monteiro, D. Costa, J.L. Zotin, D. Cardoso, Effect of metal–acid site balance on hydroconversion of decalin over Pt/Beta zeolite bifunctional catalysts, *Fuel* 160 (2015) 71–79.
- [65] H. González, O.S. Castillo, J.L. Rico, A. Gutiérrez-Alejandre, J. Ramírez, Hydroconversion of 2-Methylnaphthalene on Pt/Mordenite Catalysts. Reaction Study and Mathematical Modeling, *Ind. Eng. Chem. Res.* 52 (2013) 2510–2519.
- [66] M. Santikunaporn, J. Herrera, S. Jongpatiwut, D. Resasco, W. Alvarez, E. Sughrue, Ring opening of decalin and tetralin on HY and Pt/HY zeolite catalysts, *Journal of Catalysis* 228 (2004) 100–113.
- [67] L. Piccolo, S. Nassreddine, G. Toussaint, C. Geantet, Mechanism of tetralin ring opening and contraction over bifunctional Ir/SiO<sub>2</sub>-Al<sub>2</sub>O<sub>3</sub> Catalysts, *ChemSusChem* 5 (2012) 1717–1723.
- [68] D. Santi, T. Holl, V. Calemma, J. Weitkamp, High-performance ring-opening catalysts based on iridium-containing zeolite Beta in the hydroconversion of decalin, *Applied Catalysis A: General* 455 (2013) 46–57.
- [69] G. Bellussi, A. Haas, S. Rabl, D. Santi, M. Ferrari, V. Calemma, J. Weitkamp, Catalytic Ring Opening of Perhydroindan – Hydrogenolytic and Cationic Reaction Paths, *Chinese Journal of Catalysis* 33 (2012) 70–84.

- [70] M.A. Arribas, P. Concepción, A. Martínez, The role of metal sites during the coupled hydrogenation and ring opening of tetralin on bifunctional Pt(Ir)/USY catalysts, *Applied Catalysis A: General* 267 (2004) 111–119.
- [71] D. Kubička, N. Kumar, P. Mäki-Arvela, M. Tiitta, V. Niemi, H. Karhu, T. Salmi, D.Y. Murzin, Ring opening of decalin over zeolites. Activity and selectivity of platinum-modified zeolites, *Journal of Catalysis* 227 (2004) 313–327.
- [72] D. Kubička, N. Kumar, P. Mäki-Arvela, T. Venäläinen, M. Tiitta, T. Salmi, D.Y. Murzin, Ring opening of decalin over Pt- and Ir-modified SAPO-5 and VPI-5 zeolite catalysts, in: *Molecular sieves: From basic research to industrial applications Proceedings of the 3rd International zeolite symposium Prague, Czech Republic, August 23-26, 2005*, Elsevier, Oxford, New York, Amsterdam, op. 2005, pp. 1669–1676.
- [73] D. Kubička, T. Salmi, M. Tiitta, D.Y. Murzin, Ring-opening of decalin – Kinetic modelling, *Fuel* 88 (2009) 366–373.
- [74] R. F. Sullivan, Clark J. Egan, And G. E. Langlois, Hydrocracking of alkylbenzenes and polycyclic aromatic hydrocarbons on acidic catalysts. Evidence for cyclization of the side chains, *Journal of Catalysis* 3 (1964) 183–195.
- [75] Clark J. Egan, Hydrocracking of n-Butylbenzene, sec-Butylbenzene Benzene with Palladium on Silica-Alumina Catalysts, *Journal of Catalysis* 36 (1975) 313–319.
- [76] J. Weitkamp, Isomerization of Long-chain n -Alkanes on a Pt/CaY Zeolite Catalyst, *Ind. Eng. Chem. Prod. Res. Dev.* 21 (1982) 550–558.
- [77] H. Pichler, H. Schulz, H. O. Reitemeyer, and J. Weitkamp, Über das Hydrocracken gesättigter Kohlenwasserstoffe., *Erdöl, Kohle –Erdgas -Petrochem* 25 (1972).
- [78] J.W. Thybaut, Narasimhan, C. S. L., J.F. Denayer, G.V. Baron, P.A. Jacobs, J.A. Martens, G.B. Marin, Acid-metal balance of a hydrocracking catalyst, *Ind. Eng. Chem. Res.* 44 (2005) 5159–5169.
- [79] M. Guisnet, “Ideal” bifunctional catalysis over Pt-acid zeolites, *Catalysis Today* 218-219 (2013) 123–134.
- [80] N. Batalha, L. Pinard, Y. Pouilloux, M. Guisnet, Bifunctional Hydrogenating/Acid Catalysis, *Catal Lett* 143 (2013) 587–591.
- [81] J. Zečević, G. Vanbutsele, K.P. de Jong, J.A. Martens, Nanoscale intimacy in bifunctional catalysts for selective conversion of hydrocarbons, *Nature* 528 (2015) 245–248.
- [82] P.S.F. Mendes, J.M. Silva, M.F. Ribeiro, P. Duchêne, A. Daudin, C. Bouchy, Quantification of metal-acid balance in hydroisomerization catalysts, *AIChE J* 63 (2017) 2864–2875.
- [83] M. Guisnet, “Ideal” bifunctional catalysis over Pt-acid zeolites, *Catal Today* 218–219 (2013) 123–134.
- [84] F. Alvarez, F.R. Ribeiro, G. Perot, C. Thomazeau, M. Guisnet, Hydroisomerization and hydrocracking of alkanes - Influence of the balance between acid and hydrogenating

- functions on the transformation of n-decane on PtHY catalysts, *J. Catal.* 162 (1996) 179–189.
- [85] N. Batalha, Optimization of the balance between activity and selectivity on a hydroisomerization catalyst, Lisbon.
- [86] M.J. Girgis, Y.P. Tsao, Impact of catalyst metal acid balance in n-hexadecane hydroisomerization and hydrocracking, *Ind. Eng. Chem. Res.* 35 (1996) 386–396.
- [87] F. Alvarez, F.R. Ribeiro, G. Perot, C. Thomazeau, M. Guisnet, Hydroisomerization and Hydrocracking of Alkanes, *Journal of Catalysis* 162 (1996) 179–189.
- [88] T.F. Degnan, C.R. Kennedy, Impact of Catalyst Acid Metal Balance in Hydroisomerization of Normal Paraffins, *Aiche J.* 39 (1993) 607–614.
- [89] S. Nassreddine, L. Massin, M. Aouine, C. Geantet, L. Piccolo, Thiotolerant Ir/SiO<sub>2</sub>-Al<sub>2</sub>O<sub>3</sub> bifunctional catalysts, *Journal of Catalysis* 278 (2011) 253–265.
- [90] E. Gutierrez-Acebo, C. Leroux, C. Chizallet, Y. Schuurman, C. Bouchy, Metal/Acid Bifunctional Catalysis and Intimacy Criterion for Ethylcyclohexane Hydroconversion, *ACS Catal.* 8 (2018) 6035–6046.
- [91] M.A. Arribas, A. Martínez, G. Sastre, Simultaneous hydrogenation and ring opening of aromatics for diesel upgrading on Pt/zeolite catalysts. The influence of zeolite pore topology and reactant on catalyst performance, in: R. Aiello, G. Giordano, F. Testa (Eds.), *Impact of zeolites and other porous materials on the new technologies at the beginning of the new millennium: Proceedings of the 2nd International FEZA (Federation of the European Zeolite Associations) Conference, Taormina, Italy, September 1-5, 2002, 1st ed., Elsevier, Amsterdam, Boston, 2002, pp. 1015–1022.*
- [92] J. Weitkamp, S. Ernst, H.G. Karge, Peculiarities in the conversion of naphthenes on bifunctional catalysts, *Erdöl & Kohle, Erdgas, Petrochemie.* 37 (1984).
- [93] E. Benazzi, L. Leite, N. Marchal-George, H. Toulhoat, P. Raybaud, New insights into parameters controlling the selectivity in hydrocracking reactions, *J. Catal.* 217 (2003) 376–387.
- [94] L. Leite, Etude sur molécule modèle des paramètres régissant la sélectivité des catalyseurs d'hydrocraquage des charges lourdes, 2000.
- [95] T. Dutriez, M. Courtiade, D. Thiébaud, H. Dulot, M.-C. Hennion, Improved hydrocarbons analysis of heavy petroleum fractions by high temperature comprehensive two-dimensional gas chromatography, *Fuel* 89 (2010) 2338–2345.
- [96] V. Garaniya, D. McWilliam, L. Goldsworthy, M. Ghiji, Extensive chemical characterization of a heavy fuel oil, *Fuel* 227 (2018) 67–78.
- [97] D. Stratiev, I. Shishkova, I. Tankov, A. Pavlova, Challenges in characterization of residual oils. A review, *Journal of Petroleum Science and Engineering* 178 (2019) 227–250.
- [98] A.A. Herod, K.D. Bartle, R. Kandiyoti, Characterization of Heavy Hydrocarbons by Chromatographic and Mass Spectrometric Methods, *Energy Fuels* 21 (2007) 2176–2203.

- [99] C.S. Hsu, Q. Shi, Prospects for petroleum mass spectrometry and chromatography, *Sci. China Chem.* 56 (2013) 833–839.
- [100] S. Gutiérrez Sama, C. Barrère-Mangote, B. Bouyssière, P. Giusti, R. Lobinski, Recent trends in element speciation analysis of crude oils and heavy petroleum fractions, *TrAC Trends in Analytical Chemistry* 104 (2018) 69–76.
- [101] A.C. Clingenpeel, T.R. Fredriksen, K. Qian, M.R. Harper, Comprehensive Characterization of Petroleum Acids by Distillation, Solid Phase Extraction Separation, and Fourier Transform Ion Cyclotron Resonance Mass Spectrometry, *Energy Fuels* 32 (2018) 9271–9279.
- [102] R. Bacaud, L. Rouleau, Coupled simulated distillation-mass spectrometry for the evaluation of hydroconverted petroleum residues, *Journal of chromatography. A* 750 (1996) 97–104.
- [103] L. Carbognani, R. Meneghini, E. Hernandez, J. Lubkowitz, P. Pereira-Almao, Applications of Hydrocarbon Group-Type and Class-Type Analysis via Simulated Distillation-Mass Spectrometry for Process Upgrading Monitoring, *Energy Fuels* 26 (2012) 2248–2255.
- [104] F.T. van Beek, R. Edam, B.W.J. Pirok, W.J.L. Genuit, P.J. Schoenmakers, Comprehensive two-dimensional liquid chromatography of heavy oil, *Journal of chromatography. A* 1564 (2018) 110–119.
- [105] C. Yang, G. Zhang, M. Serhan, G. Koivu, Z. Yang, B. Hollebone, P. Lambert, C.E. Brown, Characterization of naphthenic acids in crude oils and refined petroleum products, *Fuel* 255 (2019) 115849.
- [106] F. Adam, D. Thiébaud, F. Bertoncini, M. Courtiade, M.-C. Hennion, Supercritical fluid chromatography hyphenated with twin comprehensive two-dimensional gas chromatography for ultimate analysis of middle distillates, *Journal of chromatography. A* 1217 (2010) 1386–1394.
- [107] T. Dutriez, D. Thiébaud, M. Courtiade, H. Dulot, F. Bertoncini, M.-C. Hennion, Application to SFC-GC×GC to heavy petroleum fractions analysis, *Fuel* 104 (2013) 583–592.
- [108] L. Freije-Carreló, J. García-Bellido, F. Calderón-Celis, M. Moldovan, J.R. Encinar, GC-ICP-MS/MS Instrumental Setup for Total and Speciation Sulfur Analysis in Gasolines using Generic Standards, *Analytical chemistry* 91 (2019) 7019–7024.
- [109] A. Kondyli, W. Schrader, High-resolution GC/MS studies of a light crude oil fraction, *Journal of mass spectrometry JMS* 54 (2019) 47–54.
- [110] B. Yang, Z. Yu, P. Yao, F. Jiang, J. Chen, Characterization of Oil by Micro-Solid-Phase Extraction and Gas Chromatography–Mass Spectrometry, *Analytical Letters* 48 (2015) 2493–2506.
- [111] E. Kim, E. Cho, S. Moon, J.-I. Park, S. Kim, Characterization of Petroleum Heavy Oil Fractions Prepared by Preparatory Liquid Chromatography with Thin-Layer

- Chromatography, High-Resolution Mass Spectrometry, and Gas Chromatography with an Atomic Emission Detector, *Energy Fuels* 30 (2016) 2932–2940.
- [112] R. Chakravarthy, G.N. Naik, A. Savalia, J. Kedia, C. Saravanan, A.K. Das, U. Sreedharan, K.B. Gudasi, Simultaneous Determination of Boiling Range Distribution of Hydrocarbon, Sulfur, and Nitrogen in Petroleum Crude Oil by Gas Chromatography with Flame Ionization and Chemiluminescence Detections, *Energy Fuels* 31 (2017) 3101–3110.
- [113] Y. Han, Y. Zhang, C. Xu, C.S. Hsu, Molecular characterization of sulfur-containing compounds in petroleum, *Fuel* 221 (2018) 144–158.
- [114] É.V.A. Rodrigues, S.R.C. Silva, W. Romão, E.V.R. Castro, P.R. Filgueiras, Determination of crude oil physicochemical properties by high-temperature gas chromatography associated with multivariate calibration, *Fuel* 220 (2018) 389–395.
- [115] G. Toussaint, C. Lorentz, M. Vrinat, C. Geantet, Comprehensive 2D chromatography with mass spectrometry, *Anal. Methods* 3 (2011) 2743.
- [116] W. Genuit, H. Chaabani, Comprehensive two-dimensional gas chromatography-field ionization time-of-flight mass spectrometry (GCxGC-FI-TOFMS) for detailed hydrocarbon middle distillate analysis, *International Journal of Mass Spectrometry* 413 (2017) 27–32.
- [117] G.L. Alexandrino, J. Malmborg, F. Augusto, J.H. Christensen, Investigating weathering in light diesel oils using comprehensive two-dimensional gas chromatography-High resolution mass spectrometry and pixel-based analysis, *Journal of chromatography. A* 1591 (2019) 155–161.
- [118] L.C. Santos, G.F. da Cruz, B.M.F. Ávila, V.B. Pereira, D.A. Azevedo, Exploratory Analysis of Campos Basin Crude Oils via Geochemical Parameters by Comprehensive Two-Dimensional Gas Chromatography/Time-of-Flight Mass Spectrometry, *Energy Fuels* 32 (2018) 10321–10332.
- [119] F. Bertoncini, C. Vendevre, D. Thiébaud, Interest and Applications of Multidimensional Gas Chromatography for Trace Analysis in the Petroleum Industry, *Oil & Gas Science and Technology - Rev. IFP* 60 (2005) 937–950.
- [120] G. Semard, C. Gouin, J. Bourdet, N. Bord, V. Livadaris, Comparative study of differential flow and cryogenic modulators comprehensive two-dimensional gas chromatography systems for the detailed analysis of light cycle oil, *Journal of chromatography. A* 1218 (2011) 3146–3152.
- [121] E. Adlard, Fabrice Bertoncini, Marion Courtiade-Tholance and Didier Thiébaud, *Chromatographia* 77 (2013) 525–526.
- [122] M. Jennerwein, M. Eschner, T. Wilharm, T. Gröger, R. Zimmermann, Evaluation of reversed phase versus normal phase column combination for the quantitative analysis of common commercial available middle distillates using GC × GC-TOFMS and Visual Basic Script, *Fuel* 235 (2019) 336–338.

- [123]Edmond de Hoffmann and Vincent Stroobant, *Mass Spectrometry Principles and Applications*, 3rd ed., Wiley.
- [124]R.S. Borisov, L.N. Kulikova, V.G. Zaikin, *Mass Spectrometry in Petroleum Chemistry (Petroleomics) (Review)*, *Pet. Chem.* 59 (2019) 1055–1076.
- [125]*Interpretation of Mass Spectra*, 4th ed. (McLafferty, Fred W; Turecek, Frantisek), <https://pubs.acs.org/doi/abs/10.1021/ed071pA54.5> (accessed 1.08.2019).



## TABLE OF FIGURES – CHAPTER II

---

<b>Figure 1.</b> Example of GC-FID analysis of reaction products from hydroconversion of perhydrophenanthrene over Pt/H-USY zeolite catalyst. ....	48
<b>Figure 2.</b> A) GCxGC-FID analysis of perhydrophenanthrene stereoisomers obtained by hydrogenation of phenanthrene over Pt/Al <sub>2</sub> O <sub>3</sub> catalyst. B) GCxGC-FID analysis of the heaviest reaction products obtained at 68% perhydrophenanthrene conversion over Pt/H-USY zeolite catalyst. Integrated signals are noted with blobs. The region where the perhydrophenanthrene stereoisomers appear is indicated with dashed line. Pink blobs are assigned to perhydrophenanthrene stereoisomers, yellow blobs to C <sub>14</sub> alkyladamantanes, blue to C <sub>14</sub> skeletal isomers of perhydrophenanthrene, green blobs to C <sub>14</sub> ring opening products and white blobs to C <sub>12</sub> H <sub>22</sub> molecules. ....	50
<b>Figure 3.</b> GCxGC-FID analysis of reaction products in the range C <sub>3</sub> to C <sub>14</sub> of hydroconversion of perhydrophenanthrene obtained over Pt/H-USY zeolite catalyst at 68% conversion. ....	51
<b>Figure 4.</b> Molecule families and typical examples of reaction products of perhydrophenanthrene stereoisomers hydroisomerization and hydrocracking over Pt/H-USY zeolite catalyst. ....	52
<b>Figure 5.</b> Evolution of PHP conversion with contact time on Pt/H-USY catalyst extrudates with 1 wt.% and 3 wt.% zeolite in alumina binder. ....	53
<b>Figure 6.</b> Yield of skeletal isomerization, ring-opening and cracked products against perhydrophenanthrene conversion over Pt/H-USY zeolite catalyst. ....	54
<b>Figure 7.</b> Distribution of C <sub>14</sub> H <sub>24</sub> reaction products of PHP conversion over Pt/H-USY zeolite catalyst against PHP conversion. ....	55
<b>Figure 8.</b> Distribution of skeletal isomers of PHP (excluding substituted adamantanes) at different PHP conversions over Pt/H-USY zeolite catalyst. PHA: perhydroanthracene; PHP 149: methylperhydrophenalenes; PHP CC5: perhydrophenanthrene that underwent ring-contraction. ....	56
<b>Figure 9.</b> Distribution of alkyl adamantanes at different PHP conversions over Pt/H-USY zeolite catalyst. ....	57
<b>Figure 10.</b> Distribution of ring-opening products (ROP) at different PHP conversions over Pt/H-USY zeolite catalyst. ....	58
<b>Figure 11.</b> Yield of cracked products according to the number of carbon atoms in the molecules at different levels of PHP conversion over Pt/H-USY zeolite catalyst. ....	59
<b>Figure 12.</b> Distribution of naphthenes, isoalkanes and n-alkanes in the cracked products based on C-atom content against PHP conversion over bifunctional Pt/H-USY zeolite catalyst. ....	60
<b>Figure 13.</b> Yield of cracked naphthenes per 100 mol of cracked products as a function of perhydrophenanthrene conversion over bifunctional Pt/H-USY zeolite catalyst. ....	60

---



## TABLE OF FIGURES – CHAPTER II

---

<b>Figure 14.</b> A) Distribution of C <sub>6</sub> naphthenes and B) Distribution of C <sub>7</sub> naphthenes resulting from hydrocracking of PHP over Pt/H-USY zeolite catalyst. ....	61
<b>Figure 15.</b> Distribution of C <sub>8</sub> naphthenes from hydrocracking of PHP over Pt/H-USY zeolite catalyst at different conversions.....	62
<b>Figure 16.</b> Distribution of C <sub>9</sub> naphthenes from hydrocracking of PHP over Pt/H-USY zeolite catalyst at different conversions.....	63
<b>Figure 17.</b> Distribution of C <sub>10</sub> naphthenes resulting from hydrocracking of PHP over Pt/H-USY zeolite catalyst at different conversions. ....	64
<b>Figure 18.</b> General reaction pathway for hydrocracking of perhydrophenanthrene over bifunctional Pt/H-USY zeolite catalyst.....	65
<b>Figure 19.</b> Steps of formation of alkyladamantanes over aluminum bromide sludge catalyst according to Schneider et al [40]. A similar reaction pathway is observed in this work in hydrocracking of PHP over Pt/H-USY zeolite catalyst.....	66
<b>Figure 20.</b> Proposed hydrocracking pathway to C <sub>7</sub> naphthenes (A) and C <sub>6</sub> and C <sub>8</sub> naphthenes (B) of ring-opening products originating from hydroconversion of skeletal perhydrophenanthrene isomers (R2) over Pt/H-USY zeolite catalyst. ....	68
<b>Figure 21.</b> A) Suggested hydrocracking pathway to C <sub>6</sub> and C <sub>8</sub> naphthenes of ring-opening product originating from hydroconversion of skeletal perhydrophenanthrene isomers (R3) over Pt/H-USY zeolite catalyst. B) Suggested hydrocracking pathway to C <sub>7</sub> naphthenes.....	70
<b>Figure 22.</b> Suggested hydrocracking pathway to C <sub>10</sub> naphthenes and isobutane of ring-opening product originating from hydroconversion of skeletal perhydrophenanthrene isomers (R6) over Pt/H-USY zeolite catalyst.....	71
<b>Figure 23.</b> A) Suggested hydrocracking pathway to C <sub>9</sub> naphthenes and C <sub>5</sub> isoalkanes of ring-opening product originating from hydroconversion of skeletal perhydrophenanthrene isomers (R2) over Pt/H-USY zeolite catalyst. B) Suggested hydrocracking pathway to C <sub>9</sub> naphthenes and C <sub>5</sub> isoalkanes of ring-opening product originating from hydroconversion of skeletal perhydrophenanthrene isomers (R3) over Pt/H-USY zeolite catalyst. All pathways show subsequent steps to dehydrogenation over the metal sites.....	73
<b>Figure 24.</b> Suggested hydrocracking pathways leading to C <sub>9</sub> naphthenes and C <sub>5</sub> isoalkanes departing from ring-opening product originating from hydroconversion of skeletal perhydrophenanthrene isomers (R6) over Pt/H-USY zeolite catalyst.....	75
<b>Figure 25.</b> Yield of cracked products from hydrocracking of perhydrophenanthrene over Pt/H-USY zeolite catalyst expressed as mol/100 mol PHP cracked. Total yield of cracked products at the different conversions is indicated at the bottom of the graph.....	76

---

## CHAPTER II: HYDROCONVERSION OF PERHYDROPHENANTHRENE OVER BIFUNCTIONAL Pt/H-USY ZEOLITE CATALYST

---

This chapter was published as part of an issue at ChemCatChem and may be found with slight modifications at [10.1002/cctc.201902372](https://doi.org/10.1002/cctc.201902372)

### Highlights

- Two-dimensional gas chromatography coupled to flame ionization and mass detectors allowed the separation, identification and quantification of important families of reaction products of perhydrophenanthrene
- Isomerized perhydrophenanthrene molecules undergo ring opening reactions leading to cyclic, alicyclic and small amounts of aliphatic cracked hydrocarbon molecules
- Bridging rearrangements of perhydrophenanthrene isomers lead to formation of alkyl-substituted adamantanes which resist hydrocracking

### Abstract

In petroleum refining, middle distillates are produced via hydroisomerization/hydrocracking processes using bifunctional catalysts often containing ultrastable Y (USY) zeolite. Petroleum fractions serving as feedstock for hydrocracking processes contain a majority of (poly)cyclic hydrocarbon molecules. Few studies on reaction mechanisms of hydrocracking of such polycyclic compounds are available. In this study the tricyclic phenanthrene molecule was used as model compound. Phenanthrene was hydrogenated on a Pt/alumina pre-catalyst to perhydrophenanthrene, and subsequently hydrocracked over Pt/H-USY zeolite. The feed consisted of 3 wt.% phenanthrene dissolved in n-heptane. The reaction was performed at 280°C and 60 bar, with a molar H<sub>2</sub> to total hydrocarbon ratio of 7 mol/mol. The reaction products were analyzed using GCxGC-FID/MS. This detailed analysis enabled identification of the reaction scheme involving skeletal isomerization, ring opening and fragmentation. New mechanistic insight is gained on relative reactivities of bridged and non-bridged tricyclic naphthenes. Preferential hydrocracking routes were identified. The study provides insight in the products to be expected from polycyclic hydrocarbon isomerization and hydrocracking.

**Keywords:** phenanthrene, hydroisomerization, hydrocracking, adamantanes, polycyclic aromatic, polycyclic naphthenes, bifunctional catalysis, ultrastable Y zeolite

---

## 1. Introduction

Nowadays, the oil industry faces a discrepancy between products supplied by refineries and the worldwide demand of clean hydrocarbon fuels. Refiners are using heavier crude oil fractions which are more difficult to convert, and consequently, it becomes more challenging to provide commodities that are in accordance with the market demands and strict environmental legislation. Vacuum gas oil (VGO) is a typical heavy oil cut (C<sub>20</sub>-C<sub>60</sub>) that can be converted in refineries by hydrocracking and fluid catalytic cracking [1,2]. VGO is composed mainly of polycyclic molecules (aromatics and naphthenes), the rings of which must be cracked to obtain lighter fractions, especially gasoline (less than 10 carbon atoms) and middle distillates (C<sub>10</sub>-C<sub>22</sub>), serving as diesel and kerosene. Market trends suggest that in the period from 2020 to 2040, despite an expected shrinking demand for oil products, middle distillates will remain indispensable for the industry and transportation, especially in emerging countries and, more specifically, in non OECD Asia [3,4]. In the future, conversion of VGO by hydrocracking processes will be strongly directed towards the production of high quality diesel and kerosene.

Hydrocracking catalysts are bifunctional catalysts. The reaction mechanism of bifunctional catalysis in general terms is understood as a combination of hydrogenation-dehydrogenation reactions on a metal phase, and acid catalyzed reaction steps on acid sites, typically provided by zeolites [5–8]. The reaction mechanism of bifunctional conversion of aliphatic molecules and mono- and bicyclic naphthenes is well documented [9–12]. Long alkanes undergo consecutive branching isomerization reactions to monobranched, dibranched and tribranched skeletal isomers which become more and more reactive towards cracking [13–16]. Monocyclic naphthenes undergo ring contraction and expansion, and in this way interchange carbon atoms between ring and side chain. Exocyclic cracking predominates over endocyclic cracking [17]. The grouping of short side chains by consecutive ring expansion and contraction reactions leads to isobutyl and longer branched substituents that are cracked from the ring. This reaction is known in literature as “the paring reaction” [18–20]. Bicyclic molecules like decahydronaphthalene first undergo ring opening and enter the conversion pathways of monocyclic naphthenes.

VGO is composed of hydrocarbons with many cycles [21]. Mechanistic insight in hydrocracking pathways of such molecules is difficult to obtain because of the multitude of reaction products. For mastering the conversion of VGO to middle distillates, there is a need for scientific insight in the mechanisms of hydrocracking of typical VGO molecules because extrapolation of the behavior of small molecules to larger ones of interest to VGO is not possible. The selectivity of reaction among individual cycles of a polycyclic molecule is just one example. Experimental investigations of the reaction pathways of model VGO molecules with carbon numbers higher than 20 in laboratory reactors are practically very challenging because of the solid nature of the feed at ambient temperature. In view of these challenges and needs, we opted for a stepwise approach and selected a tricyclic molecule to expand the collection of documented molecules in hydrocracking beyond naphthenes containing two rings or less [19,22–24].

The objective of this study was to explore the mechanism governing hydrocracking of perhydrophenanthrene ( $C_{14}H_{24}$ , PHP), the fully hydrogenated product from phenanthrene ( $C_{14}H_{10}$ ). The catalyst was a conventional platinum loaded USY zeolite extrudate. Key questions to be answered were about the nature of the skeletal isomerization pathways and the formation of bridged and skeletal isomers. In previous work on perhydrophenanthrene hydrocracking, substituted adamantanes have been observed among the reaction products[25]. These compounds have high cetane index and superior diesel quality[26]. Another particularity is the ring opening selectivity, and especially of the central ring compared to the extremes, and the competition between consecutive ring openings and paring reactions. Finally, the nature of the cracked products in terms of ring size and alkyl substituents is essential for estimating the octane and cetane number of gasoline and diesel fractions to be expected in industrial VGO hydrocracking processes.

## 2. Materials and methods

### 2.1. Preparation and characterization of catalysts

Commercial ultrastable Y zeolite powder (CBV 720 with a Brønsted acid site concentration of 202  $\mu\text{mol/g}$ ) from Zeolyst was shaped in extrudate using Pural SB-3 alumina binder provided by Sasol, according to a procedure described elsewhere [27]. An aqueous solution in a proportion of 62.5 g water per 100 g of dry powder, containing 6.50 g nitric acid per 100 g dry boehmite, was mixed with USY zeolite and boehmite powder, and stirred with a mixer for 30 minutes, at a frequency of 50 revolutions per minute. A solution composed of 64.5 g water per 100 g of dry powder, containing 2.5 g ammonium per 100 g of dry boehmite, was then added to the mixture, which was kneaded for 15 minutes, keeping the same frequency of stirring. This paste was then extruded into a trilobe shape extrudate with a diameter of 1.6 mm and dried overnight at 80°C. Two supports containing different contents of USY zeolite, 1 and 3 wt.%, respectively, were shaped following this procedure. A trilobe extrudate sample containing only boehmite was also prepared following the same method.

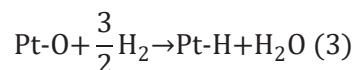
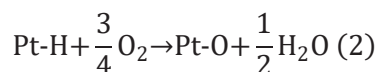
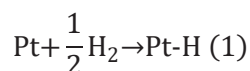
The extrudes were calcined under air flow of 1.5NL/h/g<sub>support</sub> at 600°C for 2 h. The heating rate was 5°C/min. The length of the broken extrudates was selected between 3 and 6 mm.

Selective impregnation of platinum on the alumina binder was performed via ion exchange. In this procedure, the dry support was humidified before the addition of the competitor (chloride ions). The wetted support was mixed with an aqueous solution (4g water per 1g dry support) containing 1.3 wt.% of hydrochloric acid. The suspension was stirred for 1 h and then decanted. After decantation, the extrudates were mixed with another solution (4 g water per 1g of dry support) containing dissolved chloroplatinic acid hydrate ( $\text{H}_2\text{PtCl}_6$ , Sigma-Aldrich). The amount of precursor was calculated assuming quantitative ionic exchange and based on the targeted content of Pt in the final catalyst. The suspension was then stirred for at least 24 h, decanted and dried overnight at 120°C.

After drying, calcination was carried out in air flow of 1NL/h/g<sub>dry catalyst</sub>, heating rate of 5°C/min and temperature range starting from room temperature up to 520°C, in steps with 1 h at 150°C, 250°C and 350°C, and 2 h at 520°C. The calcination in steps minimizes sintering of Pt particles [28].

Si and Al contents of the support and Pt content of the final catalyst were determined with X-ray fluorescence (ThermoFischer Scientific Advant-X instrument). To this purpose, the samples were crushed and sieved into granulometric particles smaller than 100  $\mu\text{m}$ .

The dispersion of the Pt metal on the extrudates was determined via  $\text{H}_2\text{-O}_2$  chemisorption (Gira Xisorb equipment). The samples were calcined following the procedure described above, cooled down to room temperature and purged with helium. Then, a first reduction under hydrogen flow was done at 500°C for 2h. The temperature was decreased to 20°C and the samples were purged with Helium flow. Pulses of oxygen gas were used to titrate the platinum hydride contained in the sample. Another purge under Helium flow was applied, and a second reduction with hydrogen at room temperature. After reduction, the catalyst was titrated again with pulses of oxygen gas. The procedure was repeated until the result was stable. The average volume of oxygen corresponding to both titrations is then used for estimating the platinum dispersion based on Equations 1-3 [29].



Silicon, aluminum and platinum content of the catalysts obtained with X-ray fluorescence, and platinum dispersion values acquired through  $\text{H}_2\text{-O}_2$  titration, are summarized in Table 1. Platinum particle size was estimated from the platinum dispersion by considering a spherical shape of the particles. The concentration of Brønsted acid sites (BAS) was estimated from the content of USY zeolite in the extrudate, by taking into account the concentration of BAS in the parent USY zeolite, derived from the pyridine adsorption capacity and the speciation determined using FTIR as described elsewhere [30]. Textural properties of the commercial USY zeolite are available in literature [27,31,32].

**CHAPTER II: HYDROCONVERSION OF PERHYDROPHENANTHRENE OVER  
BIFUNCTIONAL Pt/H-USY ZEOLITE CATALYST**

Table 1. Properties of Pt-loaded zeolite USY extrudates determined by X-ray fluorescence, H<sub>2</sub>-O<sub>2</sub> chemisorption and pyridine adsorption monitored with FTIR.

USY content in binder (wt. %)	Pt loading (wt. %)	Pt dispersion (%)	Pt particle size (nm)	n <sub>Pt</sub> (μmol/g)	BAS (μmol/g) <sup>a</sup>
1	0.7	45	2.5	9	2
3	0.7	89	1.3	18.8	6

<sup>a</sup>According to BAS concentration of the USY zeolite, viz. 202 μmol/g, and the zeolite content of the extrudate assuming that the zeolite it is not affected by the extrusion.

## 2.2. Catalytic tests

The reaction was carried out in a fixed-bed downflow reactor tube with an internal diameter of 19 mm. The reactor was loaded with two layers of catalysts of 2 g each, with Pt/Alumina hydrogenation catalyst mounted upfront of bifunctional Pt/H-USY zeolite catalyst. The hydrogenation pre-catalyst ensured hydrogenation of phenanthrene before reaching the hydrocracking catalyst. The catalysts were reduced *in situ* at 450°C for 2 h under a hydrogen flow of 1 NL/h/g<sub>catalyst</sub>. The heating rate to 450°C was 5°C/min. The feedstock was composed of 3 wt.% of phenanthrene (Sigma-Aldrich) diluted into 97 wt.% of n-heptane (AnalaR Normapur). With this composition, condensation of feed and reaction products in the reactor unit was avoided. A molar ratio of hydrogen to total hydrocarbons of 7 mol/mol was used. The reaction temperature was 280°C and total pressure 60 bar. In an experiment with Pt/Alumina catalyst only it was verified that all phenanthrene was hydrogenated before contacting the Pt/H-USY zeolite catalyst downstream. The weight hourly space velocity was varied from 10 to 30 g<sub>feed</sub>/g<sub>zeolite</sub>/h by varying the hydrocarbon flow entering the reactor. Catalyst deactivation was not observed over the entire range of operating conditions tested.

The reaction products were analyzed on-line as well as off-line. On-line analysis was performed with a GC-FID instrument (Varian) equipped with HP-PONA column provided by Agilent. In this on-line analysis, only the molecules up to C<sub>6</sub> could be identified and quantified (Figure 1). For heavier molecules eluting from the column at retention times longer than 50 minutes, the chromatographic peaks were too much overlapping in a broad envelope till a retention time of 75 minute because of the presence of a complex mixture of aliphatic and alicyclic hydrocarbons.

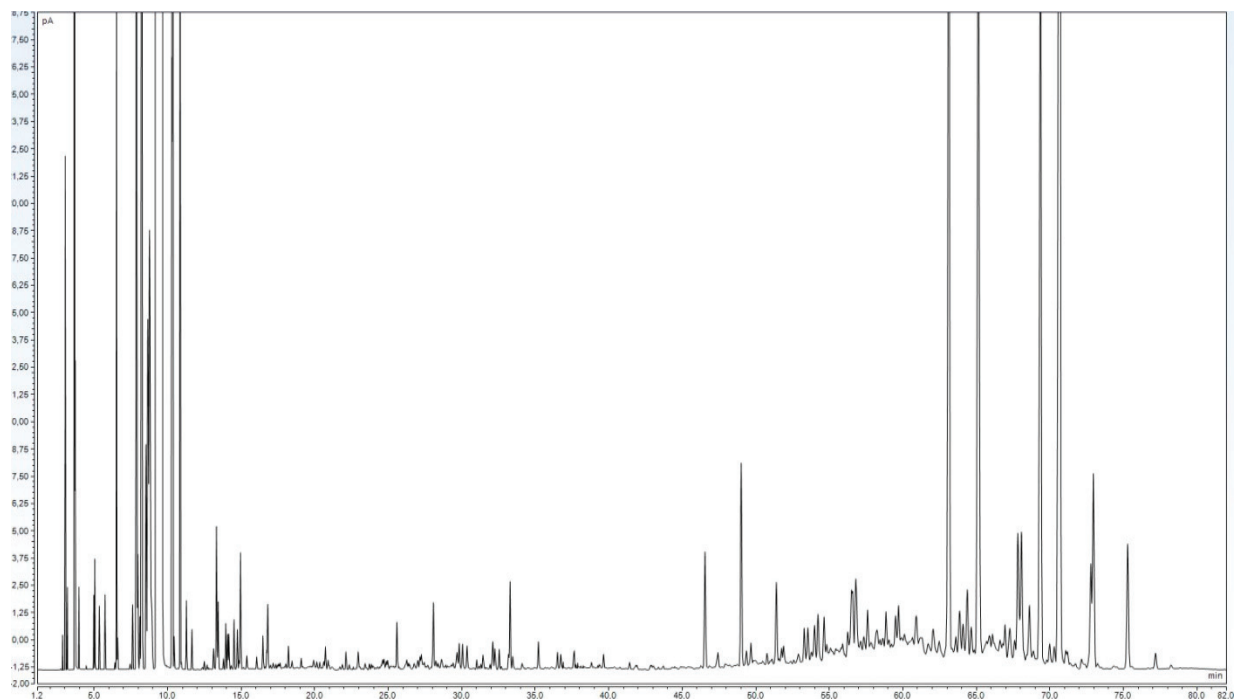


Figure 1. Example of GC-FID analysis of reaction products from hydroconversion of perhydrophenanthrene over Pt/H-USY zeolite catalyst.

For the analysis of  $C_7$  and heavier products comprehensive two-dimensional gas chromatography was used. A gas chromatograph (Agilent 6890) equipped with 50 m HP-PONA column (Agilent) with internal diameter of 0.2 mm and film thickness of 0.5  $\mu\text{m}$  enabling separation by boiling point was coupled either to a time-of-flight mass spectrometer (LECO) or to a FID. Separation in the second dimension was done with a 3 m BPX-50 column (SGE), with 0.1 mm internal diameter, and film thickness of 0.1  $\mu\text{m}$ , separating the compounds by polarity. A Zoex thermal modulator was used for controlling the flow of compounds desorbing from the first column and entering the second one. The compounds were thermally desorbed from the first column with hot air, while a nitrogen jet, cooled with a cold unit, trapped the molecules before they could move towards the analysis in the second dimension. The temperature of the hot jet was kept 15°C above the temperature of the oven with the chromatographic column. The modulation period was kept constant at 6 s during the analysis.

Both columns had the same temperature programming, starting from 40°C with heating at 2°C/min to 120°C, then from 120°C to 205°C at 1°C/min and finally from 205°C to 280°C at



10°C/min. A volume of 1 $\mu$ L of reaction effluent was injected with a split ratio of 100. High-purity helium was used as carrier gas at a constant flow rate of 10 mL/min. For MS analysis, the temperature of the ion source and the ionization energy were 200°C and 70 eV, respectively. Ionization was performed in electron ionization mode. Analysis of reaction products was carried out using GC Image 2.6 software (Zoex), and with NIST MS database (version 08) after converting the data obtained. Mass spectra were compared to those available in the NIST database and in literature [33–37].

Molar flow of a carbon number fraction ( $N_i$ ), Conversion ( $X$ ), yield ( $Y$ ) and product distributions of specific fractions ( $D$ ) were derived from the chromatographic analysis of the reaction products using Equations 4 – 8.

$$N_i = \frac{(wt./total\ wt.)_i * F_m * c_i}{(100 * M_i)} \quad (4)$$

$F_m$  is the mass flow of the feedstock and  $(wt./total\ wt.)_i$ ,  $c_i$  and  $M_i$  the mass fraction, the number of carbons and the molar mass of the component  $i$  at the outlet, respectively.

$$X = 1 - \frac{N_{PHP,out}}{\sum_{i=1}^{i=14} N_{i,out}} \quad (5)$$

$$Y_i = \frac{N_i}{\sum_{i=1}^{i=14} N_{i,out}} \quad (6)$$

$$Y_{C_i}(mol/100\ mol\ cracked) = \left( \frac{1}{i} \sum_{k=1}^{n_k} N_{i,k} / \frac{1}{14} \sum_{i=1}^{13} \sum_{k=1}^{n_k} N_{i,k} \right) \quad (7)$$

*Distribution of component  $i$  within the family  $J$ :*

$$D_{i,J} = \frac{N_{i \in J}}{\sum N_{i \in J}} \quad (8)$$

### 3. Results

#### 3.1. Identification and quantification of reaction products with GCxGC-FID/MS

The 2-dimensional analysis of the hydrogenation products of phenanthrene, obtained on the Pt/Al<sub>2</sub>O<sub>3</sub> catalyst is shown in Figure 2A. Six compounds were present, which are the stereoisomers of perhydrophenanthrene [38]. These six conformational isomers are collectively considered as the feedstock undergoing hydroisomerization and hydrocracking over the bifunctional Pt/H-USY catalyst loaded downstream of the Pt/Al<sub>2</sub>O<sub>3</sub> hydrogenation catalyst. They are collectively referred to as PHP for convenience.

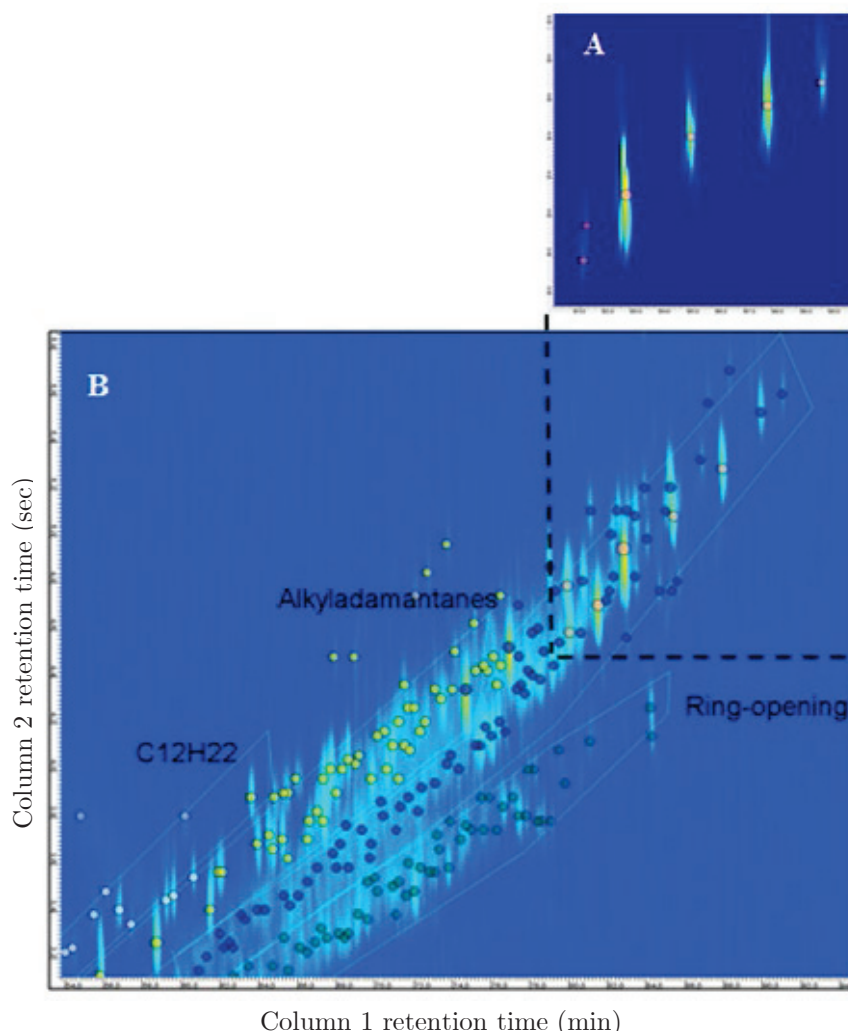


Figure 2. A) GCxGC-FID analysis of perhydrophenanthrene stereoisomers obtained by hydrogenation of phenanthrene over Pt/Al<sub>2</sub>O<sub>3</sub> catalyst. B) GCxGC-FID analysis of the heaviest reaction products obtained at

68% perhydrophenanthrene conversion over Pt/H-USY zeolite catalyst. Integrated signals are noted with blobs. The region where the perhydrophenanthrene stereoisomers appear is indicated with dashed line. Pink blobs are assigned to perhydrophenanthrene stereoisomers, yellow blobs to C<sub>14</sub> alkyladamantanes, blue to C<sub>14</sub> skeletal isomers of perhydrophenanthrene, green blobs to C<sub>14</sub> ring opening products and white blobs to C<sub>12</sub>H<sub>22</sub> molecules.

The full GCxGC-FID chromatogram of the reaction products from hydroisomerization/hydrocracking of PHP at 68% conversion is shown in Figure 3. It illustrates that the reactor effluent is a very complex mixture with over 300 different compounds.

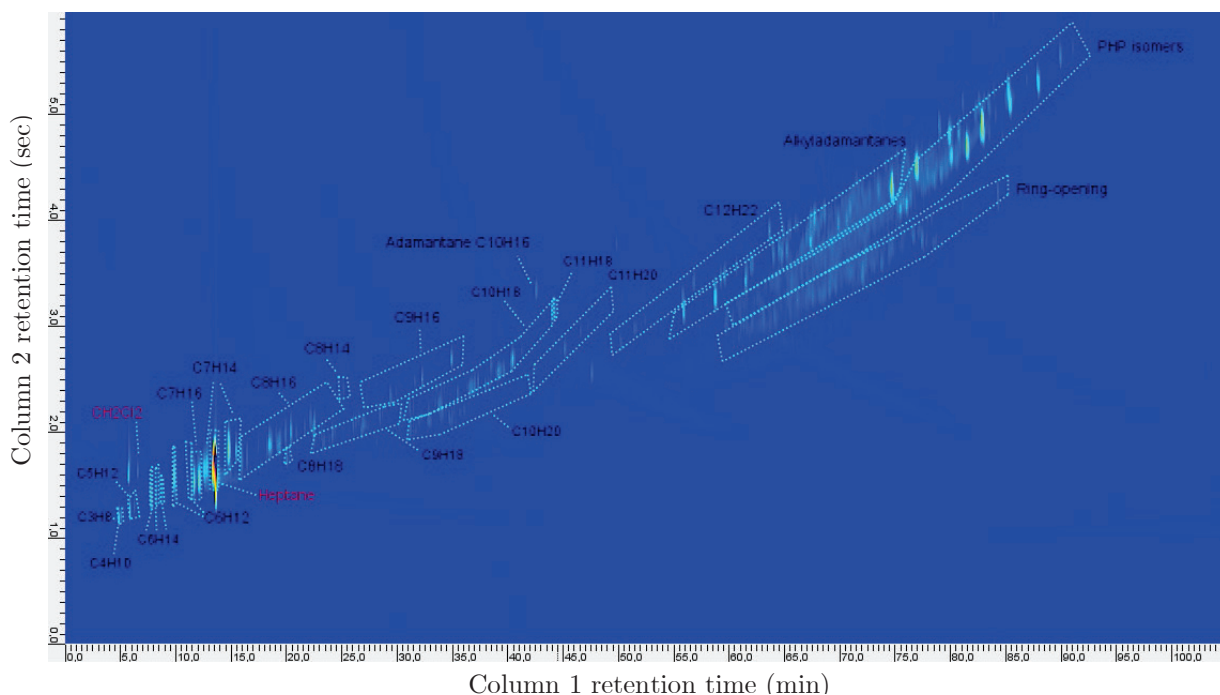


Figure 3. GCxGC-FID analysis of reaction products in the range C<sub>3</sub> to C<sub>14</sub> of hydroconversion of perhydrophenanthrene obtained over Pt/H-USY zeolite catalyst at 68% conversion.

The reaction products were lumped into families, according to their carbon number and structural formula (Figure 4). A first family obtained by skeletal isomerization of PHP is referred to as perhydrophenanthrene isomers, i.e. tricyclic compounds with chemical formula C<sub>14</sub>H<sub>24</sub>. This family is divided into two sub-families: alkyladamantanes and other skeletal isomers of PHP with different arrangements of the rings comprising e.g. perhydroanthracene, methylperhydrophenalenes and ring-contraction products of PHP. Alkyladamantanes are

particular in that all of their cycles are 6-rings having armchair conformation. Their linking by bridges makes them the thermodynamically the most stable tricyclic structures [39,40].

An additional molecule family with 14 carbon atoms are molecules containing two cycles having chemical formula  $C_{14}H_{26}$  called ring-opening products (ROP). These are alkyl-substituted decalin isomers obtained by opening of an external ring and alkyl-connected 2-cycle naphthenes obtained by opening of the central ring. Molecules with opening of two out of the three cycles of perhydrophenanthrene were not observed in this study. Figure 2B illustrates the power of two-dimensional GC analysis for separating ring-opening products and PHP skeletal isomers from PHP stereoisomers. All molecules with less than 14 C-atoms are referred to as cracking products. They essentially comprise mono- or bicyclic structures and, in small amounts, iso- and n-alkanes.

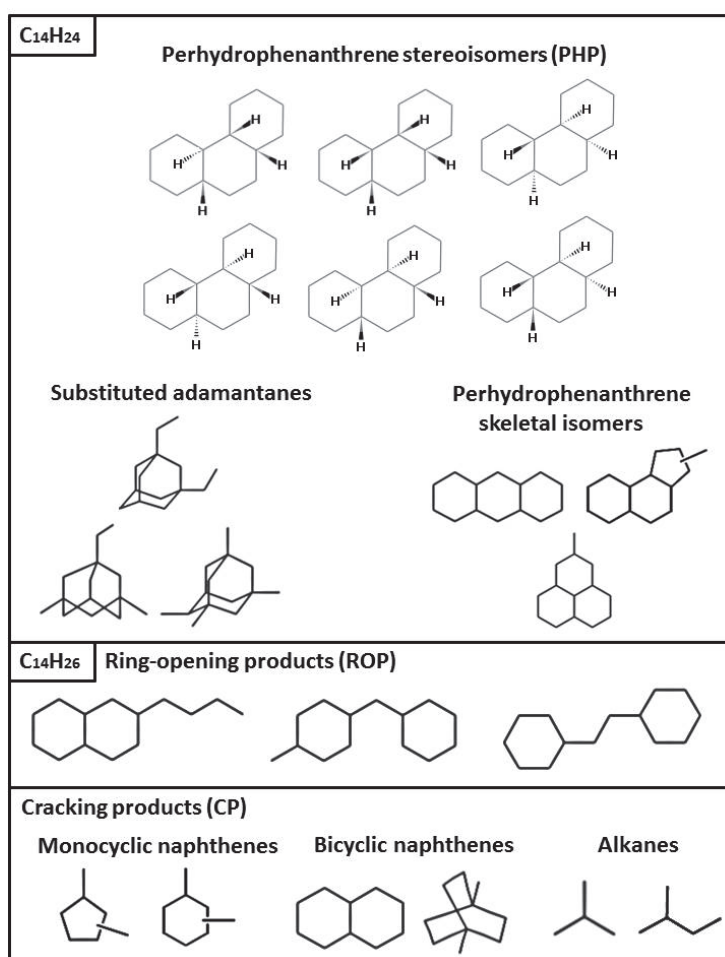


Figure 4. Molecule families and typical examples of reaction products of perhydrophenanthrene stereoisomers hydroisomerization and hydrocracking over Pt/H-USY zeolite catalyst.

### 3.2. Hydroconversion of perhydrophenanthrene

The degree of PHP conversion on the Pt/H-USY zeolite catalyst was varied by changing the contact time at a reaction temperature of 280°C. For the two types of catalyst extrudates with 1% and 3% USY zeolite, the PHP conversion is plotted against contact time in Figure 5. The catalyst containing 3% zeolite was more active than the one containing only 1% zeolite, as expected. The PHP conversion at a given contact time was roughly proportional to the zeolite loading. The data obtained over the two catalysts all together cover the conversion range from 36 % to 94%.

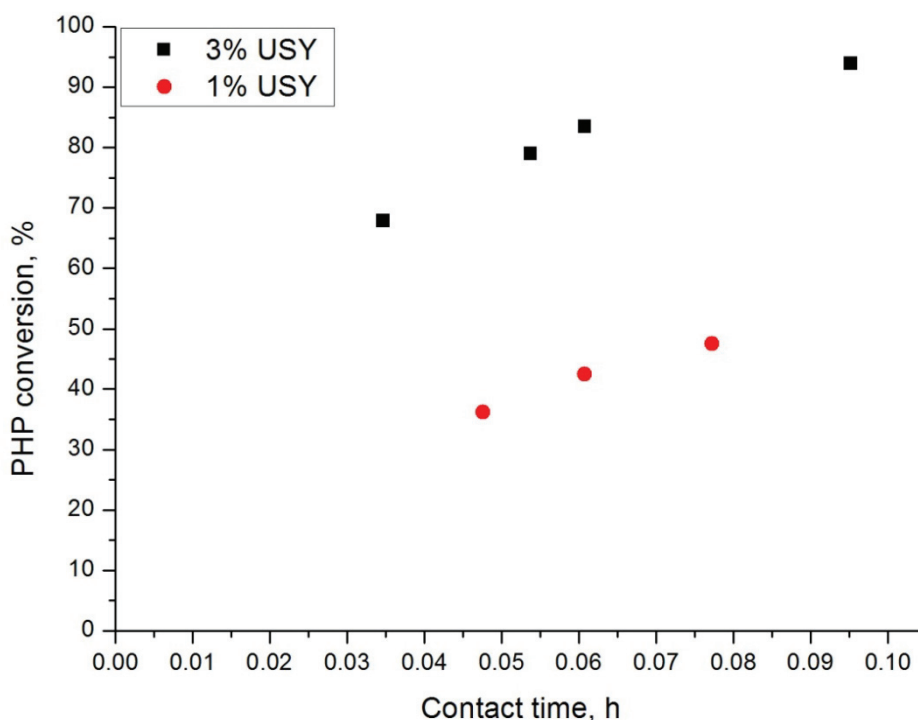


Figure 5. Evolution of PHP conversion with contact time on Pt/H-USY catalyst extrudates with 1 wt.% and 3 wt.% zeolite in alumina binder.

The yield of  $C_{14}H_{24}$  molecules (skeletal isomers of PHP and alkyladamantanes),  $C_{14}H_{26}$  molecules with one ring opening and, consequently, having two more H atoms and cracking products is presented against PHP conversion in Figure 6. PHP isomerization was the predominant reaction at low conversion. The isomerization yield reached a maximum of ca. 43% at 68% conversion.  $C_{14}H_{26}$  ring-opening products are a minority product. Ring opening products reached a maximum yield of about 8% at 80% conversion. Cracked products became

dominant above 85% conversion. From the evolution of the yields it is concluded that skeletal isomerization is the primary reaction followed by ring-opening and cracking.

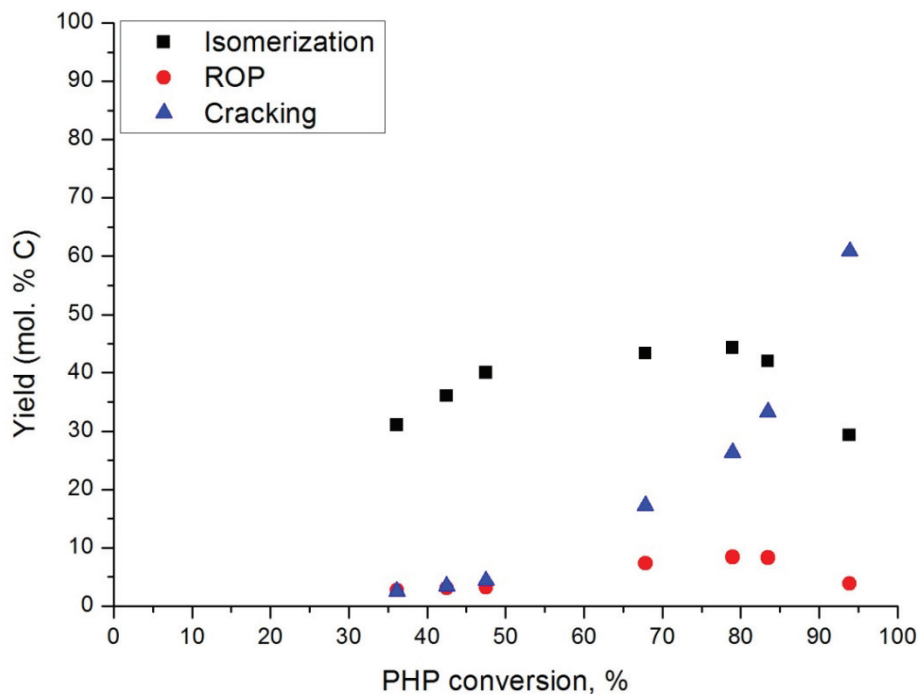


Figure 6. Yield of skeletal isomerization, ring-opening and cracked products against perhydrophenanthrene conversion over Pt/H-USY zeolite catalyst.

The evolution of the formation of alkyladamantanes and other tricyclic structures within the family of PHP skeletal isomers is presented in Figure 7. The evolution of this distribution with conversion reveals that alkyladamantanes are secondary products obtained from skeletal PHP isomers.

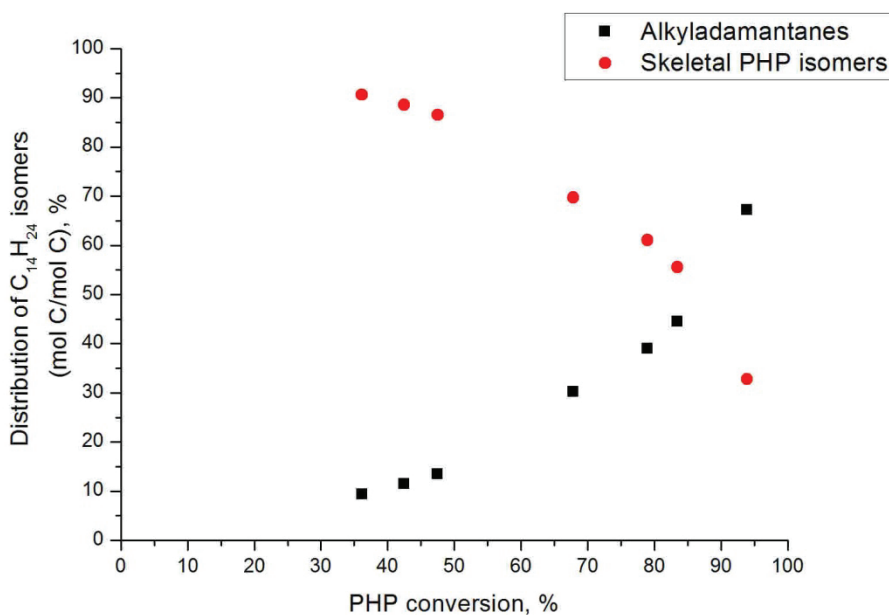


Figure 7. Distribution of  $C_{14}H_{24}$  reaction products of PHP conversion over Pt/H-USY zeolite catalyst against PHP conversion.

The detailed distribution of PHP skeletal isomers (excluding adamantanes) at different levels of PHP conversion is shown in Figure 8. The most abundant isomers were structures **I1** and **I4**, i.e. perhydroanthracene stereoisomers denoted PHA, formed by ring-shift of perhydrophenanthrene [38] and ring-contraction isomers of PHP with one 5-ring and two 6-rings. For the perhydroanthracene stereoisomers there is a discrepancy between their content at low and high PHP conversion. This could be due to an analytical difficulty at low PHP isomerization yield when these molecules are formed in small amounts, which was the case for the data points at 36, 42 and 48% PHP conversion in the experiment using the catalyst with 1% USY zeolite. Ring-contraction isomers (**I4**) formed after isomerization of an external cycle of perhydrophenanthrene were observed at all conversion levels, and their distribution did not change substantially with PHP conversion. Structures resulting from other ring-shift rearrangements of perhydrophenanthrene cycles were also observed, in particular methylperhydrophenalenes (**I3**). Methylperhydrophenalenes were quite abundant at low PHP conversion, but their proportion decreased with conversion. These compounds could be precursors for the formation of alkyladamantanes [40]. Small amounts of more exotic spiro-type compounds (**I2**), where rings are linked together through a common carbon atom,

generating a twisted naphthene, were also formed in low amounts. At low conversion, the unknown fraction accounted for nearly 20% of the distribution, while at higher conversion almost all compounds could be identified.

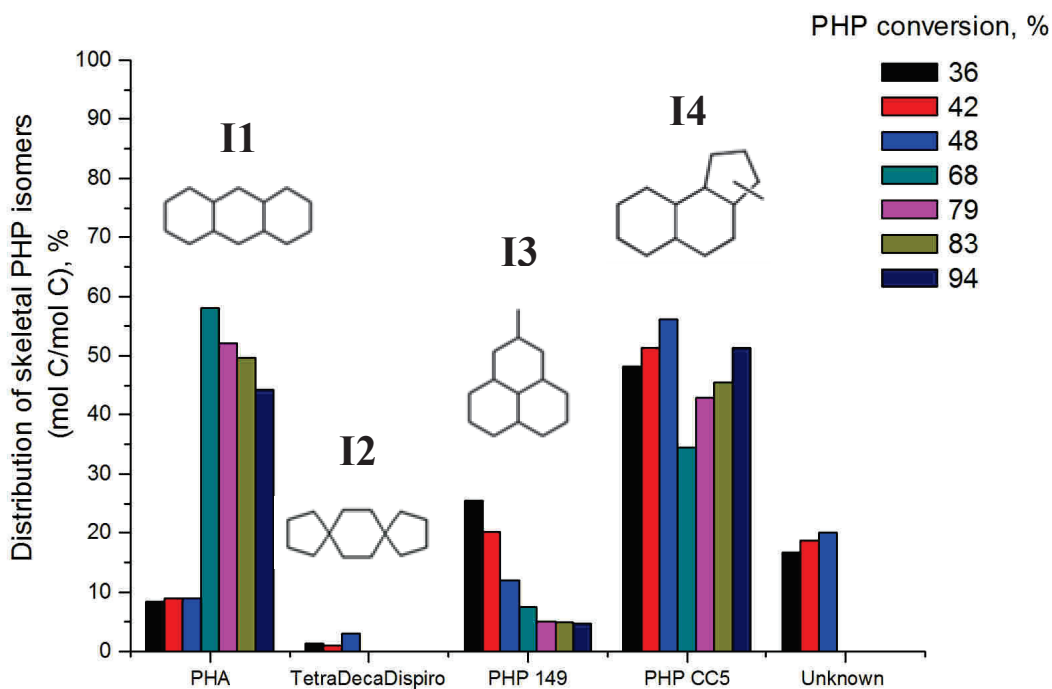


Figure 8. Distribution of skeletal isomers of PHP (excluding substituted adamantanes) at different PHP conversions over Pt/H-USY zeolite catalyst. PHA: perhydroanthracene; PHP 149: methylperhydrophenalenes; PHP CC5: perhydrophenanthrene that underwent ring-contraction.

The distribution of compounds within the alkyladamantanes subfamily is depicted in Figure 9. This product fraction was rich in structures presenting different types of alkyl substitution. The most abundant isomers were tetramethyladamantanes (**A1**) and dimethyl-ethyladamantanes (**A3**). Tetramethyladamantane in comparison to the other substituted adamantanes is the thermodynamically most stable isomer because of its higher number of quaternary carbon atoms [39]. Monoalkylsubstituted structures represented by butyladamantanes (**A5**) were only present in small amounts, and compounds like methyl-propyladamantanes (**A4**) were observed only at low conversion. The unknown fraction accounted for 10-15% of the distribution in the investigated PHP conversion range.



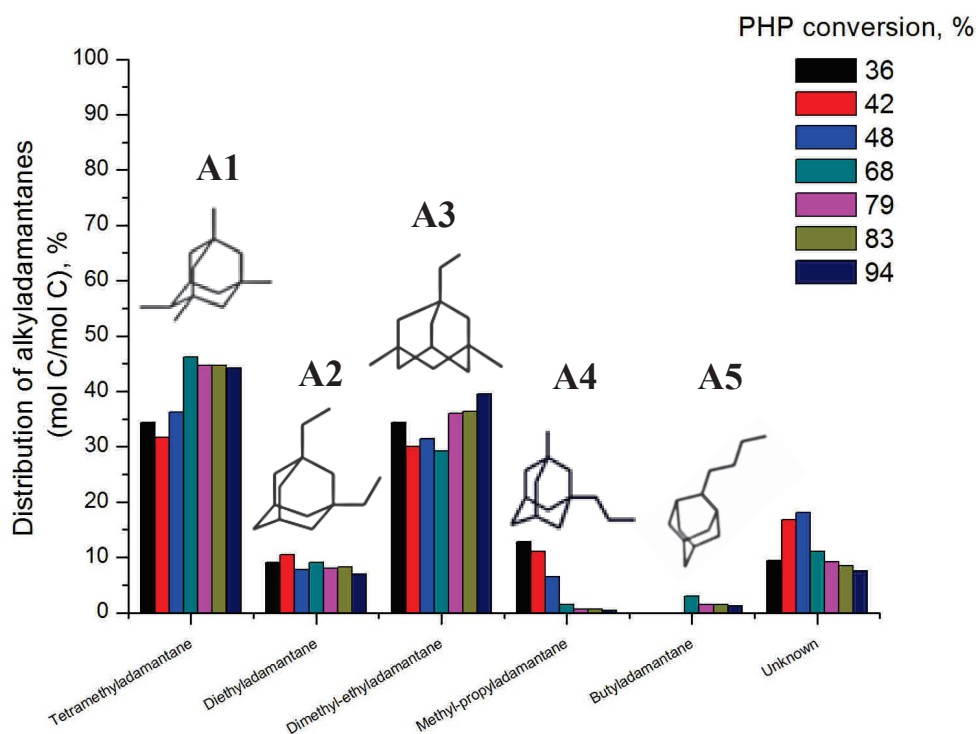


Figure 9. Distribution of alkyl adamantanes at different PHP conversions over Pt/H-USY zeolite catalyst.

The formation of cracked products from PHP needs the breaking of at least two carbon-carbon bonds. Breaking of the first carbon-carbon bond leads to ring opening and formation of alkyl chains on which a second carbon-carbon bond breaking can cause spitting of the C<sub>14</sub> molecule into two fragments. PHP stereo and skeletal isomers are more reactive than alkyladamantanes, which accumulate in the C<sub>14</sub> fraction at increasing PHP conversion (Figure 7). PHP skeletal isomers undergo bridging to form alkyladamantanes and ring-opening needed for cracking.

Ring-opening products comprise a broad spectrum of compounds in terms of substituents and degree of branching (Figure 10). The dominating structures at high PHP conversion were molecules with two cyclohexane rings connected by an alkyl-bridge (**R2** and **R3**). **R2**, **R3** and **R5** structures were presumably formed by ring-opening of the central ring of PHP isomers. Products formed by ring opening of an external ring were also observed, i.e. structures **R6** (butyl-decalins) and **R7**. Molecules resulting from further rearrangements of PHP cycles resulting in multiple alkyl substituted ROP, such as **R1** and **R4**, were also

present. The unknown fraction accounted for 10% of the distribution at low conversion. Almost all ROP compounds could be identified at high conversion levels.

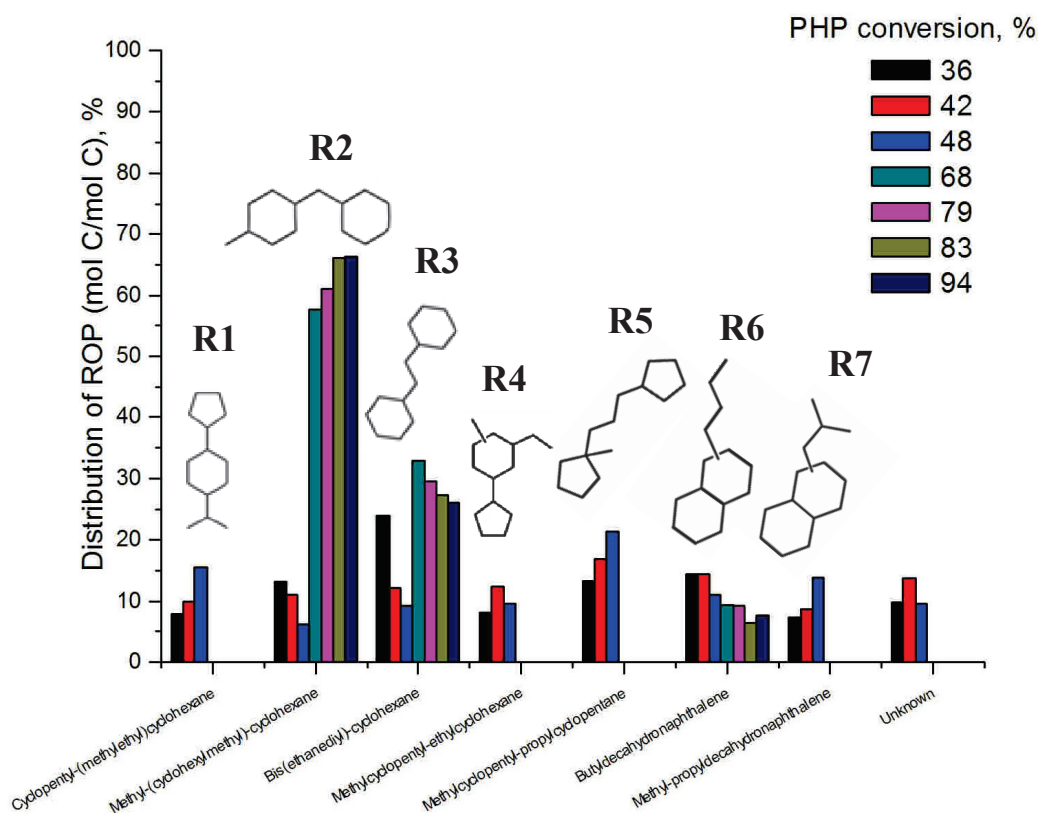


Figure 10. Distribution of ring-opening products (ROP) at different PHP conversions over Pt/H-USY zeolite catalyst.

Around 80% PHP conversion, cracked products became predominant. The yield of cracked products grouped per carbon number and expressed as the percentage of carbon atoms contained in that fraction is presented in Figure 11. Cracked products had carbon numbers in the range from 3 to 12. Methane and ethane ( $C_1$  and  $C_2$ ) and  $C_{13}$  products were not formed. Such products are difficult to obtain by bifunctional catalysis and their presence is generally interpreted as being due to hydrogenolysis on metal sites [41]. Significant amounts of  $C_{12}$  were formed especially at low conversion. The formation of  $C_{12}$  products having 2 C-atoms less than the feed molecules by cracking of feed isomers would involve elimination of 2  $C_1$  groups or a  $C_2$  group, which is difficult to rationalize with  $\beta$ -scission of alkylcarbenium ions. The yield of  $C_{12}$  reaction products did not change with increasing PHP conversion while other fragments in the  $C_4$ - $C_{10}$  range became more abundant (Figure 11). Propane ( $C_3$ ) was

almost not formed. The cracked product yield distribution according to carbon number showed maxima, *i.e.* at C<sub>4</sub>, C<sub>6</sub>, C<sub>8</sub> and C<sub>10</sub>.

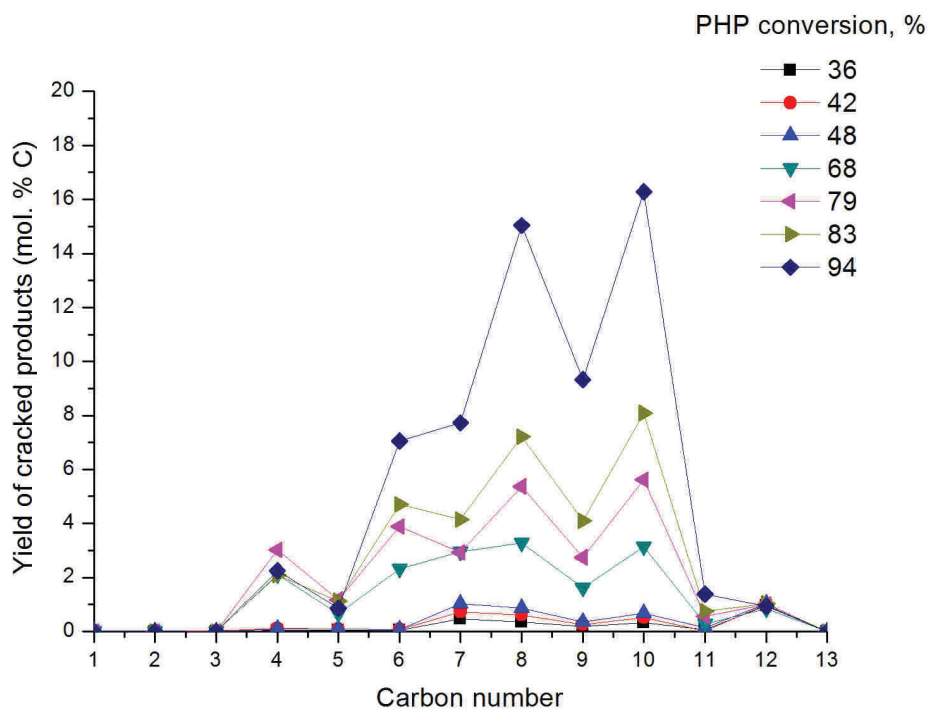


Figure 11. Yield of cracked products according to the number of carbon atoms in the molecules at different levels of PHP conversion over Pt/H-USY zeolite catalyst.

The proportion of naphthenes, isoalkanes and n-alkanes within the cracked products is revealed in Figure 12. The large majority of the cracked products were naphthenes. Only small amounts of isoalkanes, mainly isobutane, and very little n-alkanes were formed. C<sub>7</sub> isoalkanes were not taken into account, since they were considered as impurities of the solvent.

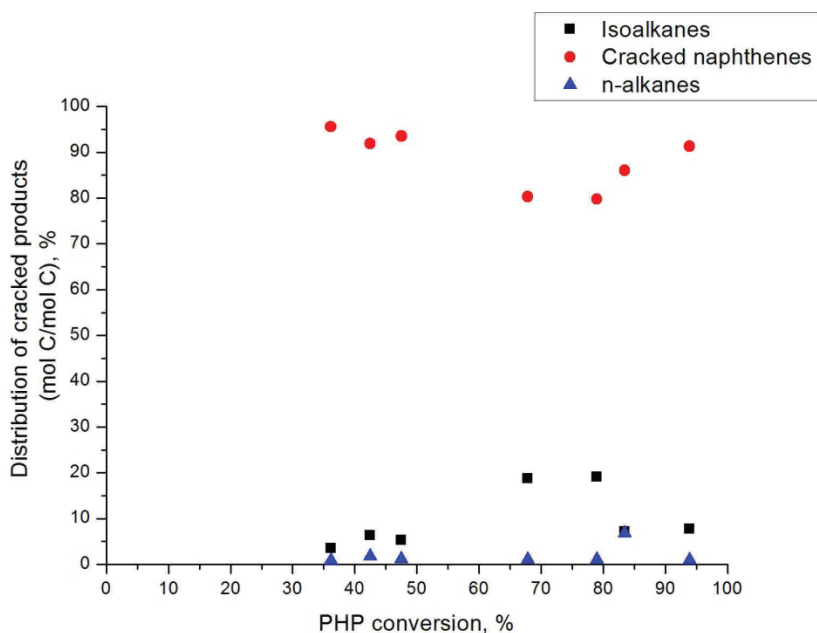


Figure 12. Distribution of naphthenes, isoalkanes and n-alkanes in the cracked products based on C-atom content against PHP conversion over bifunctional Pt/H-USY zeolite catalyst.

The yield of cracked naphthenes divided according to carbon number at increasing PHP conversion is shown in Figure 13. A preferential formation of C<sub>10</sub> and C<sub>8</sub> naphthene products was observed, followed by C<sub>9</sub>, C<sub>7</sub>, and C<sub>6</sub>. C<sub>11</sub> and C<sub>12</sub> naphthenes were minority reaction products.

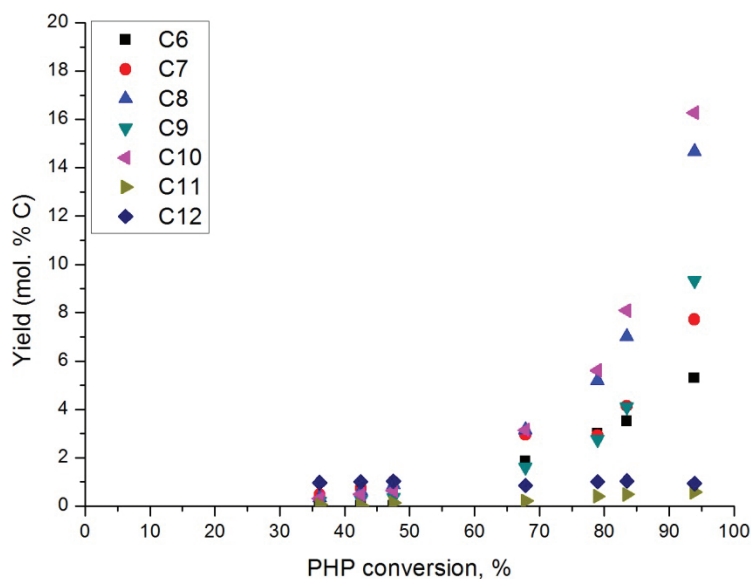


Figure 13. Yield of cracked naphthenes per 100 mol of cracked products as a function of perhydrophenanthrene conversion over bifunctional Pt/H-USY zeolite catalyst.

C<sub>6</sub> naphthenes were mainly methylcyclopentane (Figure 14A). Their distribution did not significantly change with PHP conversion. The distribution of C<sub>7</sub> naphthenes slightly varied with conversion (Figure 14B). Dimethylcyclopentane was formed primarily and isomerized to methylcyclohexane. The content of ethylcyclopentane among the C<sub>7</sub> naphthenes was almost constant.

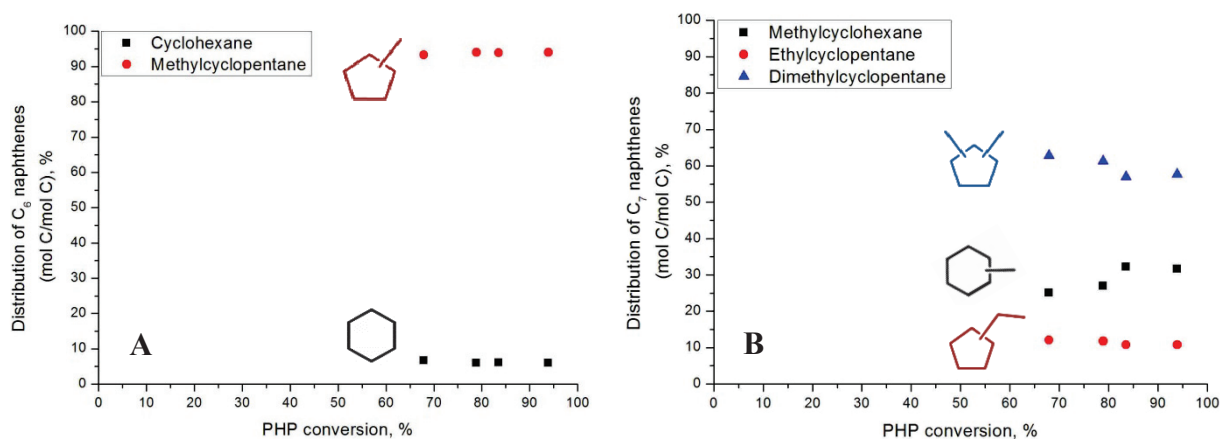


Figure 14. A) Distribution of C<sub>6</sub> naphthenes and B) Distribution of C<sub>7</sub> naphthenes resulting from hydrocracking of PHP over Pt/H-USY zeolite catalyst. .

The distribution of C<sub>8</sub> naphthenes did not significantly change with PHP conversion over Pt/H-USY zeolite catalyst (Figure 15). Major products were dimethylcyclohexane positional isomers (**C8-1**). The content of ethylcyclohexane (**C8-2**), trimethyl- and methyl-ethylcyclopentane (**C8-4** and **C8-5**, respectively) was about equal. Minor C<sub>8</sub> naphthenic products were propylcyclopentane (**C8-3**) in addition to a small and stable content of octahydropentalene (**C8-6**).

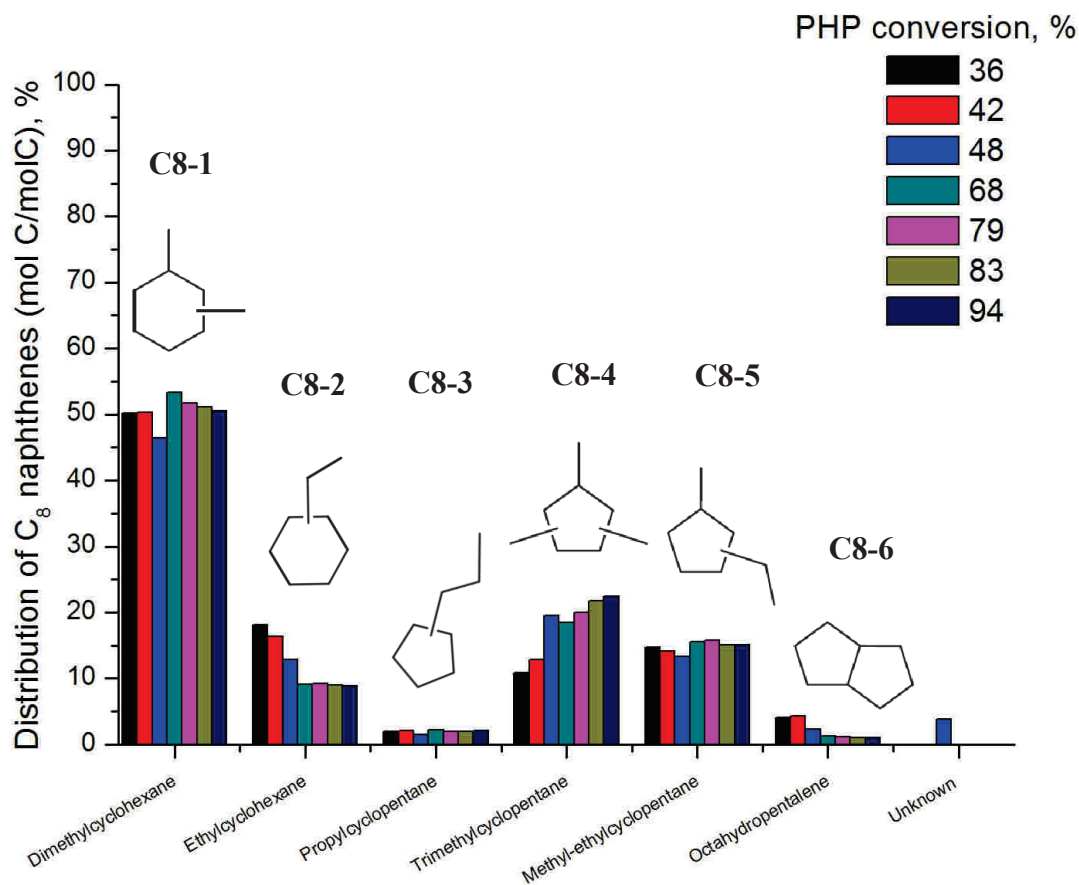


Figure 15. Distribution of C<sub>8</sub> naphthenes from hydrocracking of PHP over Pt/H-USY zeolite catalyst at different conversions.

The product distribution of C<sub>9</sub> naphthenes at different PHP conversions is shown in Figure 16. On-line analysis of these products at low PHP conversion was somewhat problematic due to the difficulty of integration of small chromatographic peaks. The distribution at 68% and higher PHP conversion is reliable. Substituted cyclohexanes, especially di- or tribranched molecules such as **C9-4** and **C9-5** were dominant at high PHP conversion. Alkyl substituted cyclopentanes were minor products among C<sub>9</sub> naphthenes.

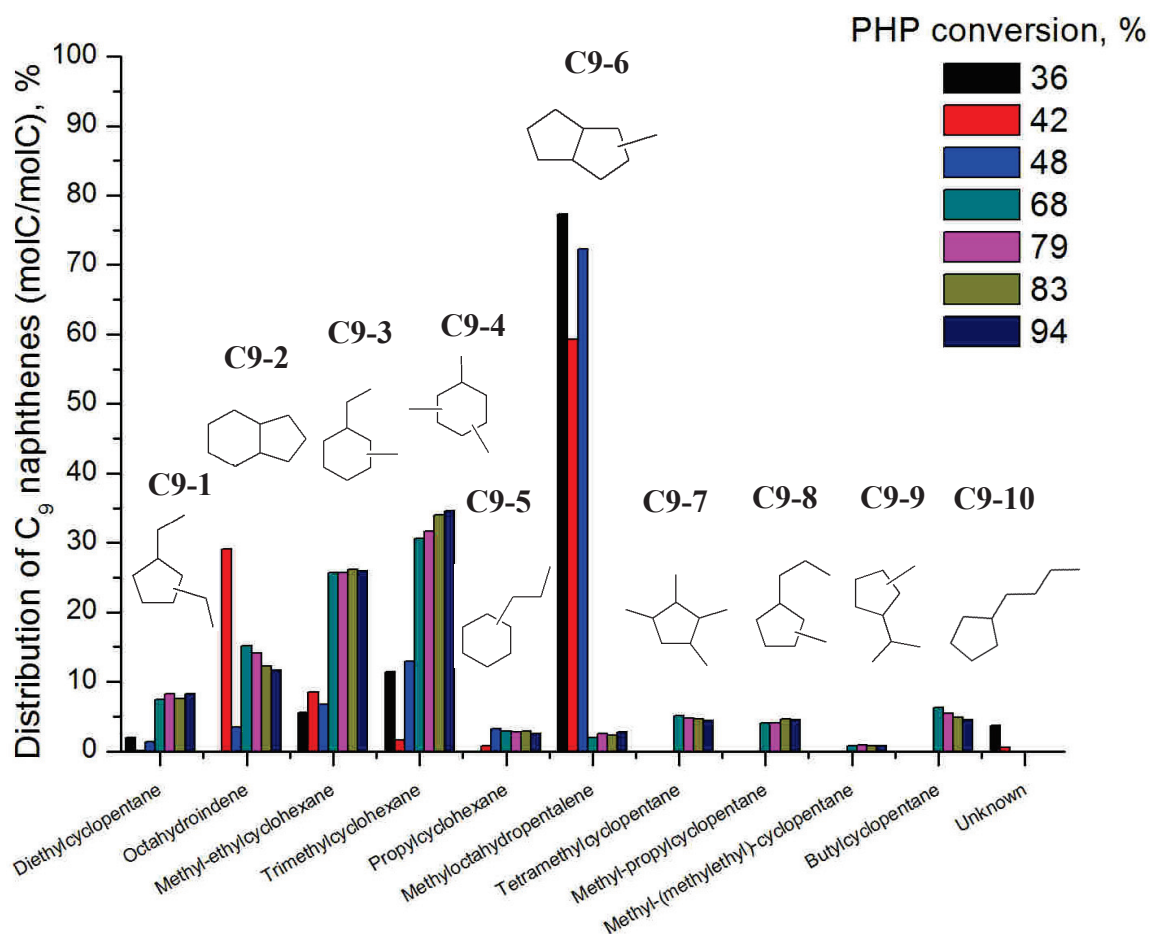


Figure 16. Distribution of C<sub>9</sub> naphthenes from hydrocracking of PHP over Pt/H-USY zeolite catalyst at different conversions.

The distribution of C<sub>10</sub> naphthenes over Pt/H-USY zeolite catalyst formed preferentially condensed bicyclic naphthenes, as decahydronaphthalene (decalin, **C10-7**) and its isomers, **C10-3** and **C10-4** (Figure 17). Non-substituted adamantane (**C10-1**), the most stable tricyclic hydrocarbon, was observed at all PHP conversion values, and its distribution remained relatively constant with PHP conversion. Minor products were constituted of substituted cyclohexanes (**C10-5** and **C10-6**, for instance) and twisted naphthenes, as spirodecane (**C10-8**).

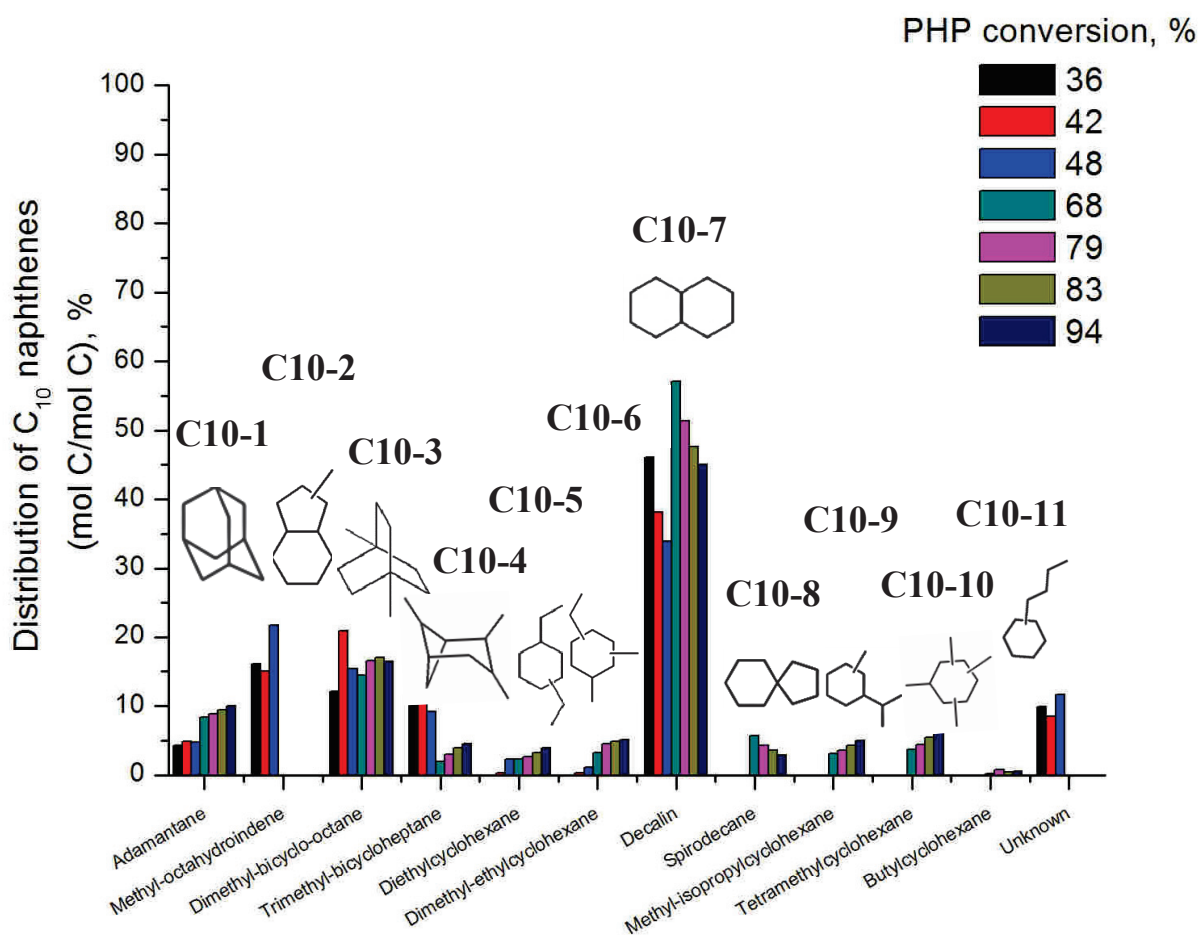


Figure 17. Distribution of C<sub>10</sub> naphthenes resulting from hydrocracking of PHP over Pt/H-USY zeolite catalyst at different conversions.

The C<sub>11</sub> and C<sub>12</sub> naphthenes were substituted decalin isomers.

## 4. Discussion

### 4.1. Hydroisomerization and hydrocracking reaction pathways

An analysis of the families of reaction products as a function of PHP conversion (Figure 6 and Figure 7) shows that the primary reaction products are ring-contraction and ring-shift isomers of PHP. Alkyladamantanes with the same number of carbon atoms are formed in a secondary reaction. Ring-opening and cracking are secondary and tertiary reaction products, respectively. Alkyladamantanes are final products (Figure 7). A small part of them may have undergone exocyclic cracking explaining the presence of non-substituted adamantane in the C<sub>10</sub> naphthene fraction (Figure 17), unless the small amount of adamantane is formed via



bridging of other C<sub>10</sub> naphthenes. Based on this analysis a general reaction scheme for hydroconversion of PHP over Pt/H-USY zeolite catalyst is proposed in Figure 18.

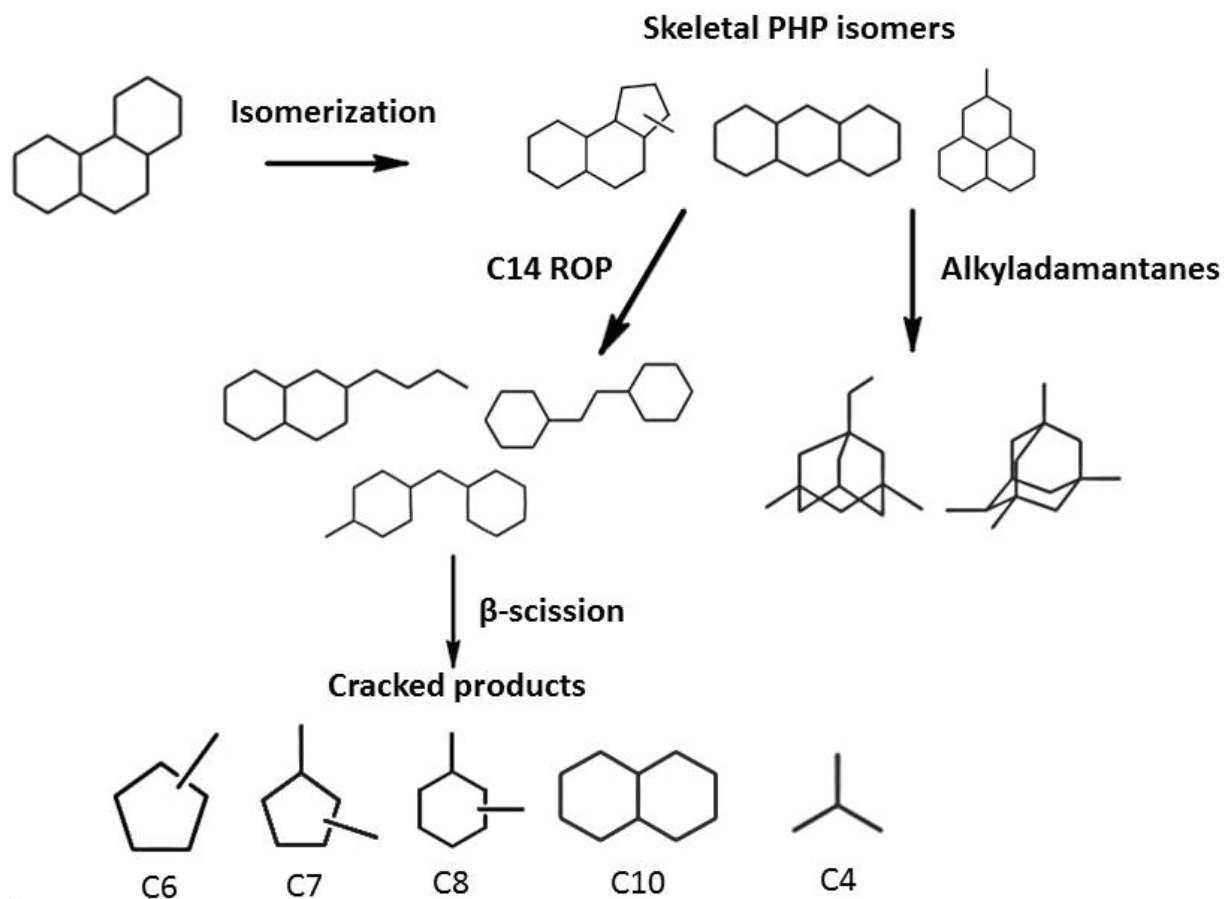


Figure 18. General reaction pathway for hydrocracking of perhydrophenanthrene over bifunctional Pt/H-USY zeolite catalyst.

Formation of alkyladamantanes from perhydrophenanthrene in the presence of aluminum bromide sludge catalyst at 0°C has been reported in literature [39,40]. It was proposed that substituted adamantanes would be the favored products resulting from isomerization of tricyclic naphthenes, such as perhydrophenanthrene isomers, due to their high thermodynamic stability. Perhydrophenanthrene and alkyladamantanes are almost strain-free molecules, therefore the thermodynamic driving force of the rearrangements is based on the increase in chain branching and the number of quaternary carbon atoms which is enhanced by the bridging in alkyladamantane structures.

The formation mechanism of alkyladamantanes proposed by Schneider *et al.* (Figure 19) departs from perhydrophenanthrene stereoisomers, which are isomerized to perhydroanthracenes, undergo ring condensation to methylperhydrophenalenes, which undergo multiple further rearrangements that ultimately lead to substituted adamantanes with methyl, ethyl, propyl or butyl substituents. Intermediates needed to produce the bridged naphthenes (Figure 19) were observed among the skeletal PHP isomers (Figure 8, structures **I1** and **I3**). It is interesting to notice the decreasing content of methylperhydrophenalene (**I3**) among the PHP skeletal isomers at increasing conversion (Figure 8), which could be explained by its conversion to alkyladamantanes (Figure 19). The formation mechanism of alkyladamantanes following the steps presented in Figure 19 originally proposed for aluminum bromide catalyst could be similar to the mechanism observed here in hydrocracking of perhydrophenanthrene over bifunctional Pt/H-USY zeolite catalyst. Tetramethyl-substituted adamantanes and ethyldimethyl-substituted adamantanes having three quaternary carbon atoms are the most stable alkyladamantanes and are most abundant in the reaction products (Figure 11). Non-substituted adamantane has a van der Waals diameter of 7.4 Å that could be accommodated in the micropores of zeolite Y [42,43]. Few previous studies mentioned the formation of alkyladamantanes among the reaction products [25,44,45]. These molecules can be overlooked due to a lack of analytical tools which could be used to properly separate and identify them.

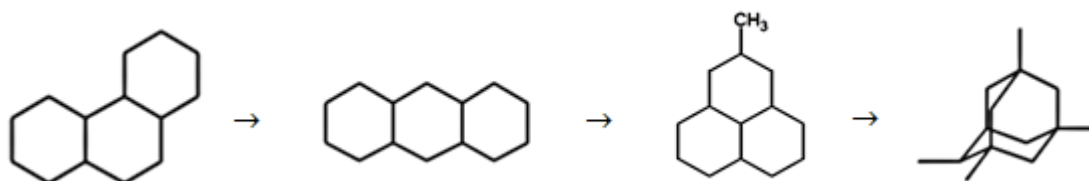


Figure 19. Steps of formation of alkyladamantanes over aluminum bromide sludge catalyst according to Schneider *et al.* [40]. A similar reaction pathway is observed in this work in hydrocracking of PHP over Pt/H-USY zeolite catalyst.

Ring-opening and cracking are consecutive reactions to skeletal PHP isomerization (Figure 18). This sequence has also been observed with bicyclic naphthenes [46–49]. Ring opening does not lead to fragmentation, but is a necessary step to enable splitting of the molecule in two parts in a next step. Interestingly, the central ring is opened preferentially (Figure 10,

structures **R2** and **R3**) and the alkyl group linking the two remaining rings is elongated from an initial methyl group (**R2**) to an ethyl (**R3**) and propyl (**R5**). The transformation of **R2** to **R3** is caused by ring contraction and expansion reaction shifting carbons from alkyl substituents on a ring to the chain linking the rings. The yield of ring-opening products is low (Figure 6) probably because these structures enable fast beta-scission pathways splitting rings from chains.

#### 4.2. Detailed analysis of the hydrocracking pathways

To shed more light on the hydrocracking reaction pathways, the reaction products to be theoretically expected by cracking through  $\beta$ -scission of the experimentally observed ROP molecules were compared with the experimental data. We opted to consider only the configurations of rings, branchings and positively charged carbon atom in carbenium ions which lead to fast beta-scission. The reaction rate of  $\beta$ -scission decreases in the order: tertiary-to-tertiary carbocation > tertiary-to-secondary carbocation and secondary-to-tertiary carbocation > secondary-to-secondary carbocation. Consequently, pathways involving the formation of primary carbocations were not considered. Ring branching is considered to occur, since this step is faster than alkyl-branching[18].

Dehydrogenation and protonation of abundant isomers **R2**, **R3** and **R6** (Figure 10) results in several possibilities of carbocations, according to the steps expected in a bifunctional mechanism. These possibilities and the cracked products to be expected are discussed here below. Isomers of structure **R2** have been evidenced in previous work on hydrocracking of perhydrophenanthrene over bifunctional catalysts[25,50]. Reasonable pathways of hydrocracking of structure **R2**, originated from the opening of a central cycle of skeletal perhydrophenanthrene isomers, are exemplified in Figure 20 (A and B). After fast formation of a tertiary carbocation through ring-contraction and hydride shifts, its hydrocracking can lead to the formation of C<sub>7</sub> naphthenes, such as dimethylcyclopentane and methylcyclohexane (Figure 20A). Dimethylcyclopentane may also isomerize into methylcyclohexane. The C<sub>7</sub> naphthene fraction contains all isomers (Figure 14B). A tertiary carbocation is also obtained after cleavage. The structure **R2** may also provide C<sub>6</sub> and C<sub>8</sub> naphthenes as reaction

products, undergoing the same type of skeletal rearrangements (Figure 20B). These are tertiary-to-tertiary alkylcarbenium ion types of beta-scission.

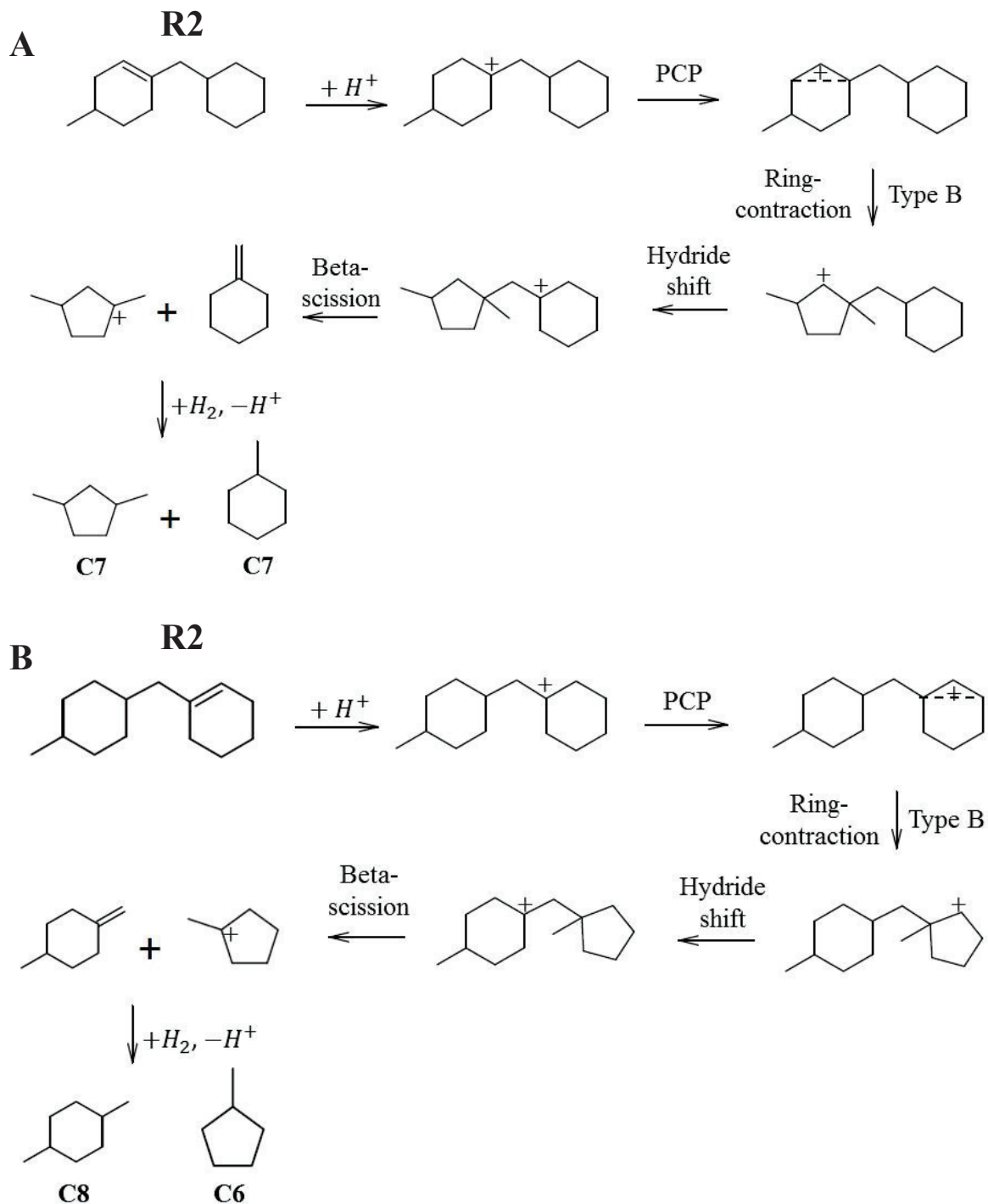
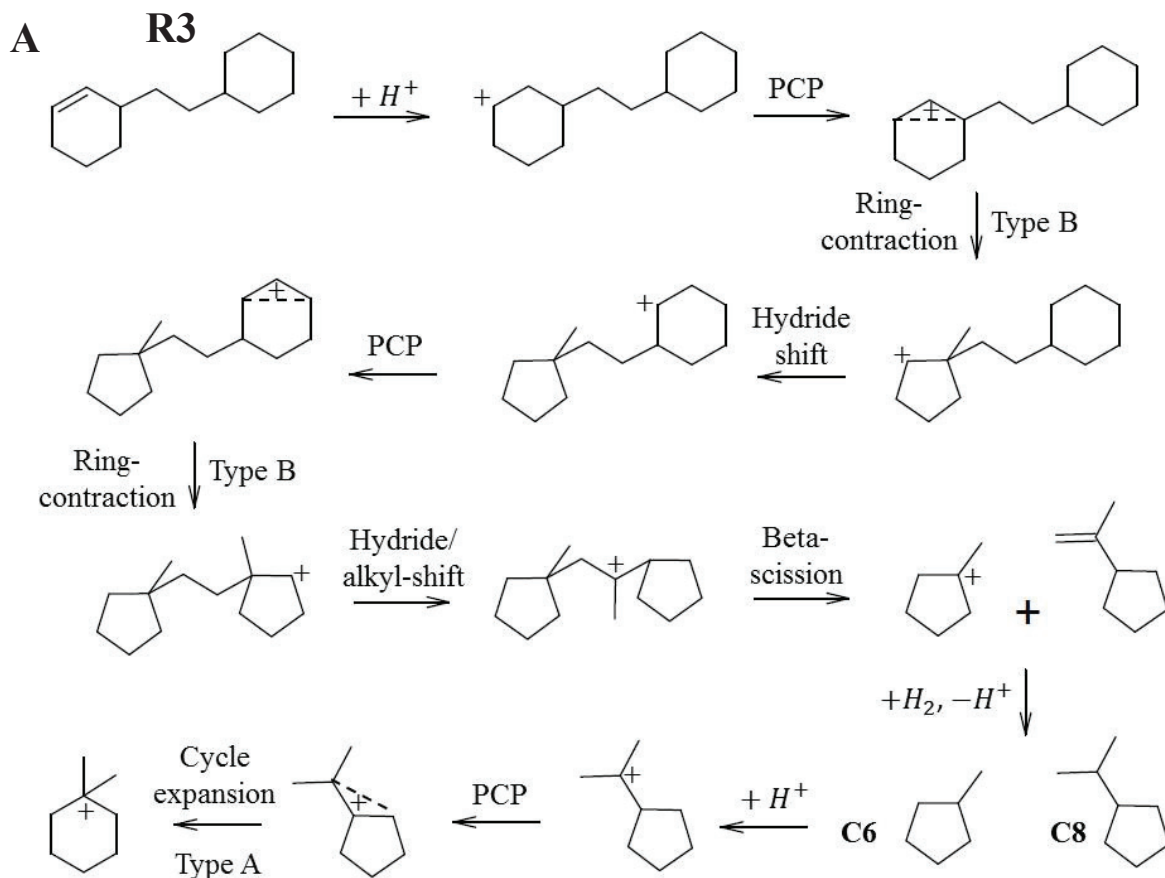


Figure 20. Proposed hydrocracking pathway to C<sub>7</sub> naphthenes (A) and C<sub>6</sub> and C<sub>8</sub> naphthenes (B) of ring-opening products originating from hydroconversion of skeletal perhydrophenanthrene isomers (R2) over Pt/H-USY zeolite catalyst.

Hydrocracking pathways of skeletal isomer **R3** (Figure 10), another ring-opening product from perhydrophenanthrene may lead to C<sub>6</sub> and C<sub>8</sub> naphthenes as cracked products, as depicted in Figure 21A. A favored configuration to fast beta-scission is achieved through hydride and alkyl-shifts. This configuration implies the formation of tertiary carbocations before and after the scission. The products illustrated in Figure 21 can easily be isomerized into 6-membered isomers, by expanding their naphthenic ring. Similar rearrangements may also generate C<sub>7</sub> cyclic structures through scission of tertiary carbocations. After scission, the positive charge is located on a secondary carbon, which causes a slower cleavage in comparison to the tertiary-to-tertiary carbocation pathway.



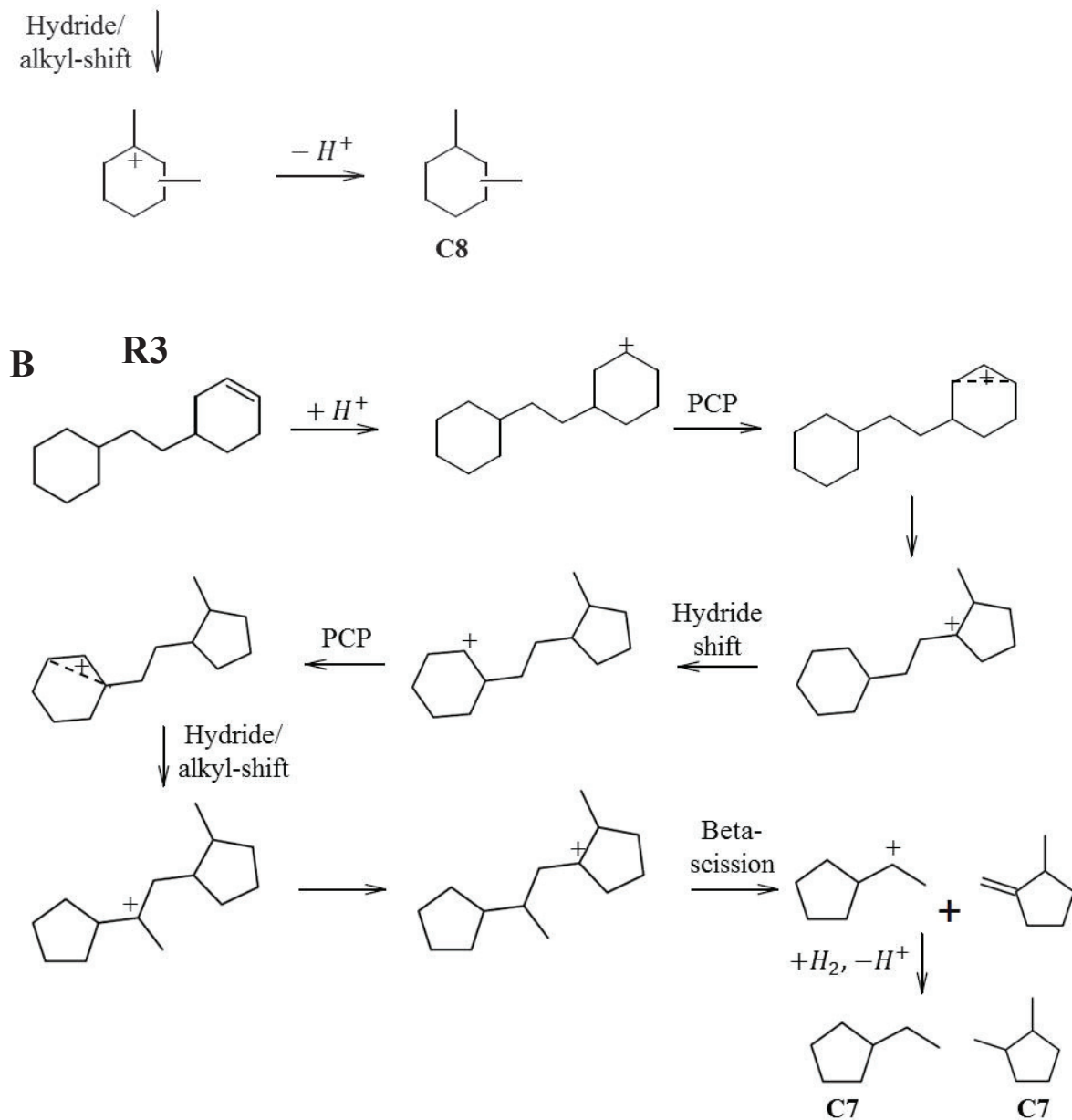


Figure 21. A) Suggested hydrocracking pathway to C<sub>6</sub> and C<sub>8</sub> naphthenes of ring-opening product originating from hydroconversion of skeletal perhydrophenanthrene isomers (R3) over Pt/H-USY zeolite catalyst. B) Suggested hydrocracking pathway to C<sub>7</sub> naphthenes.

The **R6** isomer is formed through the opening of an extreme cycle of skeletal perhydrophenanthrene isomers (Figure 10). These intermediates undergo simple rearrangements which lead to a favored configuration allowing cracking to C<sub>10</sub> naphthenes

and isobutane (Figure 22). C<sub>10</sub> naphthenes were mainly represented by decalin and its isomers (Figure 17). Cracking of butyldecalin to C<sub>6</sub>, C<sub>7</sub> and C<sub>8</sub> naphthenes can generate isoalkanes only through opening of a cycle. Since the content of isoalkanes within the cracked products was very small, these pathways will not be described here.

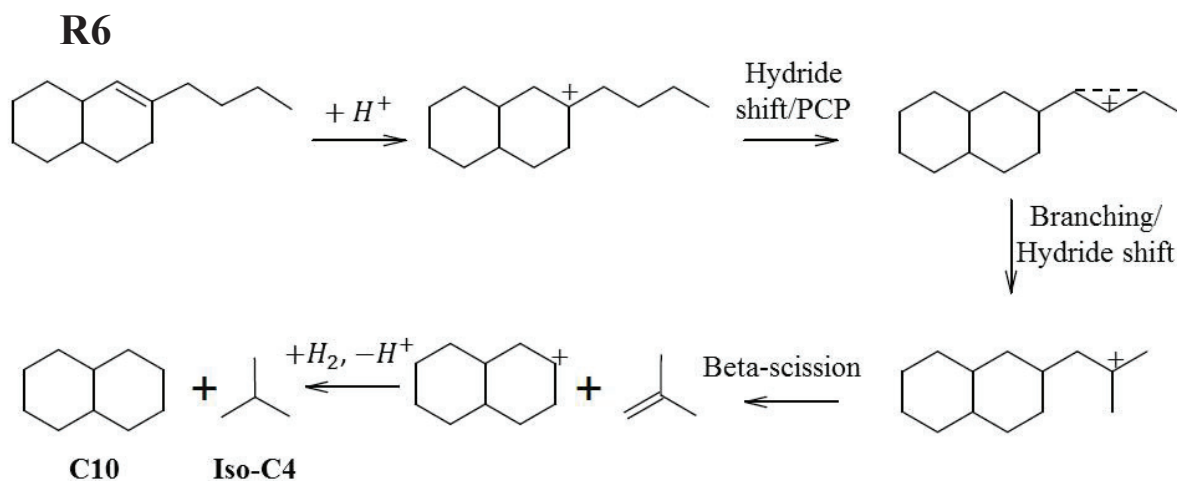
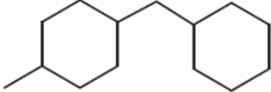
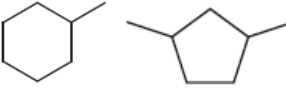
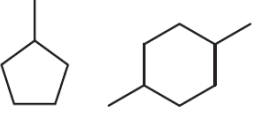
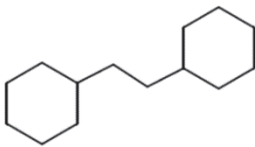
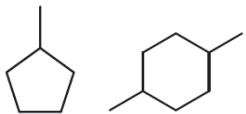
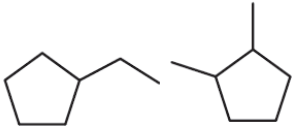
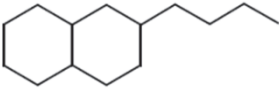
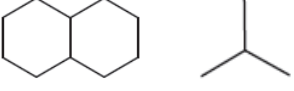


Figure 22. Suggested hydrocracking pathway to C<sub>10</sub> naphthenes and isobutane of ring-opening product originating from hydroconversion of skeletal perhydrophenanthrene isomers (R6) over Pt/H-USY zeolite catalyst.

Ring-opening reaction intermediates originated from hydroconversion of skeletal perhydrophenanthrene isomers and the compounds which they may form through bifunctional catalysis are summarized in Table 2. By comparing these compounds to the ones obtained through hydroconversion of skeletal PHP isomers over Pt/H-USY zeolite catalyst, it can be concluded that ROP may, in fact, lead to all cracked products observed in this work.

**CHAPTER II: HYDROCONVERSION OF PERHYDROPHENANTHRENE OVER  
BIFUNCTIONAL PT/H-USY ZEOLITE CATALYST**

Table 2. Ring-opening intermediates and main possible hydrocracking products according to bifunctional mechanism.

<i>ROP Intermediate</i>	<i>Cracks mainly to</i>	<i>Type of Beta-scission</i>
	 <i>C<sub>7</sub> naphthenes</i>	<i>Tertiary to tertiary</i>
	 <i>C<sub>6</sub> and C<sub>8</sub> naphthenes</i>	<i>Tertiary to tertiary</i>
	 <i>C<sub>6</sub> and C<sub>8</sub> naphthenes</i>	<i>Tertiary to tertiary</i>
	 <i>C<sub>7</sub> naphthenes</i>	<i>Tertiary to secondary</i>
	 <i>C<sub>10</sub> naphthenes and isobutane</i>	<i>Tertiary to secondary</i>

The yield of cracked products (Figure 11) shows maxima at even numbers of carbon atoms. The above analysis of hydrocracking pathways of the main ring-opening products of PHP can offer an explanation for the observed pattern. In this section we analyze why the formation of cracked products with 5 and 9 carbon atoms is suppressed. Ring-opening structures **R2** and **R3** (Figure 10) offer pathways to C<sub>7</sub>, C<sub>8</sub> and C<sub>6</sub> naphthenes, as previously discussed.



Hydrocracking pathways of these two intermediates leading to C<sub>5</sub> and C<sub>9</sub> naphthenes are presented in Figure 23. Cracking to C<sub>9</sub> naphthenes and C<sub>5</sub> isoalkanes proceeds through the opening of a ring, which is a difficult step [51]. In both cases, cracking involves secondary carbocations before and after cleavage, which does not configure a fast type of beta-scission [52].

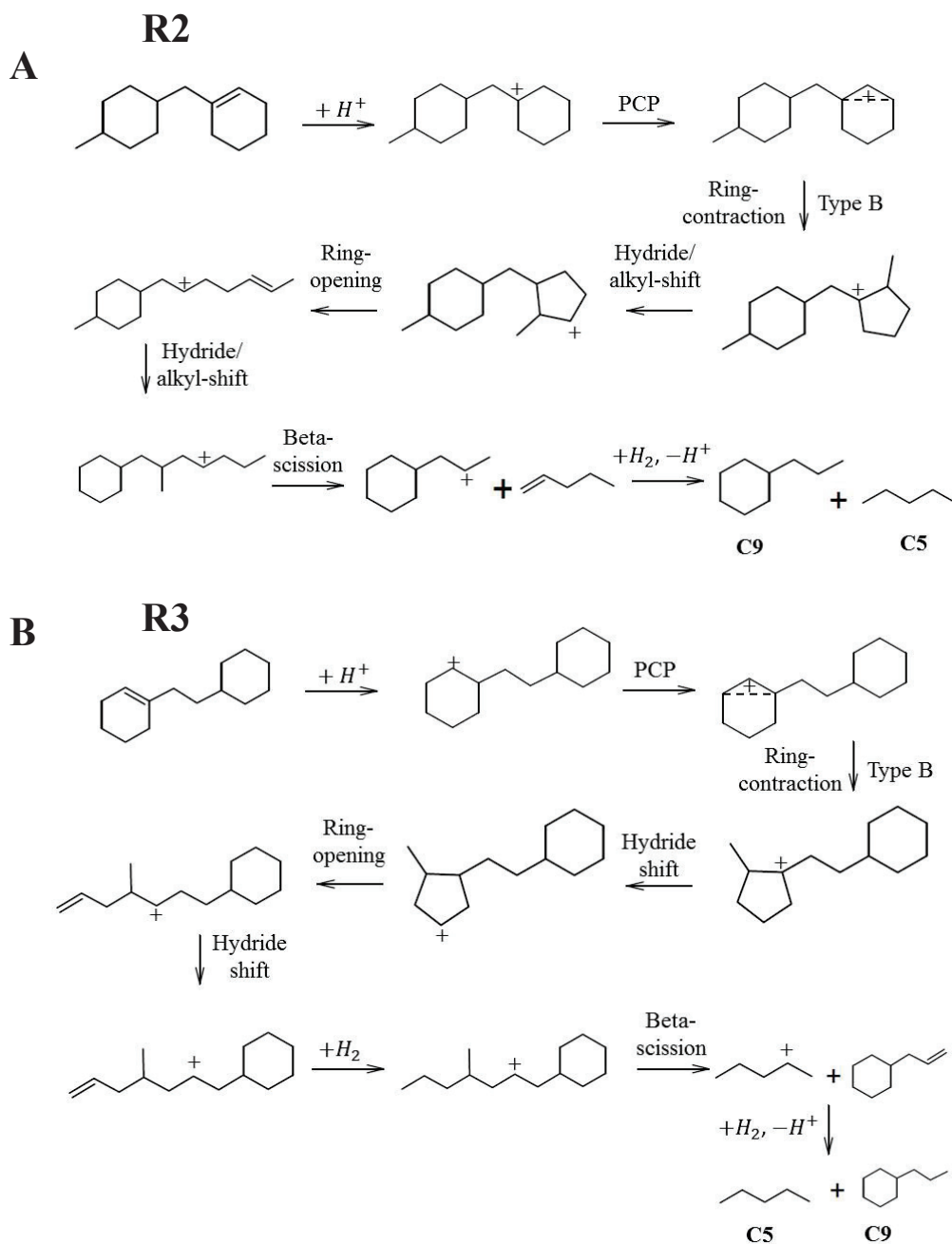
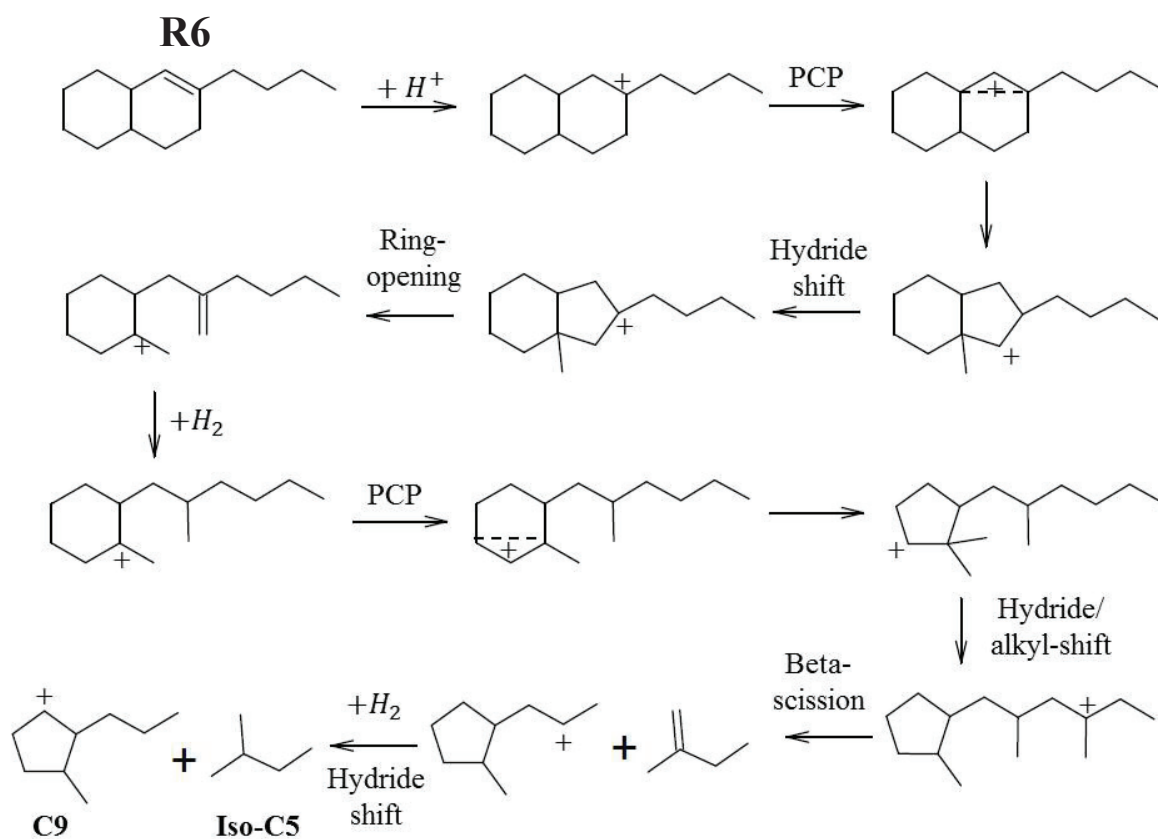


Figure 23. A) Suggested hydrocracking pathway to C<sub>9</sub> naphthenes and C<sub>5</sub> isoalkanes of ring-opening product originating from hydroconversion of skeletal perhydrophenanthrene isomers (R2) over Pt/H-USY zeolite catalyst.

B) Suggested hydrocracking pathway to C<sub>9</sub> naphthenes and C<sub>5</sub> isoalkanes of ring-opening product originating from hydroconversion of skeletal perhydrophenanthrene isomers (R3) over Pt/H-USY zeolite catalyst. All pathways show subsequent steps to dehydrogenation over the metal sites.

Butyldecalin may be converted into C<sub>9</sub> naphthenes and C<sub>5</sub> isoalkanes (Figure 24) through opening of a second ring, similar to the other intermediates. In this case, tertiary and secondary carbocations were generated before and after cleavage, respectively. The cyclic structure obtained can be isomerized to its 6-membered naphthene through expansion of the C<sub>5</sub>-cyclic structure, producing the C<sub>9</sub> isomers experimentally observed.



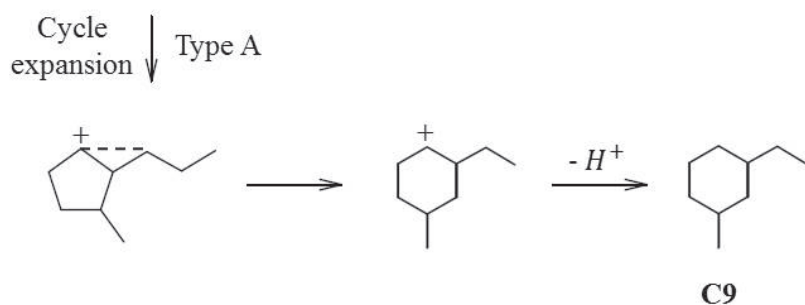


Figure 24. Suggested hydrocracking pathways leading to C<sub>9</sub> naphthenes and C<sub>5</sub> isoalkanes departing from ring-opening product originating from hydroconversion of skeletal perhydrophenanthrene isomers (R6) over Pt/H-USY zeolite catalyst.

The formation of C<sub>6</sub>, C<sub>8</sub> and C<sub>10</sub> naphthenes does not require opening of the second cycle of the reaction intermediates, which is considered a strained step in a bifunctional mechanism. Therefore, the production of compounds containing an odd number of carbon atoms, such as C<sub>9</sub> naphthenes and C<sub>5</sub> isoalkanes, would be less favored over the bifunctional catalyst. The exception is the formation of C<sub>7</sub> naphthenes, which can be easily generated from intermediates **R2** and **R3**, as previously described.

#### 4.3. Attempts to rationalize the yield of cracked products

To enable a discussion of contributions of hydrocracking pathways, it is convenient to express the cracked product yields as mol per 100 mol of PHP cracked. Primary hydrocracking results in the formation of 200 mol of cracked products per 100 mol of feed cracked. Values obtained covered, instead, a range from ca. 154 to 200 mol/100 mol of cracked PHP. Values below 200 mol per 100 mol cracked mean that next to cracking, some oligomerization of feed molecules and/or cracked products takes place.

The yields of cracked product fractions according to carbon number is presented in Figure 25.

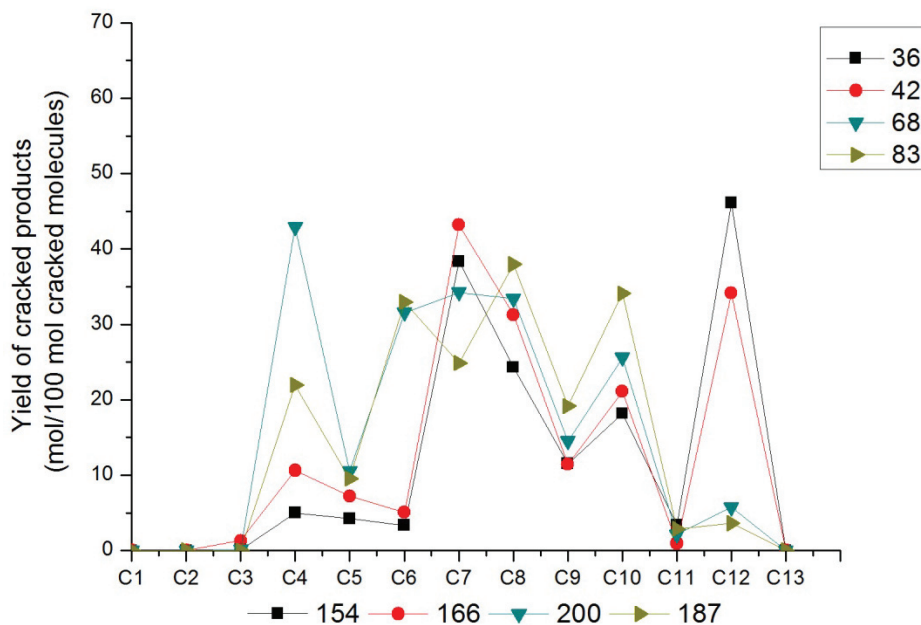


Figure 25. Yield of cracked products from hydrocracking of perhydrophenanthrene over Pt/H-USY zeolite catalyst expressed as mol/100 mol PHP cracked. Total yield of cracked products at the different conversions is indicated at the bottom of the graph.

This phenomenon has been observed in smaller molecules, as n-heptane. Blomsma et al. studied the hydroconversion of n-heptane over bifunctional Pd/H-Beta zeolite catalyst [53]. Cracking of the C<sub>7</sub> alkane resulted in non-equimolar amounts of C<sub>3</sub> and C<sub>4</sub>, in addition to formation of C<sub>5</sub> and C<sub>6</sub> alkanes. The yield of these cracked products was explained by a dimerization-cracking mechanism, where two molecules of C<sub>7</sub> would form a C<sub>14</sub> molecule cracking e.g. into 1 C<sub>4</sub> and 2 C<sub>5</sub> fragments.

In a similar way, a dimerization mechanism, in addition to classic hydrocracking, could explain the low overall molar yields of cracked products per feed molecule cracked. The oligomerization-cracking mechanisms can explain the formation of C<sub>12</sub> naphthenes at low PHP conversion. Disproportionation is a reasonable mechanism to explain such result. In fact, disproportionation has been observed in hydroconversion of naphthenes containing 9 or less carbon atoms over large-pore zeolite-based catalysts, such as Pt/CaY. Although there are no many evidences on how this reaction works, it is believed that the mechanism goes through the formation of an alkenyl cation, formed after ionic ring-opening, which could alkylate a cyclo-olefin over the acid sites of the zeolite. The resulting structure would then undergo cracking after rearranging favorably to beta-scission [54].

## 5. Conclusions

Hydroisomerization and hydrocracking of perhydrophenanthrene ( $C_{14}H_{24}$ ) were performed over Pt/H-USY zeolite catalyst in order to rationalize bifunctional mechanisms on the conversion of polycyclic naphthenes. Perhydrophenanthrene stereoisomers were formed through *in situ* hydrogenation of the parent aromatic, phenanthrene, over a Pt/ $Al_2O_3$  pre-catalyst. The conversion of perhydrophenanthrene stereoisomers over the bifunctional extrudate catalyst generated hundreds of reaction products which were exhaustively analyzed with GCxGC-FID/MS. These products were lumped into families, according to their carbon number and chemical family. The families of products regrouped isomers, ring-opening and cracking products.

The study of reaction intermediates enabled the proposition of a reaction pathway for hydroconversion of the model molecule over the bifunctional catalyst. Primary products comprised skeletal isomers of perhydrophenanthrene and alkyladamantanes. The latter are very stable molecules and resisted hydrocracking. They could be produced thanks to the size of USY pores. Ring-opening products were formed afterwards and their hydrocracking resulted mostly in cracked naphthenes. The diversity of reaction intermediates led to a broad carbon distribution over Pt/H-USY. Hydrocracking pathways of the polycyclic naphthene were studied in order to explain the cracked products obtained. The study of the yield of cracked products evidenced the contribution of other types of mechanism in addition to bifunctional pathways, as dimerization and disproportionation reactions.

## REFERENCES

- [1] J. Lee, S. Hwang, J.G. Seo, U.G. Hong, J.C. Jung, I.K. Song, Pd catalyst supported on  $SiO_2-Al_2O_3$  xerogel for hydrocracking of paraffin wax to middle distillate, *Journal of Industrial and Engineering Chemistry* 17 (2011) 310–315.
- [2] R. Sahu, B.J. Song, J.S. Im, Y.-P. Jeon, C.W. Lee, A review of recent advances in catalytic hydrocracking of heavy residues, *Journal of Industrial and Engineering Chemistry* 27 (2015) 12–24.

- [3] M. Gagnière, A. Pucci, E. Rousseau, Tackling the gasoline/middle distillate imbalance: An oligomerisation technology can produce a significant increase in middle distillate production, <https://www.axens.net/document/1003/tackling-the-gasoline-middle-distillate-imbalance/english.html>, 2013 (accessed 19.06.2019).
- [4] Organization of the Petroleum Exporting Countries (OPEC), 2040 World Oil Outlook, 2017.
- [5] M. Guisnet, “Ideal” bifunctional catalysis over Pt-acid zeolites, *Catalysis Today* 218-219 (2013) 123–134.
- [6] J. Weitkamp, Catalytic Hydrocracking-Mechanisms and Versatility of the Process, *ChemCatChem* 4 (2012) 292–306.
- [7] J.W. Thybaut, Laxmi Narasimhan, C S, J.F. Denayer, G.V. Baron, P.A. Jacobs, J.A. Martens, G.B. Marin, Acid-Metal Balance of a Hydrocracking Catalyst: Ideal versus Nonideal Behavior, *Ind. Eng. Chem. Res.* 44 (2005) 5159–5169.
- [8] H.F. Schulz, J.H. Weitkamp, Zeolite Catalysts. Hydrocracking and Hydroisomerization of n-Dodecane, *Ind. Eng. Chem. Prod. Res. Dev.* 11 (1972) 46–53.
- [9] D. Kubička, N. Kumar, P. Mäki-Arvela, M. Tiitta, V. Niemi, H. Karhu, T. Salmi, D.Y. Murzin, Ring opening of decalin over zeolitesII. Activity and selectivity of platinum-modified zeolites, *Journal of Catalysis* 227 (2004) 313–327.
- [10] V. Calemma, M. Ferrari, S. Rabl, J. Weitkamp, Selective ring opening of naphthenes, *Fuel* 111 (2013) 763–770.
- [11] G. Burnens, C. Bouchy, E. Guillon, J.A. Martens, Hydrocracking reaction pathways of 2,6,10,14-tetramethylpentadecane model molecule on bifunctional silica–alumina and ultrastable Y zeolite catalysts, *Journal of Catalysis* 282 (2011) 145–154.
- [12] J.A. Martens, P.A. Jacobs, Evidence for branching of long-chain n-alkanes via protonated cycloalkanes larger than cyclopropane, *Journal of Catalysis* 124 (1990) 357–366.
- [13] F. Alvarez, F.R. Ribeiro, G. Perot, C. Thomazeau, M. Guisnet, Hydroisomerization and Hydrocracking of Alkanes, *Journal of Catalysis* 162 (1996) 179–189.

- [14] N. Batalha, A. Astafan, J.C. Dos Reis, Y. Pouilloux, C. Bouchy, E. Guillon, L. Pinard, Hydroisomerization of n-hexadecane over bifunctional Pt-HBEA catalysts. Influence of Si/Al ratio on activity selectivity, *Reac Kinet Mech Cat* 114 (2015) 661–673.
- [15] J.A. Martens, P.A. Jacobs, J. Weitkamp, Attempts to rationalize the distribution of hydrocracked products. 1. Qualitative description of the primary hydrocracking modes of long-chain paraffins in open zeolites, *Appl Catal* 20 (1986) 239–281.
- [16] J.A. Martens, L. Uytterhoeven, P.A. Jacobs, G.F. Froment, Isomerization of Long-Chain N-Alkanes on Pt/H-Zsm-22 and Pt/H-Y Zeolite Catalysts and on Their Intimate Mixtures, *Stud. Surf. Sci. Catal.* 75 (1993) 2829–2832.
- [17] G.G. Martens, J.W. Thybaut, G.B. Marin, Single-Event Rate Parameters for the Hydrocracking of Cycloalkanes on Pt/US-Y Zeolites, *Ind. Eng. Chem. Res.* 40 (2001) 1832–1844.
- [18] W. Souverijns, R. Parton, J.A. Martens, G.F. Froment, P.A. Jacobs, Mechanism of the paring reaction of naphthenes, *Catal Lett* 37 (1996) 207–212.
- [19] C.J. Egan, G.E. Langlois, R.J. White, Selective Hydrocracking of C 9 - to C 12 - Alkylcyclohexanes on Acidic Catalysts. Evidence for the Paring Reaction, *J. Am. Chem. Soc.* 84 (1962) 1204–1212.
- [20] J. Weitkamp, S. Ernst, H.G. Karge, Peculiarities in the conversion of naphthenes on bifunctional catalysts, *Erdöl & Kohle, Erdgas, Petrochemie.* 37 (1984).
- [21] T. Dutriez, M. Courtiade, D. Thiébaud, H. Dulot, F. Bertoncini, J. Vial, M.-C. Hennion, High-temperature two-dimensional gas chromatography of hydrocarbons up to nC60 for analysis of vacuum gas oils, *Journal of chromatography. A* 1216 (2009) 2905–2912.
- [22] S.G.A. Ferraz, B.M. Santos, F.M.Z. Zotin, L.R.R. Araujo, J.L. Zotin, Influence of Support Acidity of NiMo Sulfide Catalysts for Hydrogenation and Hydrocracking of Tetralin and Its Reaction Intermediates, *Ind. Eng. Chem. Res.* 54 (2015) 2646–2656.
- [23] S. Sayan, B. Demirel, J. Paul, Methyldecalin hydrocracking over palladium/zeolite-X, *Fuel* 79 (2000) 1395–1404.

- [24] Sato, K., Iwata Y., Miki Y., Shimada H., Hydrocracking of Tetralin over NiW/USY Zeolite Catalysts: For the Improvement of Heavy-Oil Upgrading Catalysts, *Journal of Catalysis* 186 (1999) 45–56.
- [25] Lorraine Leite, Eric Benazzi, Nathalie Marchal-George, Hydrocracking of phenanthrene over bifunctional Pt catalysts, *Catalysis Today* 65 (2001) 241–247.
- [26] B.G. Harvey, K.W. Harrison, M.C. Davis, A.P. Chafin, J. Baca, W.W. Merriman, Molecular Design and Characterization of High-Cetane Alkyl Diamondoid Fuels, *Energy Fuels* 30 (2016) 10171–10178.
- [27] P.S.F. Mendes, J.M. Silva, M.F. Ribeiro, A. Daudin, C. Bouchy, From powder to extrudate zeolite-based bifunctional hydroisomerization catalysts, *Journal of Industrial and Engineering Chemistry* 62 (2018) 72–83.
- [28] P. Gallezot, The State and Catalytic Properties of Platinum and Palladium in Faujasite-type Zeolites, *Catalysis Reviews* 20 (1979) 121–154.
- [29] J.Prasad, K.R.Murthy, P.G.Menon, The stoichiometry of Hydrogen-Oxygen titration on supported Platinum catalysts, *Journal of Catalysis* 52 (1978) 515–520.
- [30] P.S.F. Mendes, G. Lapisardi, C. Bouchy, M. Rivallan, J.M. Silva, M.F. Ribeiro, Hydrogenating activity of Pt/zeolite catalysts focusing acid support and metal dispersion influence, *Applied Catalysis A: General* 504 (2015) 17–28.
- [31] S.C. Larsen, Nanocrystalline Zeolites and Zeolite Structures, *J. Phys. Chem. C* 111 (2007) 18464–18474.
- [32] D. Verboekend, N. Nuttens, R. Locus, J. van Aelst, P. Verolme, J.C. Groen, J. Pérez-Ramírez, B.F. Sels, Synthesis, characterisation, and catalytic evaluation of hierarchical faujasite zeolites, *Chemical Society reviews* 45 (2016) 3331–3352.
- [33] A. Polyakova, E. Khramova, Y. Bagrii, N. Tsitsugina, I. Lukashenko, T. Frid, P. Sanin, Mass spectrometric study of alkyladamantanes, *Petroleum Chemistry U.S.S.R.* 13 (1973) 1–10.
- [34] A.V. Kiselev, N. S. Kulikov, G. Curthoys, Gas chromatography-mass spectrometry of the stereoisomers of perhydroanthracene and perhydrophenanthrene, *Chromatographia* 18 (1984).



- [35] J.W. Greidanus, Chemistry of 2-Substituted Adamantanes. III. Mass Spectra of 1- and 2-Adamantanethiol, 2-Adamantanol, and 2-Adamantanamine.
- [36] Robert J. Waltman, A. Campbell Ling, Mass spectrometry of diamantane and some adamantane derivatives.
- [37] Interpretation of Mass Spectra, 4th ed. (McLafferty, Fred W; Turecek, Frantisek), <https://pubs.acs.org/doi/abs/10.1021/ed071pA54.5> (accessed 8.01.2019).
- [38] W.-C. Lai, C. Song, A. van Duin, J.W. de Leeuw, Ring-shift isomerization of sym-octahydrophenanthrene into sym-octahydroanthracene. Effects of zeolite catalysts and equilibrium compositions, *Catalysis Today* 31 (1996) 145–161.
- [39] M.A. McKerverey, Adamantane rearrangements, *Chem. Soc. Rev.* 3 (1974) 479.
- [40] A. Schneider, R. W. Warren, and E. J. Janoski, Formation of Perhydrophenalenes and Polyalkyladamantanes by Isomerization of Tricyclic Perhydroaromatics, *J. Org. Chem* 31 (1966) 1617–1625.
- [41] A. Haas, Ring Opening of Mono- and Bicyclic Naphthenes via Hydrogenolysis on Noble Metal Catalysts, 2012.
- [42] G.C. Lau, W.F. Maier, Polycyclic Hydrocarbon Rearrangements in Zeolites. A Mechanistic Study, *Langmuir* 3 (1987) 164–173.
- [43] Jacobus C. Jansen, Edward J. Creighton, Swie Lan Njo, Henk van Koningsveld, Herman van Bekkum, On the remarkable behaviour of zeolite Beta in acid catalysis, *Catalysis Today* 38 (1997) 205–212.
- [44] L. Wang, Y. Chen, S. Jin, X. Chen, C. Liang, Selective Ring-Shift Isomerization in Hydroconversion of Fluorene over Supported Platinum Catalysts, *Energy Fuels* 30 (2016) 3403–3412.
- [45] L.D. Rollmann, L.A. Green, R.A. Bradway, H.K.C. Timken, Adamantanes from petroleum with zeolites, *Catalysis Today* 31 (1996) 163–169.
- [46] C.A.A. Monteiro, D. Costa, J.L. Zotin, D. Cardoso, Effect of metal–acid site balance on hydroconversion of decalin over Pt/Beta zeolite bifunctional catalysts, *Fuel* 160 (2015) 71–79.

- [47] M. Kangas, D. Kubička, T. Salmi, D.Y. Murzin, Reaction Routes in Selective Ring Opening of Naphthenes, *Top Catal* 53 (2010) 1172–1175.
- [48] H. Du, C. Fairbridge, H. Yang, Z. Ring, The chemistry of selective ring-opening catalysts, *Applied Catalysis A: General* 294 (2005) 1–21.
- [49] M.A. Arribas, A. Martínez, G. Sastre, Simultaneous hydrogenation and ring opening of aromatics for diesel upgrading on Pt/zeolite catalysts. The influence of zeolite pore topology and reactant on catalyst performance, in: R. Aiello, G. Giordano, F. Testa (Eds.), *Impact of zeolites and other porous materials on the new technologies at the beginning of the new millennium: Proceedings of the 2nd International FEZA (Federation of the European Zeolite Associations) Conference, Taormina, Italy, September 1-5, 2002, 1st ed., Elsevier, Amsterdam, Boston, 2002, pp. 1015–1022.*
- [50] L. Leite, Etude sur molecule modèle des paramètres régissant la sélectivité des catalyseurs d'hydrocraquage des charges lourdes, 2000.
- [51] D.M. Brouwer, H. Hogeveen, *Recl. Trav. Chim. Pays-Bas* 89 (1970) 211–224.
- [52] J. Weitkamp, Peter A. Jacobs, J. A. Martens, Isomerization and hydrocracking of C<sub>9</sub> through C<sub>16</sub> n-alkanes on Pt/HZSM-5 zeolite, *Applied Catalysis* 8 (1983) 123–141.
- [53] E. Blomsma, J. A. Martens, P. A. Jacobs, Reaction mechanisms of isomerization and cracking of heptane on Pd/H-Beta zeolite, *Journal of Catalysis* 155 (1995) 141–147.
- [54] H.Schulz, J. Weitkamp, H.Eberth (Ed.), *5th Intern. Congr. Catalysis, North-Holland Publishing Co., Amsterdam, 1973.*



## TABLE OF FIGURES – CHAPTER III

---

<b>Figure 1.</b> GCxGC-FID analysis of reaction products from hydroconversion of perhydrophenanthrene obtained over A) Pt/H-USY zeolite catalyst at 48% conversion, B) Pt/H-Beta zeolite catalyst at 45% conversion, C) Pt/ASA catalyst at 45% conversion. ....	92
<b>Figure 2.</b> Molecule families and typical examples of molecules in the reaction products of hydroconversion of perhydrophenanthrene over Pt/H-USY, Pt/H-Beta and Pt/ASA bifunctional catalysts. ....	94
<b>Figure 3.</b> Evolution of perhydrophenanthrene conversion with contact time on Pt/H-USY, Pt/H-BETA catalysts with 3 wt.% zeolite in alumina binder; and Pt/ASA bifunctional catalysts. ....	95
<b>Figure 4.</b> Yield of isomerization, ring-opening and cracked products as a function of perhydrophenanthrene conversion over Pt/H-USY, Pt/H-BETA at 280°C and Pt/ASA bifunctional catalysts at 300°C. ....	96
<b>Figure 5.</b> Distribution of C <sub>14</sub> H <sub>24</sub> reaction products from hydrocracking of perhydrophenanthrene over Pt/H-USY, Pt/H-BETA and Pt/ASA bifunctional catalysts as a function of PHP conversion. Skeletal PHP isomers are indicated with triangles. Alkyladamantanes are assigned with squares. ....	97
<b>Figure 6.</b> Distribution of skeletal isomers of PHP (excluding substituted adamantanes) at isoconversion over Pt/H-USY, Pt/H-BETA and Pt/ASA bifunctional catalysts. PHP 149 stands for methylperhydrophenalene. PHP CC5 represents a skeletal perhydrophenanthrene isomer containing a C <sub>5</sub> -ring. ....	98
<b>Figure 7.</b> Distribution of alkyladamantanes at isoconversion over Pt/H-USY, Pt/H-Beta and Pt/ASA bifunctional catalysts. ....	99
<b>Figure 8.</b> Distribution of ring-opening products at isoconversion over Pt/H-USY, Pt/H-BETA and Pt/ASA bifunctional catalysts. ....	100
<b>Figure 9.</b> Yield of cracked products according to the number of carbon atoms at isoconversion of perhydrophenanthrene over Pt/H-USY, Pt/H-BETA and Pt/ASA bifunctional catalysts. ....	101
<b>Figure 10.</b> Distribution of cracked products as a function of perhydrophenanthrene conversion over Pt/H-USY, Pt/H-BETA and Pt/ASA bifunctional catalysts. Cracked products were assigned as naphthenes, isoalkanes and n-alkanes. ....	102
<b>Figure 11.</b> Distribution of C <sub>7</sub> naphthenes as a function of perhydrophenanthrene conversion over Pt/H-USY, Pt/H-BETA and Pt/ASA bifunctional catalysts. C <sub>7</sub> naphthenes were identified as dimethylcyclopentanes (triangles), methylcyclohexanes (squares) and ethylcyclopentanes (circles). ....	103
<b>Figure 12.</b> Distribution of skeletal isomers of perhydrophenanthrene (excluding substituted adamantanes) at isoconversion over Pt/H-USY and Pt/H-BETA bifunctional catalysts. ....	105
<b>Figure 13.</b> Distribution of ring-opening products at isoconversion over Pt/H-USY and Pt/H-BETA bifunctional catalysts. ....	107

---

## TABLE OF FIGURES – CHAPTER III

---

<b>Figure 14.</b> Simplified reaction pathway for hydrocracking of perhydrophenanthrene over bifunctional Pt/H-Beta, Pt/H-USY zeolite catalysts and Pt/ASA catalyst. Reaction intermediates obtained on each catalyst are illustrated.....	109
<b>Figure 15.</b> Suggested hydrocracking pathway to C <sub>7</sub> naphthenes of ring-opening product (R3) originated from hydroconversion of skeletal perhydrophenanthrene isomers over Pt/ASA catalyst. The pathway shows subsequent steps to dehydrogenation over the metal sites.....	112
<b>Figure 16.</b> Suggested hydrocracking pathway to C <sub>10</sub> naphthenes and isobutane of ring-opening product (R6) originated from hydroconversion of skeletal perhydrophenanthrene isomers over Pt/H-Beta zeolite catalyst.....	113
<b>Figure 17.</b> A) Suggested hydrocracking pathway to C <sub>7</sub> (major products), C <sub>6</sub> and C <sub>8</sub> naphthenes resulting from hydroconversion of ring-opening intermediate <b>R1</b> over Pt/H-Beta zeolite catalyst. B) Suggested hydrocracking pathway to C <sub>7</sub> (major products), C <sub>6</sub> and C <sub>8</sub> naphthenes resulting from hydroconversion of ring-opening intermediate <b>R4</b> over Pt/H-Beta zeolite catalyst.....	114
<b>Figure 18.</b> Suggested hydrocracking pathway to C <sub>7</sub> naphthenes of ring-opening product <b>R2</b> originated from hydroconversion of skeletal perhydrophenanthrene isomers over Pt/H-USY zeolite catalyst.....	115
<b>Figure S 1.</b> Evolution of perhydrophenanthrene conversion with contact time on Pt/H-USY, Pt/H-BETA catalysts with 1 wt.% zeolite in alumina binder at 280°C; and Pt/ASA (at 300°C) bifunctional catalysts.....	121

---

# CHAPTER III: HYDROCONVERSION OF PERHYDROPHENANTHRENE OVER BIFUNCTIONAL CATALYSTS - A COMPARISON BETWEEN PT/H-USY, PT/H-BETA AND PT/SILICA-ALUMINA

---

## Highlights

- Different intermediates are formed on each solid leading to distinct reaction products
- Preferential formation of certain intermediates over each zeolite can be rationalized by their preferential adsorption, as demonstrated by molecular simulation
- Linear structures are favored over Beta zeolites, USY zeolites process bulky molecules

## Abstract

Hydroconversion of perhydrophenanthrene was performed over Pt/H-Beta and Pt/ASA bifunctional catalysts, and compared to results obtained on Pt/H-USY zeolite catalyst, under the same operating conditions. Perhydrophenanthrene resulted from hydrogenation of the parent aromatic, phenanthrene, on a Pt/Alumina pre-catalyst. All three bifunctional catalysts followed the general reaction pathway observed previously, i.e. isomerization of perhydrophenanthrene by ring-shift and ring-contraction, followed either by the formation of alkyladamantanes or by ring-opening. The ring opening products crack to smaller naphthenes. Yet, the intermediates of this general reaction network differed very clearly from one catalyst to another. These shape selectivity effects could be explained by GCMC simulations of the adsorption selectivities of different intermediates. Bulky intermediates were mostly adsorbed on USY zeolites, whereas Beta zeolites processed preferentially linear structures. The products distribution on Beta zeolites was explained through formation of a ring-opening intermediate which cracked rapidly to C<sub>7</sub> naphthenes. USY-based catalysts were the most active among the solids tested, while Beta zeolites were slightly more selective to generate cracked products.

**Keywords:** phenanthrene, hydroisomerization, hydrocracking, polycyclic naphthenes, bifunctional catalysis, ultrastable Y zeolite, Beta zeolite, silica-alumina, shape-selectivity, pore-mouth catalysis

## 1. Introduction

In petroleum refining, hydrocracking plays an important role for upgrading heavy oil fractions, as Vacuum Gas Oil (VGO), to more valuable fractions, such as middle distillates [1–3]. Hydrocracking employs bifunctional catalysts, which comprise acid and metal functions. In order to process heavy fractions as VGO, large-pore catalysts must be employed to avoid diffusional limitations [4–7]. Zeolites and amorphous silica-alumina (ASA) are commonly used in hydrocracking units as the acid function of bifunctional catalysts [8–11]. The acid function works in synergy with a strong hydrogenating component, as Pt or promoted MoS<sub>2</sub>, which becomes more active than Pt if the environment contains high H<sub>2</sub>S concentrations [12–14].

Bifunctional catalysts operate by dehydrogenating the feedstock over the metal sites to create an olefin that will diffuse towards the acidic support. The olefin is protonated on the acid sites and it is susceptible to undergo isomerization and cracking, according to the chemistry of carbocations. The isomerized or cracked olefins diffuse towards the metal sites of the bifunctional catalysts to be hydrogenated [15–17].

VGO fractions are rich in cyclic molecules, as naphthenes and aromatics [18]. Hydroconversion of monocyclic naphthenes has been well reported in literature [19–24], as well as the reaction pathways alkanes [25–34]. The knowledge of reaction routes leading to conversion of polycyclic naphthenes containing at least 3 cycles is scarcer [10,35–40]. In our preceding study, we established hydroisomerization and hydrocracking pathways of perhydrophenanthrene, a 3-cycle naphthene, over a bifunctional Pt/H-USY catalyst (Chapter II). The model molecule was first isomerized to ring-shift and ring-contraction compounds. These isomers generated ring-opening products or went through further isomerization to produce alkyladamantanes. The latter are very stable molecules and resisted hydrocracking. The opening of one cycle (central or extreme) of perhydrophenanthrene isomers was followed by cracking, resulting in a broad distribution of carbon atoms.

In a prior study, Leite and coworkers addressed pore size selectivity on hydroconversion of perhydrophenanthrene over bifunctional catalysts [41,42]. Grand Canonical Monte Carlo simulation was performed in order to obtain adsorption energies of key reaction intermediates on large-pore zeolites topologies. It was established from experimental and theoretical results that isomerization products were predominant on catalysts presenting the biggest pore opening. In spite of the formation of different intermediates on each solid, the same reaction products were obtained on USY, Beta and ASA based catalysts.

In this work, we aim to compare reaction pathways on hydroconversion of perhydrophenanthrene over Pt/H-USY, Pt/H-Beta and Pt/ASA bifunctional catalysts. The main objective is to investigate reaction intermediates and cracked products generated on each solid, the occurrence of shape selective effects and their impact on the reaction products and distribution of carbon atoms. Monte Carlo simulation\* was carried out to access adsorption selectivities to probe intermediates on FAU and BEA topologies. We also address the question whether the formation of adamantanes is limited to mesopores/external surface of zeolites or whether it can occur in the micropores of large-pore zeolites.

\*Simulations were performed by J. Perez, from Catalysis, Biocatalysis and Separation Division (IFP Energies Nouvelles).

## 2. Materials and methods

### 2.1. Preparation and characterization of catalysts

Ultra Stable-Y (CBV720) and Beta (CP814e) zeolites were provided by Zeolyst. The powder was mixed with alumina binder (Pural SB3), furnished by Sasol, and extruded, according to a protocol described elsewhere (Chapter II and [43]). Zeolite loading corresponded to 1 or 3 wt.% of the dried support. Amorphous silica-alumina (Siralox 30) was supplied by Sasol in its extrudate form. All supports were calcined at 600°C, under air flow of 1.5 NL/h/g<sub>support</sub>. The extrudates were sorted to a length from 3 to 6 mm. Impregnation of the Pt precursor (H<sub>2</sub>PtCl<sub>6</sub> from Sigma-Aldrich) on the alumina binder was achieved by assuming total ionic exchange. Hydrochloric acid was applied as competitor. Further details on preparation of catalysts may be found in previous work (Chapter II). Pt-based catalysts were calcined at



520°C for 2h, under air flow of 1NL/h/gcatalyst. A 0.8 wt.% Pt/Al<sub>2</sub>O<sub>3</sub> pre-catalyst was synthesized using the same procedure.

The content of Pt in the catalysts was determined with X-ray fluorescence and dispersion of Pt on the alumina binder was measured by H<sub>2</sub>-O<sub>2</sub> chemisorption. Pt particles were considered to be spheric for the calculation of their size. The concentration of Brønsted acid sites (BAS) of the parent zeolites was determined from pyridine adsorption followed by FTIR. Concentration of BAS in USY and BETA parent zeolites corresponded to ca. 200 and 220 μmol/g, respectively. The BAS concentration of the final catalysts was estimated by a rule of proportionality, considering that extrusion did not affect the acidity of the shaped support. The BAS acidity of ASA was below the limit of reliable quantification. These properties are summarized in Table 1.

Table 1. Properties of Pt-loaded zeolite and amorphous catalysts determined by X-ray fluorescence, H<sub>2</sub>-O<sub>2</sub> chemisorption and pyridine adsorption monitored with FTIR.

Type of support	Zeolite content in binder (wt. %)	Pt loading (wt. %)	Pt dispersion (%)	Pt particle size (nm)	n <sub>Pt</sub> (μmol/g)	BAS (μmol/g)
USY (CBV720)	1	0.60	48	2.3	9.0	2.0
Beta (CP814e)	1	0.65	45	2.5	9.0	2.2
USY (CBV720)	3	0.66	89	1.3	18.8	6.0
Beta (CP814e)	3	0.69	85	1.3	15.8	6.6
ASA (Siralox 30)	-	0.60	84	1.3	15.8	n.d.

## 2.2. Catalytic tests

A downflow fixed-bed reactor was used to perform catalytic tests at 280 or 300°C and 60 bar. The reactor was loaded with a stacking of 2g of Pt/Alumina and 2g of bifunctional catalyst. Prior to the tests, the solids were reduced *in situ*, at 450°C for 2h under hydrogen flow of 1NL/h/gcatalyst. The feedstock was composed of 3 wt.% perhydrophenanthrene (Alfa Aesar) diluted in 97 wt.% n-heptane (AnalaR Normapur). A high hydrogen to hydrocarbons molar ratio of 7 mol/mol was applied for all tests and ensured total hydrogenation of the parent

aromatic to the naphthenic molecule. This ratio also avoided catalyst deactivation throughout the tests. Different conversion degrees of perhydrophenanthrene were obtained by changing the feed flow entering the reactor. Gas phase reaction products were analyzed online with a GC-FID apparatus (Varian). Liquid phase reaction products were collected for offline identification and quantification, with GCxGC-FID/MS. Further details on the analysis of reaction products are available elsewhere (Chapter II).

Molar flow of a carbon number fraction ( $N_i$ ) along with catalytic descriptors comprising conversion of perhydrophenanthrene ( $X$ ), yield of reaction products ( $Y$ ) and distribution of a given product  $i$  within a family  $J$  ( $D$ ), were calculated according to Equations 1-4.

$$N_i = \frac{(wt.\%)_i * F_m * c_i}{(100 * M_i)} \quad (1)$$

$F_m$  is the mass flow of the feedstock and  $(wt.\%)_i$ ,  $c_i$  and  $M_i$  the mass fraction, the number of carbons and the molar mass of the component  $i$  at the outlet, respectively.

$$X = 1 - \frac{N_{PHP,out}}{\sum_{i=1}^{i=14} N_{i,out}} \quad (2)$$

$$Y_i = \frac{N_i}{\sum_{i=1}^{i=14} N_{i,out}} \quad (3)$$

$$D_{i,J} = \frac{N_{i \in J}}{\sum N_{i \in J}} \quad (4)$$

### 2.3. Molecular simulation with Grand Canonical Monte Carlo (GCMC)

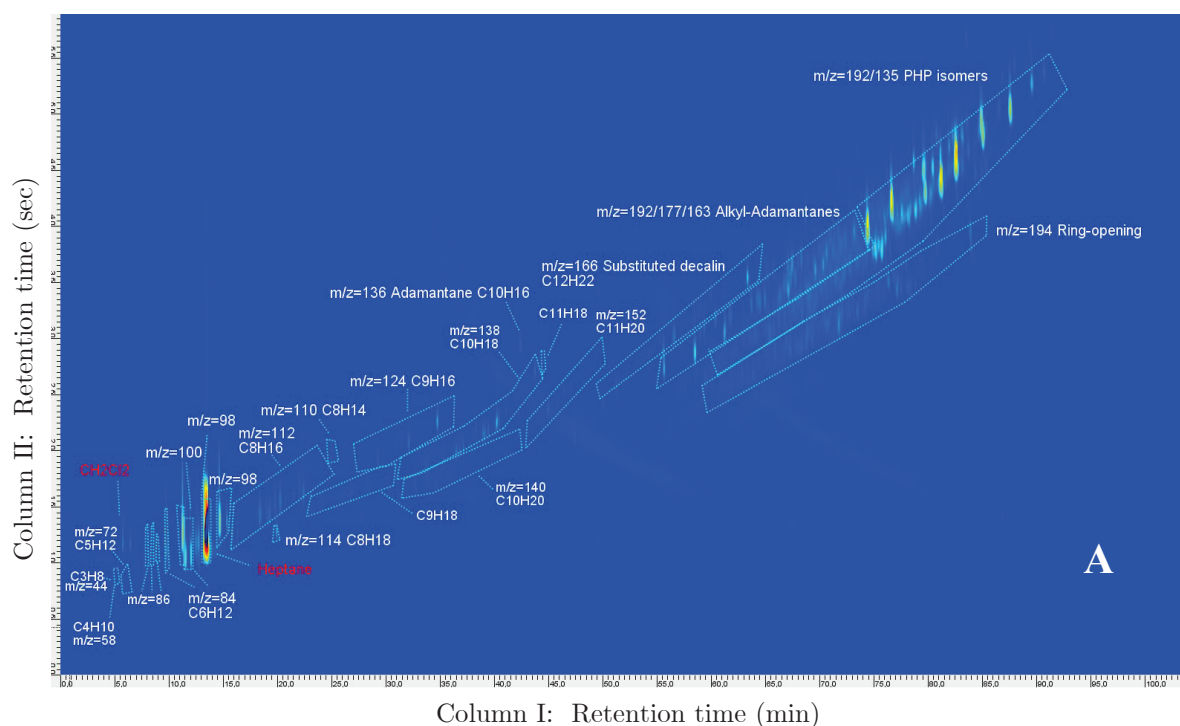
Grand Canonical Monte Carlo simulations combined with a bias scheme for the insertion of the centre of mass of the guest molecules were performed at 280°C to calculate selectivities to hydrocarbon mixtures in zeolite Beta and faujasite. The structure was represented by a 2x2x2 purely siliceous cell of FAU and of the A polymorph of \*BEA (taken from the IZA database 65), respectively. The simulations were performed using the code GIBBS 9.3. The adsorbate molecules were described according to the anisotropic united atom (AUA) for hydrocarbons 66, while the description of the zeolite was based on a “Kiselev type” potential 67 where the depth of the potential was slightly modified in order to better match the experimental

adsorption data available for pure linear alkanes (octane and hexadecane) in \*BEA and FAU. 50 million Monte Carlo steps were accumulated for mixtures.

### 3. Results

#### 3.1. Identification and quantification of reaction products with GCxGC-FID/MS

The reaction products resulting from hydroisomerization and hydrocracking of perhydrophenanthrene over Pt/H-USY, Pt/H-Beta and Pt/ASA bifunctional catalysts were identified and quantified with two-dimensional GC coupled to FID and MS detectors. The chromatograms at isoconversion of perhydrophenanthrene are illustrated in Figure 1. The conversion of phenanthrene, the parent aromatic, to the tricyclic naphthene was complete under operating conditions applied during the catalytic tests. The method to distinguish non-transformed perhydrophenanthrene, i.e. the reactant, from reaction products was the same as applied for the hydroconversion of the model molecule over Pt/H-USY zeolite catalyst (Chapter II).



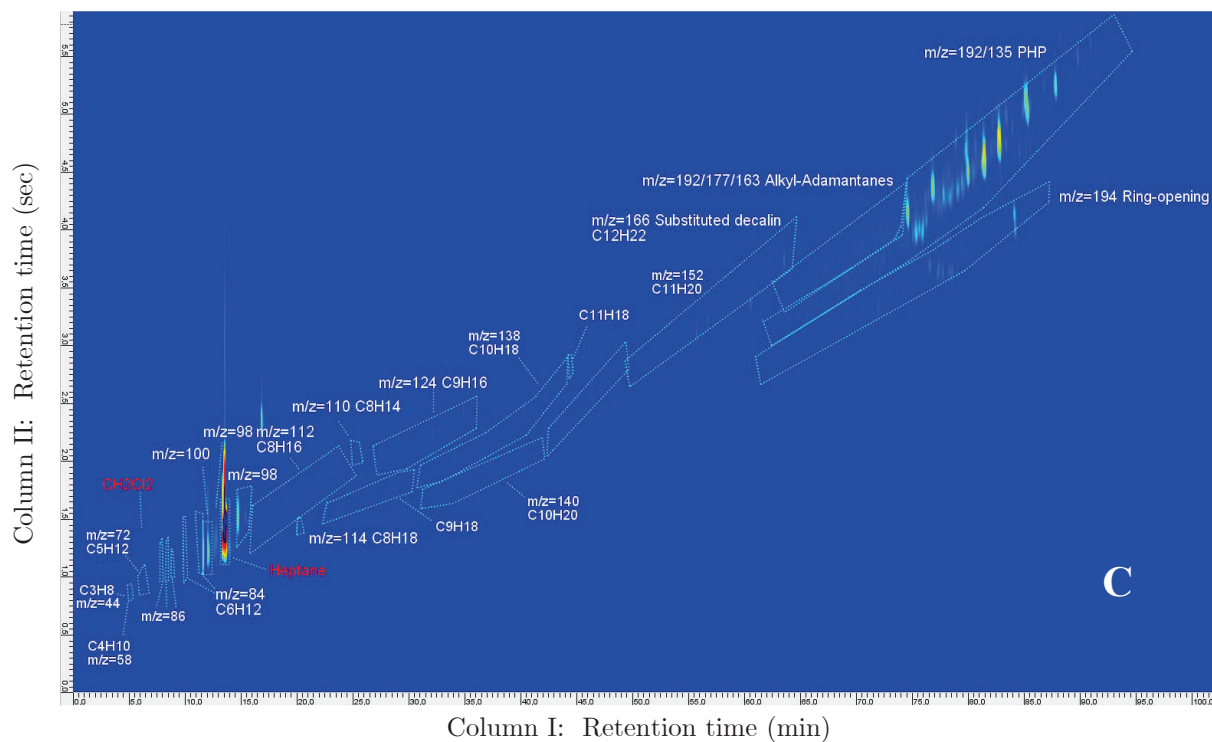
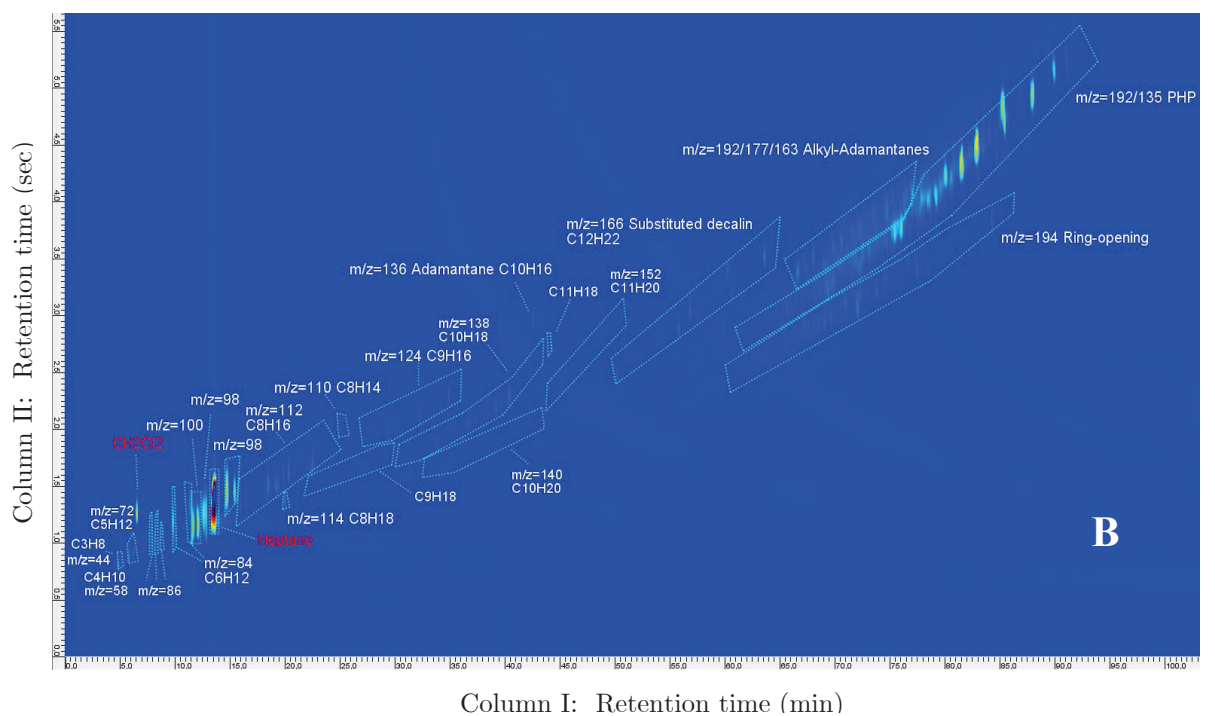


Figure 1. GCxGC-FID analysis of reaction products from hydroconversion of perhydrophenanthrene obtained over A) Pt/H-USY zeolite catalyst at 48% conversion, B) Pt/H-Beta zeolite catalyst at 45% conversion, C) Pt/ASA catalyst at 45% conversion.

The reaction products were lumped into families, according to their number of carbon atoms and chemical similarity. The six stereoisomers of perhydrophenanthrene, obtained over the pre-catalyst Pt/Al<sub>2</sub>O<sub>3</sub>, were considered as the reactants, which underwent hydroisomerization and hydrocracking over the zeolite or silica-alumina catalysts.

Isomerization products (C<sub>14</sub>H<sub>24</sub>) were then divided into substituted adamantanes and skeletal PHP isomers. Among the latter, two subgroups of ring-shift (perhydroanthracene and methylperhydrophenalenes) and ring-contraction isomers were distinguished. Ring-opening products (ROP, C<sub>14</sub>H<sub>26</sub>) were characterized by compounds presenting the same number of carbon atoms than PHP and only two naphthenic cycles.

Ring-opening of two out of three cycles of perhydrophenanthrene was not observed among the reaction products. Finally, cracked products comprised all the molecules with less than 14 carbon atoms and were mainly constituted of naphthenes. Globally, the similar reaction products were observed over the three catalysts, as summarized in Figure 2, except for some ring-contraction isomers of perhydrophenanthrene which were not produced on Beta-based catalysts, as will be discussed in the next sections.

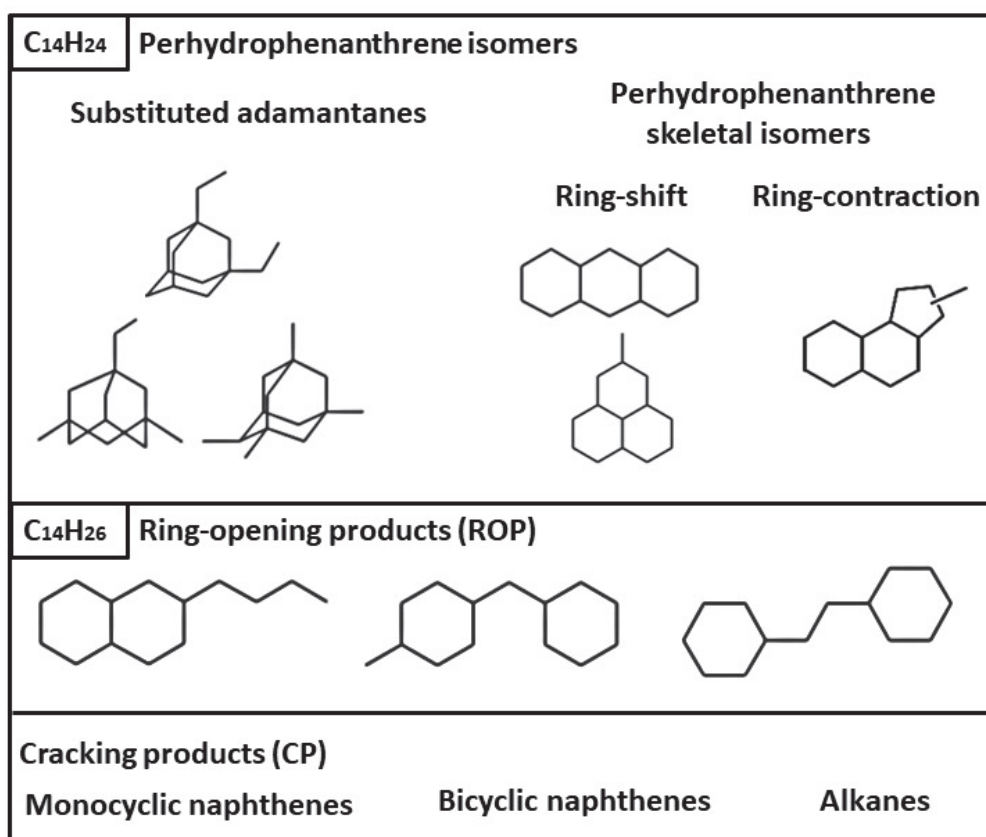


Figure 2. Families and typical examples of molecules in the reaction products of hydroconversion of perhydrophenanthrene over Pt/H-USY, Pt/H-Beta and Pt/ASA bifunctional catalysts.

### 3.2. Hydroconversion of perhydrophenanthrene

Conversion of perhydrophenanthrene over Pt/H-USY, Pt/H-Beta and Pt/ASA bifunctional catalysts, as a function of contact time, is depicted in Figure 3. The catalysts containing 3 wt.% of zeolite were the most active among the solids tested. Results obtained with 1 wt.% zeolite loading and Pt/ASA (the latter at 300°C) are available in supporting information. USY-based catalysts gave higher PHP conversion than Beta zeolite, irrespective of the zeolite loading in alumina binder. The activity of Pt/ASA at 280°C was very low compared to zeolite catalysts. We, therefore, raised the temperature to 300°C, in order to achieve a reasonable range of PHP conversions (30 to 45%). In the rest of the manuscript, the 300°C data will be presented for ASA and compared with the zeolite data at 280°C.

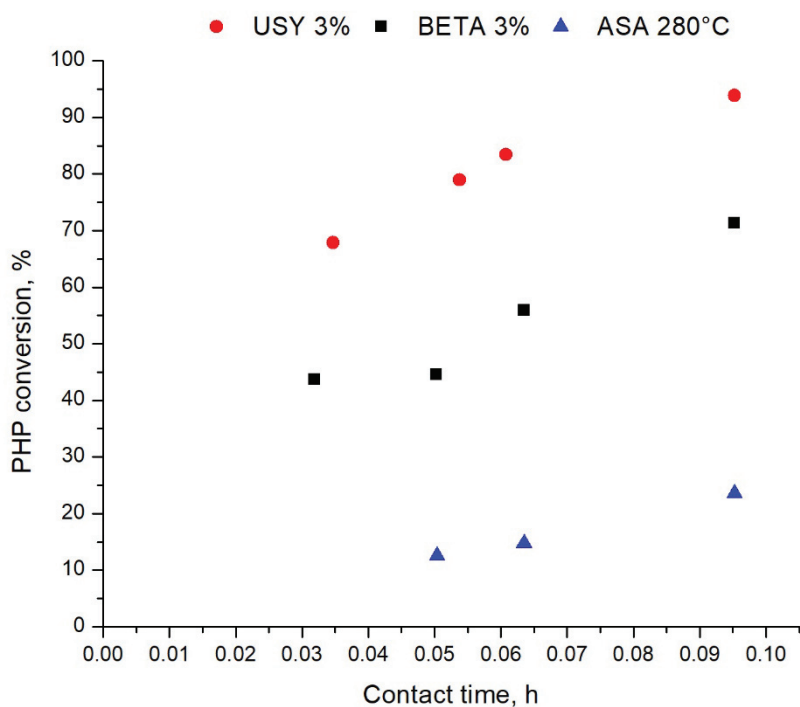


Figure 3. Evolution of perhydrophenanthrene conversion with contact time on Pt/H-USY, Pt/H-BETA catalysts with 3 wt.% zeolite in alumina binder; and Pt/ASA bifunctional catalysts.

The yield of isomerization, ring-opening and cracking products in a carbon molar basis over Pt/H-USY, Pt/H-BETA and Pt/ASA bifunctional catalysts is illustrated in Figure 4. Isomerization products comprised skeletal PHP isomers and alkyladamantanes. Isomerization was the predominant reaction at low conversion over zeolite and ASA-based catalysts. Over Pt/H-USY, a maximum yield of isomerization of ca. 43% was obtained at 68% conversion. We presume that Beta catalysts reach approximately the same maximum at equivalent PHP conversion, despite of a lack of higher conversion data. As only low conversion degrees were obtained over Pt/ASA catalysts, it was not possible to determine a maximum yield of isomerization over these solids. Similar to isomerization products, ring-opening profiles also reached a maximum, whereas cracked products increased with PHP conversion over the three catalysts. On Pt/H-Beta, the profile of ROP and cracking followed the same trend as observed on Pt/H-USY, but it is not possible to determine, in this case, if there is a maximum yield of ROP, nor at which conversion cracking became the predominant reaction over Beta-based catalysts. Ring-opening and cracking over Pt/ASA were minority reactions

in comparison to isomerization. In each case, isomerization was the primary reaction, followed by ring-opening and cracking.

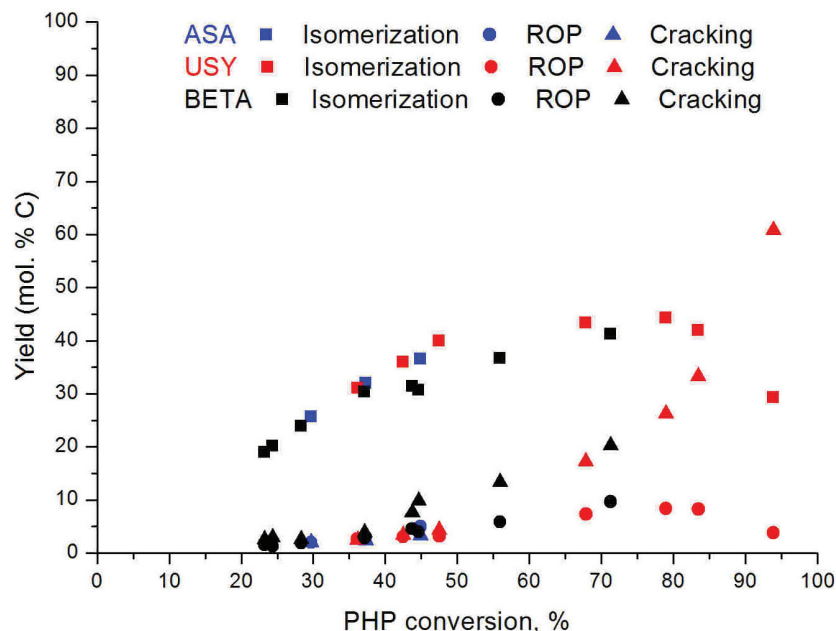


Figure 4. Yield of isomerization, ring-opening and cracked products as a function of perhydrophenanthrene conversion over Pt/H-USY, Pt/H-BETA at 280°C and Pt/ASA bifunctional catalysts at 300°C.

Globally, all catalysts behaved similarly, but with slight differences regarding selectivity to reaction products. At 45% conversion, Beta zeolites were, to a small degree, more selective to cracking products than USY and ASA, which is indicated by a lower yield of isomerization products in comparison to the other catalysts. In addition, USY zeolite and ASA presented virtually the same selectivity to isomerization products at isoconversion (although the catalytic tests of ASA were performed at 300°C). At higher PHP conversion, a direct comparison between Beta and USY zeolites indicated the same trend, i.e., cracking was slightly favored over Pt/H-Beta bifunctional catalysts.

The distribution of PHP isomers, represented by skeletal isomers and alkyladamantanes, over Pt/H-USY, Pt/H-Beta and Pt/ASA bifunctional catalysts is revealed in Figure 5. The proportion of alkyladamantanes increased with PHP conversion, whereas the proportion of skeletal PHP isomers decreased. Among the solids tested, USY zeolite seems to be the most suitable for alkyladamantanes production, in particular at high conversions. ASA-based catalysts were the least selective towards the formation of substituted adamantanes.



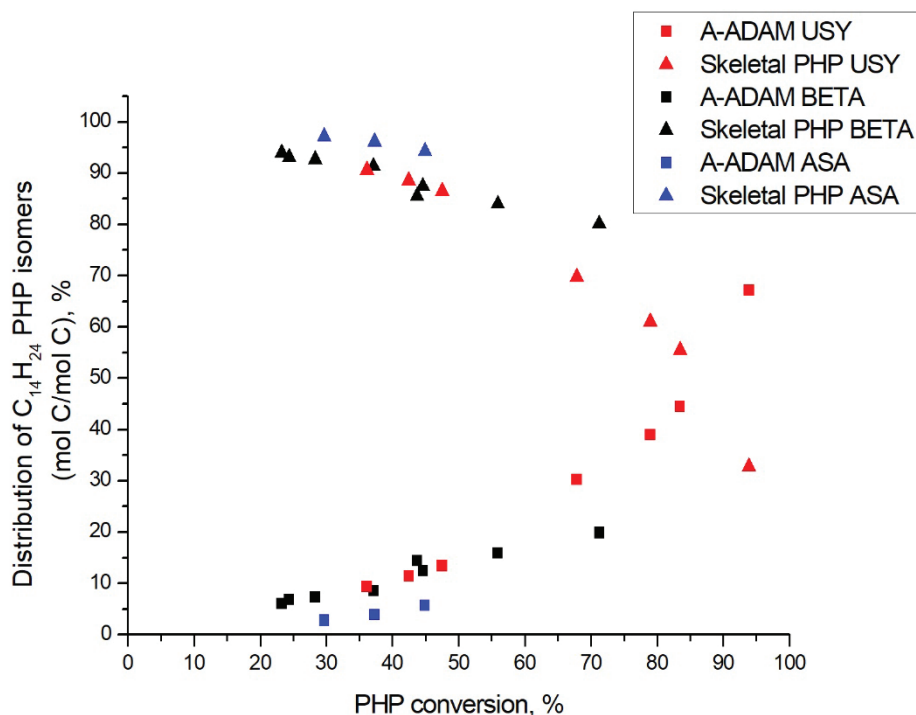


Figure 5. Distribution of  $C_{14}H_{24}$  reaction products from hydrocracking of perhydrophenanthrene over Pt/H-USY, Pt/H-BETA and Pt/ASA bifunctional catalysts as a function of PHP conversion. Skeletal PHP isomers are indicated with triangles. Alkyladamantanes are assigned with squares.

The distribution of skeletal PHP isomers over Pt/H-USY, Pt/H-Beta and Pt/ASA bifunctional catalysts at isoconversion is depicted in Figure 6. The only compound which was not formed over Beta catalysts is represented by structure **I4**, corresponding to a ring-contraction product of perhydrophenanthrene. In contrast, this molecule was the major intermediate on USY zeolite and ASA at this conversion. This difference between USY and beta had already been reported by Leite *et al.* Structure **I1**, a ring-shift isomers of perhydrophenanthrene (perhydroanthracene), was widely favored over Pt/H-Beta at this conversion level, in comparison to the other catalysts. Precursors of alkyladamantanes, characterized by methylperhydrophenalenes (**I3**), were more favored over Beta and ASA catalysts than over USY. Finally, spiro-type compounds, as isomers **I2**, were almost not perceived over USY zeolites, and formed to a small extent over Beta and ASA based catalysts. At this conversion, the unknown fraction accounted for 20% of the distribution.

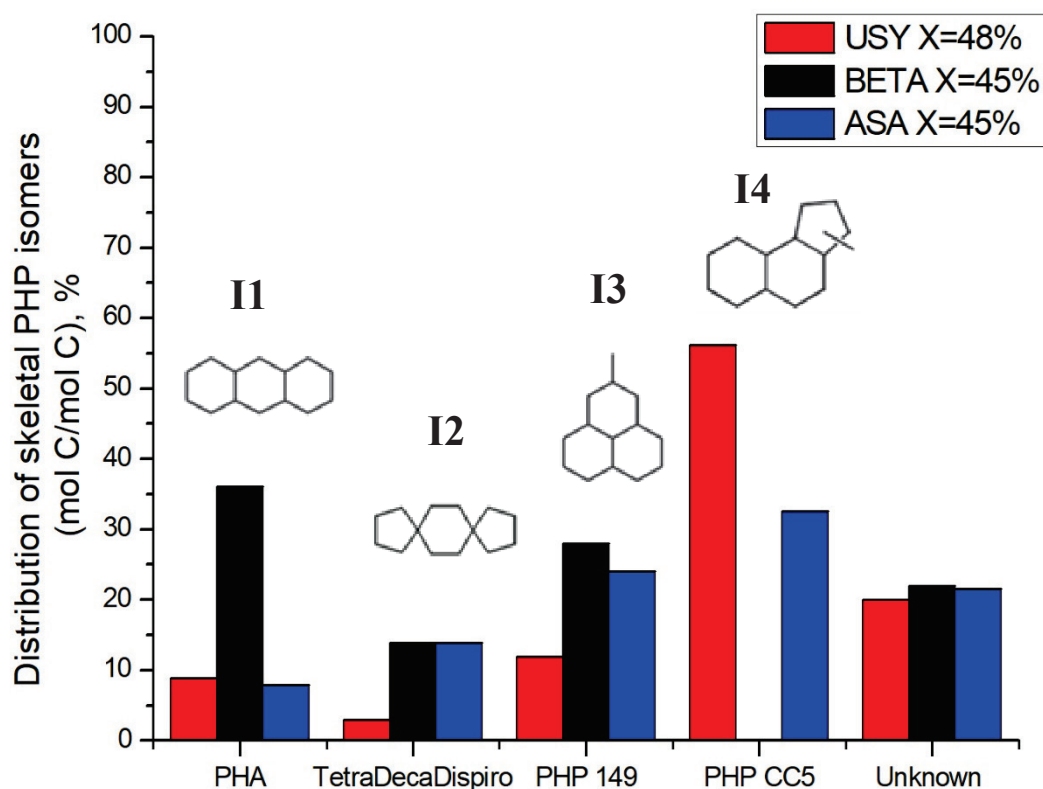


Figure 6. Distribution of skeletal isomers of PHP (excluding substituted adamantanes) at isoconversion over Pt/H-USY, Pt/H-BETA and Pt/ASA bifunctional catalysts. PHP 149 stands for methylperhydrophenalene. PHP CC5 represents a skeletal perhydrophenanthrene isomer containing a C<sub>5</sub>-ring.

The distribution of substituted adamantanes over Pt/H-USY, Pt/H-Beta and Pt/ASA catalysts at isoconversion is presented in Figure 7. USY zeolite formed preferentially multibranched isomers, as tetramethyladamantanes (**A1**), the thermodynamically most stable substituted adamantane [46], and dimethyl-ethyladamantanes (**A3**), whereas Beta zeolites produced mainly isomers **A1** and **A2** (diethyladamantanes). Methylpropyladamantanes (**A4**), in addition to isomers **A3** and **A1**, were perceived almost at the same proportion over ASA. The unknown fraction accounted for about 20% of the distribution of alkyladamantanes on each solid tested.

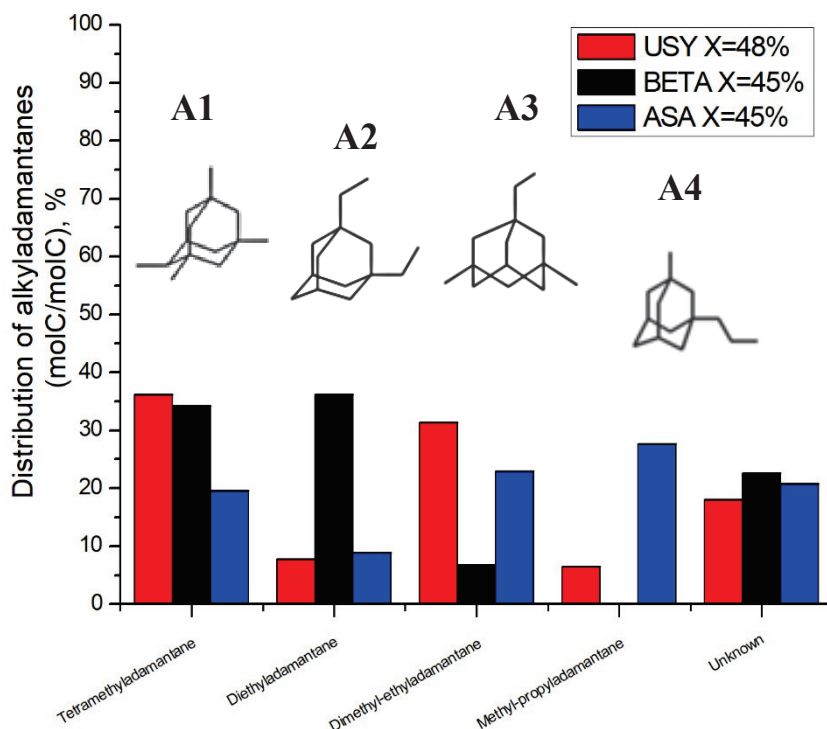


Figure 7. Distribution of alkyladamantanes at isoconversion over Pt/H-USY, Pt/H-Beta and Pt/ASA bifunctional catalysts.

Ring-opening products were represented by molecules presenting different degrees of branching, opening of external or central cycle of the model molecule and ring-contraction intermediates (Figure 8). At this PHP conversion, USY zeolites processed preferentially structures **R5**, **R1** (opening of central cycle of perhydrophenanthrene) and **R6**, **R7** (opening of external cycle of perhydrophenanthrene). Similarly, Beta zeolites mainly generated structures **R1**, **R4** (cyclopentyl-cyclohexane structures) and **R6**. ASA catalysts produced mostly **R3** and **R6** intermediates, corresponding respectively to opening of central and external cycle of perhydrophenanthrene. The unknown fraction varied from 10% to 25% of the distribution.

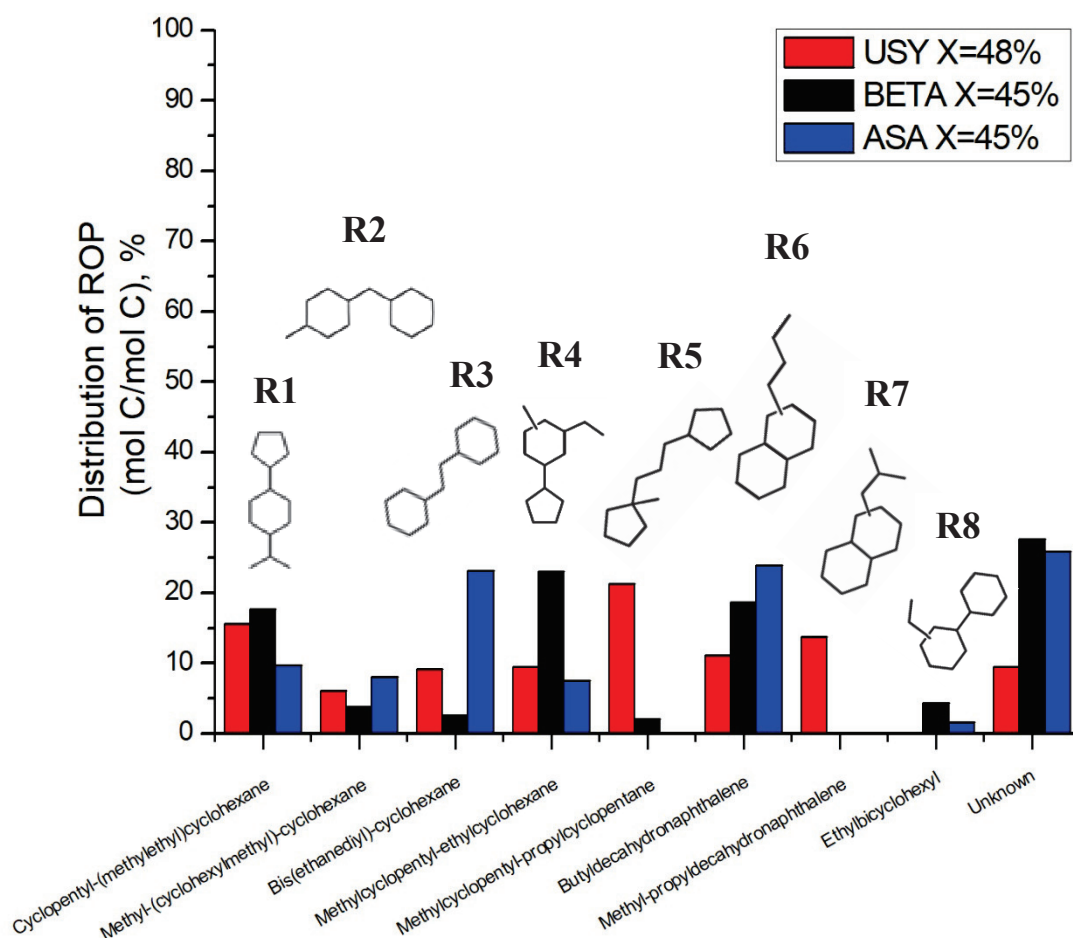


Figure 8. Distribution of ring-opening products at isoconversion over Pt/H-USY, Pt/H-BETA and Pt/ASA bifunctional catalysts.

The yield of cracked products resulting from hydroconversion of perhydrophenanthrene over Pt/H-USY, Pt/H-Beta and Pt/ASA bifunctional catalysts is illustrated in Figure 9. At 37% conversion, a predominant cracking to C<sub>7</sub> compounds was observed over the three catalysts, followed by the production of C<sub>12</sub> cracked products. Note that the production of C<sub>12</sub> was not accompanied by the formation of light components, as methane and ethane. Cracking to C<sub>12</sub> molecules has been discussed in a previous work (Chapter II), where reaction pathways of hydrocracking of perhydrophenanthrene over Pt/H-USY leading to such products were understood as a contribution of non-classical bifunctional mechanisms, such as disproportionation and addition-cracking reactions. When conversion increased, USY catalysts gave a broader distribution of carbon atoms as cracked products, while, over Beta

zeolites and ASA, a central cracking of perhydrophenanthrene to C<sub>7</sub> molecules remained predominant.

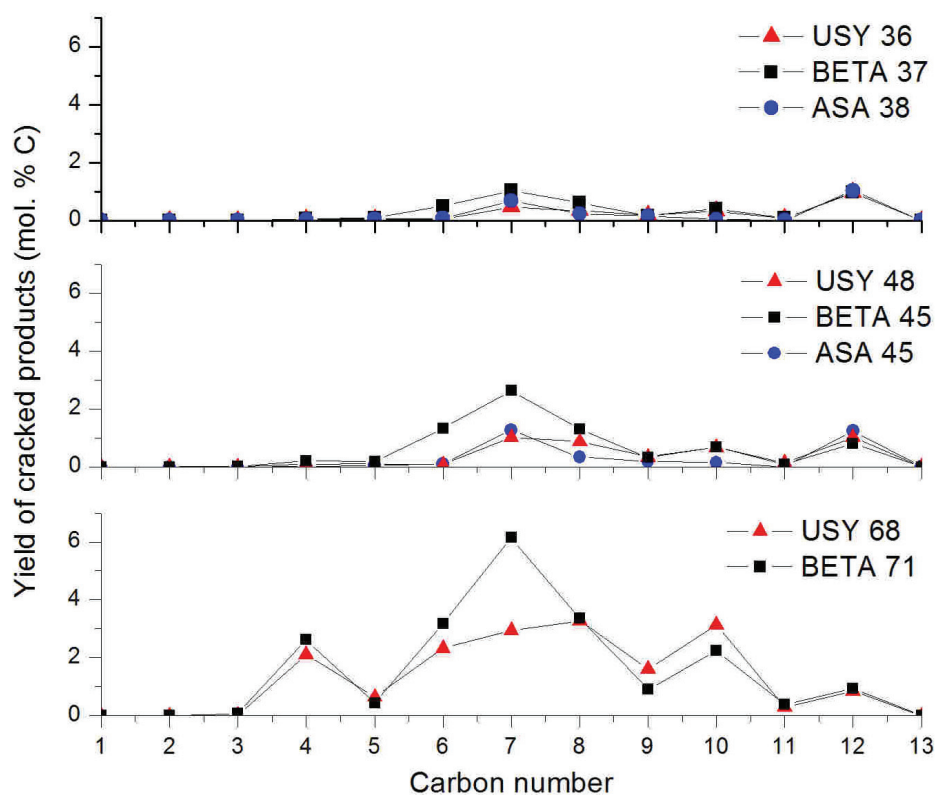


Figure 9. Yield of cracked products according to the number of carbon atoms at isoconversion of perhydrophenanthrene over Pt/H-USY, Pt/H-BETA and Pt/ASA bifunctional catalysts.

Cracked products were lumped into naphthenes, iso- and n-alkanes subfamilies (Figure 10). The relative distribution of cracked compounds indicated a high proportion of naphthenes among reaction products generated in hydroconversion of perhydrophenanthrene. It is worth mentioning that C<sub>7</sub> isoalkanes are not counted in the distribution of cracked products, since it was not possible to determine whether they resulted from hydrocracking of the tricyclic model molecule or from impurities of the solvent. Either way, the distribution of cracked products remained almost constant throughout PHP conversion. No alkane longer than 8 carbon atoms was formed over the catalysts studied.

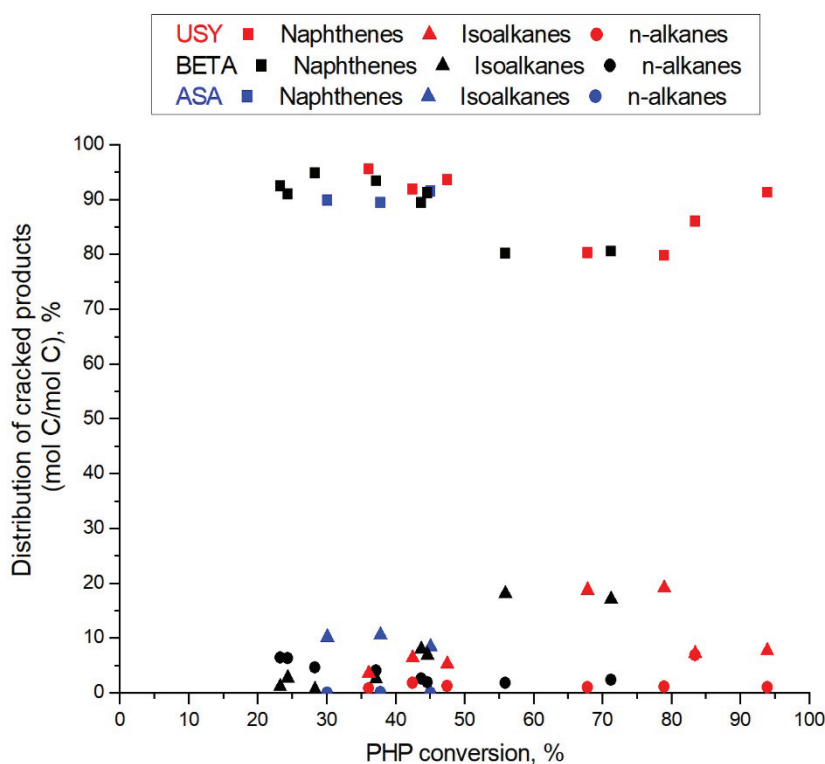


Figure 10. Distribution of cracked products as a function of perhydrophenanthrene conversion over Pt/H-USY, Pt/H-BETA and Pt/ASA bifunctional catalysts. Cracked products were assigned as naphthenes, isoalkanes and n-alkanes.

The yield and distribution of cracked products (Figures 9 and 10) showed a predominant cracking to  $C_7$  naphthenes over Beta zeolites and ASA. Reaction products resulting from hydroconversion of perhydrophenanthrene over Pt/H-USY zeolite catalyst have been exhaustively described elsewhere (Chapter II). The distribution of  $C_7$  naphthenes over Pt/H-USY, Pt/H-Beta and Pt/ASA is presented in Figure 11. Over Beta zeolites and ASA, primary  $C_7$  cyclic compounds were composed of methylcyclohexanes, whereas dimethylcyclopentanes seemed to be formed in a primary route over Pt/H-USY bifunctional catalyst. The proportion of dimethylcyclopentanes increased with conversion over Pt/H-Beta and Pt/ASA catalysts. Over the three catalysts, ethylcyclopentane was observed to a small extent within this subfamily. These results indicate that Beta zeolites and silica-alumina supports differ from USY catalysts not only in terms of carbon distribution, but also with respect to the nature of primary products formed.

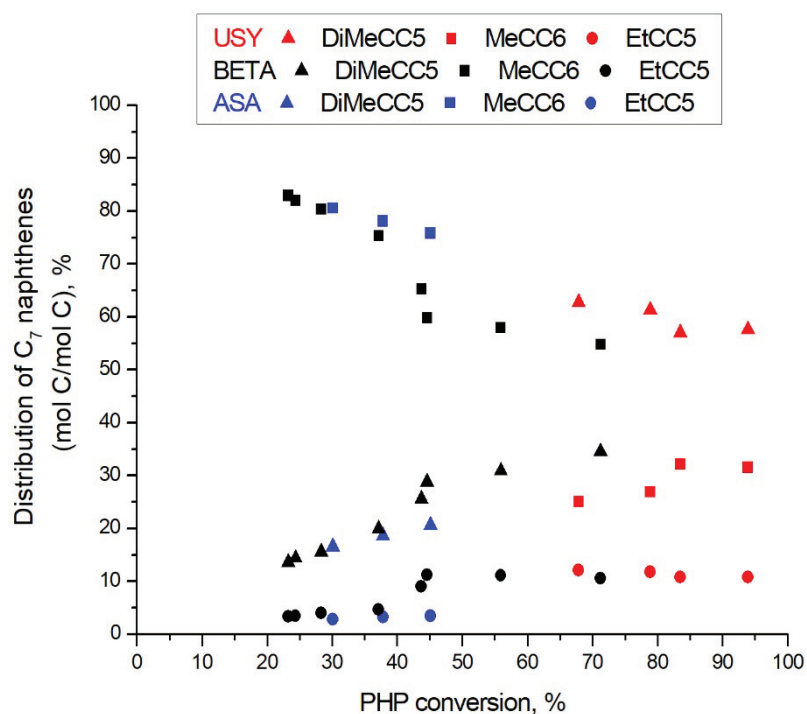


Figure 11. Distribution of  $C_7$  naphthenes as a function of perhydrophenanthrene conversion over Pt/H-USY, Pt/H-BETA and Pt/ASA bifunctional catalysts.  $C_7$  naphthenes were identified as dimethylcyclopentanes (triangles), methylcyclohexanes (squares) and ethylcyclopentanes (circles).

At higher conversion, other cracked products, in addition to  $C_7$  naphthenes, were also produced, as evidenced in Figure 9. At 71% conversion, molar equivalence was observed between  $C_6$  and  $C_8$  compounds, as well as between  $C_4$  (mainly isobutane) and  $C_{10}$  molecules. The detailed composition of each family of cracked products will not be presented herein, since similar results were observed in hydrocracking of perhydrophenanthrene over Pt/H-USY zeolite catalyst (for further detail on distribution of reaction products, see Chapter II).  $C_6$  and  $C_8$  reaction products were mainly represented by dimethylcyclopentanes and ethylcyclohexanes, while  $C_{10}$  structures were assigned as decalin (decahydronaphthalene) and its isomers.

### 3.3. *Molecular simulation*

Figures 6 and 8 show that the distribution of PHP isomers and of ring opening products is quite different on the three catalysts, i.e. we observe shape selectivity. Shape selectivity is often related to the fact that one isomer is preferentially adsorbed over another in a given zeolite [44,45]. In order to explore this hypothesis, a series of molecular simulations of the adsorption of selected intermediates was performed in the crystal structure of USY (FAU) and Beta (BEA) zeolites. The amorphous silica-alumina was not evaluated with this method because this support does not present a crystallographic structure. Adsorption of the most representative molecules from PHP isomers and ring-opening families were compared at the same operating conditions as catalytic tests were performed, corresponding to ca. 70% perhydrophenanthrene conversion. This conversion degree revealed distinct selectivities to isomerization and ring-opening intermediates on each zeolite, based on the profiles illustrated in Figures 4, 5 and 9. These results could indicate the existence of shape selectivity to isomerization and ring-opening pathways, leading to different distribution of carbon atoms over USY and Beta zeolites.

As a first step, we wanted to rationalize the preferential formation of skeletal PHP isomers or alkyladamantanes on each zeolite. The choice of representative intermediates was made based on the distribution of skeletal PHP isomers and alkyladamantanes (Figures 6, 7 and 12). Isomer **I4** (PHP CC5) was selectively formed over USY zeolites and ASA. In contrast, perhydroanthracene isomers (**I1**) seemed to be favored over Beta zeolites, especially at high PHP conversion (Figure 12). Within the subfamily of alkyladamantanes, secondary products of isomerization of perhydrophenanthrene, different selectivities to tetramethyl- (**A1**) and diethyladamantanes (**A2**) were noticed over the zeolites at high PHP conversion. Although not representative of bridged PHP isomers, C<sub>10</sub> adamantane was chosen as probe molecule in the simulation, due to a lack of proper adsorption model to represent C<sub>14</sub> alkyladamantanes.



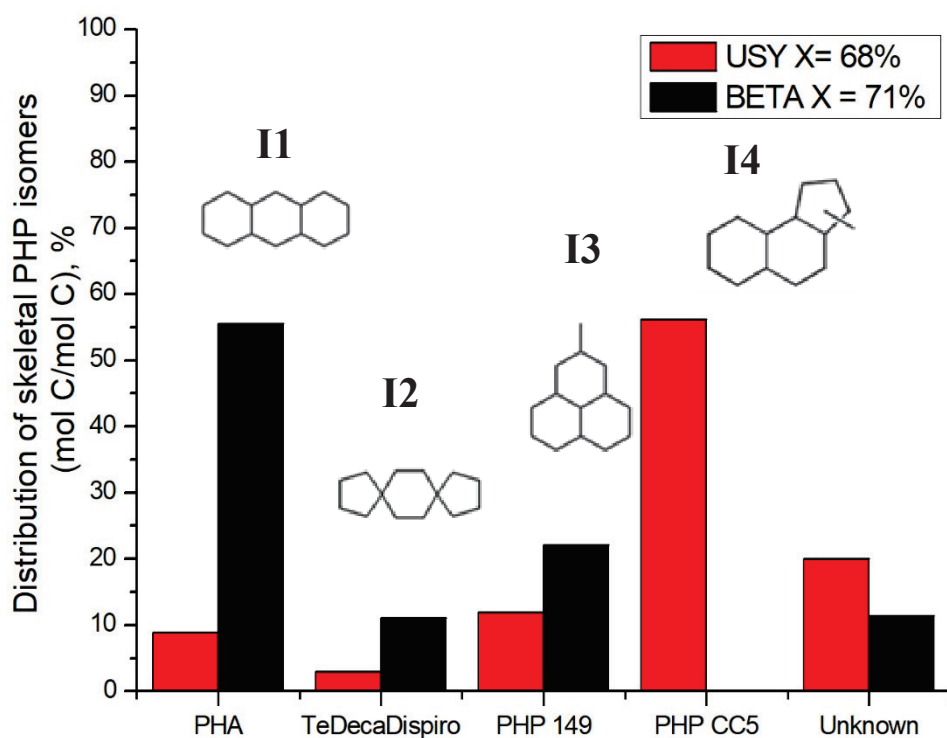


Figure 12. Distribution of skeletal isomers of perhydrophenanthrene (excluding substituted adamantanes) at isoconversion over Pt/H-USY and Pt/H-Beta bifunctional catalysts.

We, thus, carried out a simulation of the adsorption of an equimolar mixture of the reactant PHP, perhydroanthracene (**I1**), the ring contraction isomer **I4** and adamantane, in the presence of n-heptane as a solvent. The chosen partial pressures were representative of the reaction conditions. The aim of this simulation was to estimate the inclination of the system to form either skeletal PHP isomers or adamantanes. The quantity of molecules adsorbed per volume is provided in Table 2. Clearly, both zeolites preferred the adsorption of PHP isomers **I1** and **I4** over the adsorption of adamantane. The adsorption of adamantane was especially unfavorable on zeolite Beta. One may wonder whether the weak adsorption of adamantane in the mixture was caused by steric hindrance or by the lower molecular weight of adamantane. We, therefore, carried out simulations with pure adamantane at 1 bar. Even in that case, the amount of adsorbed adamantane was extremely low ( $q_{FAU}=0.70$  vs  $q_{Beta}=0.043$  molecules/nm<sup>3</sup>), which proves that steric hindrance is responsible of the low adsorption. We can, thus, safely conclude that C<sub>14</sub> alkyladamantanes would be even less adsorbed.

Furthermore, adsorption of the ring-shift isomer perhydroanthracene (**I1**) was more favored in zeolite BEA, in comparison to bulky molecules as isomer **I4**. These trends were confirmed by carrying out simulation with a mixture containing only isomers **I1** and **I4** (Table 3). The **I1/I4** selectivity was ca. 3.2 for BEA, but only 1.06 for FAU. We can, therefore, assume that the preferential adsorption of PHA in BEA is partially responsible for the abundant formation of this intermediate in zeolite Beta.

Table 2 further demonstrates that the PHP reactant is hardly adsorbed in the zeolite BEA, whereas the FAU is quite favorable for the adsorption of PHP.

Table 2. Quantity of molecules adsorbed per unit cell as a function of zeolite topology. Operating conditions were equivalent to that of catalytic tests: T=280°C, partial pressure of each component = 10 mbar, partial pressure of n-heptane = 8 bar.

Zeolite topology	PHP reactant	$q_i$ (molecule/nm <sup>3</sup> )			
		<b>A1</b> Adamantane	<b>I4</b> (PHP CC5)	<b>I1</b> (PHA)	n-C <sub>7</sub>
FAU	0.197	0.002	0.087	0.119	0.548
BEA	0.008	0	0.055	0.207	0.820

Table 3. Quantity of molecules adsorbed per unit cell as a function of zeolite topology. Operating conditions were equivalent to that of catalytic tests: T=280°C, partial pressure of each component = 10 mbar, partial pressure of n-heptane = 8 bar.

Zeolite topology	$q_i$ (molecule/ nm <sup>3</sup> )		Selectivity
	<b>I4</b> (PHP CC5)	<b>I1</b> (PHA)	<b>I1/I4</b>
FAU	0.310	0.328	1.06
BEA	0.215	0.684	3.18

The same approach was applied to ring-opening intermediates. At high PHP conversion, Beta zeolites processed mainly multibranched products (**R1**) and butyldecalin (**R6**) (Figure 13). In contrast, USY-based catalysts favored the opening of the central cycle of perhydrophenanthrene isomers, resulting in ring-opening products **R2** and **R3**.

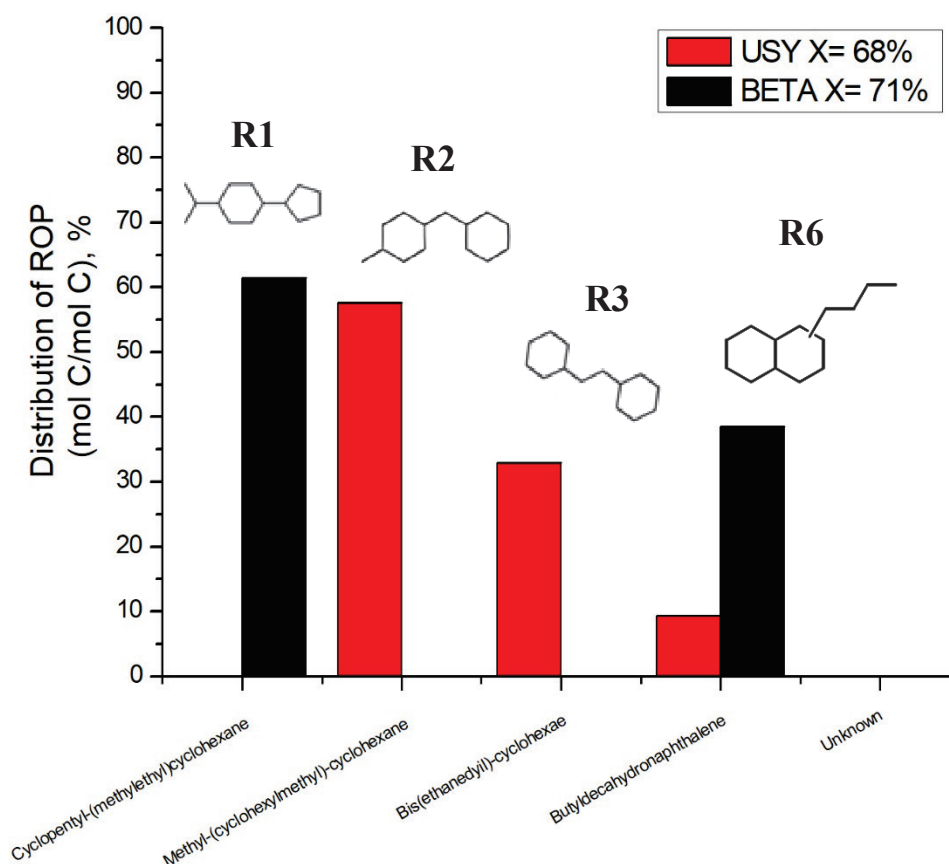


Figure 13. Distribution of ring-opening products at isoconversion over Pt/H-USY and Pt/H-BETA bifunctional catalysts.

Molecular simulations were performed by taking ring-opening intermediates **R1** and **R2** as probe molecules, as described in Table 4. Both ring-opening products could adsorb in both zeolites, the adsorption of **R2** being favored over the adsorption of **R1**. In FAU, the adsorption selectivity **R2**/ **R1** was 9.62. In BEA, the selectivity was only 0.842. The simulations do not explain why **R1** is absent in zeolite USY, while **R2** is absent in zeolite beta, but the tendency that the USY zeolite has a stronger preference for intermediate **R2** is reproduced.

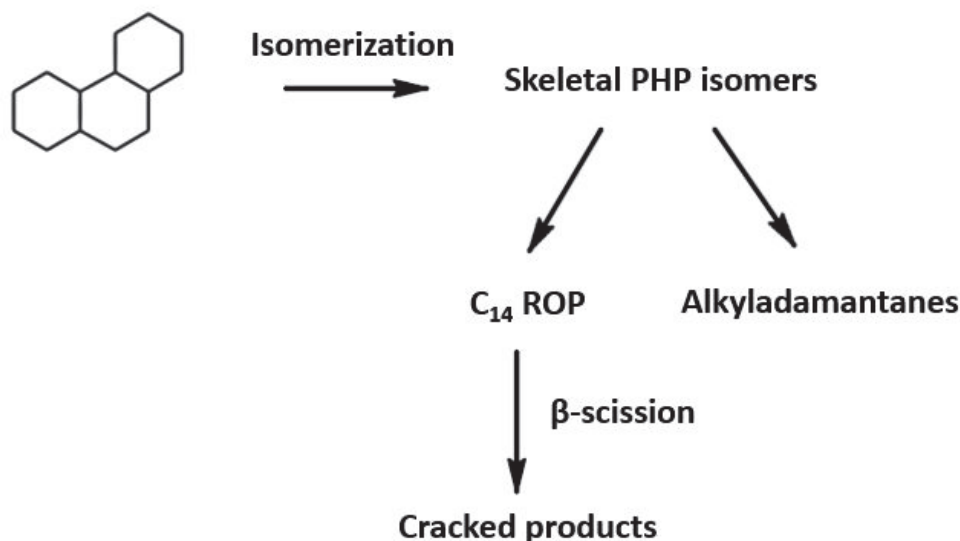
Table 4. Quantity of ring-opening products adsorbed per unit cell as a function of zeolite topology. Operating conditions were equivalent to that of catalytic tests: T=280°C, partial pressure of each component = 10 mbar

Zeolite topology	$q_i$ (molecule/nm <sup>3</sup> )		Selectivity
	<b>R1</b>	<b>R2</b>	<b>R2/R1</b>
FAU	0.016	0.154	9.62
BEA	0.404	0.340	0.842

## 4. Discussion

### 4.1. Attempts to rationalize hydrocracking pathways

Reaction pathways for hydrocracking of perhydrophenanthrene over Pt/H-Beta and Pt/ASA bifunctional catalysts were rationalized from the analysis of reaction product yields, together with the study of reaction intermediates, i.e. PHP isomers and ring-opening products, and cracked compounds. A global pathway and the reaction intermediates attributed to each catalyst are illustrated in Figure 14. USY zeolite-based catalysts were the most active among the solids tested, followed by Beta and ASA catalysts, irrespective of the zeolite loading in the alumina binder. ASA bifunctional catalyst gave the lowest activity constants even at higher temperature (300°C).



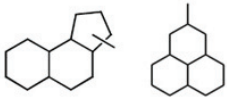
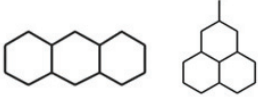
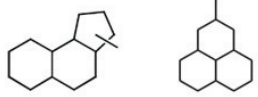
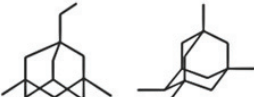
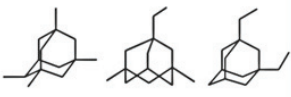
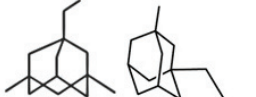
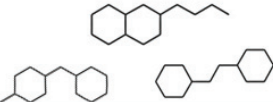
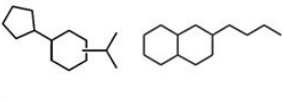
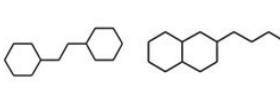
Intermediates	USY	Beta	ASA
Skeletal PHP isomers			
Alkyladamantanes			
ROP			
Cracked products	Distribution from C <sub>4</sub> to C <sub>10</sub> , with minima at C <sub>5</sub> and C <sub>9</sub>	C <sub>7</sub> is the dominating product	C <sub>7</sub> is the dominating product

Figure 14. Simplified reaction pathway for hydrocracking of perhydrophenanthrene over bifunctional Pt/H-Beta, Pt/H-USY zeolite catalysts and Pt/ASA catalyst. Reaction intermediates obtained on each catalyst are illustrated.

Isomerization to ring-shift and ring-contraction perhydrophenanthrene isomers was the primary reaction over the whole set of catalysts studied, followed by ring-opening and cracking or by the formation of alkyladamantanes (Figure 4). The proportion of alkyladamantanes within the family of PHP isomers increased with conversion, whereas the fraction of skeletal PHP isomers diminished. This result reveals the primary character of skeletal PHP isomers. Alkyladamantanes were not easily converted through hydrocracking to C<sub>10</sub> adamantanes and isobutane, which is coherent with their high thermodynamic stability. A detailed analysis on formation of alkyladamantanes starting from perhydrophenanthrene may be found in our previous work (Chapter II).

Cracking can only take place after opening of at least one cycle of skeletal PHP isomers. The yield of ring-opening products was very low over USY, Beta and ASA, indicating that cracking occurred rapidly after opening of a central or external cycle of PHP isomers.

Both zeolites and ASA-based catalysts generated similar isomerization intermediates on hydroconversion of perhydrophenanthrene, with different selectivities. Isomer **I3** (methylperhydrophenalene), formed after ring-shift of perhydrophenanthrene, was observed over the three solids throughout PHP conversion. Methylperhydrophenalenes are known to be important intermediates in the synthesis of alkyladamantanes [46,47]. In contrast, ring-contraction PHP isomer **I4** (Figure 6) was exclusively formed in the presence of USY and ASA. Its absence on zeolite beta had already been pointed out by Leite et al. [42]. Our molecular simulations show that the adsorption of **I4** in zeolite beta is quite unfavorable compared to more linear isomers. BEA adsorbed preferentially more linear structures, represented by perhydroanthracene stereoisomers. It is clear that shape-selectivity excluded the production of bulky molecules on Beta zeolites, due to their more strained pore system.

Molecular simulations showed that even unsubstituted adamantanes are not easily adsorbed in the micropores of USY and beta zeolites. Still, both zeolites produced significant amounts of alkyladamantanes, whereas ASA had a much lower selectivity to these products. At ca. 37% conversion, selectivity to alkyladamantanes on USY zeolite corresponded to 8% vs 3.4% on ASA catalyst. The low adamantane selectivity of ASA is coherent with previous work [40], where the hydroconversion of fluorene over Pt/ASA produced only very little adamantane products. This result is somewhat surprising, since ASA may accommodate large molecules as alkyladamantanes thanks to its large pore size (pore diameter of 70-80 Å). On the other hand, the easiness to generate alkyladamantanes in USY zeolites was previously attributed to the presence of supercages of 7.4 Å diameter, which corresponds to Van der Waals diameter of non-substituted adamantane [40,48], but our simulations do not confirm that hypothesis of a good fit. We may infer from our results that a large pore size is not a sufficient criterion to form alkyladamantanes. The weak acid sites in amorphous silica-alumina are apparently not good catalysts for adamantane formation. Their production might be favored on the more strongly acidic zeolites, although the very bulky molecules cannot be easily accommodated in the micropores, in particular for zeolite beta. This allows us to assume that alkyladamantanes formation probably takes place in the pore mouths.

In spite of zero adsorption of adamantanes in zeolite BEA (according to the simulations), at high levels of perhydrophenanthrene conversion, the selectivity to alkyladamantanes over Pt/H-Beta and Pt/H-USY bifunctional catalysts corresponded to ca. 10% and 20%,

respectively, in a carbon molar basis (Figures 4 and 5). The higher alkyladamantanes selectivity of USY vs. Beta is coherent with the literature. In a previous study, Rolmann and coworkers compared the effectiveness to convert perhydrofluorene, a tricyclic naphthene, to trimethyladamantanes over Pt or Pd/USY and Pt or Pd/Beta zeolite catalysts. At similar operating conditions, the yield of alkyladamantanes obtained over USY-based catalysts corresponded to 27%, whereas a yield of only 3% was acquired with Beta zeolites. In a similar work, Wang *et al.* studied the hydroconversion of fluorene on Pt-supported catalysts. Higher yield of perhydrophenalene, precursors of alkyladamantanes, and propyladamantanes were obtained over USY zeolite, in comparison to Beta. Figure 6 illustrates the distribution of skeletal PHP isomers at isoconversion on Pt-supported catalysts. As aforementioned, methylperhydrophenalene is an important intermediate for the production of alkyladamantanes. Methylperhydrophenalene isomers accumulated within the skeletal PHP isomers fraction over Beta zeolites, while they were consumed on USY zeolites to generate alkyladamantanes or ring-opening products. It is likely that Beta zeolites did not easily convert such intermediates, hindering the further isomerization of methylperhydrophenalene to alkyladamantanes on their pores.

In order to explain the formation of cracked products, it is necessary to analyze pathways of hydrocracking of ring-opening products resulting from hydroconversion of perhydrophenanthrene over Pt/H-Beta and Pt/ASA bifunctional catalysts. Hydrocracking pathways over Pt/H-USY were exhaustively studied in our previous work (Chapter II). Ring-opening products processed over ASA-based catalysts mainly comprised structures **R3** and **R6**. No formation of C<sub>10</sub> compounds, followed by C<sub>4</sub> isoalkanes, was observed among reaction products over the amorphous catalyst, suggesting that butyldecalin (**R6**) did not undergo hydrocracking over Pt/ASA. A major cracking to C<sub>7</sub> naphthenes was favored at all PHP conversion levels, according to the yield of cracked products presented in Figure 9. A hydrocracking pathway of intermediate **R3** is depicted in Figure 15. Cleavage involved tertiary and secondary carbocations before and after scission, respectively. The same intermediate was produced over Pt/H-USY zeolite catalyst.

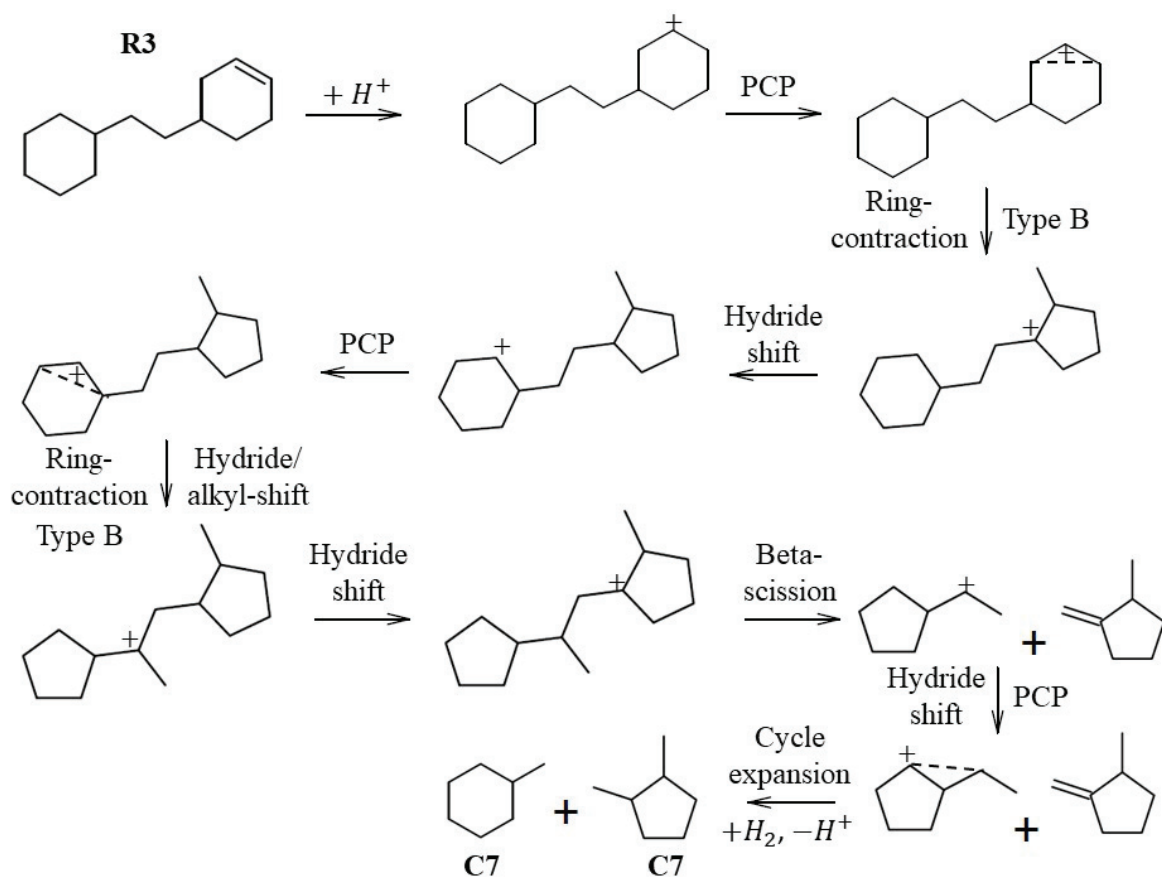


Figure 15. Suggested hydrocracking pathway to C<sub>7</sub> naphthenes of ring-opening product (R3) originated from hydroconversion of skeletal perhydrophenanthrene isomers over Pt/ASA catalyst. The pathway shows subsequent steps to dehydrogenation over the metal sites.

Beta zeolites processed mainly structures **R1**, **R4** and **R6**, according to the distribution presented in Figure 8. The cracking of butyldecalin (**R6**) to C<sub>10</sub> naphthenes, represented by decalin and its isomers, and isobutane is observed at high PHP conversion (Figure 16).



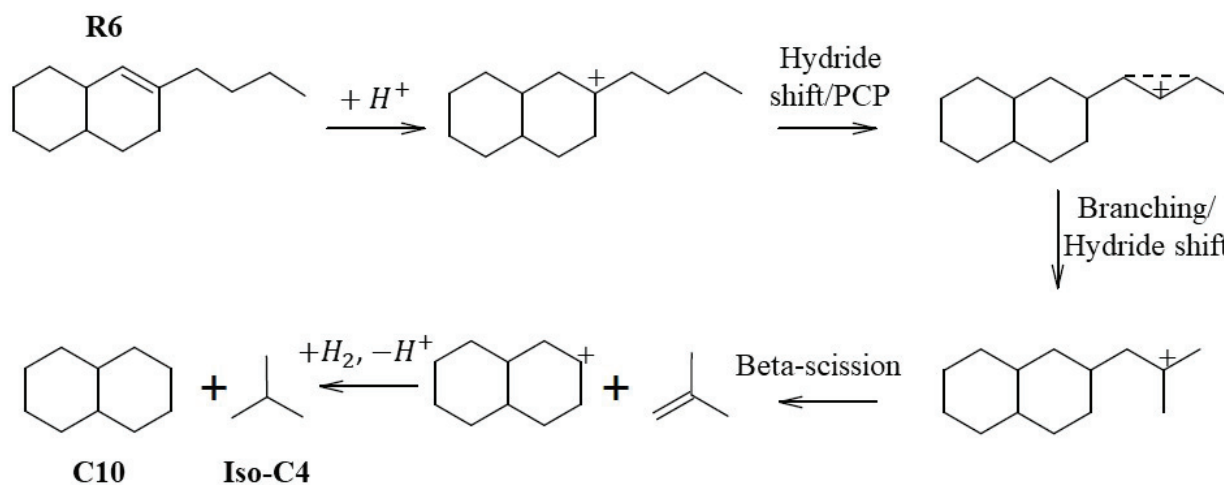


Figure 16. Suggested hydrocracking pathway to C<sub>10</sub> naphthenes and isobutane of ring-opening product (R6) originated from hydroconversion of skeletal perhydrophenanthrene isomers over Pt/H-Beta zeolite catalyst.

We tried to construct reaction pathways for the cracking of intermediates **R1** and **R4** to C<sub>7</sub> naphthenes, the main products over Pt/H-Beta zeolite catalysts (Figure 17, A and B). Several rearrangements, including a slow step of ring-contraction (type B isomerization) were necessary to achieve a configuration allowing fast beta-scission. In both cases, cracking leading to C<sub>6</sub> and C<sub>8</sub> was more easily obtained through exocyclic alkylshifts, generating dimethylcyclopentanes and ethylcyclohexanes. In spite of the apparent easiness to form C<sub>6</sub> and C<sub>8</sub>, they were only observed at high PHP conversion, in contrast to C<sub>7</sub> naphthenes, which were major reaction products. We infer that both **R1** and **R4** intermediates were not predominantly cracked on Pt/H-Beta bifunctional catalyst. In addition, cracking of ring-opening **R2** and **R3** intermediates on Pt/H-USY led to primary production of dibranched C<sub>7</sub> naphthenes, in contrast to Pt/H-Beta zeolite catalysts.

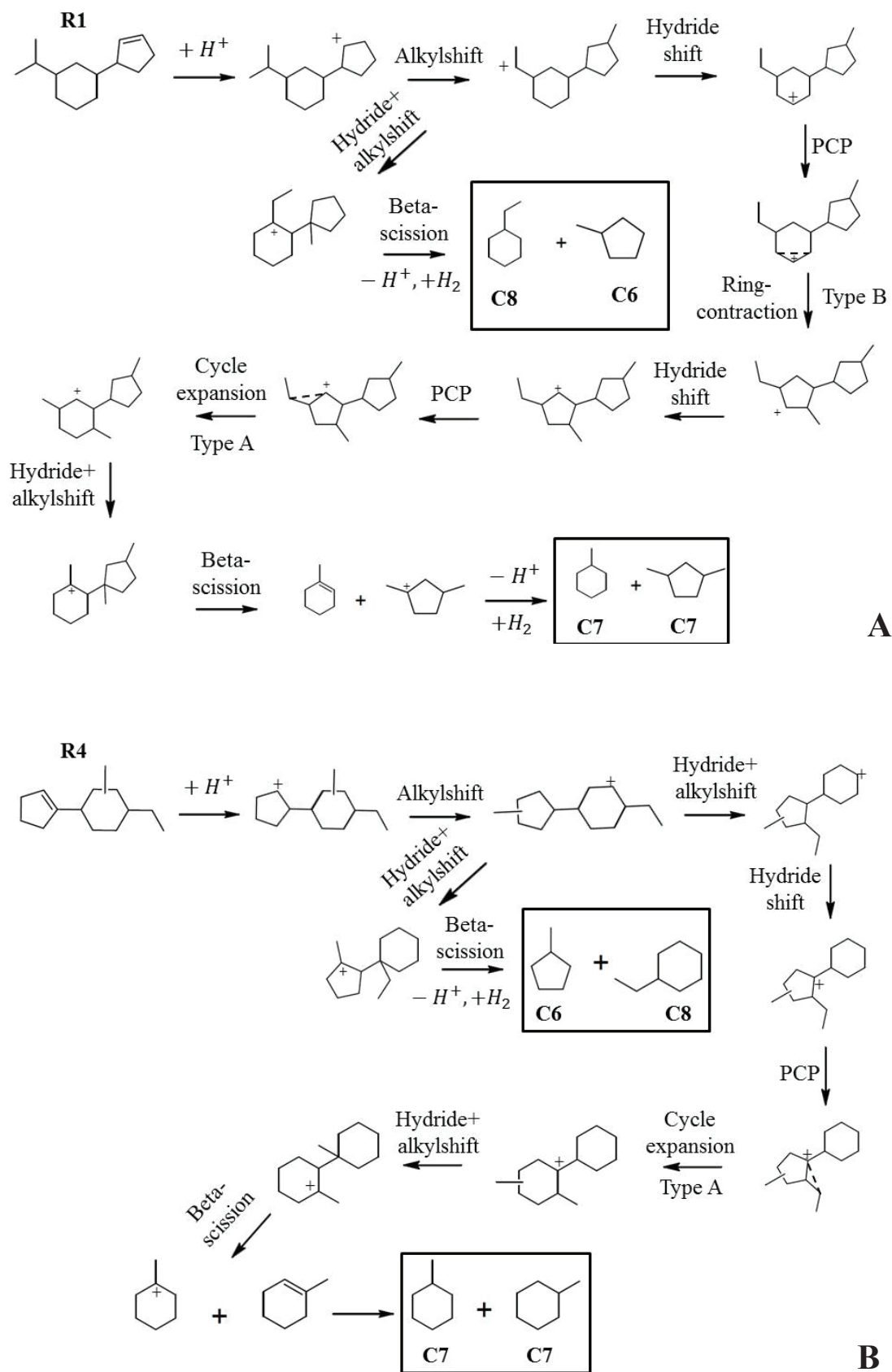


Figure 17. A) Suggested hydrocracking pathway to C<sub>7</sub> (major products), C<sub>6</sub> and C<sub>8</sub> naphthenes resulting from

hydroconversion of ring-opening intermediate **R1** over Pt/H-Beta zeolite catalyst. B) Suggested hydrocracking pathway to C<sub>7</sub> (major products), C<sub>6</sub> and C<sub>8</sub> naphthenes resulting from hydroconversion of ring-opening intermediate **R4** over Pt/H-Beta zeolite catalyst.

Preferential cracking to C<sub>7</sub> naphthenes over Beta zeolites can be rationalized from the fast consumption of **R2** intermediate. The distribution of ROP (Figures 8 and 13) shows that R2 accounts for ca. 10% of the distribution at low PHP conversion, and its content decreases to virtually zero at high PHP conversion. Besides, the simulations pointed out an equilibrated adsorption of intermediates **R1** and **R2** on BEA structure, therefore it is likely that the formation of either **R1** or **R2** ring-opening products is favored over Beta-supported catalysts. **R2** intermediates can easily lead to C<sub>7</sub> naphthenes as cracked products, after alkylshift promoting a fast tertiary-tertiary beta-scission, as illustrated in Figure 18. This constitutes then the main hydrocracking pathway over Pt/H-Beta zeolite catalyst and it is in accordance with the exclusive formation of methylcyclohexane as primary C<sub>7</sub> products on Beta zeolites, as indicated in Figure 11.

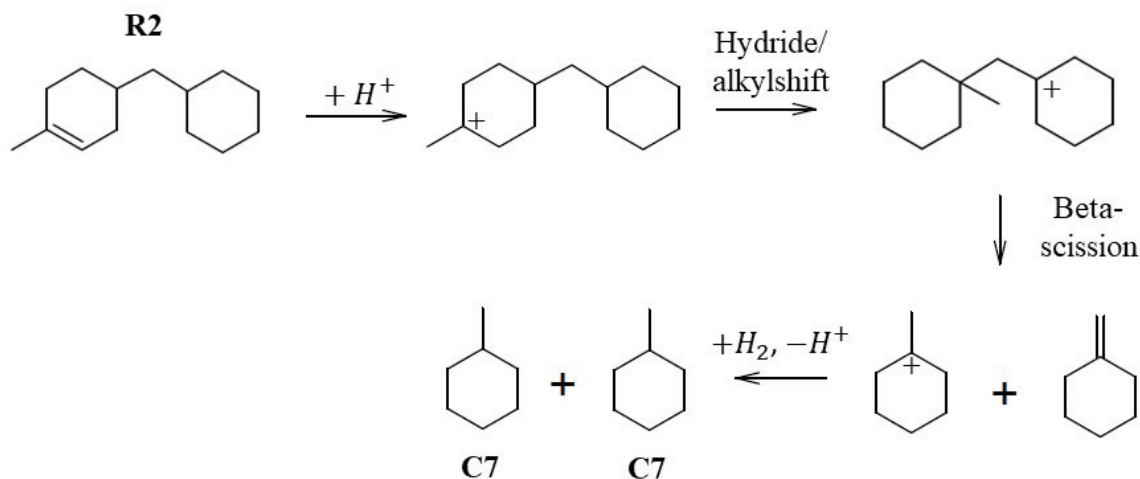


Figure 18. Suggested hydrocracking pathway to C<sub>7</sub> naphthenes of ring-opening product **R2** originated from hydroconversion of skeletal perhydrophenanthrene isomers over Pt/H-USY zeolite catalyst.

## 5. Conclusions

Hydroisomerization and hydrocracking of perhydrophenanthrene were performed over Pt/H-Beta and Pt/ASA bifunctional catalysts and compared to results obtained with Pt/H-USY zeolite catalyst, under the same operating conditions. The common reaction pathway consisted of converting the reactant into skeletal perhydrophenanthrene isomers, which were further transformed into substituted adamantanes or ring-opening products. The latter underwent hydrocracking, unlike alkyladamantanes, which are very stable compounds.

Shape selectivity effects were evidenced by comparing the large-pore zeolites and ASA at isoconversion. Thanks to their pore system, USY zeolites and ASA were more suitable to process bulky molecules, such as ring-contraction isomers of perhydrophenanthrene. Beta zeolites favored the conversion of linear structures, as perhydroanthracene stereoisomers, and were less effective to convert methylperhydrophenalene isomers, important precursors of alkyladamantanes.

Despite of the presence of mesopores, ASA catalysts did not favor the formation of alkyladamantanes, due to their poor acidity. The simulations indicated a hindered adsorption of adamantanes on FAU and BEA topologies. Therefore, the high selectivity to the bridged isomers over both zeolites cannot be attributed to the pore system of either USY or Beta catalysts. It seems that pore-mouth catalysis is crucial to attain further isomerization of perhydrophenanthrene to alkyladamantanes.

Beta zeolites processed mainly cyclopentyl-cyclohexane as ring-opening products, whereas bicyclohexyl-like compounds, i.e. ring-opening intermediates favored on USY zeolites, accounted for a low proportion within ring-opening products at low PHP conversion and were absent at high PHP conversion. On the other hand, simulation results indicated a more equilibrated adsorption of ring-opening products on BEA topology. The preferential cracking to C<sub>7</sub> naphthenes over Pt/H-Beta was rationalized from fast beta-scission (tertiary-tertiary) of substituted bicyclohexyl- intermediates, whereas more branched ROP accumulated at high PHP conversion. ASA catalysts also favored cracking to C<sub>7</sub> naphthenes, with hydrocracking pathways similar to the ones suggested for Pt/H-USY zeolite catalyst.

USY-based catalysts were the most active among the solids tested, whereas the ASA support resulted in lower conversion degrees of perhydrophenanthrene compared to both zeolites, even at higher temperature. Molecular simulation pointed out a weak adsorption of PHP reactant on the pores of BEA structure, which strongly correlates with the order of activity of USY and Beta zeolites on hydroconversion of perhydrophenanthrene.

## REFERENCES

- [1] M.S. Rana, V. Sámano, J. Ancheyta, Diaz, J. A. I., A review of recent advances on process technologies for upgrading of heavy oils and residua, Special Issue: Mexican Congress on Chemical Reaction Engineering 2006 86 (2007) 1216–1231.
- [2] G. Valavarasu, M. Bhaskar, K.S. Balaraman, Mild hydrocracking - A review of the process, catalysts, reactions, kinetics, and advantages, *Pet. Sci. Technol.* 21 (2003) 1185–1205.
- [3] Bloomingdale, IL, US (Wang, Li), Hydrocracking Catalyst Containing Beta and Y Zeolites, and Process for its use to make Distillate.
- [4] A. Corma, M.J. Diaz-Cabanas, C. Lopez, A. Martinez, Hydrocracking catalysts based on the new large-pore ITQ-21 zeolite for maximizing diesel products, *Stud Surf Sci Catal* 154 (2004) 2380–2386.
- [5] A. Chica, A. Corma, Comparison of large pore zeolites for n-octane hydroisomerization: Activity, selectivity and kinetic features, *Chem-Ing-Tech* 79 (2007) 857–870.
- [6] Degnan, ThomasF, Jr., Applications of zeolites in petroleum refining, *Top Catal* 13 (2000) 349–356.
- [7] W.M. Zhang, P.G. Smirniotis, Effect of zeolite structure and acidity on the product selectivity and reaction mechanism for n-octane hydroisomerization and hydrocracking, *J. Catal.* 182 (1999) 400–416.
- [8] M.A. Ali, T. Tatsumi, T. Masuda, Development of heavy oil hydrocracking catalysts using amorphous silica-alumina and zeolites as catalyst supports, *Appl Catal a-Gen* 233 (2002) 77–90.
- [9] K. Sato, Y. Nishimura, K. Honna, N. Matsubayashi, H. Shimada, Role of HY Zeolite Mesopores in Hydrocracking of Heavy Oils, *Journal of Catalysis* 200 (2001) 288–297.
- [10] H.W. Haynes, J.F. Parcher, N.E. Helmer, Hydrocracking Polycyclic Hydrocarbons over a Dual-Functional Zeolite (Faujasite)-Based Catalyst, *Ind. Eng. Chem. Process Des. Dev.* 22 (1983) 401.
- [11] V.Y. Pereyma, P.P. Dik, O.V. Klimov, S.V. Budukva, K.A. Leonova, A.S. Noskov, Hydrocracking of vacuum gas oil in the presence of catalysts NiMo/Al<sub>2</sub>O<sub>3</sub>-amorphous

- aluminosilicates and NiW/Al<sub>2</sub>O<sub>3</sub>-amorphous aluminosilicates, *Russ J Appl Chem* 88 (2015) 1969–1975.
- [12] C.-E. Hédoire, C. Louis, A. Davidson, M. Breyse, F. Maugé, M. Vrinat, Support effect in hydrotreating catalysts: hydrogenation properties of molybdenum sulfide supported on  $\beta$ -zeolites of various acidities, *Journal of Catalysis* 220 (2003) 433–441.
- [13] N. Guernalec, T. Cseri, P. Raybaud, C. Geantet, M. Vrinat, Influence of H<sub>2</sub>S on the hydrogenation activity of relevant transition metal sulfides, *Catal Today* 98 (2004) 61–66.
- [14] N. Guernalec, C. Geantet, T. Cseri, M. Vrinat, H. Toulhoat, P. Raybaud, Compensation effect and volcano curve in toluene hydrogenation catalyzed by transition metal sulfides, *Dalton Trans.* 39 (2010) 8420–8422.
- [15] A. Soualah, J.L. Lemberon, L. Pinard, M. Chater, P. Magnoux, K. Mojord, Hydroisomerization of long-chain n-alkanes on bifunctional Pt/zeolite catalysts, *Appl Catal a-Gen* 336 (2008) 23–28.
- [16] M. Roussel, J.L. Lemberon, M. Guisnet, T. Cseri, E. Benazzi, Mechanisms of n-decane hydrocracking on a sulfided NiW on silica-alumina catalyst, *J. Catal.* 218 (2003) 427–437.
- [17] J. Weitkamp, Catalytic Hydrocracking-Mechanisms and Versatility of the Process, *ChemCatChem* 4 (2012) 292–306.
- [18] T. Dutriez, M. Courtiade, D. Thiébaud, H. Dulot, F. Bertoncini, J. Vial, M.-C. Hennion, High-temperature two-dimensional gas chromatography of hydrocarbons up to nC<sub>60</sub> for analysis of vacuum gas oils, *Journal of chromatography. A* 1216 (2009) 2905–2912.
- [19] R. Nageswara Rao, N. You, S. Yoon, D.P. Upare, Y.-K. Park, C.W. Lee, Selective Ring Opening of Methylcyclopentane and Methylcyclohexane Over Iridium Bifunctional Catalysts Supported on Surface Modified  $\gamma$ -Al<sub>2</sub>O<sub>3</sub>, SiO<sub>2</sub> and Ultra Stable Y Zeolites, *Catal Lett* 141 (2011) 1047–1055.
- [20] H. Ziaei-Azad, A. Sayari, Bifunctional MCM-41 aluminosilicate supported Ir with adjusted metal and acid functionality for catalytic ring opening of 1,2-dimethylcyclohexane, *Journal of Catalysis* 344 (2016) 729–740.
- [21] S. Mignard, N. Marchal-George, Décyclisation du méthylcyclohexane en des conditions d'hydroconversion sur des catalyseurs de type Pt/USY influence du rapport H/A., 1995.
- [22] E. Gutierrez-Acebo, C. Leroux, C. Chizallet, Y. Schuurman, C. Bouchy, Metal/Acid Bifunctional Catalysis and Intimacy Criterion for Ethylcyclohexane Hydroconversion, *ACS Catal.* 8 (2018) 6035–6046.
- [23] S.A. D'Ippolito, C. Especel, L. Vivier, F. Epron, C.L. Pieck, Influence of the Brønsted acidity, SiO<sub>2</sub>/Al<sub>2</sub>O<sub>3</sub> ratio and Rh–Pd content on the ring opening. Part II. Selective ring opening of methylcyclohexane, *Applied Catalysis A: General* 469 (2014) 541–549.
-

- [24] J. Weitkamp, S. Ernst, Comparison Of The Reactions Of Ethylcyclohexane And 2-Methylheptane On Pd/Lay Zeolite, in: B. Imelik, C. Naccache, G. Coudurier, Y. Ben Taarit, J.C. Vedrine (Eds.), *Catalysis by Acids and Bases*, Elsevier, 1985, pp. 419–426.
- [25] P.S.F. Mendes, F.M. Mota, J.M. Silva, M.F. Ribeiro, A. Daudin, C. Bouchy, A systematic study on mixtures of Pt/zeolite as hydroisomerization catalysts, *Catal. Sci. Technol.* 7 (2017) 1095–1107.
- [26] R. Kenmogne, A. Finiels, C. Cammarano, V. Hulea, F. Fajula, Hydroconversion of n-hexadecane over bifunctional microporous and mesoporous model catalysts. Influence of pore architecture on selectivity, *Journal of Catalysis* 329 (2015) 348–354.
- [27] N. Batalha, L. Pinard, C. Bouchy, E. Guillon, M. Guisnet, n-Hexadecane hydroisomerization over Pt-HBEA catalysts. Quantification and effect of the intimacy between metal and protonic sites, *Journal of Catalysis* 307 (2013) 122–131.
- [28] F. Alvarez, G. Giannetto, M. Guisnet, G. Perot, Hydroisomerization and hydrocracking of n-Alkanes. 2. n-Heptane transformation on a Pt-dealuminated Y zeolite - comparison with a Pt-Y zeolite, *Appl Catal* 34 (1987) 353–365.
- [29] G.E. Giannetto, G.R. Perot, M.R. Guisnet, Hydroisomerization and hydrocracking of n-alkanes. 1. Ideal hydroisomerization PtHY catalysts, *Ind. Eng. Chem. Prod. Res. Dev.* 25 (1986) 481–490.
- [30] F. Alvarez, F.R. Ribeiro, G. Giannetto, F. Chevalier, G. Perot, M. Guisnet, Hydroisomerization and Hydrocracking of Alkanes. 5. Hydroisomerization and Hydrocracking of N-Hexane and N-Heptane on Pt-HY Catalysts. Effect of the Distribution of Metallic and Acid Sites, in: A. Galarneau, F. Fajula F. Di Renzo, J. Vedrine (Eds.), *Studies in Surface Science and Catalysis*, Elsevier, 2001, pp. 1339–1348.
- [31] N. Batalha, L. Pinard, Y. Pouilloux, M. Guisnet, Bifunctional Hydrogenating/Acid Catalysis, *Catal. Lett.* 143 (2013) 587–591.
- [32] G. Burnens, C. Bouchy, E. Guillon, J.A. Martens, Hydrocracking reaction pathways of 2,6,10,14-tetramethylpentadecane model molecule on bifunctional silica-alumina and ultrastable Y zeolite catalysts, *J. Catal.* 282 (2011) 145–154.
- [33] M.C. Claude, J.A. Martens, Monomethyl-branching of long n-alkanes in the range from decane to tetracosane on Pt/H-ZSM-22 bifunctional catalyst, *J. Catal.* 190 (2000) 39–48.
- [34] J. Weitkamp, P.A. Jacobs, J.A. Martens, Isomerization and hydrocracking of C<sub>9</sub> through C<sub>16</sub> n-alkanes on Pt/HZSM-5 zeolite, *Appl Catal* 8 (1983) 123–141.
- [35] S.C. Korre, M.T. Klein, R.J. Quann, Polynuclear Aromatic Hydrocarbons Hydrogenation. 1. Experimental Reaction Pathways and Kinetics, *Ind. Eng. Chem. Res.* 34 (1995) 101–117.
- [36] T. Isoda, S. Maemoto, K. Kusakabe, S. Morooka, Hydrocracking of Pyrenes over a Nickel-Supported Y-Zeolite Catalyst and an Assessment of the Reaction Mechanism Based on MD Calculations, *Energy Fuels* 13 (1999) 617–623.
-



- [37] Arunas T. Lapinas, Michael T. Klein and Bruce C. Gates, Catalytic Hydrogenation and Hydrocracking of Fluorene: Reaction Pathways, Kinetics, and Mechanisms, *Ind. Eng. Chem. Res.* 30 (1991) 42–50.
- [38] Lorraine Leite, Eric Benazzi, Nathalie Marchal-George, Hydrocracking of phenanthrene over bifunctional Pt catalysts, *Catalysis Today* 65 (2001) 241–247.
- [39] S.-U. Lee, Y.-J. Lee, J.-R. Kim, E.-S. Kim, T.-W. Kim, H.J. Kim, C.-U. Kim, S.-Y. Jeong, Selective ring opening of phenanthrene over NiW-supported mesoporous HY zeolite catalyst depending on their mesoporosity, *Materials Research Bulletin* 96 (2017) 149–154.
- [40] L. Wang, Y. Chen, S. Jin, X. Chen, C. Liang, Selective Ring-Shift Isomerization in Hydroconversion of Fluorene over Supported Platinum Catalysts, *Energy Fuels* 30 (2016) 3403–3412.
- [41] E. Benazzi, L. Leite, N. Marchal-George, H. Toulhoat, P. Raybaud, New insights into parameters controlling the selectivity in hydrocracking reactions, *Journal of Catalysis* 217 (2003) 376–387.
- [42] L. Leite, Etude sur molecule modèle des paramètres régissant la sélectivité des catalyseurs d'hydrocraquage des charges lourdes, 2000.
- [43] P.S.F. Mendes, J.M. Silva, M.F. Ribeiro, A. Daudin, C. Bouchy, From powder to extrudate zeolite-based bifunctional hydroisomerization catalysts, *Journal of Industrial and Engineering Chemistry* 62 (2018) 72–83.
- [44] B. Smit, T.L.M. Maesen, Towards a molecular understanding of shape selectivity, *Nature* 451 (2008) 671–678.
- [45] P. Bai, M.Y. Jeon, L. Ren, C. Knight, M.W. Deem, M. Tsapatsis, J.I. Siepmann, Discovery of optimal zeolites for challenging separations and chemical transformations using predictive materials modeling, *Nature communications* 6 (2015) 5912.
- [46] A. Schneider, R. W. Warren, and E. J. Janoski, Formation of Perhydrophenalenes and Polyalkyladamantanes by Isomerization of Tricyclic Perhydroaromatics, *J. Org. Chem* 31 (1966) 1617–1625.
- [47] M.A. McKerverey, Adamantane rearrangements, *Chem. Soc. Rev.* 3 (1974) 479.
- [48] L.D. Rollmann, L.A. Green, R.A. Bradway, H.K.C. Timken, Adamantanes from petroleum with zeolites, *Catalysis Today* 31 (1996) 163–169.



## Supporting Information

Figure S1

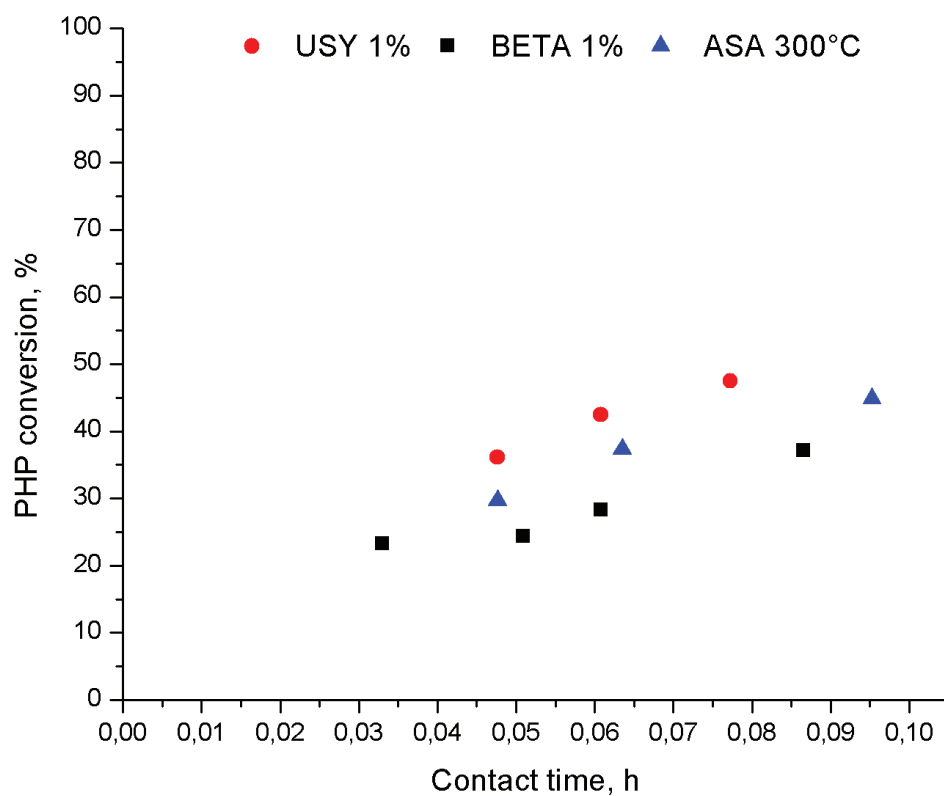


Figure S 1. Evolution of perhydrophenanthrene conversion with contact time on Pt/H-USY, Pt/H-BETA catalysts with 1 wt.% zeolite in alumina binder at 280°C; and Pt/ASA (at 300°C) bifunctional catalysts.



---

## TABLE OF FIGURES – CHAPTER IV

---

<b>Figure 1.</b> GCxGC-FID analysis of reaction products from hydroconversion of octylcyclohexane obtained over Pt/H-USY zeolite catalyst at 71% conversion. ....	132
<b>Figure 2.</b> Molecule families and typical examples of molecules in the reaction products of hydroconversion of octylcyclohexane over Pt/H-USY zeolite catalyst.....	134
<b>Figure 3.</b> Evolution of octylcyclohexane conversion with contact time on Pt/H-USY extrudate catalyst with 1 wt.% zeolite in alumina binder. ....	135
<b>Figure 4.</b> Selectivity to isomerization, ring-opening and cracked products as a function of octylcyclohexane conversion over Pt/H-USY zeolite catalyst.....	136
<b>Figure 5.</b> Distribution of positional and ring-contraction isomers of octylcyclohexane over Pt/H-USY bifunctional catalyst.....	137
<b>Figure 6.</b> Yield of cracked products according to the number of carbon atoms at different levels of octylcyclohexane conversion over Pt/H-USY zeolite catalyst. ....	138
<b>Figure 7.</b> Distribution of cracked products as a function of octylcyclohexane conversion over bifunctional Pt/H-USY zeolite catalyst.....	139
<b>Figure 8.</b> Distribution of cracked naphthenes as a function of octylcyclohexane conversion over bifunctional Pt/H-USY zeolite catalyst.....	139
<b>Figure 9.</b> A) Distribution of C <sub>6</sub> naphthenes as a function of octylcyclohexane conversion over bifunctional Pt/H-USY zeolite catalyst. B) Distribution of C <sub>7</sub> naphthenes as a function of octylcyclohexane conversion over bifunctional Pt/H-USY zeolite catalyst. ....	140
<b>Figure 10.</b> Distribution of C <sub>8</sub> naphthenes as a function of octylcyclohexane conversion over bifunctional Pt/H-USY zeolite catalyst.....	141
<b>Figure 11.</b> Distribution of C <sub>9</sub> naphthenes as a function of octylcyclohexane conversion over bifunctional Pt/H-USY zeolite catalyst.....	142
<b>Figure 12.</b> Distribution of C <sub>10</sub> naphthenes as a function of octylcyclohexane conversion over bifunctional Pt/H-USY zeolite catalyst.....	143
<b>Figure 13.</b> Distribution of alkanes as a function of octylcyclohexane conversion over bifunctional Pt/H-USY zeolite catalyst.....	144
<b>Figure 14.</b> A) Distribution of C <sub>6</sub> isoalkanes as a function of octylcyclohexane conversion over bifunctional Pt/H-USY zeolite catalyst. B) Distribution of C <sub>8</sub> isoalkanes as a function of octylcyclohexane conversion over bifunctional Pt/H-USY zeolite catalyst. ....	144
<b>Figure 15.</b> Suggested reaction pathway for isomerization of octylcyclohexane towards methyl-heptylcyclohexane ( <b>12</b> ) over Pt/H-USY zeolite catalyst, in accordance with Souverijns <i>et al.</i> ....	147

---

## TABLE OF FIGURES – CHAPTER IV

---

<b>Figure 16.</b> A) Suggested reaction pathway for isomerization of octylcyclohexane towards isomer <b>I4</b> starting from methyl-heptylcyclohexane ( <b>I2</b> ) over Pt/H-USY zeolite catalyst. B) Suggested reaction pathway for isomerization of octylcyclohexane towards isomer <b>I6</b> starting from structure i-C14 over Pt/H-USY zeolite catalyst.....	149
<b>Figure 17.</b> Yield of cracked products per 100 mol of cracked products resulting from hydroconversion of octylcyclohexane over bifunctional Pt/H-USY zeolite catalyst. Values indicated in the graph correspond to total yield of cracked products per 100 mol of cracked molecules. ....	151
<b>Figure 18.</b> Suggested cracking pathway towards formation of methylcyclohexane and isoheptane from hydroconversion of octylcyclohexane over Pt/H-USY zeolite catalyst. ....	152
<b>Figure 19.</b> Suggested cracking pathway towards formation of structure C10-5 and isobutane from hydrocracking of <b>I5</b> isomer over Pt/H-USY zeolite catalyst. ....	153
<b>Figure 20.</b> Suggested cracking pathway towards formation of structure <b>C9-3</b> and methylbutane from hydrocracking of <b>I6</b> isomer over Pt/H-USY zeolite catalyst.....	154
<b>Figure 21.</b> A) Suggested cracking pathway towards formation of methyl-ethylcyclopentane and methylpentane from hydrocracking of <b>I6</b> isomer over Pt/H-USY zeolite catalyst. B) Suggested cracking pathway towards formation of ethylcyclohexane and methylpentane from hydrocracking of <b>I8</b> isomer over Pt/H-USY zeolite catalyst.....	155
<b>Figure 22.</b> Reaction pathways and isomers that may lead to observed cracked compounds. ....	157

---

# CHAPTER IV: HYDROCONVERSION OF OCTYLCYCLOHEXANE OVER BIFUNCTIONAL Pt/H- USY ZEOLITE CATALYST

---

## Highlights

- Distribution of isomers and cracked products explained according to the degree of branching of reaction intermediates.
- Less branched isomers are more likely to crack, while multibranched structures accumulate within the isomers fraction.

## Abstract

Hydroisomerization and hydrocracking of octylcyclohexane ( $C_{14}H_{28}$ ), obtained after *in situ* hydrogenation of the parent aromatic compound, phenyloctane ( $C_{14}H_{22}$ ), on a Pt/ $Al_2O_3$  pre-catalyst, were performed over a bifunctional Pt/H-USY zeolite catalyst, at 300°C, 60 bar and a molar ratio  $H_2/HC$  of 7 mol/mol. The reaction products were identified and quantified with GCxGC-FID/MS and then lumped into families according to carbon number and chemical similarity. Reaction pathways leading to isomers and cracked products were studied in detail. A mechanistic analysis suggests that, despite the formation of multibranched isomers, the conversion of less branched structures would be the preferential route to generate cracked products on Pt/H-USY zeolite catalyst.

**Keywords:** octylcyclohexane, hydroisomerization, hydrocracking, substituted naphthenes, bifunctional catalysis, ultrastable Y zeolite

## 1. Introduction

Hydrocracking is a versatile process allowing the conversion of heavy oil fractions, mainly represented by Vacuum gas oil (VGO), to desired products, as diesel and jet fuel [1–3]. VGO cuts are rich in cyclic molecules, i.e. aromatics and naphthenes, in addition to aliphatic hydrocarbons [4,5]. Hydroconversion mechanisms of alkanes have been exhaustively reported in literature [6–14] and follow a bifunctional pathway [15–17] over metal supported zeolite or amorphous-based catalysts. These steps comprise dehydrogenation of the feed over the metal sites of the bifunctional catalyst, diffusion of the generated olefin towards its acidic sites, rearrangements and cracking of the reaction intermediate over the acidic support, and diffusion of the isomerized or cracked species towards the metallic sites of the catalyst, where they undergo hydrogenation. In the absence of shape-selectivity effects, i.e. for large pore zeolite catalysts, the rates of isomerization and cracking steps of alkanes depend on the stability of the carbocation-like transition states. The product distribution can, thus, be fairly well rationalized/predicted from the rules of carbocation chemistry. This also holds true for long-chain alkanes, which are within or close to the VGO boiling range [12,18–21].

The hydrocracking chemistry of heavy naphthenes has been much less studied than that of long-chain alkanes. Several practical limitations restrict the size and type of naphthenic molecules that can be employed in a model system. Most hydrocracking studies of cyclic molecules concerned naphthenes presenting two cycles or less [22–27]. It has been shown that such molecules undergo the same reactions as alkanes, e.g. isomerization and cracking [16,28–30].

Rearrangements of the naphthenic cycle comprise alkyl-shifts, ring-contraction or expansion, which may change the degree of branching of the molecule. Naphthenes may contract or expand their cycle through a cyclic Protonated CycloPropane (PCP) intermediate. This transition state is also involved in alkyl-shifts that take place around the cycle (endocyclic alkyl-shifts) and move towards the substituent alkyl-chain (exocyclic alkyl-shifts). Finally, there is also a possibility of creating a branching directly in the alkyl-chain through the PCP intermediate. The composite activation energy of these reaction rearrangements were reported in literature [31].

Monocyclic naphthenes undergo isomerization of the cycle, i.e. ring-contraction or expansion, without opening it. The opening of the unique ring of a monocyclic naphthene is considered to be a difficult step, due to orbital hindrance [32]. The main consequence of this strained reaction is that a substituted monocyclic naphthene undergoes isomerization of its ring or of its alkyl-chains until a favored configuration to fast beta-scission is achieved. This effect has been verified for naphthenes containing 9 to 12 carbon atoms and it is called “paring” reaction. Egan and coworkers observed, e.g., that a substituted C<sub>10</sub> naphthene would crack selectively to cyclic C<sub>6</sub> (cyclohexane or methylcyclopentane) and isobutane [33], irrespective of the native naphthene configuration. In addition, Souverijns *et al.* studied the hydroisomerization of a C<sub>14</sub> naphthene, octylcyclohexane, over Pt/H-USY bifunctional catalyst [34]. The distribution of isomers indicated that branching was kinetically favored in positions close to the ring. These results strongly suggested that branching of the cycle, formed through ring-contraction, was faster than chain branching. The generated branching would then propagate towards the alkyl-substituent.

Another interesting point resulting from “paring” reactions is the formation of compounds presenting different degrees of branching, starting from a monobranched molecule. The degree of branching is designated by the number of tertiary and quaternary carbon atoms in the compound [34].

Reaction pathways of bicyclic naphthenes on bifunctional catalysts accumulate the routes observed in hydroconversion of monocyclic naphthenes, with the possibility of opening one of their rings after isomerization of the cycle. Polycyclic naphthenes react similarly, with ring-opening playing an important role in their hydrocracking network, as it has been verified through hydroconversion of perhydrophenanthrene over Pt/H-USY zeolite catalyst in previous works [35,36]. The rate of ring-opening decreases with the number of remaining rings in the molecule [37]. Furthermore, the conversion of polycyclic compounds significantly increases the complexity of the reactions network, and it becomes challenging to predict the distribution of cracked products. As it was evidenced in our previous works, hydroisomerization and hydrocracking pathways of perhydrophenanthrene on bifunctional catalysts (Chapters II and III) led to hundreds of reaction products, and shape selective effects, together with pore-mouth catalysis, were a key factor to promote the formation of important isomerization compounds, e.g. perhydroanthracene and alkyladamantanes.

---

After having studied the reaction pathway of the tricyclic molecule perhydrophenanthrene, we address here the reactivity of a long-chain substituted monocyclic naphthene. Octylcyclohexane (C<sub>14</sub>H<sub>28</sub>) was evaluated as model molecule. In order to provide mechanistic insights in its hydrocracking reaction pathways on a bifunctional Pt/H-USY zeolite catalyst, we followed the formation of isomerization products presenting different degrees of branching and related them to the resulting cracking products, so as to elucidate the competition between hydroisomerization and hydrocracking.

## 2. Materials and methods

### 2.1. Preparation and characterization of catalysts

Catalyst supports based on commercial ultrastable Y zeolite (CBV720), supplied in powder form by Zeolyst, with bulk Si/Al ratio of 17.7 and a Brønsted acid site concentration of 202 μmol/g, were shaped into extrudates with alumina binder (Pural SB3) provided by Sasol, according to procedures described elsewhere (Chapter II and [38]). The shaped acidic support contained 1 wt.% of USY zeolite. A pure alumina support was also prepared. In both cases, the length of the extrudates was equal to 3-6 mm, with a diameter of 1.6 mm. Calcination was performed at 520°C during 2h according to a protocol reported in Chapter II.

Impregnation of Platinum over the alumina binder was achieved through ionic exchange, by using chloroplatinic acid hydrate (H<sub>2</sub>PtCl<sub>6</sub> from Sigma-Aldrich) as Platinum precursor. A complete procedure of the impregnation process, as well as thermal treatments applied on the final catalysts, may be found in previous work (Chapter II).

The impregnated extrudates were characterized by X-ray fluorescence in order to determine the Pt contents of the final catalyst; hydrogen-oxygen chemisorption was implemented in order to calculate Pt dispersion and size of Pt particles, considering a spherical shape, according to a procedure described in literature [39].

Results are shown in Table 1.



Table 1. Properties of Pt/H-USY zeolite catalyst determined by X-ray fluorescence, H<sub>2</sub>-O<sub>2</sub> chemisorption and pyridine adsorption followed by FTIR.

USY content in binder (wt. %)	Pt loading (wt. %)	Pt dispersion (%)	Pt particle size (nm)	n <sub>Pt</sub> (μmol/g)	BAS (μmol/g) <sup>a</sup>
1	0.65	45	2.5	9	2

<sup>a</sup> Deduced from the BAS concentration of the native USY zeolite, i.e. 202 μmol/g, assuming that it is not affected by the shaping procedure.

## 2.2. Catalytic tests

Hydroconversion of octylcyclohexane was performed as a model reaction over Pt/H-USY in order to study bifunctional mechanisms of a long side chain substituted monocyclic naphthene. The reaction took place at 300°C in a fixed-bed downflow reactor with internal diameter of 19 mm and total pressure of 60 bar. Phenyloctane (C<sub>14</sub>H<sub>22</sub>, Alfa Aesar) was diluted into n-heptane (AnalaR Normapur) in a proportion of 5/95 wt. %. The parent aromatic was used due to the difficulty of obtaining its corresponding naphthene commercially. A high molar ratio of hydrogen to total hydrocarbons of 7 mol/mol was used to prevent coke formation, and guarantee the full conversion to the model naphthene, octylcyclohexane (C<sub>14</sub>H<sub>28</sub>). Two catalysts were loaded into the reactor, comprising 2 g of monofunctional Pt/Al<sub>2</sub>O<sub>3</sub> and 2 g of bifunctional Pt/H-USY zeolite catalyst. The metallic catalyst was employed to ensure total hydrogenation of the aromatic compound into octylcyclohexane, whereas the zeolite-based catalyst carried out isomerization and cracking reactions. Both extrudate catalysts, similar in length (3-6 mm) and diameter (1.6 mm), underwent *in situ* reduction in presence of hydrogen, as described in our previous work (Chapters II and III).

Gas and liquid fractions corresponding to the reaction products of hydrocracking of octylcyclohexane over Pt/H-USY extrudate catalyst were analyzed by gas chromatography (GC) coupled to flame ionization (FID) and mass detectors. Further details on the analysis of liquid reaction products are provided in the next section. Gas products were analyzed with a GC-FID apparatus (Nexis GC – 2030, by Shimadzu) coupled online to the catalytic unit. This apparatus allowed the separation and quantification of hydrocarbons up to 7 carbon

atoms. Heavier compounds, if present, could not be resolved and eluted with peaks corresponding to C<sub>7</sub> hydrocarbons.

Catalytic performance was analyzed through calculation of octylcyclohexane conversion, yield, selectivity and distribution in a molar basis. The molar flow of the component  $i$  by taking into account the number of carbon atoms is represented in Equation 1. Conversion of octylcyclohexane was calculated as the molar flow in a carbon basis of the reaction products divided by the total molar flow in a carbon basis at the outlet (Equation 2). The yield of a component  $i$  was calculated as the total molar of this component divided by the molar flow of the reactant, octylcyclohexane (Equation 3). The molar yield of a cracked product fraction with carbon number  $c_i$  was calculated as the number of mol of a product  $k$  divided by the number of mol of cracked products (Equation 4). The yield of cracked products is expressed as mol per 100 mol cracked. The selectivity to a given product was calculated as the number of mol of a component  $i$  divided by the number of mol of reaction products (Equation 5). The distribution of a given product was calculated as the total molar flow of the product  $i$ , in a group  $J$ , divided by the total molar flow of the group  $J$  (Equation 6).

*Molar flow in respect to the number of carbons*

$$N_i = \frac{(wt.\%)_i * F_m * c_i}{(100 * M_i)} \quad (1)$$

Where  $F_m$  is the mass flow of the feedstock and  $(wt.,\%)_i$ ,  $c_i$  and  $M_i$  corresponds to the mass fraction, the number of carbons and the molar mass of the component  $i$  at the outlet, respectively.

*Conversion of octylcyclohexane*

$$X = 1 - \frac{N_{OCC6,out}}{\sum_{i=1}^{i=14} N_{i,out}} \quad (2)$$

*Yield on a carbon basis*

$$Y_i = \frac{\frac{N_i}{c_i}}{\frac{100}{196}} \quad (3)$$

*Molar yield of cracked products*

$$Y_{C_i} = \left( \frac{1}{c_i} \sum_{k=1}^{n_k} N_{i,k} / \frac{1}{14} \sum_{c_i=1}^{13} \sum_{k=1}^{n_k} (N_{i,k}/c_i) \right) * 100\% \quad (4)$$

*Selectivity to a given component*

$$S_i = \frac{\frac{N_i}{c_i}}{\sum_{i=1}^{i=14} \frac{N_{i,out}}{c_i}} \quad (5)$$

*Distribution of component i within the family J*

$$D_{i,J} = \frac{N_{i \in J}}{\sum N_{i \in J}} \quad (6)$$

Deactivation of the catalysts was not perceived in the range of operating conditions tested.

### 2.3. Methodology of analysis of liquid reaction products

As in our previous work on the hydrocracking of perhydrophenanthrene (Chapters II and III), two-dimensional comprehensive gas chromatography was carried out on a gas chromatograph (Agilent) coupled either to a time of flight mass spectrometer (TOF/MS provided by LECO) or to a flame ionization detector (FID). Detailed procedure regarding this setup are available in our previous work.

Both columns operated at the same temperature programming, starting from 40°C, with a holding time of 5 minutes, to 120°C at 1.5°C/min; then from 120°C to 135°C at 0.75°C/min, holding 10 minutes at this temperature; following from 135°C to 160°C at 0.75°C/min, holding 5 minutes at this temperature; and finally from 160°C to 230°C, at 5°C/min, holding 5 minutes at the final temperature. 1µL of the reaction effluent was injected with a split ratio of 100. High-purity Helium was used as carrier gas at a constant rate of 10 mL/min. The configuration used in identification of reaction products through mass spectrometry, as well as data treatment, was the same as applied in the analysis of reaction products of hydrocracking of perhydrophenanthrene (Chapters II and III).

### 3. Results

#### 3.1. Identification and quantification of reaction products with GCxGC – FID/MS

The parent aromatic compound, phenyloctane, was hydrogenated *in situ* over the Pt/Al<sub>2</sub>O<sub>3</sub> pre-catalyst. GC analysis confirmed that its conversion to naphthenic molecules was complete at 300°C. The pre-catalyst formed octylcyclohexane and its only monobranched isomer, nonylcyclopentane. This mixture constituted the reactant which underwent hydroisomerization and hydrocracking over the bifunctional Pt/H-USY zeolite catalyst. For the sake of clarity, herein the reactant will be referred to only as octylcyclohexane.

The analysis of reaction products generated from hydroconversion of octylcyclohexane over bifunctional Pt/H-USY zeolite catalyst is illustrated in Figure 1. The GCxGC-FID chromatogram, obtained at 71% conversion, assembles more than 200 products that have been individually assigned. This chromatogram is less complex than the ones obtained through hydroconversion of perhydrophenanthrene over the same bifunctional catalyst, since there are less reaction possibilities than in the hydroconversion of polycyclic naphthenes.

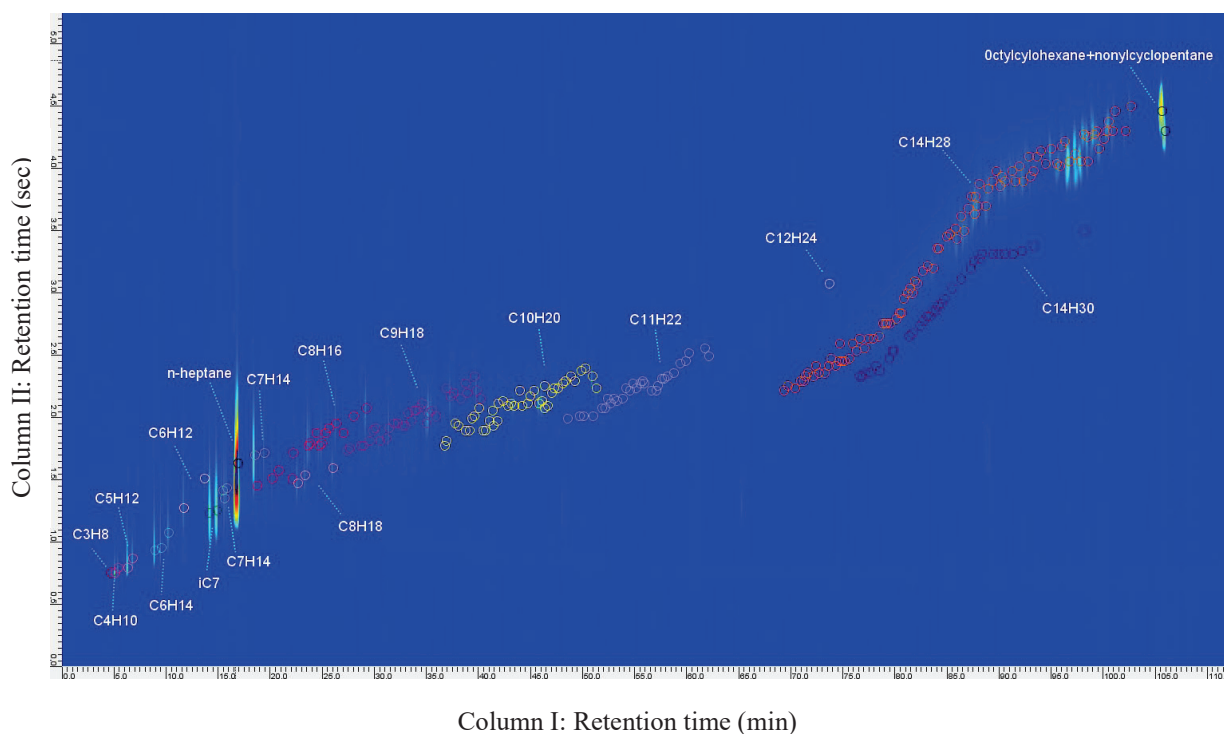


Figure 1. GCxGC-FID analysis of reaction products from hydroconversion of octylcyclohexane obtained over

Pt/H-USY zeolite catalyst at 71% conversion.

After an individual identification of reaction products generated from hydroconversion of octylcyclohexane over Pt/H-USY zeolite catalyst, they were lumped into different groups according to their carbon number and chemical family (Figure 2).

Isomers of octylcyclohexane ( $C_{14}H_{28}$ ) were divided into positional and ring-contraction isomers. The former subfamily assembled substituted cyclohexanes, comprising multiple structures presenting different degrees of branching, while the latter was constituted of substituted cyclopentanes, represented by di- or multibranched molecules.

Ring-opening products ( $C_{14}H_{30}$ ), i.e., alkanes containing 14 carbon atoms, were detected only in small amounts, since the opening of a naphthenic cycle is a difficult reaction [32]. They were mostly represented by mono- or dibranched isoalkanes. Finally, products containing less than 14 carbon atoms were assigned as cracking products. They were divided into naphthenes, n- and isoalkanes.

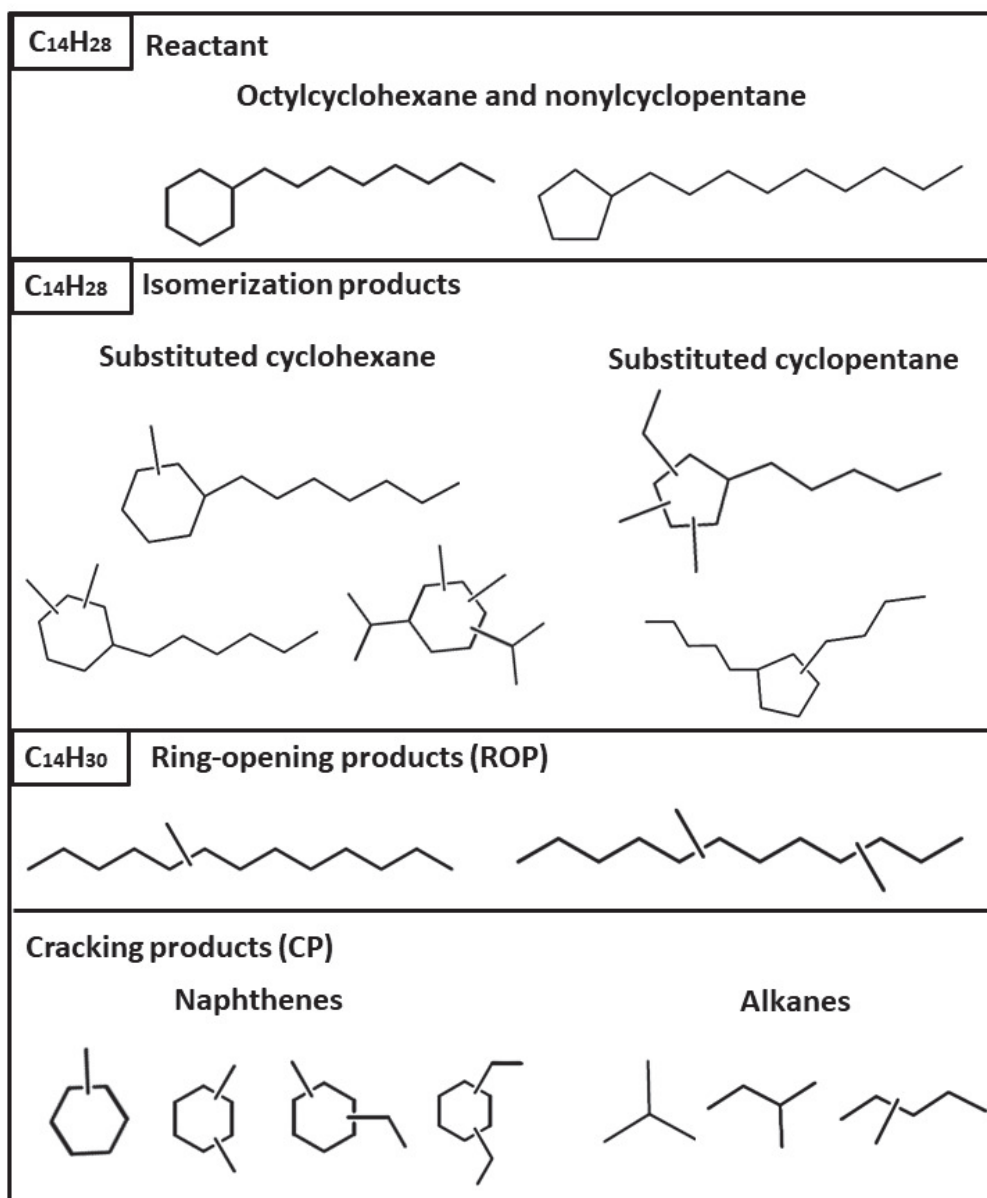


Figure 2. Molecule families and typical examples of molecules in the reaction products of hydroconversion of octylcyclohexane over Pt/H-USY zeolite catalyst.

### 3.2. Hydroconversion of octylcyclohexane

Different levels of conversion of octylcyclohexane over the catalyst containing 1% of USY zeolite in the alumina binder were obtained by changing the contact time at a reaction temperature of 300°C, as depicted in Figure 3. The degree of octylcyclohexane conversion covered a range from ca. 48% to 86%.

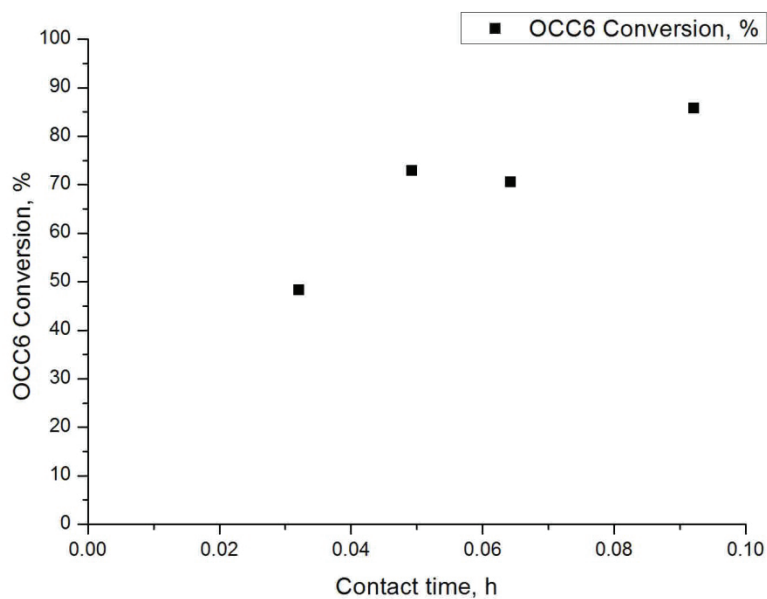


Figure 3. Evolution of octylcyclohexane conversion with contact time on Pt/H-USY extrudate catalyst with 1 wt.% zeolite in alumina binder.

The selectivity, expressed in mol per mol of reaction products, to isomerization, ring-opening and cracked compounds, is illustrated in Figure 4. The profiles reveal a primary character of isomerization reactions, followed by cracking, as expected in bifunctional mechanisms [17,40]. At higher conversion, cracked products were favored. Selectivity to ring-opening products accounted for less than 1% at all conversion degrees, since the opening of a cycle is a difficult reaction.

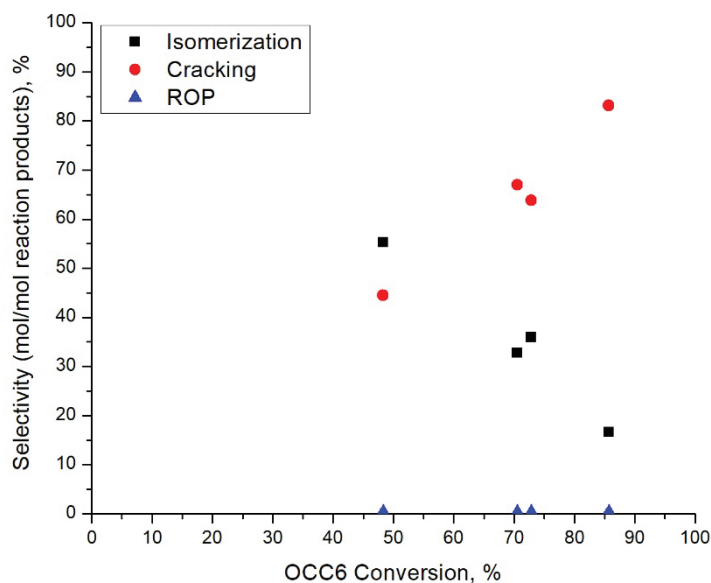


Figure 4. Selectivity to isomerization, ring-opening and cracked products as a function of octylcyclohexane conversion over Pt/H-USY zeolite catalyst.

The distribution of  $C_{14}H_{28}$  isomers as a function of octylcyclohexane conversion over Pt/H-USY zeolite catalyst is shown in Figure 5. Several compounds presenting different degrees of branching were identified. Dibranched structures were assigned as **I2**, **I4** and **I8**. The only tribranched isomer was represented by structure **I7**. Isomers with at least four branchings were characterized by **I1**, **I3**, **I5** and **I6** molecules. Ring-contraction products were assigned as **I4**, **I6** and **I8** molecules. The most abundant isomers were dibranched structures **I2** and **I4**, and multibranch compound **I6**. Other multibranch isomers as **I1**, **I3** and **I5** were less favored at all conversion levels. Globally, the distribution of isomers did not considerably change with octylcyclohexane conversion. The unknown fraction accounted for 20 % of the distribution in average.



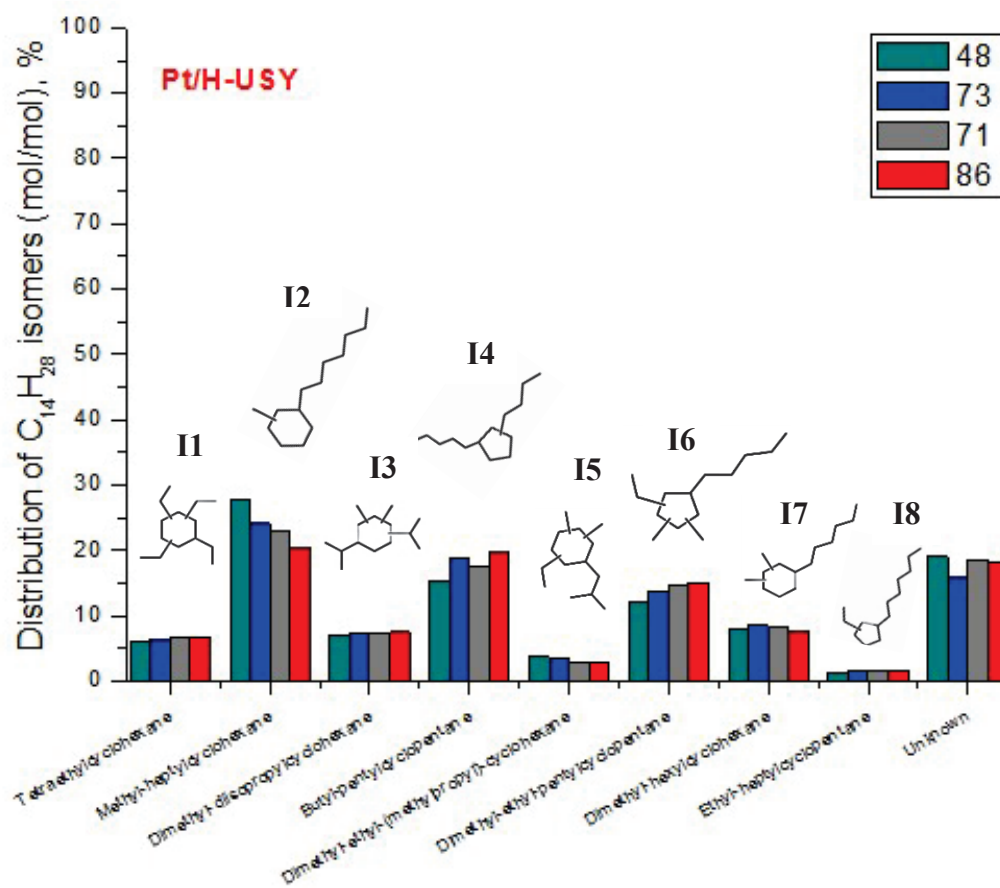


Figure 5. Distribution of positional and ring-contraction isomers of octylcyclohexane over Pt/H-USY bifunctional catalyst.

The yield of cracked products per mol of octylcyclohexane according to carbon number is presented in Figure 6. Cracked products became predominant in hydrocracking of octylcyclohexane over Pt/H-USY zeolite catalyst around 70% conversion. Cracked compounds covered a range of carbon numbers from 1 to 12. The profiles revealed in Figure 6 show a preferential formation of C<sub>7</sub> compounds, followed by an almost symmetrical distribution from C<sub>4</sub> to C<sub>10</sub> cracked molecules at all conversion degrees. It is important to note that C<sub>7</sub> compounds comprise only cyclic molecules, since the distinction between C<sub>7</sub> isoalkanes derived from the solvent n-heptane and C<sub>7</sub> isoalkanes generated from hydroconversion of octylcyclohexane was not possible. Yield of light compounds as methane and ethane represented less than 0.5 and 0.06 mol per mol octylcyclohexane, respectively, and could be associated to the cracking of the model molecule to C<sub>12</sub> naphthenes (0.08-0.11

mol.%) and light products, which characterizes hydrogenolysis [41,42]. Since the contents of C<sub>1</sub>, C<sub>2</sub> and C<sub>12</sub> products were very low, they will not be further discussed in this work.

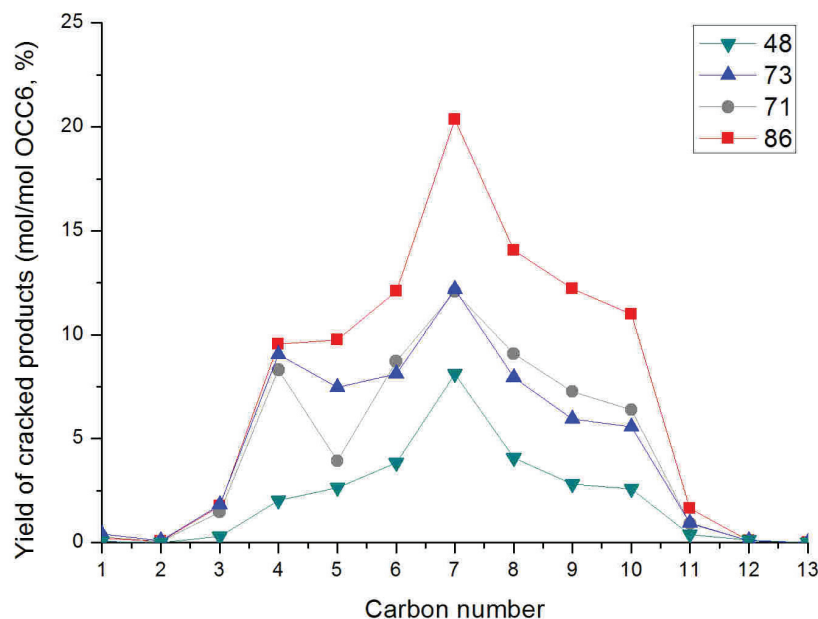


Figure 6. Yield of cracked products according to the number of carbon atoms at different levels of octylcyclohexane conversion over Pt/H-USY zeolite catalyst.

Cracked products were divided into naphthenes, isoalkanes and n-alkanes, as illustrated in Figure 7. Their distribution was fairly stable as a function of octylcyclohexane conversion over Pt/H-USY zeolite catalyst and indicated a predominant formation of naphthenes, followed by iso- and n-alkanes. Each mol of octylcyclohexane that is cracked should result in an equimolar mixture of naphthenes and alkanes, if secondary cracking does not take place. The distribution presented in Figure 7 does not confirm this behavior, since C<sub>7</sub> isoalkanes were not counted as reaction products. Therefore, alkanes were underestimated in comparison to cracked naphthenes.

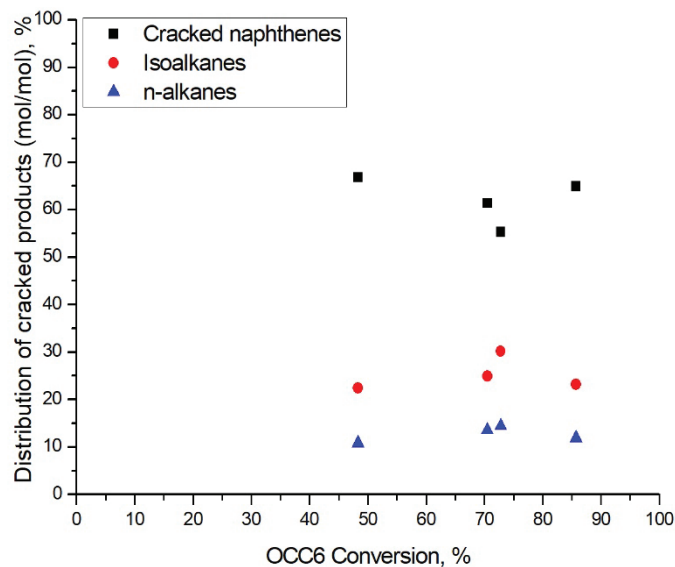


Figure 7. Distribution of cracked products as a function of octylcyclohexane conversion over bifunctional Pt/H-USY zeolite catalyst.

The distribution of cracked naphthenes obtained from hydroconversion of octylcyclohexane over Pt/H-USY zeolite catalyst is shown in Figure 8. C<sub>7</sub> naphthenes were the major products. Their percentage slightly decreased with conversion. C<sub>8</sub>, C<sub>9</sub> and C<sub>10</sub> cyclic molecules were also abundant products, followed by smaller amounts of C<sub>6</sub> naphthenes. C<sub>11</sub> and C<sub>12</sub> naphthenes (not represented) accounted altogether for less than 4% of the distribution.

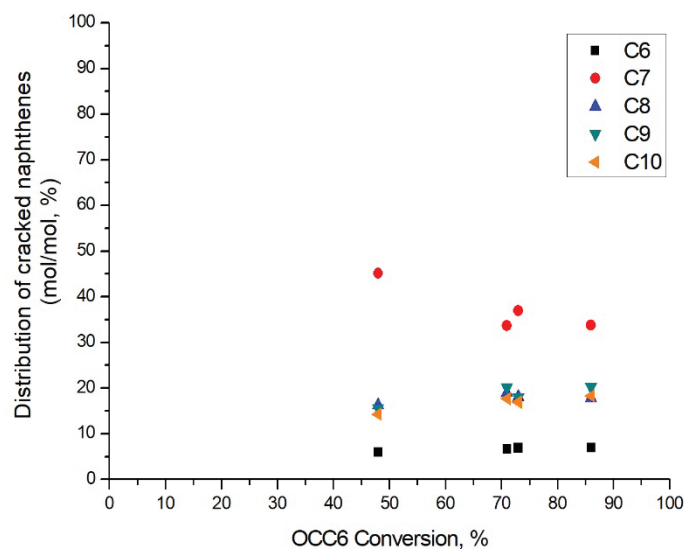


Figure 8. Distribution of cracked naphthenes as a function of octylcyclohexane conversion over bifunctional Pt/H-USY zeolite catalyst.

The distribution of C<sub>6</sub> naphthenes over Pt/H-USY zeolite catalyst, as depicted in Figure 9A, was composed of methylcyclopentane and cyclohexane. Methylcyclopentane was favored at all conversion levels over its 6-membered isomer due to its greater stability at higher temperature [43]. With respect to C<sub>7</sub> naphthenes (Figure 9B), the main primary product was methyl-cyclohexane. The distribution then evolved towards the formation of dimethylcyclopentane through type B isomerization of methylcyclohexane. Ethylcyclopentane was a minor product in this fraction. This result differed from hydrocracking of perhydrophenanthrene (Chapter II) over the same catalyst, where the primary formation of the dibranched 5-membered naphthenic isomer was observed. This also confirms that the distribution of the naphthene cracking products is not an equilibrium distribution, but related to structure of the C<sub>14</sub> isomer, which undergoes cracking.

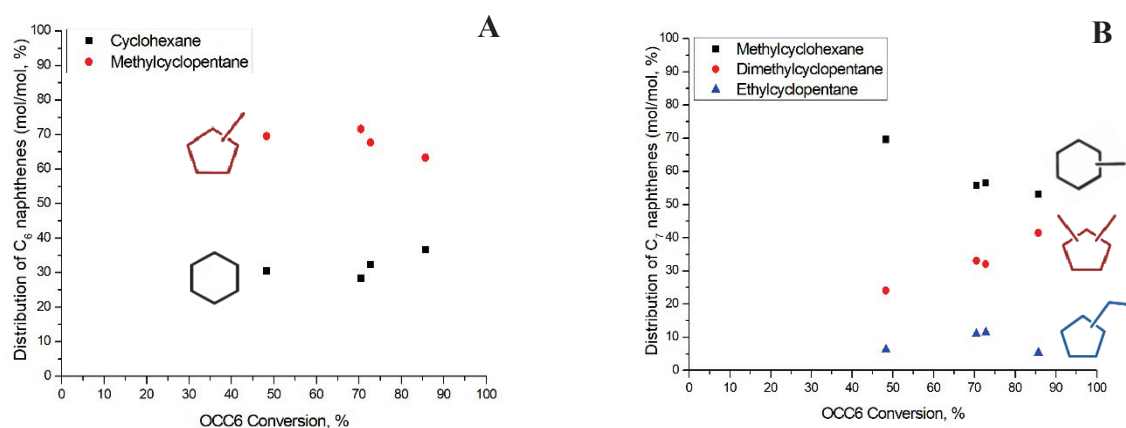


Figure 9. A) Distribution of C<sub>6</sub> naphthenes as a function of octylcyclohexane conversion over bifunctional Pt/H-USY zeolite catalyst. B) Distribution of C<sub>7</sub> naphthenes as a function of octylcyclohexane conversion over bifunctional Pt/H-USY zeolite catalyst.

C<sub>8</sub> naphthenes comprised mono-, di- and tribranched structures (Figure 10). Major C<sub>8</sub> cyclic compounds were represented by dimethylcyclohexane (dibranched), whose proportion increased slightly with octylcyclohexane conversion. An equimolar and stable distribution of ethylcyclohexane (monobranched) and its ring-contraction isomer methyl-ethylcyclopentane (dibranched) was observed. The only tribranched structure corresponded to

trimethylcyclopentane, a minor product among the compounds identified. The distribution of C<sub>8</sub> naphthenes suggests that the dimethylcyclohexane concentration increases through type B isomerization of ethylcyclohexane or type A isomerization of methyl-ethylcyclopentane. Unknown structures constituted about 10% of the distribution at all conversion degrees.

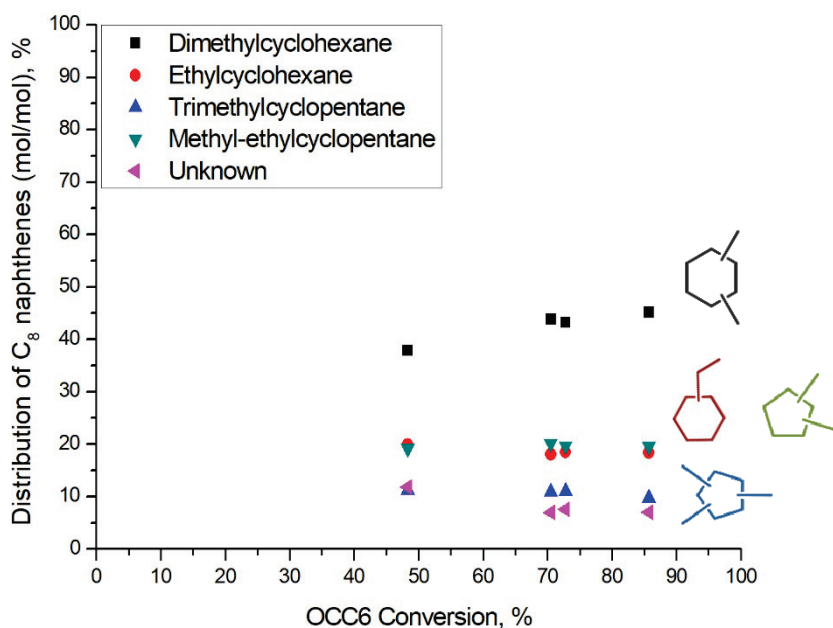


Figure 10. Distribution of C<sub>8</sub> naphthenes as a function of octylcyclohexane conversion over bifunctional Pt/H-USY zeolite catalyst.

The distribution of C<sub>9</sub> naphthenes over Pt/H-USY zeolite catalyst is revealed in Figure 11. Major cyclic C<sub>9</sub> isomers included structures such as methyl-ethylcyclohexane (**C9-3**, dibranched), followed by trimethylcyclohexane (**C9-1**, tribranched) and 5-membered isomers represented by diethylcyclopentane molecules (**C9-2**, dibranched). The latter can be directly obtained through ring-contraction, i.e., type B isomerization, of methyl-ethylcyclopentane. Minor compounds corresponded to n- and isopropylcyclohexane (**C9-5** and **C9-4**, respectively), followed by substituted cyclopentane, as butyl- and tetramethylcyclopentane (**C9-7** and **C9-6**, respectively). The distribution of C<sub>9</sub> naphthenes did not change with octylcyclohexane conversion. Unknown compounds accounted for less than 5% of the distribution.

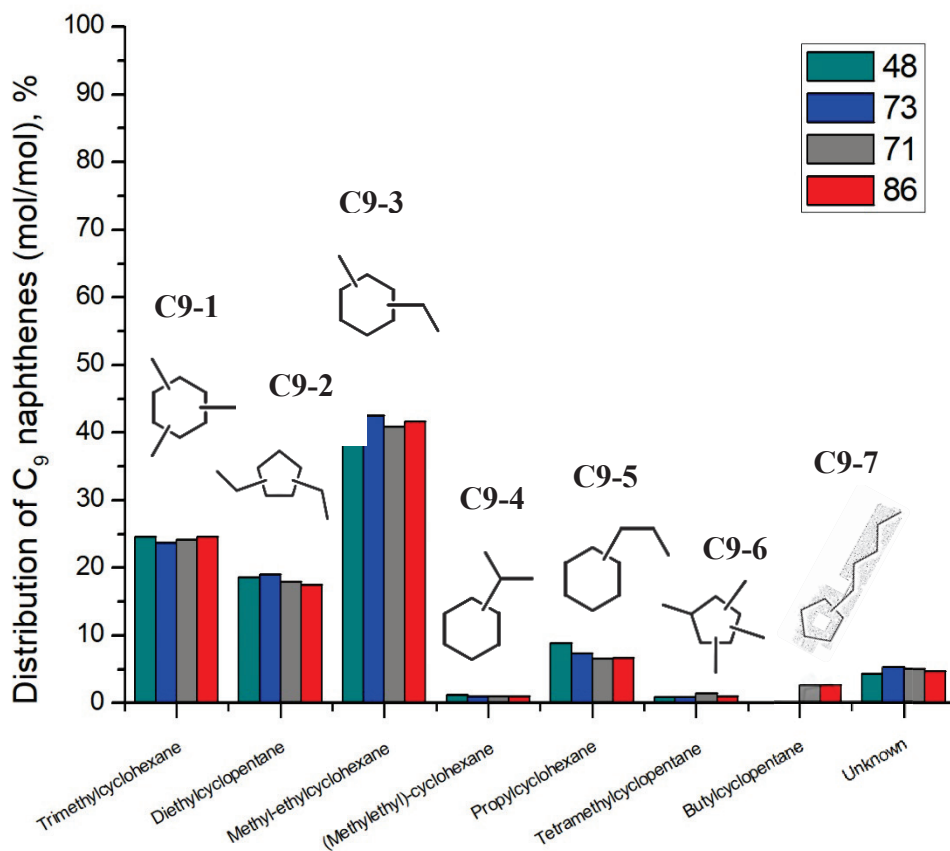


Figure 11. Distribution of C<sub>9</sub> naphthenes as a function of octylcyclohexane conversion over bifunctional Pt/H-USY zeolite catalyst.

C<sub>10</sub> naphthenes followed a stable distribution over Pt/H-USY zeolite catalyst, as indicated in Figure 12. Several structures with different substituents and degrees of branching were identified, especially substituted cyclohexane. Major compounds were identified as ethylcyclohexane (dibranched) and methyl-isopropylcyclohexane (tribranched), assigned as structures **C10-5** and **C10-1**, respectively. Minor C<sub>10</sub> products comprised multibranch molecules, as tetramethylcyclohexane (**C10-4**) and dimethyl-isopropylcyclopentane (**C10-9**). Unknown molecules represented, in average, 10% of the distribution.

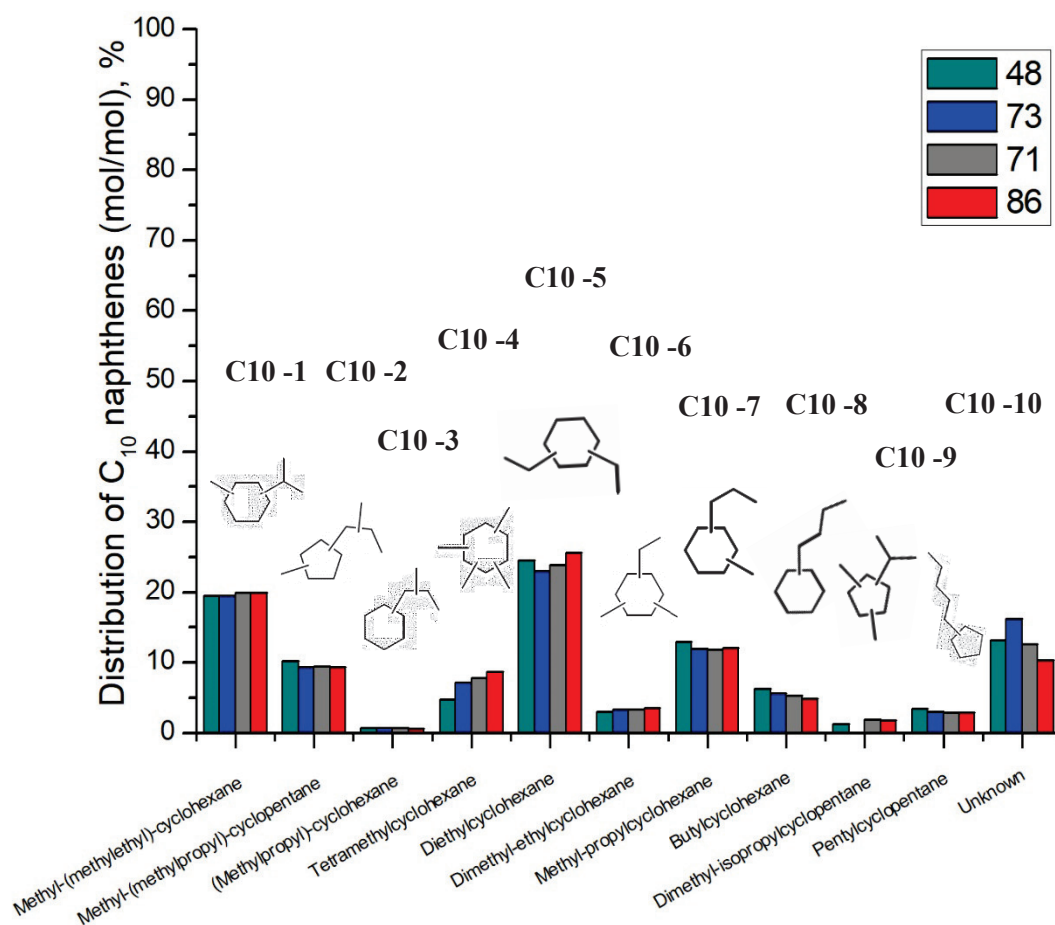


Figure 12. Distribution of C<sub>10</sub> naphthenes as a function of octylcyclohexane conversion over bifunctional Pt/H-USY zeolite catalyst.

Iso- and n-alkanes were minor cracked products from hydroconversion of octylcyclohexane over Pt/H-USY extrudate catalyst. Their distribution is presented in Figure 13. Alkanes heavier than 8 carbon atoms were not formed through hydrocracking of the model molecule. Isoalkanes were preferentially formed over linear isomers, they accounted for ca. 65 mol.% of the distribution. Branched molecules as isobutane, methylbutane and methylpentane were favored over iso-C<sub>8</sub> compounds. Among n-alkanes, n-hexane was the major product.

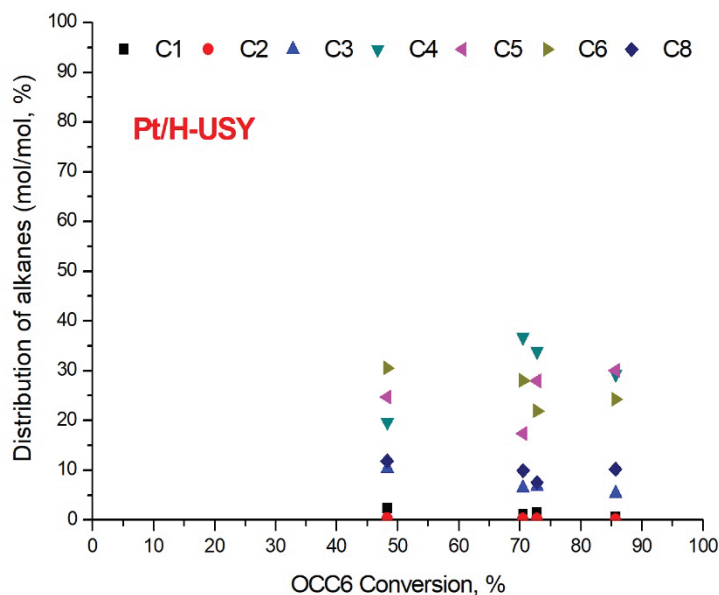


Figure 13. Distribution of alkanes as a function of octylcyclohexane conversion over bifunctional Pt/H-USY zeolite catalyst.

Only two main groups of isomers of C<sub>6</sub> and C<sub>8</sub> isoalkanes were identified over Pt/H-USY zeolite catalyst, and their distribution is presented in Figure 14. All the isoalkanes were mono-branched, preferentially in position 2. The distribution was fairly stable with conversion.

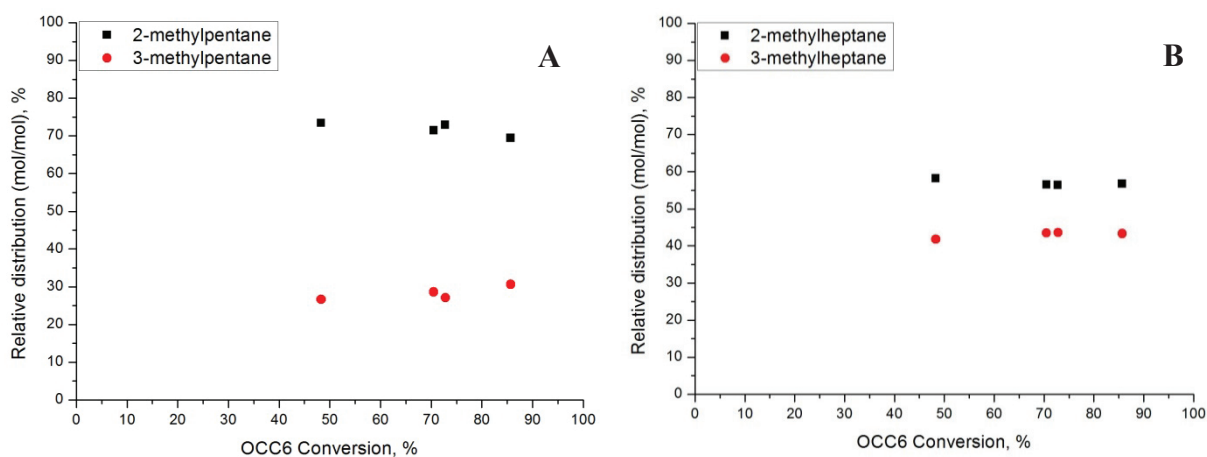


Figure 14. A) Distribution of C<sub>6</sub> isoalkanes as a function of octylcyclohexane conversion over bifunctional Pt/H-USY zeolite catalyst. B) Distribution of C<sub>8</sub> isoalkanes as a function of octylcyclohexane conversion over bifunctional Pt/H-USY zeolite catalyst.

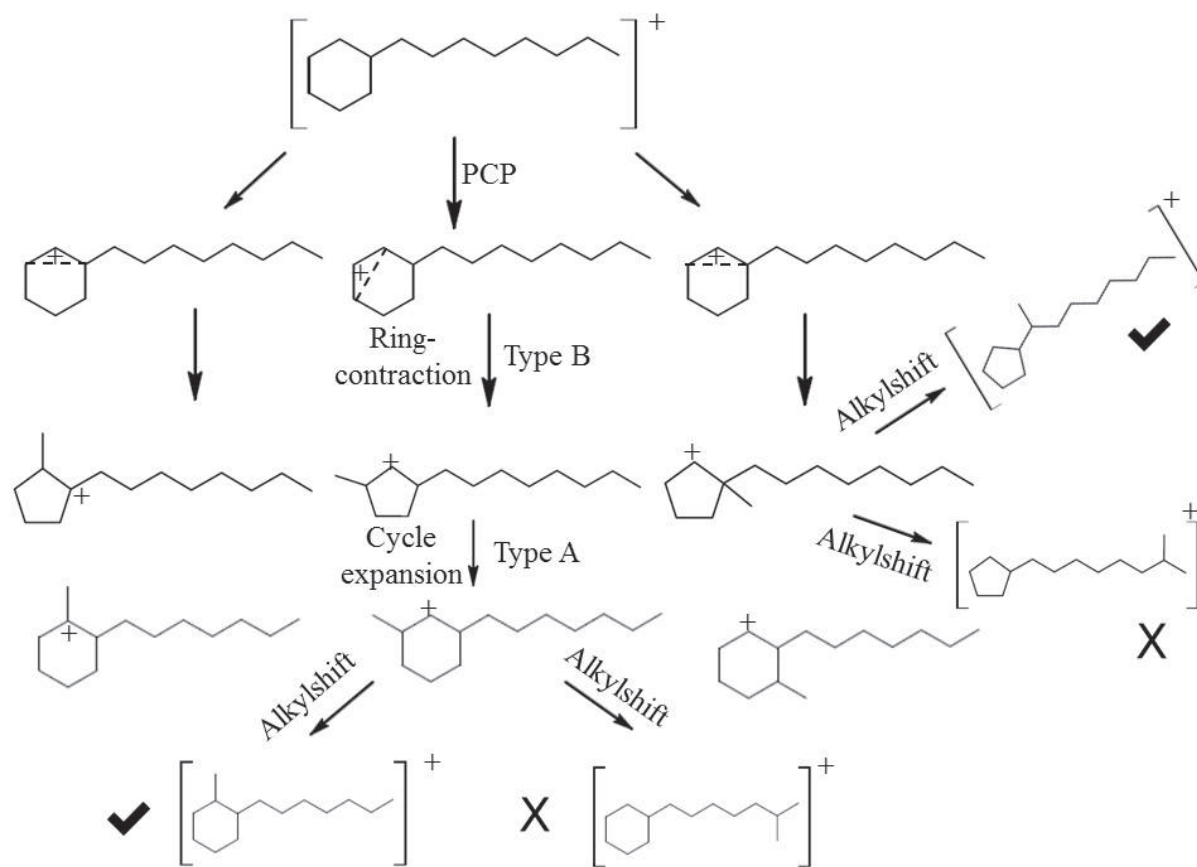


## 4. Discussion

### 4.1. Attempts to rationalize isomerization pathways

A large spectrum of isomers was formed through hydroconversion of octylcyclohexane over Pt/H-USY zeolite catalyst (Figure 5). This diversity was achieved thanks to endocyclic rearrangements and exocyclic alkyl-shifts. Carbocation chemistry shows that type B rearrangements are required to generate an additional branching on the ring or on the alkyl chain substituent. The branching on the alkyl chain preferentially occurs in 2-position, via a PCP involving the naphthene cycle. The generated methyl-substituents can then change position on the ring or on the alkyl chain by endo- or exo-cyclic alkyl shifts, respectively. From an energetic point of view, Martens *et al.* [31] showed that endocyclic alkyl-shifts as well as type A ring-contraction and ring-expansion, require less activation energy than type B arrangements, covering a range from 21-25 kJ/mol vs 27-42 kJ/mol, respectively. Activation energies for exocyclic alkyl-shifts were in the range of 10-15 kJ/mol.

By taking into account the results previously mentioned, the reaction pathways presented herein will describe the formation of the most abundant isomers (structures **I2**, **I4** and **I6**) through ring-contraction (branching occurring in the ring) and cycle expansion, with eventual alkyl-shifts around the ring (endocyclic alkyl-shift) or towards a substituent alkyl-chain (exocyclic alkyl-shift). The majority of isomerization products were branched on the cycle, and not on the substituent alkyl-chain, as previously reported by Souverijns *et al.* [34]. Branching occurred first in the ring through type B isomerization, forming a methyl-octylcyclopentane. Alkyl shifts can then transfer the methyl-branching to different positions on the ring and also to the initial alkyl substituent chain (Scheme 1).



Scheme 1. Isomerization pathways of octylcyclohexane over Pt/H-Y according to Souverijns *et al.*

Methyl-heptylcyclohexane (**I2**), for instance, could be obtained through initial ring-contraction to methyl-octylcyclopentane, followed by hydride shift and cycle expansion to form the 6-membered dibranched naphthene through type A isomerization (Figure 15). The distribution of  $C_{14}H_{28}$  isomers indicated that the content of methyl-heptylcyclohexane decreased slightly with conversion, suggesting that it would be the primary isomerization product from hydroconversion of octylcyclohexane, which is then further converted to other isomers or cracking products. All the suggested isomerization pathways go through the formation of methyl-heptylcyclohexane as initial intermediate, which confirms the primary character of this isomer.

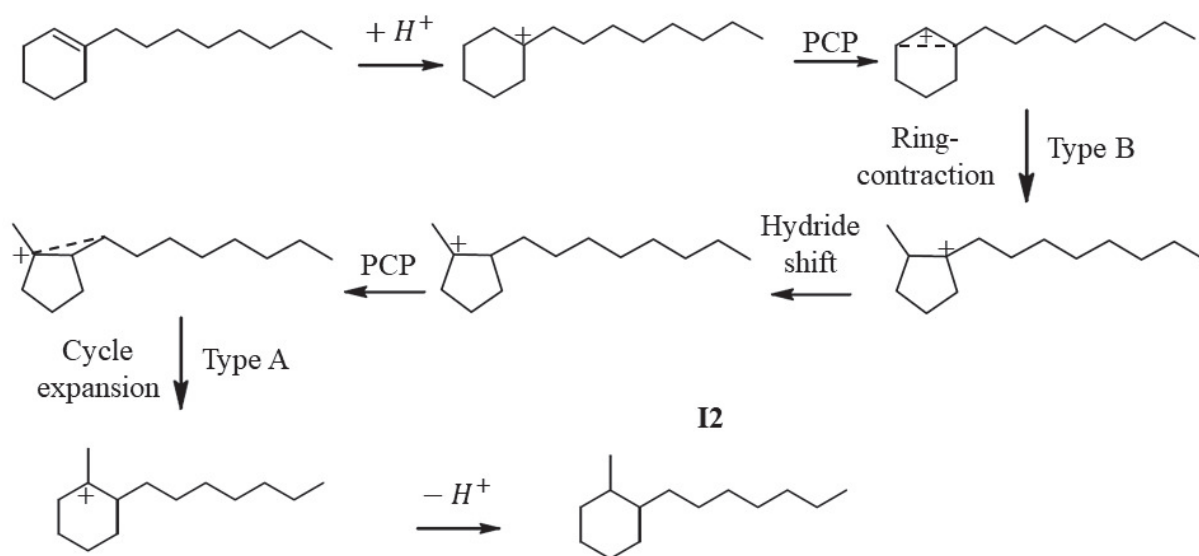
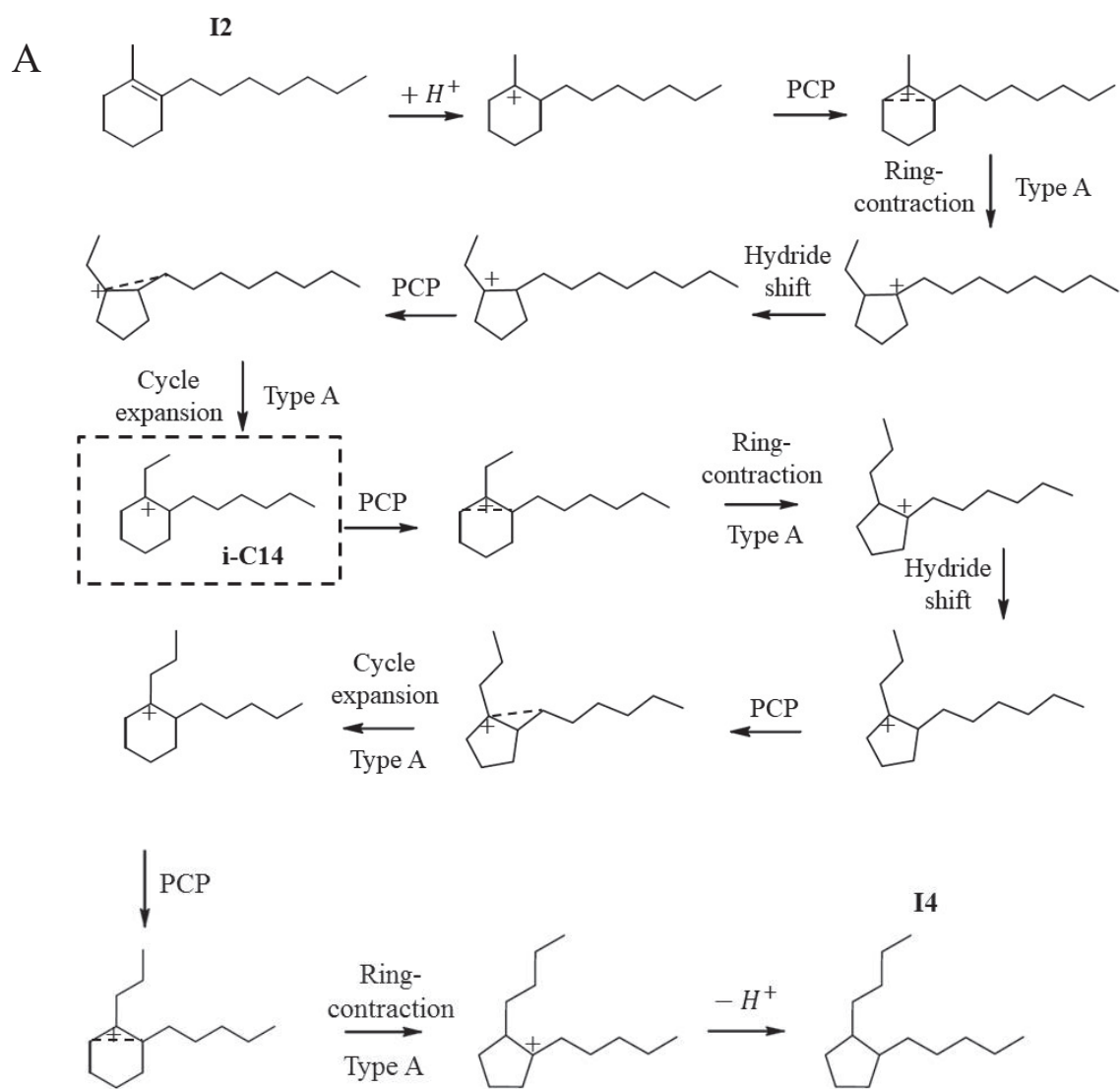


Figure 15. Suggested reaction pathway for isomerization of octylcyclohexane towards methyl-heptylcyclohexane (**I2**) over Pt/H-USY zeolite catalyst, in accordance with Souverijns *et al.*

Structures **I4** and **I6** were similarly obtained, but with an increasing number of the sequential steps previously described in comparison to methyl-heptylcyclohexane, as illustrated in Figure 16 A and B. Transformation of the latter to isomers **I4** and **I6** share a common intermediate which was assigned as **i-C14**. A significant difference in respect to these two compounds (**I4** and **I6**) regards the degree of branching. Structure **I4** is a dibranched molecule, with two alkyl-chains as substituents, whereas structure **I6** is a tetrabranched isomer, containing smaller substituents. In order to change the degree of branching, the model molecule must undergo a higher number of type B isomerization, which is indeed the case for isomer **I6**, as evidenced in Figure 16B.



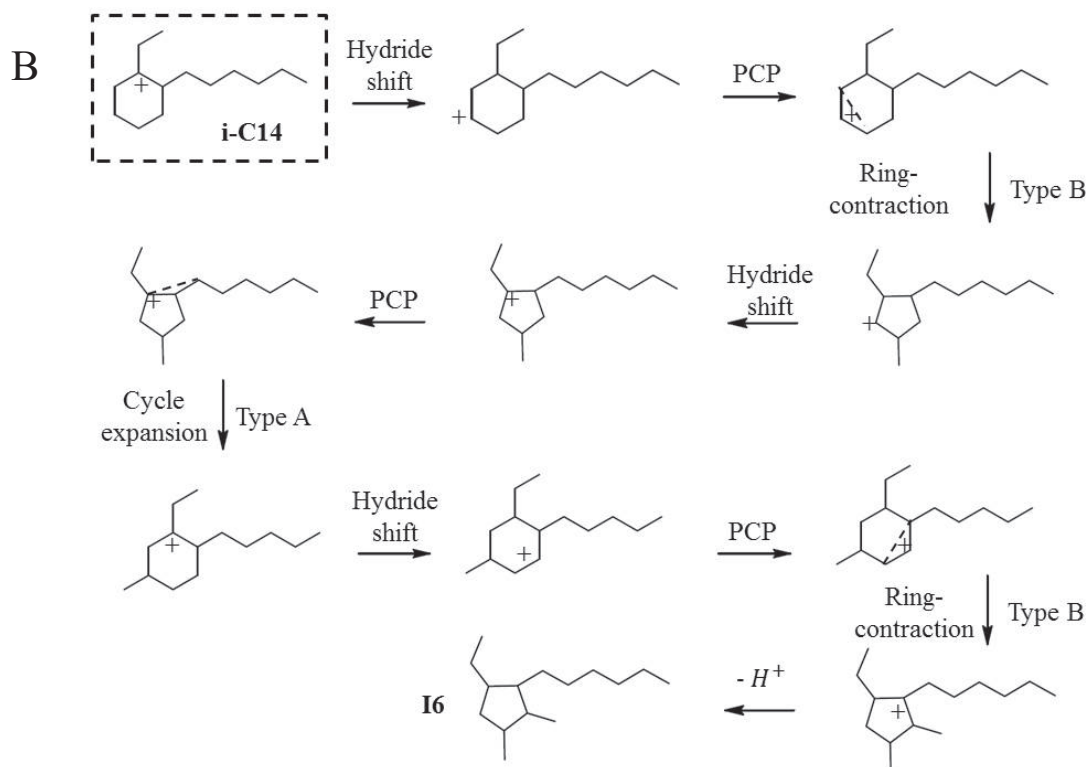


Figure 16. A) Suggested reaction pathway for isomerization of octylcyclohexane towards isomer **I4** starting from methyl-heptylcyclohexane (**I2**) over Pt/H-USY zeolite catalyst. B) Suggested reaction pathway for isomerization of octylcyclohexane towards isomer **I6** starting from structure **i-C14** over Pt/H-USY zeolite catalyst.

The easiness to form a given isomer should be associated to the number of reaction steps needed for their formation. These data allow us to rationalize the distribution of isomers presented in Figure 5. For carrying out this exercise, the number of branchings on cycle and on alkyl-chain, as well as the total number of type B ring-contraction required to produce a specific isomer are recapitulated in Table 2. According to Table 2, structures **I2**, **I4** and **I8**, and to a lesser extent **I7**, should be the most favored among isomerization products over Pt/H-USY zeolite catalyst. The reaction pathways (type B isomerization) leading to structures **I1**, **I6**, **I3** and **I5** should be much slower.

Major isomerization products comprised methyl-heptylcyclohexane (**I2**), **I4** and **I6** structures. Conversely, **I7** and **I8** molecules were only observed to a small extent. The dibranched structures **I7** and **I8** can be easily formed through isomerization of methyl-heptylcyclohexane, but they can also crack very fast, as it will be discussed in next section. On the other

extreme, the highly branched compounds **I3** and **I5** were the least abundant in the isomer fraction, which correlates well to the number of slow reactions steps involved to form such molecules. The high abundance of the tetra-branched compound I6 indicates that this molecule is not easily converted to subsequent cracking products.

Table 2. Number of branchings on rings or on chain, and type B ring-contraction required to produce isomers from octylcyclohexane over Pt/H-USY zeolite catalyst.

Isomer	Branchings on ring	Branchings on chain	Number of type B branchings required for formation of isomer
I2	2	-	1
I8	2	-	1
I4	2	-	1
I7	3	-	2
I1	4	-	3
I6	4	-	3
I5	4	1	4
I3	4	2	5

#### 4.2. Attempts to rationalize hydrocracking pathways

Cracked products were formed rapidly after isomerization and became predominant around 70% of octylcyclohexane conversion (Figure 4). In order to verify the nature of cracking reactions, i.e., if secondary cracking takes place or if non-classical cracking mechanisms contribute to hydroconversion of octylcyclohexane over Pt/H-USY, the yield of a given cracked product per 100 mol of cracked products is analyzed as a function of octylcyclohexane conversion, as depicted in Figure 17. Values of total yield covered a range from ca. 200 to 210 mol per 100 mol of cracked products. These values correspond globally to cracking of one molecule into two other ones, as expected for a single cracking event. However, it should be emphasized that, as C<sub>7</sub> isoalkanes were not accounted among reaction products, the cracking yields are underestimated, i.e. they should be higher than 200 mol per

100 mol of cracked product, indicating that secondary cracking took place. This contrasts with the hydrocracking of perhydrophenanthrene, where the analysis of the yield of cracked products revealed values below 200 mol/mol, indicating an important contribution of addition-cracking mechanisms (Chapter II).

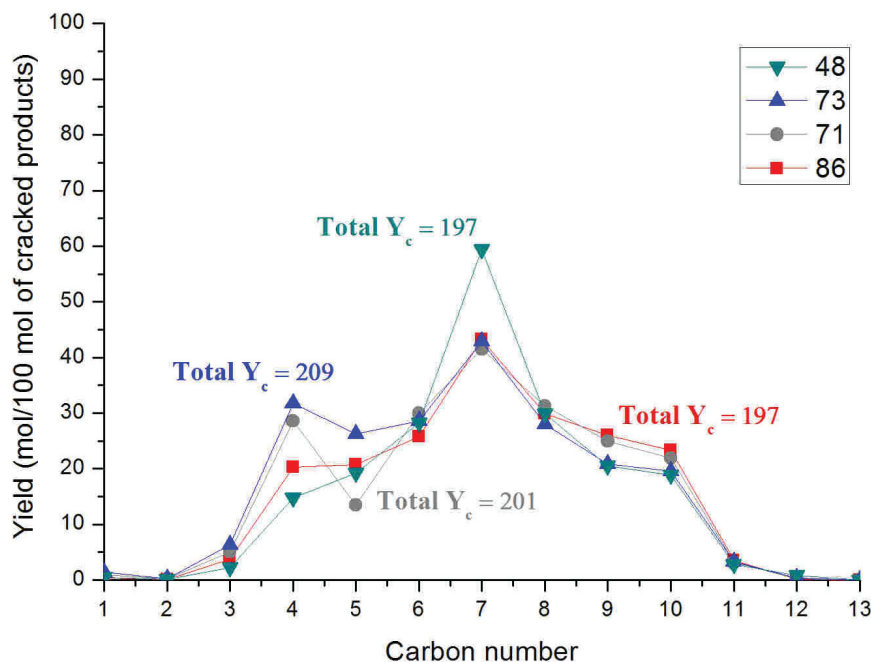


Figure 17. Yield of cracked products per 100 mol of cracked products resulting from hydroconversion of octylcyclohexane over bifunctional Pt/H-USY zeolite catalyst. Values indicated in the graph correspond to total yield of cracked products per 100 mol of cracked molecules.

The yield of cracked products presented in Figure 6 and Figure 17 suggests a predominant cracking to C<sub>7</sub> compounds, followed by an almost symmetrical distribution varying from 4 to 10 carbon atoms. Starting from a molecule containing 14 carbon atoms, there are at least four possibilities of cracking it to lighter compounds, generating in this way a smaller naphthene and an alkane. The main pathway would lead to the formation of C<sub>7</sub> naphthenes and C<sub>7</sub> alkanes. The distribution of C<sub>7</sub> naphthenes depicted in Figure 9B indicated a primary formation of methylcyclohexane. A presumed reaction pathway would therefore produce monobranched methylcyclohexane along with methylhexane as C<sub>7</sub> reaction products, resulting from hydrocracking of a tribranched C<sub>14</sub>H<sub>28</sub> isomer. Among isomerization products, **I7** is the only tribranched structure, and only an exocyclic alkyl-shift must take place prior to its cracking in order to obtain the desired product. On the other hand, its formation requires a

superior number of type B isomerization in contrast to dibranched molecules, such as **I2** and **I8**. These isomers may easily be converted to C<sub>7</sub> compounds by creating a branching on the substituent alkyl-chain. It is worth mentioning that **I8** results from a type A ring-contraction of isomer **I2**. A suggested reaction pathway for hydrocracking of isomer **I2** towards major C<sub>7</sub> naphthene (methylcyclohexane) and 2-methylhexane is presented in Figure 18.

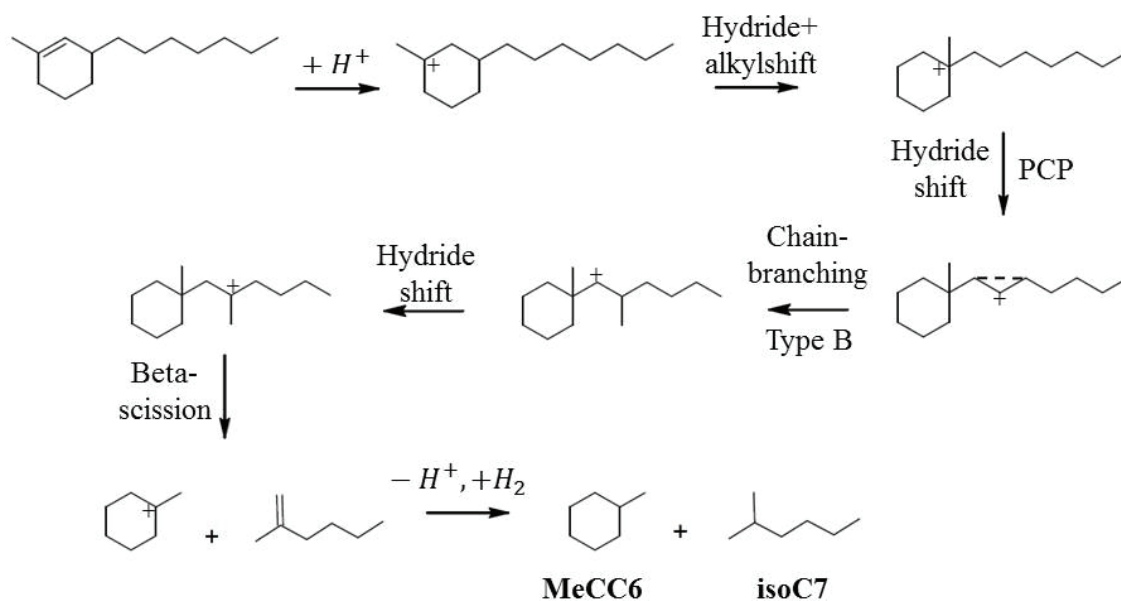


Figure 18. Suggested cracking pathway towards formation of methylcyclohexane and isoheptane from hydroconversion of octylcyclohexane over Pt/H-USY zeolite catalyst.

Another possible pathway is cracking of C<sub>14</sub>H<sub>28</sub> isomers into C<sub>10</sub> naphthenes and C<sub>4</sub> alkanes. An almost equimolar correlation between C<sub>10</sub> and C<sub>4</sub> compounds was obtained, indicating that isomers of octylcyclohexane may undergo this cracking pathway. C<sub>10</sub> compounds were represented in Figure 12 and comprised several structures presenting different degrees of branching, especially diethylcyclohexane (**C10-5**, dibranched) and methylisopropylcyclohexane (**C10-1**, tribranched).

This implies that isomers containing at least four branchings cracked to C<sub>10</sub> naphthenes, i.e. **I1**, **I3**, **I5** and **I6**. Structures **I1** and **I3** present short side chains and would have to isomerize multiple times to get to a favored cracking conformation leading to C<sub>10</sub> naphthenes and isobutane. To this end, additional type B ring-contraction and type A cycle-expansion are necessary, increasing the number of total (and slow) reaction steps before cracking. The **I6** molecule can crack to C<sub>10</sub> naphthenes, but it is even more suitable for cracking to C<sub>9</sub>



naphthenes and C<sub>5</sub> isoalkanes, as it will be explained further on. **I5**-type structures can undergo hydrocracking to tri-branched products within C<sub>10</sub> naphthenes fraction after a small number of type A rearrangements, because an isobutyl group is already attached to the naphthenic cycle. The formation of di-branched C<sub>10</sub> naphthenes (**C10-5**, for example) from **I5** is also possible, after an additional type B isomerization step, see Figure 19.

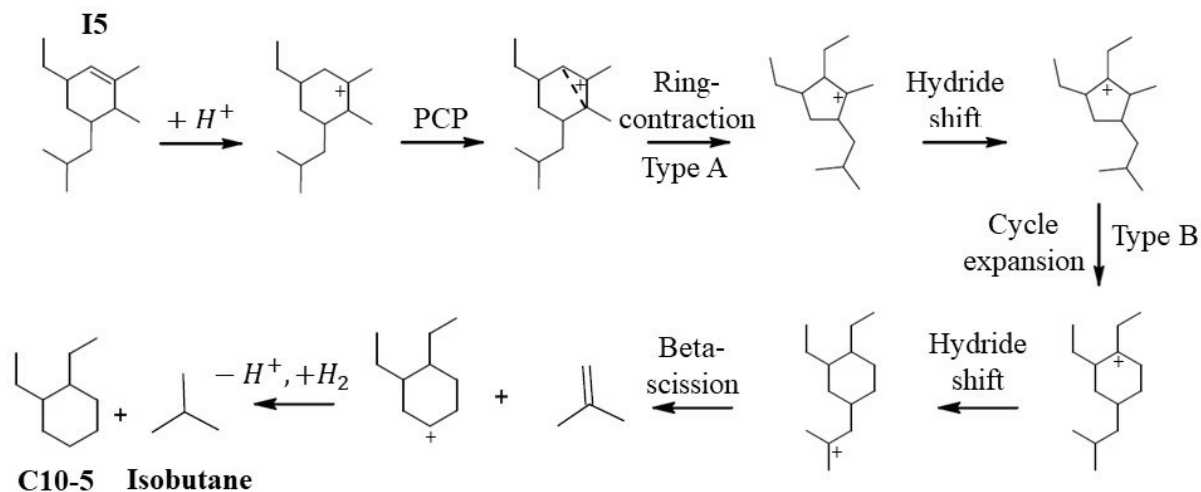


Figure 19. Suggested cracking pathway towards formation of structure C<sub>10</sub>-5 and isobutane from hydrocracking of **I5** isomer over Pt/H-USY zeolite catalyst.

Following the same procedure, the profiles illustrated in Figure 6 and Figure 17 suggest a molar equivalence between C<sub>5</sub> and C<sub>9</sub> compounds. According to Figure 11 and Figure 13, major C<sub>9</sub> products corresponded to **C9-3**, **C9-1** and **C9-2** structures, whereas methylbutane predominated among C<sub>5</sub> molecules.

The distribution of C<sub>9</sub> naphthenes was mainly constituted of dibranched and tribranched molecules (Figure 11). Thus, they should be formed after hydrocracking of at least tetrabranched isomers, e.g. **I1**, **I3**, **I5** and **I6**. As previously mentioned, **I1** and **I3** need to isomerize back to longer side chains, via slow steps, before allowing a cleavage configuration leading to C<sub>9</sub> naphthenes. The same argument may be applied to **I5** compounds. Within the isomers fraction, structure **I6** is the only molecule that can be easily converted to major C<sub>9</sub> reaction products, e.g., **C9-3**. The pathway goes through a cycle expansion without changing its degree of branching before cracking to **C9-3** molecules and methylbutane, as presented in

Figure 20. It is worth mentioning that formation of **I6** by isomerization is difficult, as recapitulated in Table 2.

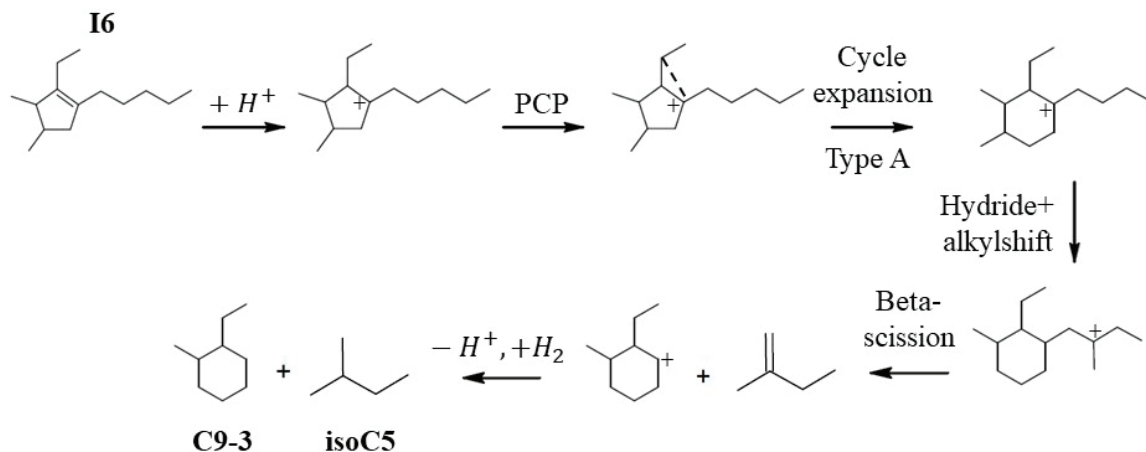


Figure 20. Suggested cracking pathway towards formation of structure **C9-3** and methylbutane from hydrocracking of **I6** isomer over Pt/H-USY zeolite catalyst.

Finally, the last pathway to be considered is hydrocracking of the isomerized model molecule into  $C_6$  and  $C_8$  compounds. According to Figure 14, the major  $C_6$  isoalkane is 2-methylpentane, whereas primary  $C_8$  naphthenes corresponded to ethylcyclohexane and methyl-ethylcyclopentane.

$C_8$  naphthenes were predominantly constituted of di- and monobranched molecules. Among isomerization products, tetrabranched **I6** and dibranched **I8** molecules are the most suitable structures to generate dibranched and monobranched  $C_8$  compounds, respectively, without needing to go through several slow rearrangements (type B isomerization). **I6** isomers may be easily converted into methyl-ethylcyclopentane and methylpentane only via hydride- and alkylshifts, while **I8** isomers may react through ring-expansion (type A isomerization) and chain branching (type B isomerization) to produce ethylcyclohexane and iso $C_6$  (Figure 21, A and B respectively). The transformation of these isomers into the aforementioned compounds correspond to the minimum number of type B rearrangements required to achieve beta-scission. In addition, all the pathways indicated the production of 2-methylpentane as primary isoalkane  $C_6$ , which avoids the formation of primary carbocations.

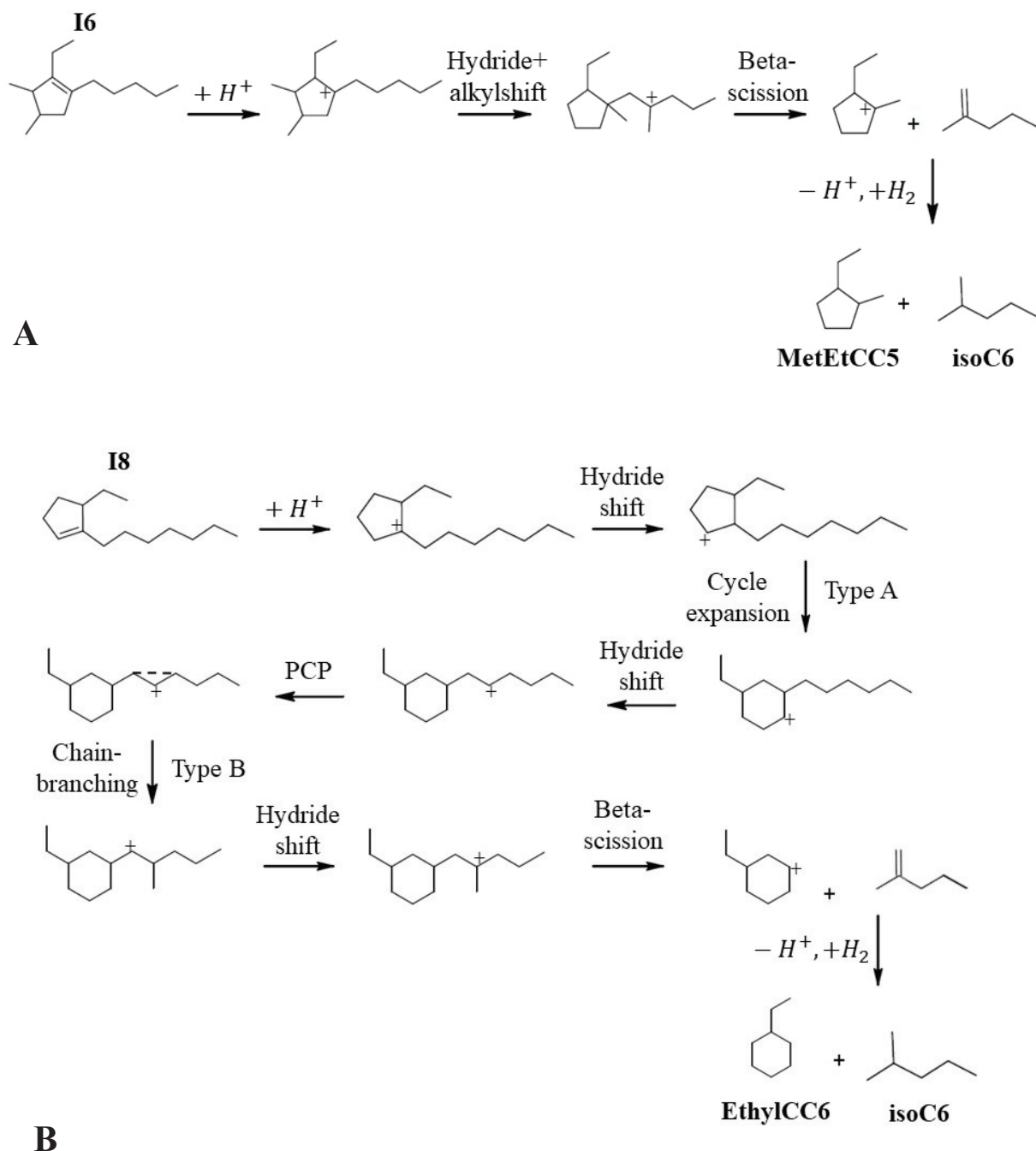


Figure 21. A) Suggested cracking pathway towards formation of methyl-ethylcyclopentane and methylpentane from hydrocracking of **I6** isomer over Pt/H-USY zeolite catalyst. B) Suggested cracking pathway towards formation of ethylcyclohexane and methylpentane from hydrocracking of **I8** isomer over Pt/H-USY zeolite catalyst.

Cracking to cyclohexane and isoC<sub>8</sub> is a minor reaction pathway and is, therefore, not discussed in detail.

### 4.3. Rationalization of the products distribution

In the previous section, hydrocracking pathways of octylcyclohexane isomers favoring the formation of cracked products on bifunctional Pt/H-USY catalyst were analyzed. In this section, we aim to explain the distribution of cracked compounds based on the degree of branching of the starting isomer molecule.

Cracked products, essentially constituted of naphthenes, were mainly comprised of monobranched C<sub>7</sub> compounds (Figure 9), which may be formed through hydrocracking of tribranched isomers. From the previous section, the best compromise to obtain C<sub>7</sub> molecules is through conversion of methyl-heptylcyclohexane (**I2**) and ethyl-heptylcyclopentane (**I8**) after alkyl-branching via PCP intermediate (type B isomerization). In addition to C<sub>7</sub> compounds, hydrocracking of octylcyclohexane on Pt/H-USY resulted in a flat distribution varying from 4 to 10 carbon atoms (Figure 6).

Most cracked C<sub>8</sub> to C<sub>10</sub> naphthenes were dibranched structures, therefore they originated from at least tetra-branched isomers, i.e. one more branching than the isomers, which can crack to methyl-cyclohexane. This additional branching competes with the cracking of tri-branched isomers. The tetra-branched isomers themselves can either branch further (to **I5** and **I3**), or crack to C<sub>8</sub>, C<sub>9</sub> and C<sub>10</sub> naphthenes. This competition can explain why the latter naphthenes are less abundant than C<sub>7</sub> naphthenes.

It is also remarkable that C<sub>8</sub>, C<sub>9</sub> and C<sub>10</sub> naphthenes are formed in equimolar amounts (Figure 8). This result suggests that a fast interconversion between the different tetrabranched compounds, which lead to C<sub>8</sub> to C<sub>10</sub> products, is possible, through alkyl-shifts and ring-contraction or expansion.

Finally, if branching continues to produce many short side chains (**I1** and **I3**), cracking becomes unfavored. A minimum of 4 carbon atoms is required to achieve a configuration allowing beta-scission.

The proportion of different isomers is result of compromise between formation and consumption by consecutive reactions, which is not easy to rationalize. Nevertheless, it seems that isomers which preferentially crack are constituted of long alkyl-substituents, i.e. less branched structures. Even if it is easier to crack multibranched structures, due to their higher

number of tertiary carbon atoms, a greater number of rearrangements will be required to achieve such conformations, leading to the preferential cleavage of more linear compounds. Multibranched isomers tend, therefore, to accumulate within the isomers subfamily. The following figure summarizes the reaction pathways discussed herein and present C<sub>14</sub>H<sub>28</sub> isomers that could easily lead to cracked compounds.

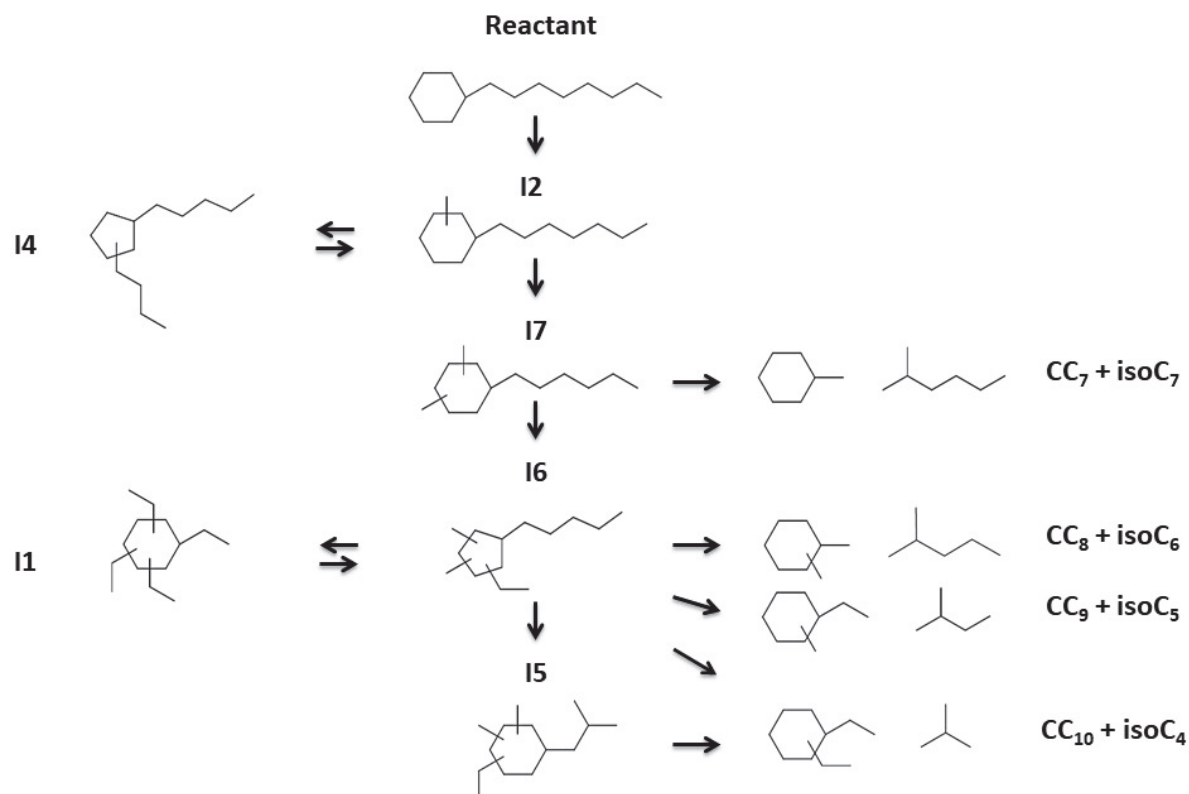


Figure 22. Reaction pathways and isomers that may lead to observed cracked compounds.

## 5. Conclusions

Hydroisomerization and hydrocracking of octylcyclohexane were performed over a bifunctional Pt/H-USY zeolite catalyst at 300°C and 60 bar. Octylcyclohexane was obtained through *in situ* hydrogenation of the parent aromatic compound, phenyloctane, over a metallic pre-catalyst, Pt/Al<sub>2</sub>O<sub>3</sub>. The reaction products were identified and quantified with comprehensive GCxGC-FID/MS analysis, and lumped into groups, according to carbon

number and chemical family. Hydroconversion of octylcyclohexane over the bifunctional catalyst resulted in several isomerization products, presenting distinct degrees of branching. Cracked products became predominant even at average conversion, while ring-opening products were almost not perceived throughout the reaction.

Hydrocracking of octylcyclohexane over Pt/H-USY zeolite catalyst generated a broad distribution of cracked products, comprised mainly of C<sub>7</sub> naphthenes. Pathways leading to major cracked products were also depicted, revealing the preferential formation of dibranched naphthenes. The reaction steps needed to form isomers and cracked products were analyzed in detail, by taking into account rearrangements of the cycle, i.e. ring-contraction or expansion, alkyl-shifts, and branching of the alkyl-substituent.

A correlation between the number of slow steps to form each isomer (type B rearrangement) and their proportion within the C<sub>14</sub>H<sub>28</sub> family showed that multibranched structures require a high number of type B rearrangements to be synthesized, and are less favored in comparison to less branched compounds.

On the other hand, multibranched isomers may easily undergo hydrocracking due to their higher number of tertiary carbon atoms, but their formation requires a greater number of rearrangements than less branched structures. Therefore, structures that present long alkyl-substituents are more suitable to be cracked and generate the reaction products obtained from hydroconversion of octylcyclohexane on Pt/H-USY bifunctional catalyst.

## REFERENCES

- [1] B. Viswanathan, Chapter 2 - Petroleum, in: B. Viswanathan (Ed.), *Energy Sources*, Elsevier, Amsterdam, 2017, pp. 29–57.
- [2] J.G. Speight, Thermal Decomposition of Hydrocarbons, in: J.G. Speight (Ed.), *Handbook of industrial hydrocarbon processes*, Elsevier/Gulf Professional Publishing, Amsterdam, Boston, 2011, pp. 395–428.
- [3] R. Sahu, B.J. Song, J.S. Im, Y.-P. Jeon, C.W. Lee, A review of recent advances in catalytic hydrocracking of heavy residues, *Journal of Industrial and Engineering Chemistry* 27 (2015) 12–24.
- [4] A. K.H., M.M. Boduszynski, *Composition and analysis of heavy petroleum fractions*, Marcel Dekker, New York, 1993.

- [5] Thomas Dutriez, *Chromatographie multidimensionnelle vers une caractérisation moléculaire étendue des charges type distillat sous vide et la compréhension de leur réactivité à l'hydrotraitement*, Paris, 2010.
- [6] F. Alvarez, F.R. Ribeiro, G. Perot, C. Thomazeau, M. GUISET, Hydroisomerization and Hydrocracking of Alkanes, *Journal of Catalysis* 162 (1996) 179–189.
- [7] V. Calemme, S. Peratello, C. Perego, Hydroisomerization and hydrocracking of long chain n-alkanes on Pt/amorphous SiO<sub>2</sub>-Al<sub>2</sub>O<sub>3</sub> catalyst, *Applied Catalysis A: General* 190 (2000) 207–218.
- [8] M.C. Claude, G. Vanbutsele, J.A. Martens, Dimethyl Branching of Long n-Alkanes in the Range from Decane to Tetracosane on Pt/H-ZSM-22 Bifunctional Catalyst, *Journal of Catalysis* 203 (2001) 213–231.
- [9] J. Weitkamp, Peter A. Jacobs, J. A. Martens, Isomerization and hydrocracking of C9 through C16 n-alkanes on Pt/HZSM-5 zeolite, *Applied Catalysis* 8 (1983) 123–141.
- [10] Y. Bi, G. Xia, W. Huang, H. Nie, Hydroisomerization of long chain n-paraffins, *RSC Adv.* 5 (2015) 99201–99206.
- [11] Johan A. Martens, Mia Tielen and Peter A. Jacobs, Attempts To Rationalize The Distribution Of Hydrocracked Products., *Catalysis Today* 1 (1987) 435–453.
- [12] J.A. Martens, P.A. Jacobs, Evidence for branching of long-chain n-alkanes via protonated cycloalkanes larger than cyclopropane, *Journal of Catalysis* 124 (1990) 357–366.
- [13] E. Blomsma, J. A. Martens, P. A. Jacobs, Reaction mechanisms of isomerization and cracking of heptane on Pd/H-Beta zeolite, *Journal of Catalysis* 155 (1995) 141–147.
- [14] G. Burnens, C. Bouchy, E. Guillon, J.A. Martens, Hydrocracking reaction pathways of 2,6,10,14-tetramethylpentadecane model molecule on bifunctional silica–alumina and ultrastable Y zeolite catalysts, *Journal of Catalysis* 282 (2011) 145–154.
- [15] G. Noh, Z. Shi, S.I. Zones, E. Iglesia, Isomerization and  $\beta$ -scission reactions of alkanes on bifunctional metal-acid catalysts, *Journal of Catalysis* 368 (2018) 389–410.
- [16] P.A. Jacobs, J.A. Martens, Chapter 12 Introduction to Acid Catalysis with Zeolites in Hydrocarbon Reactions, in: H. van Bekkum, E.M. Flanigen, J.C. Jansen (Eds.), *Introduction to zeolite science and practice*, Elsevier, Amsterdam, New York, 1991, pp. 445–496.
- [17] J. Weitkamp, Catalytic Hydrocracking-Mechanisms and Versatility of the Process, *ChemCatChem* 4 (2012) 292–306.
- [18] A. Soualah, J.L. Lemberon, L. Pinard, M. Chater, P. Magnoux, K. Mojord, Hydroisomerization of long-chain n-alkanes on bifunctional Pt/zeolite catalysts, *Appl Catal a-Gen* 336 (2008) 23–28.

- [19] J. Weitkamp, Isomerization of Long-chain n -Alkanes on a Pt/CaY Zeolite Catalyst, *Ind. Eng. Chem. Prod. Res. Dev.* 21 (1982) 550–558.
- [20] M.C. Claude, J.A. Martens, Monomethyl-branching of long n-alkanes in the range from decane to tetracosane on Pt/H-ZSM-22 bifunctional catalyst, *J. Catal.* 190 (2000) 39–48.
- [21] M.C. Claude, G. Vanbutsele, J.A. Martens, Dimethyl branching of long n-alkanes in the range from decane to tetracosane on Pt/H-ZSM-22 bifunctional catalyst, *J. Catal.* 203 (2001) 213–231.
- [22] S. Sayan, B. Demirel, J. Paul, Methyldecalin hydrocracking over palladium/zeolite-X, *Fuel* 79 (2000) 1395–1404.
- [23] Tobias Holl, Competitive Hydroconversion of Decalin and n-Decane on Noble-Metal Catalysts and the Evaluation of Molybdenum Carbide as Ring-Opening Catalyst.
- [24] Sato, K., Iwata Y., Miki Y., Shimada H., Hydrocracking of Tetralin over NiW/USY Zeolite Catalysts: For the Improvement of Heavy-Oil Upgrading Catalysts, *Journal of Catalysis* 186 (1999) 45–56.
- [25] S.G.A. Ferraz, B.M. Santos, F.M.Z. Zotin, L.R.R. Araujo, J.L. Zotin, Influence of Support Acidity of NiMo Sulfide Catalysts for Hydrogenation and Hydrocracking of Tetralin and Its Reaction Intermediates, *Ind. Eng. Chem. Res.* 54 (2015) 2646–2656.
- [26] R. Nageswara Rao, N. You, S. Yoon, D.P. Upare, Y.-K. Park, C.W. Lee, Selective Ring Opening of Methylcyclopentane and Methylcyclohexane Over Iridium Bifunctional Catalysts Supported on Surface Modified  $\gamma$ -Al<sub>2</sub>O<sub>3</sub>, SiO<sub>2</sub> and Ultra Stable Y Zeolites, *Catal Lett* 141 (2011) 1047–1055.
- [27] J. Weitkamp, P.A. Jacobs, S. Ernst, Shape Selective Isomerization and Hydrocracking of Naphthenes Over Pt/Hzsm-5 Zeolite, in: P.A. Jacobs, N.I. Jaeger, P. Jírů, V.B. Kazansky, G. Schulz-Ekloff (Eds.), *Structure and Reactivity of Modified Zeolites*, Elsevier, 1984, pp. 279–290.
- [28] J. Weitkamp, S. Ernst, Comparison Of The Reactions Of Ethylcyclohexane And 2-Methylheptane On Pd/Lay Zeolite, in: B. Imelik, C. Naccache, G. Coudurier, Y. Ben Taarit, J.C. Vedrine (Eds.), *Catalysis by Acids and Bases*, Elsevier, 1985, pp. 419–426.
- [29] J.A.M. Arroyo, J.W. Thybaut, G.B. Marin, P.A. Jacobs, J.A. Martens, G.V. Baron, Reaction Pathways of 1-Cyclohexyloctane in Admixture with Dodecane on Pt/H-ZSM-22 Zeolite in Three-Phase Hydroconversion, *Journal of Catalysis* 198 (2001) 29–40.
- [30] J. Weitkamp, S. Ernst, H.G. Karge, Peculiarities in the conversion of naphthenes on bifunctional catalysts, *Erdöl & Kohle, Erdgas, Petrochemie.* 37 (1984).
- [31] G.G. Martens, J.W. Thybaut, G.B. Marin, Single-Event Rate Parameters for the Hydrocracking of Cycloalkanes on Pt/US-Y Zeolites, *Ind. Eng. Chem. Res.* 40 (2001) 1832–1844.



- [32] D.M. Brouwer, H. Hogeveen, *Recl. Trav. Chim. Pays-Bas* 89 (1970) 211–224.
- [33] C.J. Egan, G.E. Langlois, R.J. White, Selective Hydrocracking of C<sub>9</sub> - to C<sub>12</sub> - Alkylcyclohexanes on Acidic Catalysts. Evidence for the Paring Reaction, *J. Am. Chem. Soc.* 84 (1962) 1204–1212.
- [34] W. Souverijns, R. Parton, J.A. Martens, G.F. Froment, P.A. Jacobs, Mechanism of the paring reaction of naphthenes, *Catal Lett* 37 (1996) 207–212.
- [35] L. Leite, E. Benzzi, N. Marchal-George, H. Toulhoat, Hydrocracking of phenanthrene over Pt/SiO<sub>2</sub>-Al<sub>2</sub>O<sub>3</sub>, Pt/H-Y, Pt/H-β and Pt/H-ZSM-5 catalysts: Reaction pathway and products distribution, in: A. Corma (Ed.), 12th International Congress on Catalysis: Proceedings of the 12th ICC, Granada, Spain, July 9-14, 2000, 1st ed., Elsevier, Amsterdam, New York, 2000, pp. 2495–2500.
- [36] Lorraine Leite, Eric Benazzi, Nathalie Marchal-George, Hydrocracking of phenanthrene over bifunctional Pt catalysts, *Catalysis Today* 65 (2001) 241–247.
- [37] V.A. Filimonov, Popov A.A., Khavkin V.A., Perezhigina I.Y., L.N. Osipov, S.P. Rogov, A.V. Agafonov, *Int Chem Eng* 12 (1972).
- [38] P.S.F. Mendes, J.M. Silva, M.F. Ribeiro, A. Daudin, C. Bouchy, From powder to extrudate zeolite-based bifunctional hydroisomerization catalysts, *Journal of Industrial and Engineering Chemistry* 62 (2018) 72–83.
- [39] J.Prasad, K.R.Murthy, P.G.Menon, The The stoichiometry of Hydrogen-Oxygen titration on supported Platinum catalysts, *Journal of Catalysis* 52 (1978) 515–520.
- [40] M. Guisnet, “Ideal” bifunctional catalysis over Pt-acid zeolites, *Catalysis Today* 218-219 (2013) 123–134.
- [41] A. Haas, Ring Opening of Mono- and Bicyclic Naphthenes via Hydrogenolysis on Noble Metal Catalysts, 2012.
- [42] G. McVicker, Selective Ring Opening of Naphthenic Molecules, *Journal of Catalysis* 210 (2002) 137–148.
- [43] C. Marcilly, D. Decroocq, T. Jones, *Acido-basic catalysis*, Ed. Technip, Paris, 2005 - 2006.



<b>Figure 1.</b> GCxGC-FID analysis of reaction products from hydroconversion of octylcyclohexane obtained over A) Pt/H-USY zeolite catalyst at 71% conversion (300 °C); B) Pt/H-Beta zeolite catalyst at 72% conversion (280 °C); C) Pt/ASA amorphous catalyst at 71% conversion (300 °C).....	174
<b>Figure 2.</b> Molecule families and typical examples of molecules in the reaction products of hydroconversion of octylcyclohexane over Pt/zeolites, Pt/ASA and sulfide bifunctional catalysts. Further details on reaction products are available in our previous work. (ref).....	175
<b>Figure 3.</b> Evolution of octylcyclohexane conversion with contact time at 300°C on Pt and NiMoS/H-USY (red triangles), Pt and NiMoS/H-BETA (black squares) catalyst extrudates with 1 wt.% zeolite in alumina binder; and Pt and NiMoS/ASA catalysts (blue circles). Hollow and full symbols correspond to NiMoS- and Pt-based bifunctional catalysts, respectively.....	176
<b>Figure 4.</b> Selectivity to isomerization, ring-opening and cracked products as a function of octylcyclohexane conversion over A) Pt-based catalysts; and B) sulfide catalysts. Data obtained at 280°C are indicated in the legend box. ....	178
<b>Figure 5.</b> Distribution of substituted cyclopentane and substituted cyclohexane isomers of octylcyclohexane over A) Pt/H-USY and Pt/H-Beta zeolite catalyst and B) Pt/H-USY and Pt/ASA bifunctional catalysts at isoconversion. ....	180
<b>Figure 6.</b> Yield of cracked products according to the number of carbon atoms at different levels of octylcyclohexane conversion over Pt-supported bifunctional catalysts.....	181
<b>Figure 7.</b> Yield of cracked products according to the number of carbon atoms at different levels of octylcyclohexane conversion over Pt (top) and NiMoS-based (bottom) bifunctional catalysts. ....	182
<b>Figure 8.</b> Distribution of cracked products as a function of octylcyclohexane conversion over A) bifunctional Pt/ zeolites and Pt/ASA catalysts and B) bifunctional sulfide catalysts....	184
<b>Figure 9.</b> Distribution of C <sub>6</sub> naphthenes as a function of octylcyclohexane conversion over bifunctional Pt/H-USY and Pt/H-Beta zeolite catalysts.....	185
<b>Figure 10.</b> Distribution of alkanes as a function of octylcyclohexane conversion over bifunctional Pt/H-USY and Pt/H-Beta zeolite catalysts.....	186
<b>Figure 11.</b> Yield of cracked products expressed in mol per 100 mol of cracked products on A) Pt/H-USY (top left) and NiMoS/H-USY (top right) zeolite catalysts; B) Pt/H-Beta (bottom left) and NiMoS/H-Beta (bottom right) zeolite catalysts. ....	189
<b>Figure S 1.</b> Distribution of positional and ring-contraction isomers of octylcyclohexane over A) Pt/H-USY, B) Pt/H-Beta and C) Pt/ASA bifunctional catalysts. ....	198

---

## TABLE OF FIGURES – CHAPTER V

---

<b>Figure S 2.</b> Distribution of C7 naphthenes as a function of octylcyclohexane conversion over bifunctional NiMoS/H-USY and NiMoS/H-Beta zeolite catalysts. ....	199
<b>Figure S 3.</b> Distribution of alkanes as a function of octylcyclohexane conversion over bifunctional NiMoS/H-USY and NiMoS/H-Beta zeolite catalysts. ....	199
<b>Figure S 4.</b> Conversion of n-hexadecane as a function of temperature over Pt/H-USY, Pt/H-Beta and Pt/ASA bifunctional catalysts. ....	200

---

# CHAPTER V: HYDROCONVERSION OF OCTYLCYCLOHEXANE OVER BIFUNCTIONAL CATALYSTS: USY VS. BETA VS. SILICA-ALUMINA AND PT VS. MO<sub>2</sub>S

---

## Highlights

- Similar reaction pathways resulted from hydroconversion of octylcyclohexane over Pt/zeolites and NiMoS/zeolites catalysts. Sulfide catalysts led to over-cracking.
- Beta zeolites were more effective to process linear molecules, as octylcyclohexane and n-hexadecane, while USY zeolites were more active in the conversion of bulky naphthenes.

## Abstract

Hydroisomerization and hydrocracking of octylcyclohexane (C<sub>14</sub>H<sub>28</sub>) were performed over Pt and NiMoS-supported catalysts, at 300°C and 60 bar, with a molar H<sub>2</sub> to hydrocarbon ratio of 7 mol/mol. The feed, composed of 5 wt.% phenyloctane dissolved in n-heptane, was initially hydrogenated *in situ* over a pre-catalyst, Pt or NiMoS/Al<sub>2</sub>O<sub>3</sub>. The C<sub>14</sub> naphthene underwent isomerization and cracking under high hydrogen pressure over the bifunctional catalysts, whose acid function was represented by large-pore zeolites (USY, Beta) or amorphous silica-alumina (ASA). Similar reaction intermediates resulted from hydroconversion of octylcyclohexane over Pt and NiMoS bifunctional catalysts, thus the reaction pathway was not affected by the hydrogenating function tested. Sulfide catalysts were less well equilibrated than Pt ones and led to over-cracking. Pt/H-Beta was more active in hydroconversion of octylcyclohexane and n-hexadecane, an opposite trend to that observed on conversion of perhydrophenanthrene, confirming the preferential transformation of linear molecules over Beta-supported zeolites.

**Keywords:** octylcyclohexane, hydroconversion, Pt, ultrastable Y zeolite, Beta zeolite, amorphous silica-alumina, sulfide catalysts

## 1. Introduction

Hydrocracking is a refining process for the upgrading of heavy oil fractions. Bifunctional catalysts are employed in hydrocracking. Their structure comprises a hydrogenating function, generally represented by molybdenum sulfides, promoted by nickel or cobalt [1–3]; and an acid function, characterized by zeolites or amorphous silica-alumina [4–8]. Stronger hydrogenating components, as Pt or Pd, may be used in a sulfide-free environment [9–12], but this condition can only be achieved in two-stage hydroprocessing of heavy oil fractions [13]. Sulfide catalysts are therefore widely used in hydrocracking units thanks to their resistance to H<sub>2</sub>S, generated by hydrodesulfurization of the oil [14–17].

In an ideal case, bifunctional catalysts are designed to be equilibrated, which means that the (de)hydrogenating function operates close to thermodynamic equilibrium and that conversion and product distribution only depend on the properties of the acid function [18–23]. Sulfide catalysts are much less active in (de)hydrogenation than Pt or Pd catalysts. Thus, they are generally not equilibrated and tend to produce lighter products by over-cracking, even when very high metal loadings (up to 30% MoO<sub>3</sub>) are used.

The selectivity towards desired hydrocracked products may be tuned as a function of the acid phase [24–30]. Amorphous silica-alumina catalysts give higher selectivity to middle distillates, whereas zeolite hydrocracking catalysts are more selective towards naphtha.

In our previous works on hydroconversion of a tricyclic naphthene (perhydrophenanthrene, PHP) over Pt-supported bifunctional catalysts, shape selective effects played an important role in the formation of specific reaction intermediates according to the type of acid catalyst. Bridged perhydrophenanthrene isomers, referred to as alkyladamantanes, and ring-contraction skeletal isomers were preferentially processed on USY zeolites, whereas Beta-supported catalysts favored ring-shift compounds, as perhydroanthracene stereoisomers. This was attributed to the pores system of USY zeolites, large enough to accommodate bulky molecules. Molecular simulation indicated a hindered adsorption of alkyladamantanes and ring-contraction isomers on Pt/H-Beta catalyst. In spite of their mesopores, ASA catalysts did not produce large molecules as alkyladamantanes.

Shape selectivity effects were also decisive in the formation of ring-opening products leading to different distributions of carbon atoms over each zeolite. While USY catalysts gave a broad distribution of cracked products, Beta zeolites privileged cracking to C<sub>7</sub> compounds.

With respect to hydroconversion of octylcyclohexane, previous work carried out over bifunctional Pt/H-USY catalyst (Chapter IV) evidenced a complex distribution of isomerization products, that led to major cracking to C<sub>7</sub> molecules and homogeneous distribution of remaining carbon atoms, i.e. from C<sub>4</sub> to C<sub>10</sub> compounds. The distribution of cracked products was rationalized from the degree of branching of octylcyclohexane isomers. It was elucidated that less branched isomers were more suitable to undergo hydrocracking than multibranched ones, because of the small number of type B isomerization necessary to produce the former.

The goal of this work is to compare the activity of Pt and sulfide bifunctional catalysts and hydrocracking pathways in the hydroconversion of a long alkyl-chain substituted monocyclic naphthene, represented by octylcyclohexane (C<sub>14</sub>H<sub>28</sub>). For that purpose, commercial large-pore zeolites, as ultrastable Y zeolite (CBV720) and Beta (CP814e), along with amorphous silica-alumina (Siralox 30, abbreviated as ASA) were tested in a sulfide-free environment and in the presence of H<sub>2</sub>S. Key points to be addressed are the reactivity of the model molecule in these distinct environments, and if hydrocracking pathways are changed according to the equilibrium of metal and acid functions on both systems tested.

Further objectives consist of analyzing the reaction pathways of hydroconversion of perhydrophenanthrene and octylcyclohexane, assess the reactivity of both model molecules and compare it to hydroconversion of n-hexadecane, a long alkyl-substituent alkane.

## 2. Materials and methods

### 2.1. Preparation and characterization of catalysts

Commercial supports for USY (CBV720) and Beta (CP814e) zeolite catalysts were provided in powder form by Zeolyst. They were mixed with alumina binder (Pural SB3 from Sasol) and extruded, according to a procedure described elsewhere (Chapters II and III; [31]).

Commercial silica-alumina supports (Siralox 30) were obtained from Sasol already in their extruded shape. Calcination of the supports was performed at 600°C, under air flow of 1.5 NL/h/g<sub>support</sub>. Impregnation of Platinum on the alumina binder was performed through ionic exchange, employing chloroplatinic acid hydrate (H<sub>2</sub>PtCl<sub>6</sub> from Sigma-Aldrich) as Pt precursor and hydrochloric acid as competitor. The detailed preparation of Pt-supported catalysts can be found in previous works (Chapters II and III). Pt catalysts were calcined at 520°C, under air flow of 1 NL/h/g<sub>catalyst</sub>. A pre-catalyst 0.8 wt.% Pt/Al<sub>2</sub>O<sub>3</sub> was also prepared using the same method. The length of the extrudates was kept between 3 and 6 mm.

The same supports were used for the preparation of sulfide catalysts. For this purpose, a solution containing the metal precursors Ni, Mo and P was formulated by aiming a weight fraction of 24 wt.% MoO<sub>3</sub>, with a molar Ni to Mo ratio of 0.4 mol/mol, and a molar P to Mo ratio of 0.48 mol/mol on the dried catalyst. For the synthesis of the catalyst NiMoS/Al<sub>2</sub>O<sub>3</sub>, citric acid was added to the solution, with a molar citric acid to Mo ratio of 0.3 mol/mol. The solution containing (heteropoly)molybdates, phosphates and Ni<sup>2+</sup> cations was heated to 80°C for 12h to dissolve all components and then cooled down to room temperature. After incipient wetness impregnation of the supports, the humidified catalysts were placed in a reservoir overnight, in order to achieve a uniform distribution of the metallic phase over the alumina binder. The extrudates were then dried at 120°C during 15h and sorted to lengths varying from 3 to 6 mm.

Pt-catalysts were characterized with X-ray fluorescence and H<sub>2</sub>-O<sub>2</sub> chemisorption (Table 1). The concentration of Brønsted Acid Sites (BAS) in the shaped zeolites was calculated by considering that it was proportional to that of the parent zeolite, i.e. presuming that the extrusion process did not affect its acidity. The concentration of BAS of parent zeolites was provided from pyridine adsorption followed by FTIR, as described in literature [31]. The content of molybdenum, nickel and phosphorus precursors impregnated over the alumina binder in sulfide catalysts, obtained with X-ray fluorescence, is indicated in Table 2. The compacted bulk density (CBD) of each catalyst is also recapitulated.



Table 1. Properties of Pt-loaded zeolite and amorphous catalysts determined by X-ray fluorescence, H<sub>2</sub>-O<sub>2</sub> chemisorption and pyridine adsorption monitored with FTIR.

Type of support	Zeolite content in binder (wt. %)	Pt loading (wt. %)	Pt dispersion (%)	Pt particle size (nm)	n <sub>Pt</sub> (μmol/g)	BAS (μmol/g)
USY (CBV720)	1	0.60	48	2.3	9.0	2.0
Beta (CP814e)	1	0.65	45	2.5	9.0	2.2
ASA (Siralox 30)	-	0.60	84	1.3	15.8	n.d.

Table 2. Properties of bifunctional sulfide catalysts determined by X-ray fluorescence, and respective compacted bulky density (CBD).

Type of support	Zeolite content in binder (wt. %)	MoO <sub>3</sub> (wt. %)	NiO (wt.%)	P <sub>2</sub> O <sub>3</sub> (wt.%)	CBD (g/cm <sup>3</sup> )
USY (CBV720)	1	24.0	4.9	5.7	1.12
Beta (CP814e)	1	24.9	5.2	5.9	1.14
ASA (Siralox 30)	-	23.9	4.9	5.7	0.97

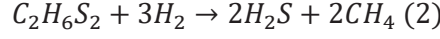
## 2.2. Catalytic tests

Hydroconversion of octylcyclohexane was performed over Pt and sulfide catalysts, following slightly different setups and protocols. Pt-based supported catalysts were tested at 300°C and 60 bar, in a fixed-bed downflow reactor, which was loaded with 2 g of a metallic (Pt/Al<sub>2</sub>O<sub>3</sub>) and 2 g of the bifunctional catalyst (Pt/zeolite or Pt/ASA). Both solids were reduced *in situ*

at 450°C under hydrogen flow of 1 NL/h/g<sub>catalyst</sub> prior to the tests. The metallic catalyst was employed to hydrogenate the aromatic feedstock, constituted of 5 wt.% phenyloctane (Alfa Aesar) diluted into 95 wt.% n-heptane (AnalaR Normapur), to the naphthenic model molecule. A hydrogen to hydrocarbons molar ratio of 7 mol/mol prevented the deactivation of the catalysts and promoted hydrogenation of phenyloctane (C<sub>14</sub>H<sub>22</sub>) to octylcyclohexane (C<sub>14</sub>H<sub>28</sub>). The hydrogenated feedstock was isomerized and cracked afterwards over the zeolite or amorphous silica-alumina catalysts. The conversion of octylcyclohexane was regulated by changing the feed flow entering the reactor. The reaction products were analyzed with GC-FID and GCxGC-FID/MS, according to a protocol described in a previous work (Chapter II).

Sulfide catalysts were tested in another fixed-bed downflow micro-reactor of 16 cm<sup>3</sup> volume. Similarly, the tests were carried out at 280 or 300°C and 60 bar, in total gas-phase conditions. The hydrogen to hydrocarbon molar ratio as well as the composition of the feedstock were equivalent to Pt-based catalytic tests. The reactor was charged with both metallic (NiMoS/Al<sub>2</sub>O<sub>3</sub>) and bifunctional (NiMoS/zeolite or NiMoS/ASA) catalysts. The same volume of catalyst was used throughout the tests, corresponding to 2 cm<sup>3</sup> per solid. The conversion of the apparent first-order constant per volume of catalyst ( $k_v$ ) to the apparent constant per mass of catalyst ( $k_m$ ) is given in Equation 1. The contact time on sulfide-based catalytic tests was corrected according to  $k_m$ . The solids were reduced *in situ* prior to the catalytic tests. The sulfidation feedstock was composed of 94.12 wt.% cyclohexane and 5.88 wt.% dimethyl-disulfide (DMDS). Under hydrogen flow, DMDS decomposes itself to H<sub>2</sub>S at 220°C, according to Equation 2. The activation was executed during 5h at 350°C, until the beginning of the test. The aromatic feedstock was hydrogenated to octylcyclohexane over NiMoS/Al<sub>2</sub>O<sub>3</sub>, before being isomerized and cracked over the bifunctional catalysts. All reaction products were quantified in gas phase with a GC-FID apparatus (Agilent) coupled online to the catalytic unit. A handmade collector allowed the sampling of reaction products in liquid phase. The liquid phase was only used for identification of reaction products with GC-MS. Quantification was done with the online gas phase analysis. A detailed description of the analysis of reaction products is provided in next section.

$$k_m = k_v \frac{\rho_{feed}}{CBD} \cdot \frac{1}{(1 - \sum \text{metal oxides wt. \%})(1 - LOI)} \quad (1) \quad \therefore k_v = \frac{Q_{feedstock} \left[ \frac{cm^3}{h} \right]}{V_{catalyst} [cm^3]} \cdot \ln \frac{1}{1 - X}$$



Octylcyclohexane conversion (X), yield (Y), yield of cracked products (Y<sub>Ci</sub>) and distribution (D) of a product (i) within a given family (J) were calculated through Equations 4-8. They allow to evaluate the catalytic performance of the solids tested, according to the approach applied in our previous work (Chapter II).

*Molar flow in respect to the number of carbons*

$$N_i = \frac{(wt. \%)_i * F_m * c_i}{(100 * M_i)} \quad (4)$$

Where  $F_m$  is the mass flow of the feedstock and (wt., %) <sub>i</sub>,  $c_i$  and  $M_i$  corresponds to the mass fraction, the number of carbons and the molar mass of the component  $i$  at the outlet.

*Conversion of octylcyclohexane*

$$X = 1 - \frac{N_{OCC6,out}}{\sum_{i=1}^{i=14} N_{i,out}} \quad (5)$$

*Yield on a carbon basis*

$$Y_i = \frac{N_i}{\frac{100}{196}} \quad (6)$$

*Molar yield of cracked products*

$$Y_{C_i} = \left( \frac{1}{i} \sum_k^{n_k} N_{i,k} / \frac{1}{14} \sum_{i=1}^{13} \sum_k^{n_k} N_{i,k} \right) * 100\% \quad (7)$$

*Distribution of component i within a family J*

$$D_{i,J} = \frac{N_{i \in J}}{\sum N_{i \in J}} \quad (8)$$

### 2.3. Methodology of analysis of reaction products

The analysis of reaction products resulting from hydroconversion of octylcyclohexane over sulfide catalysts was effected with gas chromatography (Agilent) coupled either to a FID or MS detectors (Single Quadrupole provided by LECO). The chromatograph was equipped with a 50 m H-PONA column from Agilent, with internal diameter of 0.2 mm and film thickness of 0.5  $\mu\text{m}$ , separating the components by boiling point. The temperature programming of the oven started at 40°C, holding it during 5 minutes; the temperature was increased to 120°C, with a heating rate of 1.5°C/min; then from 120°C to 135°C at 0.75°C/min and holding it during 10 minutes; next from 135°C to 160°C at 0.75°C/min, holding it during 5 minutes; and finally from 160°C to 230°C, holding it during 5 minutes. A 1  $\mu\text{L}$  volume of the products sample was injected, with a split ratio of 100. Helium was used as carrier gas at a constant flow rate of 10 mL/min. The flame ionization detector temperature was set at 300°C. Regarding the mass spectrometry analysis, the ion source temperature was kept at 230°C, while the ionization energy was configured at 70 eV. The analysis of mass spectra was carried out with NIST MS database (version 8) and compared to data available in literature [32,33].

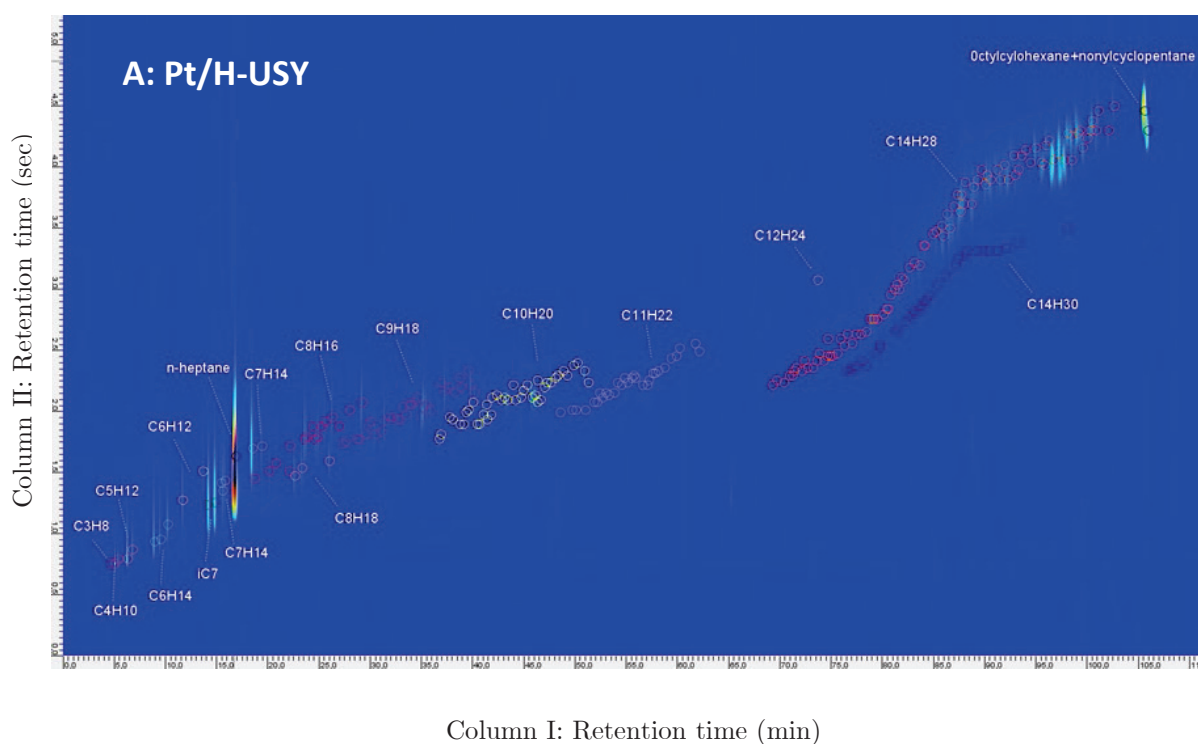
## 3. Results

### 3.1. Identification and quantification of reaction products with GCxGC – FID/MS

Prior to hydroisomerization and hydrocracking of the naphthenic model molecule, octylcyclohexane, the initial feedstock composed of phenyloctane diluted into n-heptane was completely hydrogenated *in situ* on a pre-catalyst Pt/Al<sub>2</sub>O<sub>3</sub> or NiMoS/Al<sub>2</sub>O<sub>3</sub>. Only octylcyclohexane and its isomer, nonylcyclopentane, were identified among the hydrogenated products. Both compounds were considered as the model reactant which underwent hydroconversion over the zeolite and amorphous bifunctional catalysts. For the sake of simplification, the reactant will be herein referred to as octylcyclohexane.

The reaction products resulting from hydroconversion of octylcyclohexane over Pt-supported bifunctional catalysts were individually identified and quantified with GCxGC-FID/MS.

These analysis enabled the quantification of more than 200 compounds, as displayed in the following chromatograms (Figure 1). They were obtained at similar octylcyclohexane conversion, ca. 70%. Figure 1 suggests that at first sight, the product distribution is quite similar for the three catalysts. For the analysis of the global reaction pathways, the products were lumped into isomers of octylcyclohexane (C<sub>14</sub>H<sub>28</sub>), ring-opening products (C<sub>14</sub>H<sub>30</sub>) and cracked products with a carbon number lower than 14 (Figure 2). Ring opening products were only quantified as trace compounds, which confirms that opening of the ring of a monocyclic naphthene is a difficult reaction [34].



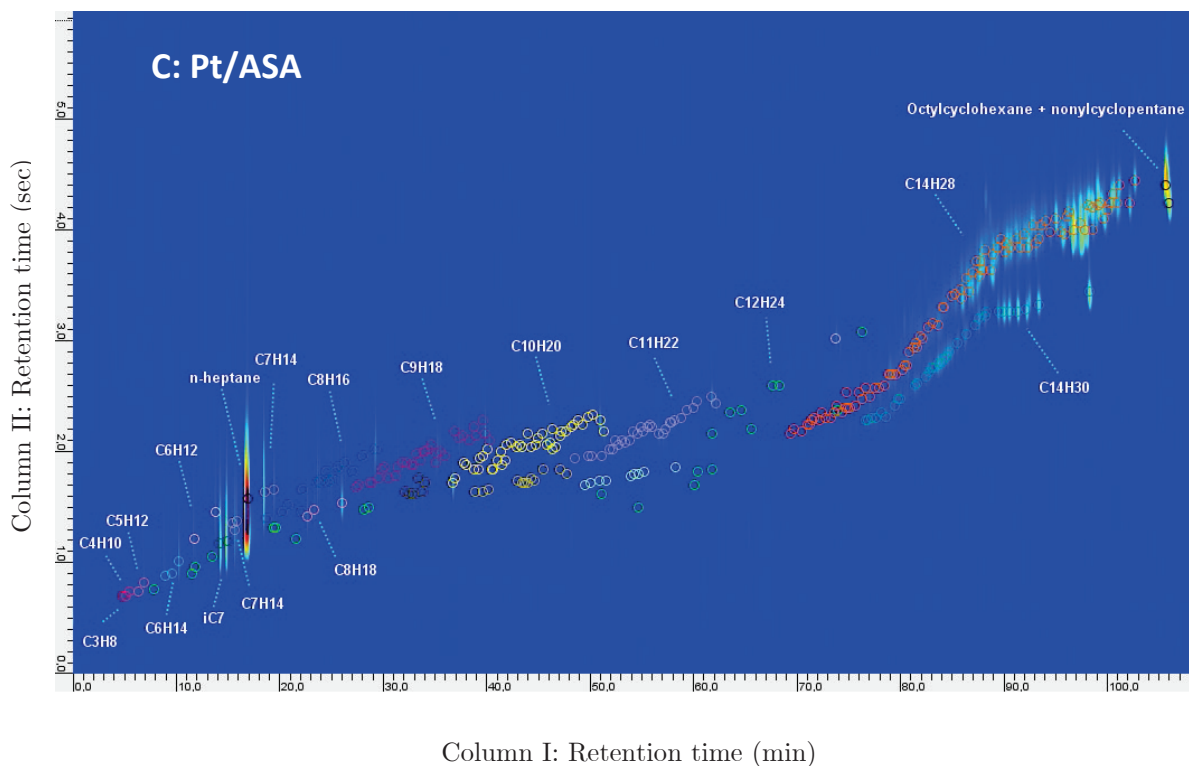
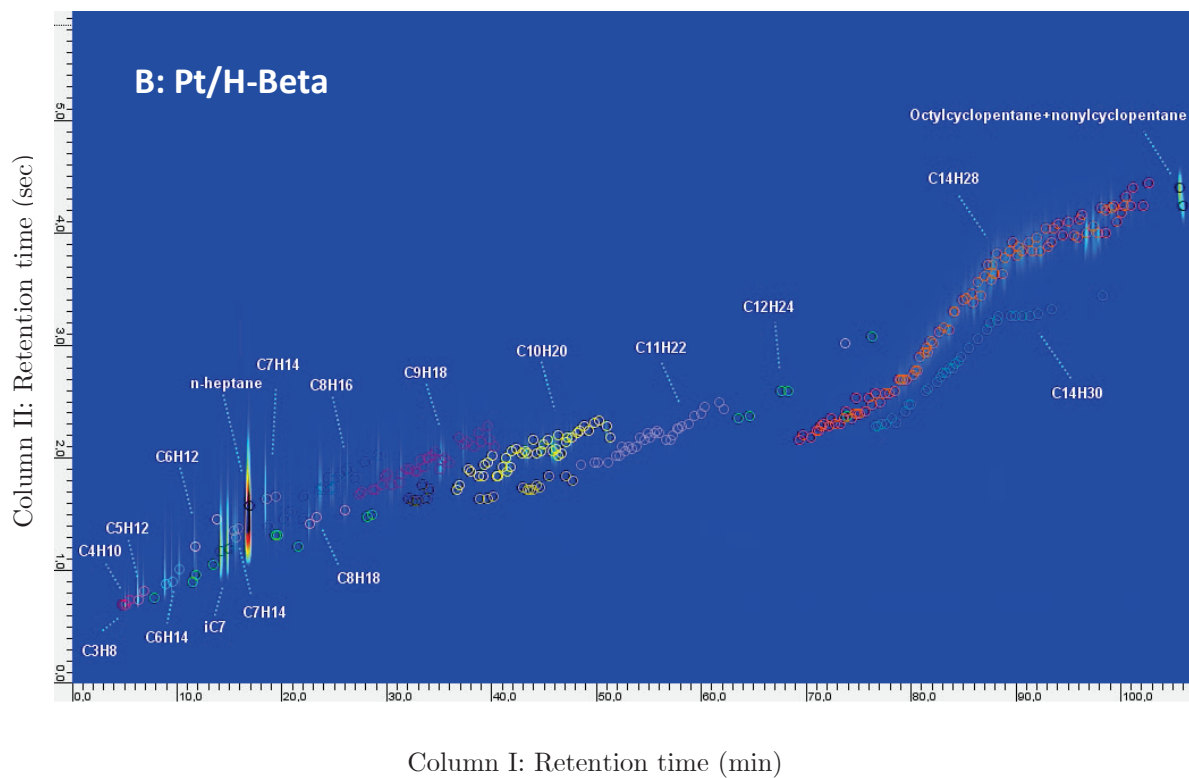


Figure 1. GCxGC-FID analysis of reaction products from hydroconversion of octylcyclohexane obtained over A) Pt/H-USY zeolite catalyst at 71% conversion (300 °C); B) Pt/H-Beta zeolite catalyst at 72% conversion (280 °C);

C) Pt/ASA amorphous catalyst at 71% conversion (300 °C).

The compounds generated on sulfide catalysts were identified with GC/MS and quantified with GC-FID. The one-dimensional GC analysis did not allow distinguishing ring-opening products from C<sub>14</sub>H<sub>28</sub> isomers, but since the former were only trace products, this should not have much impact on the interpretation of the results.

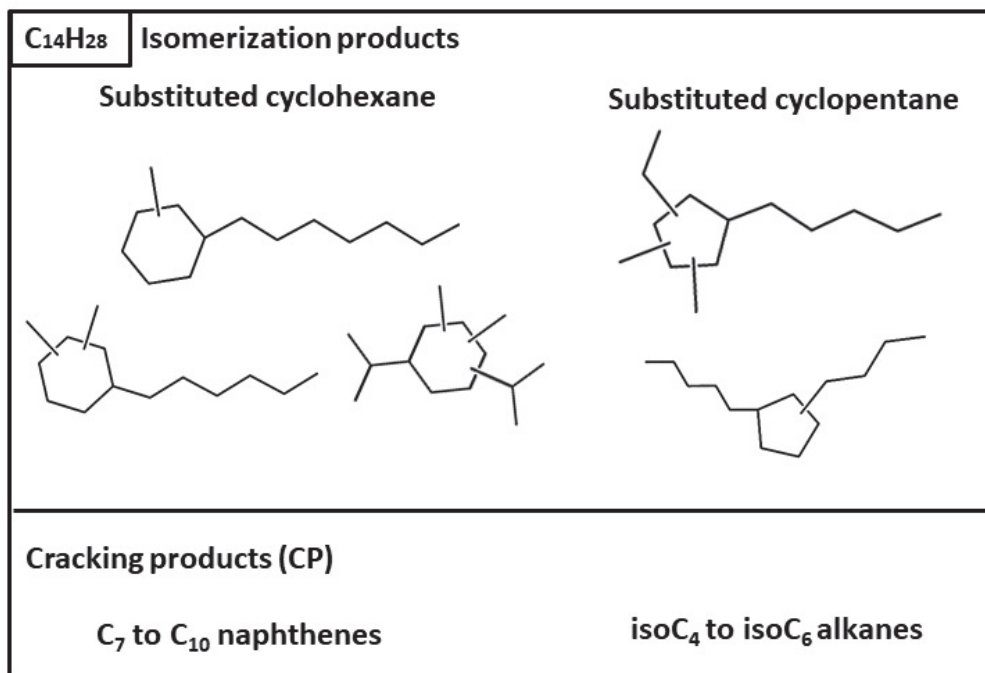


Figure 2. Molecule families and typical examples of molecules in the reaction products of hydroconversion of octylcyclohexane over Pt/zeolites, Pt/ASA and sulfide bifunctional catalysts. Further details on reaction products are available in our previous work. (ref)

### 3.2. Hydroconversion of octylcyclohexane

The evolution of octylcyclohexane conversion with contact time at 300°C, for Pt- and NiMoS-based catalysts, is illustrated in Figure 3. Zeolite-supported solids contained 1 wt.% of zeolite in alumina binder. Pt-catalysts were significantly more active than sulfide catalysts. For the Pt-catalysts, the order of activity was Pt/H-Beta > Pt/H-USY > Pt/ASA. For the sulfide catalysts, we found the ranking NiMoS/H-Beta ≈ NiMoS/H-USY >> NiMoS/ASA.

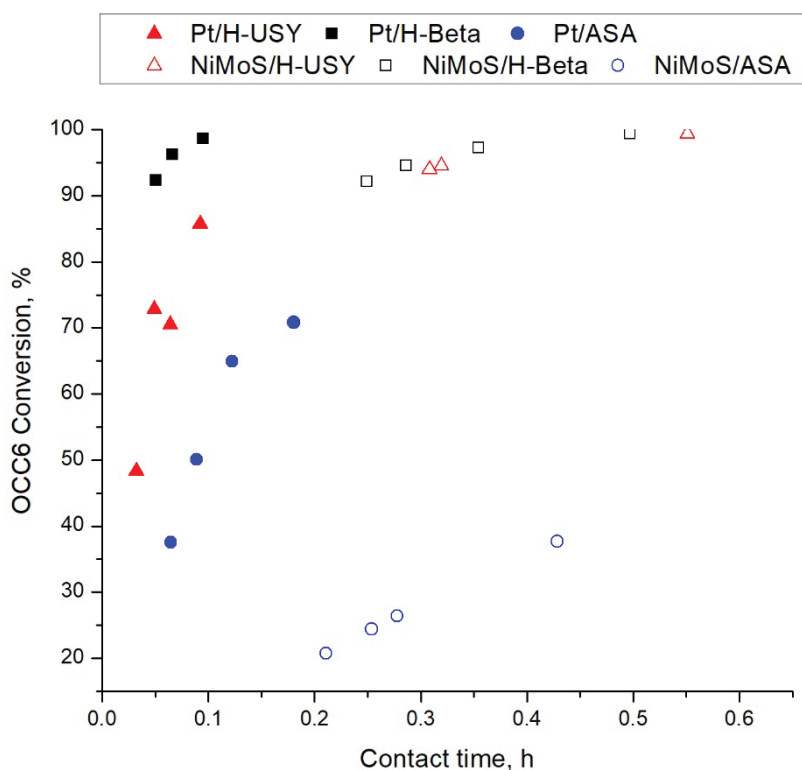


Figure 3. Evolution of octylcyclohexane conversion with contact time at 300°C on Pt and NiMoS/H-USY (red triangles), Pt and NiMoS/H-BETA (black squares) catalyst extrudates with 1 wt.% zeolite in alumina binder; and Pt and NiMoS/ASA catalysts (blue circles). Hollow and full symbols correspond to NiMoS- and Pt-based bifunctional catalysts, respectively.

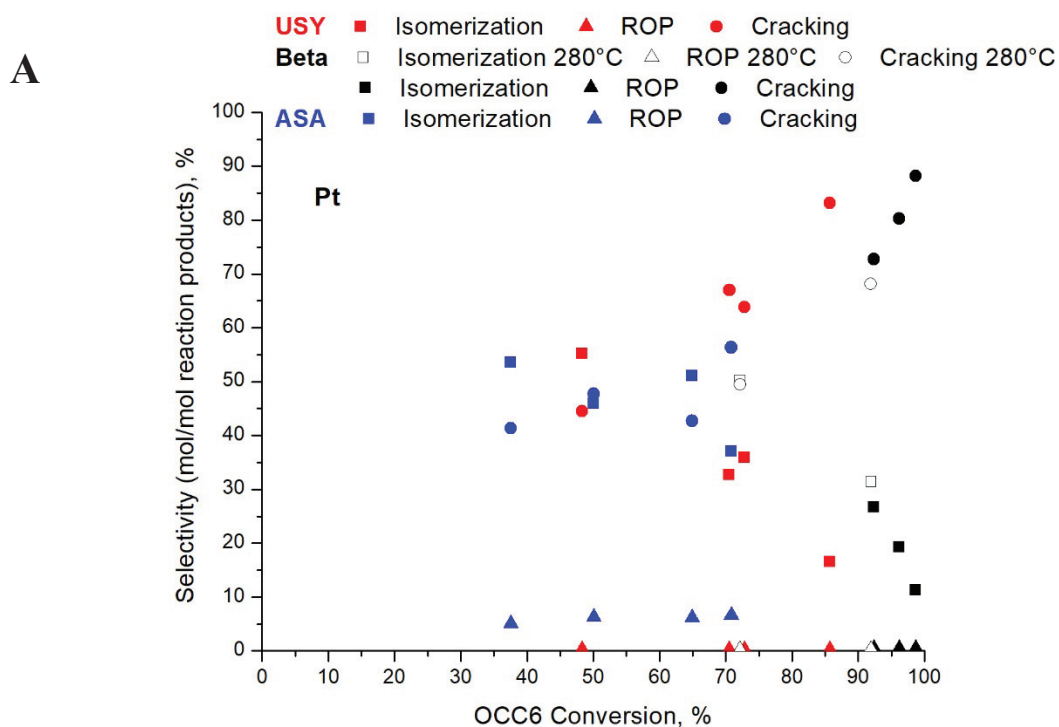
The reaction products resulting from hydroconversion of octylcyclohexane on Pt and sulfide catalysts were lumped into isomerization, ring-opening and cracking subfamilies. The selectivity, expressed in mol per mol of reaction products is illustrated in Figure 4 (A and B). Regarding Beta- catalysts, we included the results at 280°C in Figure 4, in order to better rationalize the selectivity to families of reaction products at lower octylcyclohexane conversion levels. The continuity of the profiles at 280 and 300°C shows that temperature had minor impact on the catalysts reactivity.

Pt/H-USY and Pt/ASA catalysts gave similar octylcyclohexane conversion values and therefore can be compared at the same conditions. The amorphous catalyst was more selective to isomerization and to ring-opening products than Pt/H-USY zeolite catalyst at isoconversion. The selectivity to ring-opening products on Pt/ASA accounted for ca. 6 mol/mol reaction products throughout the conversion degrees. Over the zeolite catalysts,



ring-opening was almost not perceived. Compared to Pt/H-USY, Pt/H-beta was more selective to isomerization products and less prone to cracking.

Similar results were obtained with sulfide catalysts (Figure 4B). Up to 60% conversion, isomerization was the major reaction. It is worth mentioning that ring-opening products could not be separated from the isomerization subgroup and were, therefore, counted as isomers, if present.. NiMoS/H-USY was slightly more selective to cracking products than NiMoS/H-beta.



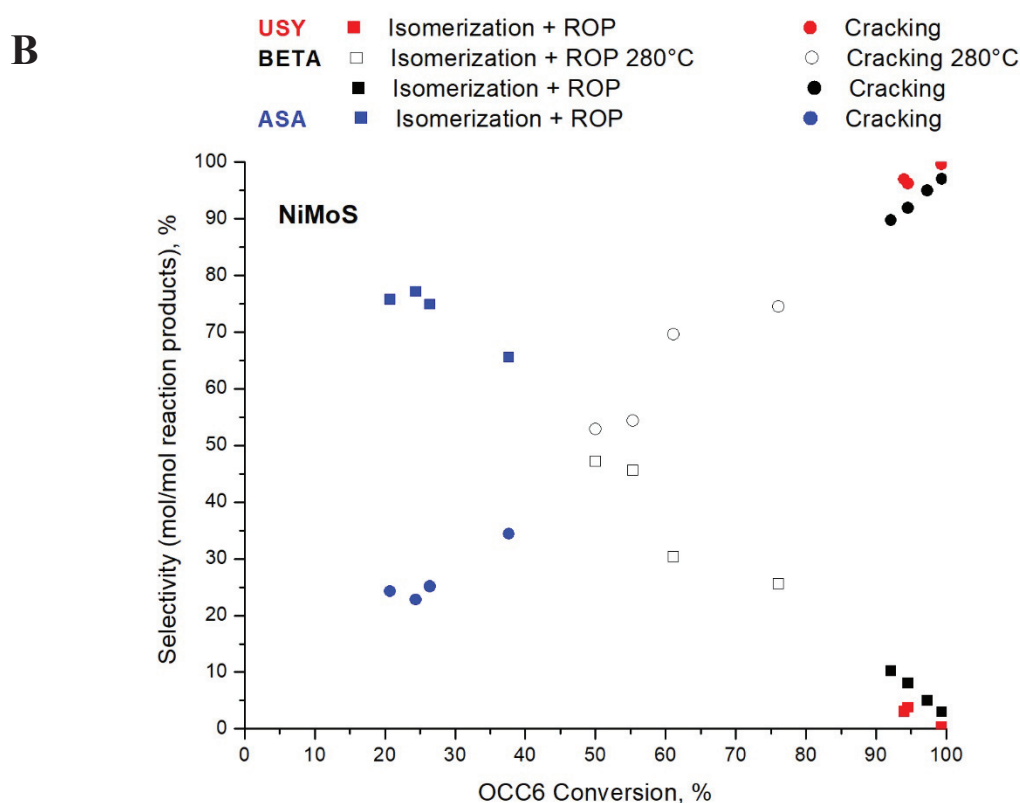


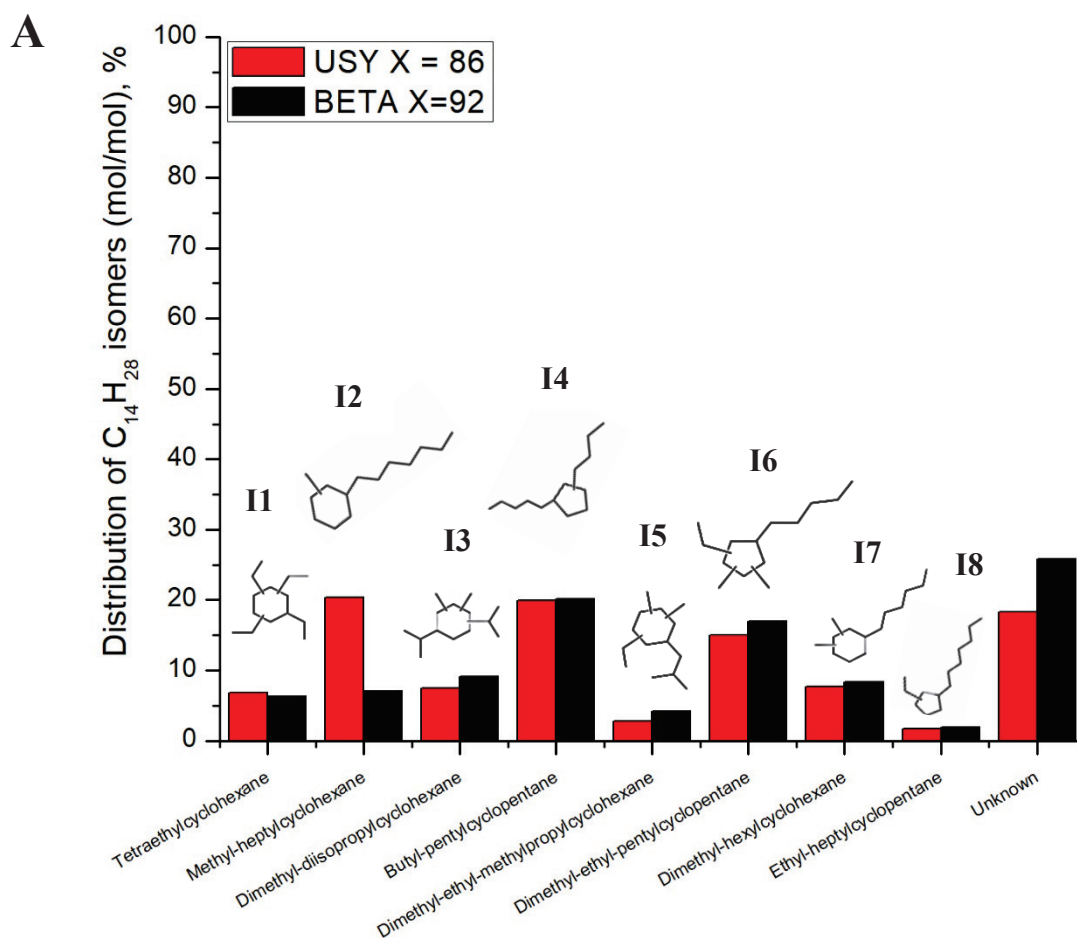
Figure 4. Selectivity to isomerization, ring-opening and cracked products as a function of octylcyclohexane conversion over A) Pt-based catalysts; and B) sulfide catalysts. Data obtained at 280°C are indicated in the legend box.

Globally, the yield of cracked products over NiMoS/H-Beta was always superior to that observed at isoconversion over Pt/H-Beta. At 92% conversion, for instance, these values corresponded to ca. 99 and 154 mol/mol octylcyclohexane over Pt- and sulfide-based bifunctional catalysts, respectively. The same behavior was noticed with bifunctional ASA-supported catalysts. At 38% conversion, the sulfide catalyst gave a yield of cracked products equivalent to 90 mol/mol octylcyclohexane against 17 mol/mol octylcyclohexane over Pt/ASA bifunctional catalyst.

Isomers of octylcyclohexane were analyzed in detail for the Pt-based catalysts (Figure 5 A and B). As aforementioned, reaction products resulting from hydroconversion of octylcyclohexane on sulfide catalysts were detected and quantified with online 1D GC-FID, therefore detailed isomer distributions could not be obtained for these catalysts. A few offline

GCxGC analyses of the collected liquids confirmed, however, that the same type of compounds were formed over Pt and sulfide catalysts.

Structures identified over Pt/zeolites and Pt/ASA bifunctional catalysts at isoconversion were equivalent. They were assigned as dibranched (**I2**, **I4** and **I8**), tribranched (**I7**) and more highly branched (**I1**, **I3**, **I5** and **I6**) isomers. Over Pt/H-USY, major isomerization products were represented by dibranched compounds (**I2** and **I4**) and multibranch structure **I6**. On Pt/H-Beta, in comparison with Pt/H-USY, isomer **I2** was quantified to a smaller extent, while **I4** and **I6** remained as major products within the isomerization family (Figure 5A). A comparison at isoconversion between Pt/ASA and Pt/H-USY revealed that the distribution shifted towards the preferential formation of multibranch structures, characterized by **I3** and **I6** isomers, over the amorphous catalyst (see supporting information for further details on the distribution of octylcyclohexane isomers).



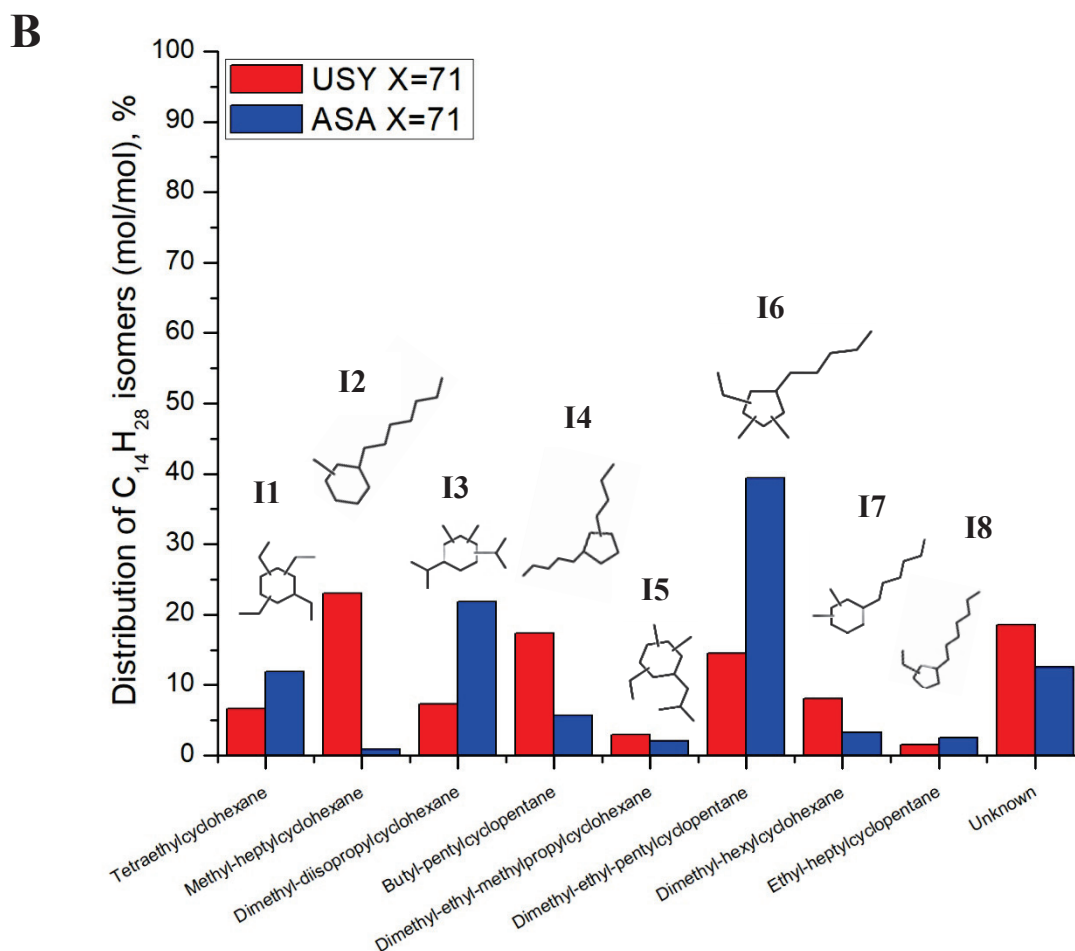


Figure 5. Distribution of substituted cyclopentane and substituted cyclohexane isomers of octylcyclohexane over A) Pt/H-USY and Pt/H-Beta zeolite catalyst and B) Pt/H-USY and Pt/ASA bifunctional catalysts at isoconversion.

The yield of cracked products over Pt- and sulfide-based catalysts, expressed in mol per mol of octylcyclohexane, is illustrated in Figure 6. The profiles were grouped at the same values of octylcyclohexane conversion. Cracked products were observed at a range from 1 to 13 carbon atoms. Pt/ASA bifunctional catalyst resulted in a central cracking to C<sub>7</sub> compounds and formation of light cracked products, represented by production of methane, ethane and propane through hydrogenolysis. At similar conversion degrees, Pt/H-USY zeolite catalyst generated a wider range of cracked products than Pt/ASA, mainly centered at C<sub>7</sub> molecules.

Pt/H-USY and Pt/H-Beta catalysts behaved similarly, presenting almost the same yield of cracked products.

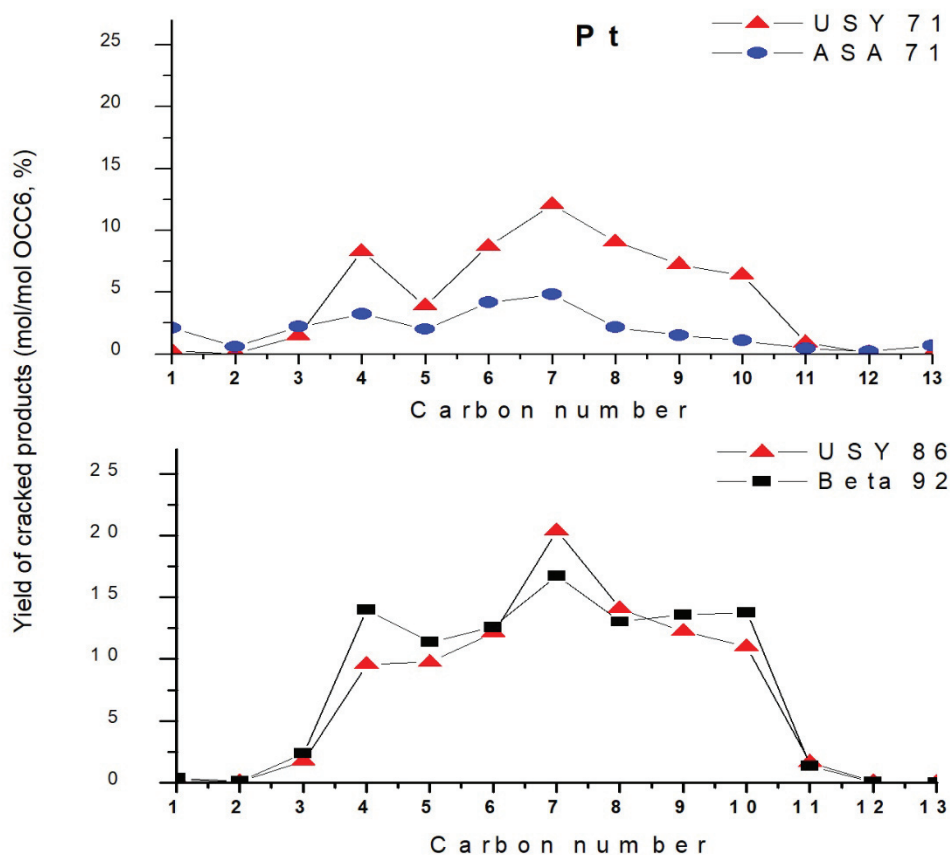


Figure 6. Yield of cracked products according to the number of carbon atoms at different levels of octylcyclohexane conversion over Pt-supported bifunctional catalysts.

Considering sulfide catalysts, the major distinction in respect to the Pt series corresponded to the higher yield of cracked products obtained over the former (Figure 7). A comparison between USY and Beta zeolite catalysts at conversion levels superior to 90% showed that the cracking yield has maxima at even carbon numbers, i.e. C<sub>4</sub>, C<sub>6</sub> and C<sub>8</sub> compounds, except for C<sub>10</sub> compounds, which probably underwent secondary cracking. Among zeolites, USY gave slightly higher yields of cracked products. In order to evaluate the behavior of zeolites and amorphous catalysts at isoconversion, the ASA catalysts was tested at 320°C and the beta catalyst at 280°C. In spite of the higher temperature, the NiMoS/ASA catalyst resulted in lower yields of cracked products. Furthermore, these profiles indicated a behavior close to

that seen with Pt-based catalysts: Beta zeolite generated a broad distribution in terms of carbon atoms, whereas the amorphous catalyst promoted cracking to lighter compounds, specially, in this case, to C<sub>6</sub> molecules.

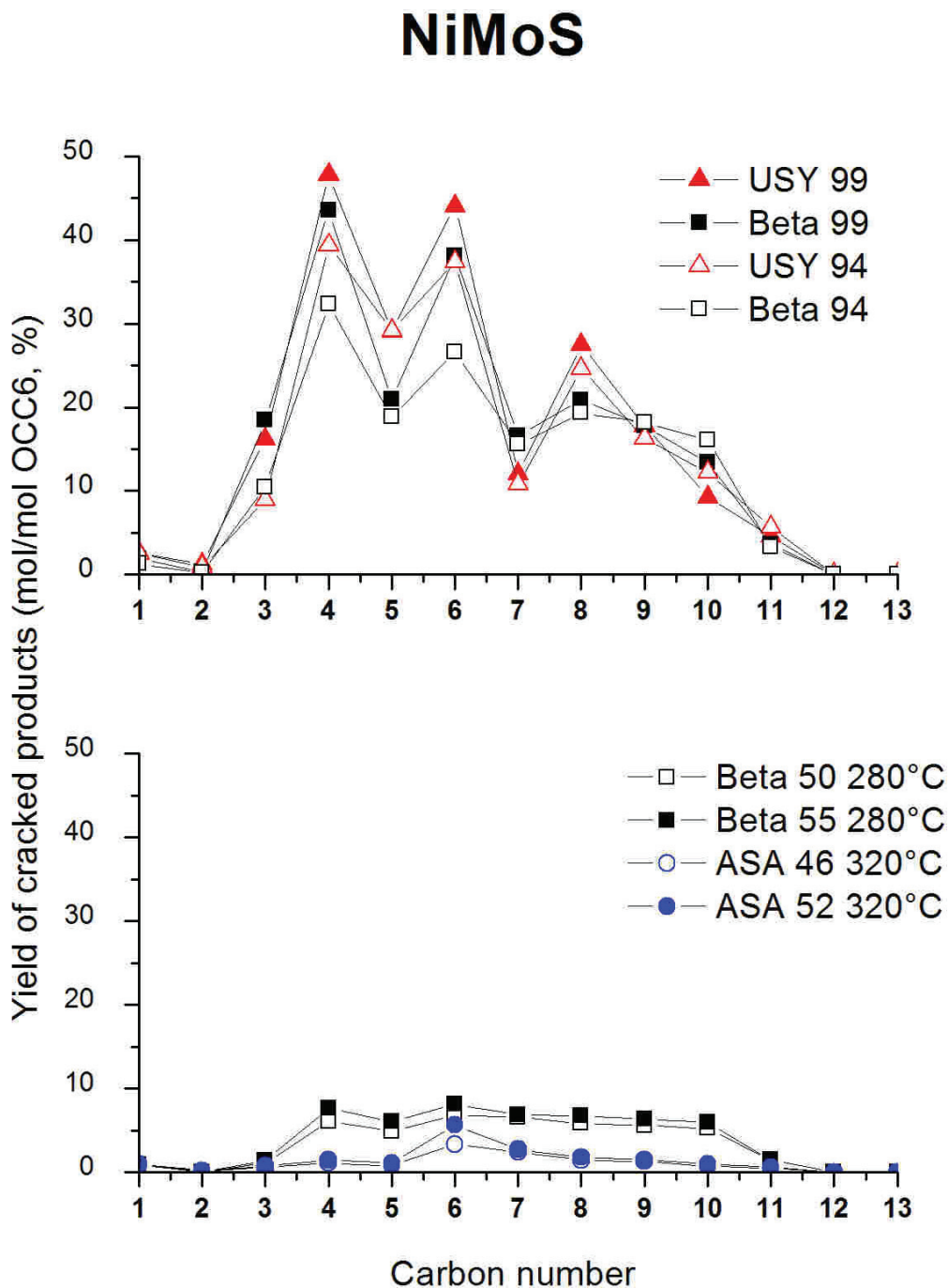
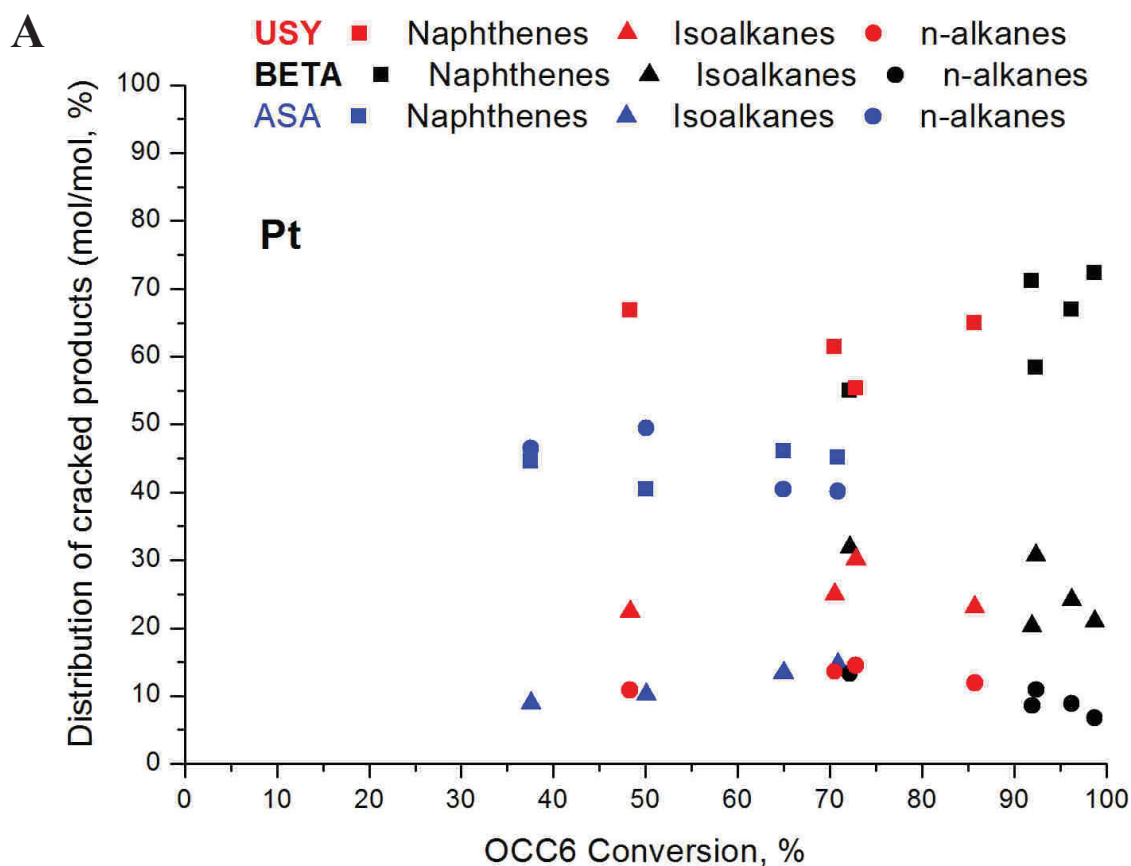


Figure 7. Yield of cracked products according to the number of carbon atoms at different levels of octylcyclohexane conversion over Pt (top) and NiMoS-based (bottom) bifunctional catalysts.

Cracked products were assembled into naphthenes, iso- and n-alkanes subgroups (Figure 8). From the hydrocracking of the model molecule, an equimolar proportion of naphthenes and alkanes was expected in the absence of secondary cracking. Within the Pt-series of catalysts, the proportion of naphthenes was superior to that of iso- and n-alkanes over the zeolite catalysts, which may be explained by the fact that C<sub>7</sub> isoalkanes were not accounted among reaction products, as they were assigned as impurities of the solvent (n-heptane). With respect to Pt/ASA bifunctional catalyst, a close equivalence of naphthenes and n-alkanes was observed, which could indicate cracking through hydrogenolysis, as aforementioned.

Within the sulfide series, zeolites and amorphous catalysts also behaved differently. Over the former, almost the same proportion of naphthenes and isoalkanes was obtained. Since C<sub>7</sub> isoalkanes were not taken into account as previously described, we may presume that a higher proportion of isoalkanes would be generated over sulfide catalysts, which may indicate a secondary cracking.



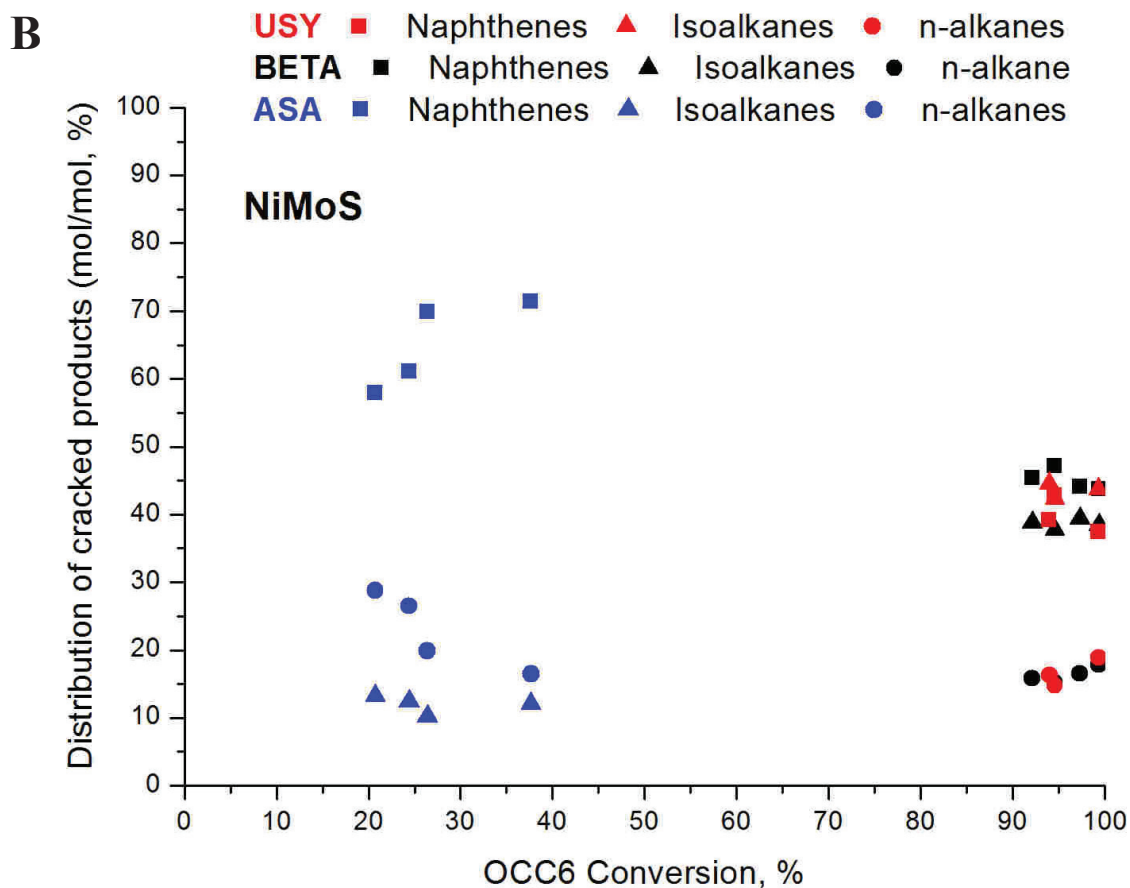


Figure 8. Distribution of cracked products as a function of octylcyclohexane conversion over A) bifunctional Pt/zeolites and Pt/ASA catalysts and B) bifunctional sulfide catalysts.

From previous results, it is possible that hydrogenolysis contributed to form cracked products, in addition to bifunctional mechanisms, in hydrocracking of octylcyclohexane over the Pt/ASA catalyst. Therefore, the distribution of major cracked products on the amorphous catalyst will not be analyzed herein. The distribution of C<sub>7</sub> naphthenes over Pt zeolite catalysts is presented in Figure 9. Over Pt and sulfide catalysts, methylcyclohexane was primarily produced, followed by the formation of dimethylcyclopentane. In addition, much less dimethylcyclopentane is formed over sulfide catalysts, especially over NiMoS/H-USY (see supporting information for the distribution of C<sub>7</sub> products on sulfide catalysts).



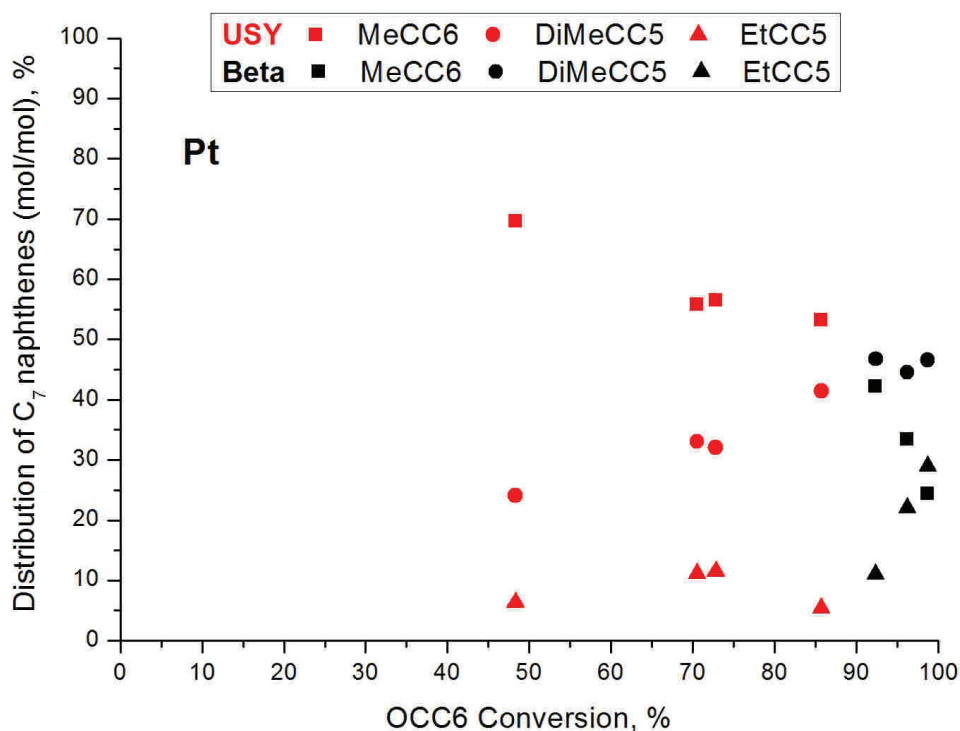


Figure 9. Distribution of C<sub>7</sub> naphthenes as a function of octylcyclohexane conversion over bifunctional Pt/H-USY and Pt/H-Beta zeolite catalysts.

As indicated in Figures 6 and 7, cracked products comprised, in addition to C<sub>7</sub> naphthenes, C<sub>6</sub>, C<sub>8</sub>, C<sub>9</sub> and C<sub>10</sub> compounds. The detailed analysis of cracked reaction products originating from hydrocracking of octylcyclohexane over Pt/H-USY is available elsewhere (Chapter IV). The same distributions of cracked naphthenes were obtained over Pt/H-Beta zeolite catalyst. Minor differences regarding the sulfide series of catalysts were observed and may be attributed to inaccuracies related to the analysis method.

The distribution of alkanes over Pt-zeolite catalysts is revealed in Figure 10. Further details on the distribution of sulfide catalysts are available in supporting information. Except for ASA (not represented), they were minor reaction products. Only alkanes containing 8 carbon atoms or less were formed, whereas C<sub>9</sub> branched acyclic compounds were quantified to a low extent over the sulfide solids. Pt- and also sulfide catalysts generated preferentially isoalkanes as isobutane, methylbutane and methylpentane and few n-alkanes. Iso-alkanes were preferentially branched in position 2. Amongst the n-alkanes, n-hexane was the major product

over Pt catalysts, while propane was the most abundant n-alkane on sulfide-based zeolite catalysts.

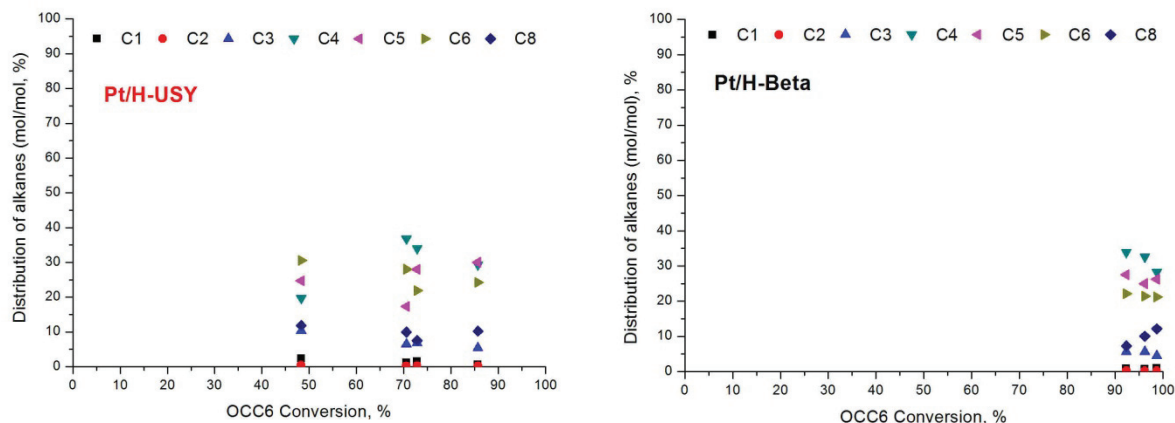


Figure 10. Distribution of alkanes as a function of octylcyclohexane conversion over bifunctional Pt/H-USY and Pt/H-Beta zeolite catalysts.

## 4. Discussion

### 4.1. Comparison of isomerization and cracked products

Isomers of octylcyclohexane were assigned according to their degree of branching. Globally, the same structures were identified over Pt/zeolites and Pt/ASA bifunctional catalysts, although minor discrepancies regarding their distribution within the isomers subfamily were evidenced. The formation of each isomer was thoroughly explained in our previous work on hydrocracking of octylcyclohexane over Pt/H-USY zeolite catalyst (Chapter IV). To this purpose, the reactions steps leading to each isomer were carefully addressed and classified according to the type of rearrangement, i.e. type A or B isomerization. Such reactions are characterized as ring-contraction or expansion; endocyclic or exocyclic alkyl-shifts; and chain-branching. They all occur through a PCP intermediate that require more or less reaction steps to be achieved.

From the results obtained in hydrocracking of octylcyclohexane over Pt/H-USY zeolite catalyst, it has been verified that compounds which require the most reduced number of type B rearrangements could be preferentially formed over the solids studied. These molecules

correspond to di- or tribranched structures presented in Figure 5, such as **I2**, **I7** and **I8**. Furthermore, it was established that isomer **I2** was primarily formed after fast rearrangement of the model molecule.

Over Pt/H-Beta catalyst, at high octylcyclohexane conversion, structures **I4** (dibranched) and **I6** (multibranched) were major isomerization products. Compound **I2** (dibranched) accounted for less than 10% of the distribution. Dibranched molecule **I8** was only perceived to a small extent. These results imply that, at these conversion levels, over Beta-supported catalysts, isomers containing a long alkyl-substituent were preferentially cracked. In opposition, multibranched isomers accumulate within this fraction, despite their higher number of tertiary carbon atoms.

In respect to Pt/ASA catalyst, major isomerization products were multibranched structures **I3** and **I6**. The formation of such isomers involves a high number of type B rearrangement steps, in comparison to dibranched compounds, which were minor isomerization products over the ASA catalyst. In this case, it is likely that, besides hydrocracking, less branched structures underwent further isomerization to multibranched compounds, given the low cracking activity of these catalysts.

In terms of distribution of carbon atoms, hydrocracking of octylcyclohexane over Pt-supported catalysts resulted in a major central cracking to C<sub>7</sub> naphthenes and an almost molar equivalent distribution of the other carbon atoms. A major cracking to C<sub>7</sub> naphthenes implies formation of C<sub>7</sub> isoalkanes as reaction products. According to Figure 9, C<sub>7</sub> naphthenes were primarily represented by methylcyclohexane over all Pt-supported catalysts tested. A hydrocracking pathway leading to such compounds would be equivalent to that proposed to hydrocracking of the model molecule over Pt/H-USY (Chapter IV), with probable production of 2-methylhexane along with methylcyclohexane.

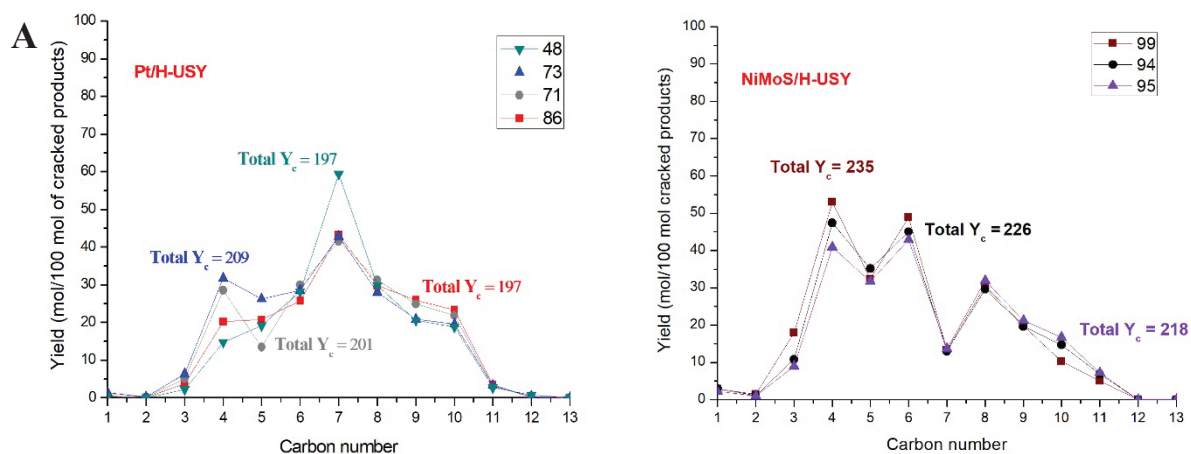
#### 4.2. Pt vs. NiMoS catalysts

Cracked compounds were the main reaction products over zeolite-based bifunctional catalysts. In order to establish if secondary cracking took place or if a non-classical cracking mechanism contributed to the bifunctional pathway, the yield, expressed in mol per 100 mol

of cracked products, was analyzed as illustrated in Figure 11. In a classical bifunctional mechanism, if secondary cracking is prevented, we may expect that each molecule will crack at least once. In this scenario, a yield of 200 mol per 100 mol of cracked products should be obtained.

Bifunctional Pt/H-USY and Pt/H-Beta zeolite catalysts gave a yield range varying from ca. 180 to 201 mol per 100 mol of cracked products. It should be emphasized that C<sub>7</sub> isoalkanes were not accounted as reaction products, since it was difficult to predict if they resulted from hydroconversion of the model molecule or from the transformation of the solvent (n-heptane) at the operating conditions. Consequently, the values of yield of cracked products must be greater than the ones acquired. For that reason, it can be inferred that, over Pt-based catalysts, only bifunctional mechanisms participated to the formation of reaction compounds.

Sulfide catalysts, in opposition, provided higher yield degrees, covering a range from ca. 218 to 235 mol per 100 mol of cracked products. Such values do not take into account C<sub>7</sub> isoalkanes, as aforementioned, which may indicate that superior values of yield should be obtained on NiMoS/H-USY and NiMoS/H-Beta zeolite catalysts. Accordingly, these results suggest that secondary cracking occurred over these catalysts.



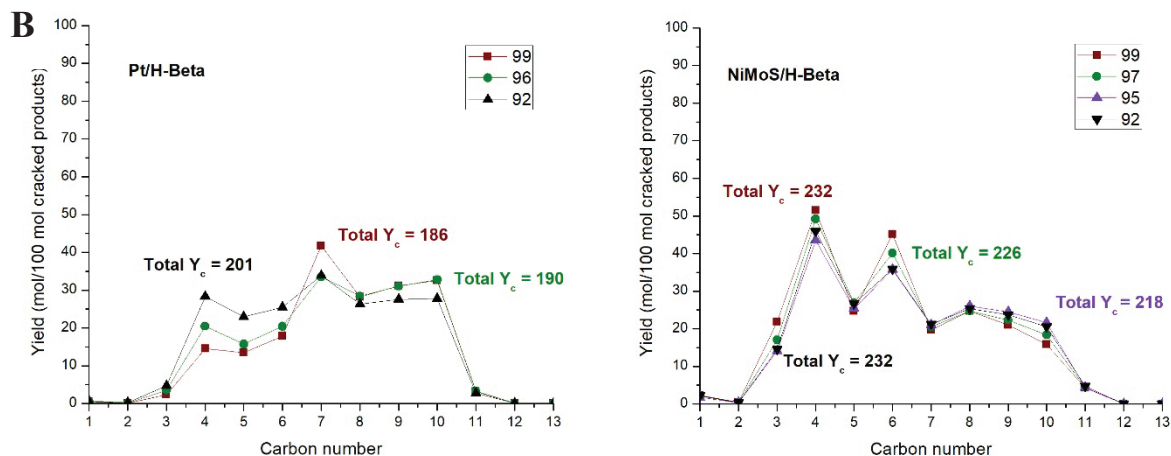


Figure 11. Yield of cracked products expressed in mol per 100 mol of cracked products on A) Pt/H-USY (top left) and NiMoS/H-USY (top right) zeolite catalysts; B) Pt/H-Beta (bottom left) and NiMoS/H-Beta (bottom right) zeolite catalysts.

Bifunctional sulfide catalysts are less well equilibrated than Pt-based ones. The hydrogenating function of the former is not strong enough to saturate the cracked olefins produced on the acidic sites of zeolites. This leads to secondary cracking, i.e. the formation of lighter compounds. Since Pt is a strong hydrogenating component, Pt/H-USY and Pt/H-Beta catalysts are referred to as well equilibrated and, in this case, only primary cracking, along with a more homogeneous distribution, was observed.

No preferential central cracking to C<sub>7</sub> naphthenes was evidenced over the less equilibrated sulfide catalysts. Moreover, because of secondary cracking, lighter compounds containing 4 and 6 carbon atoms were generated. Therefore, no molar equivalence was found between C<sub>10</sub> naphthenes and isobutane, nor between C<sub>8</sub> naphthenes and 2- methylpentane over both zeolite catalysts.

These results propose that, over sulfide catalysts, the model molecule containing 14 carbon atoms cracked to C<sub>10</sub> naphthenes and C<sub>4</sub>, in an equimolar proportion. C<sub>10</sub> naphthenes were cracked again to C<sub>6</sub> naphthenes and C<sub>4</sub> (mainly isobutane). In parallel, the other possible routes contribute to increase the yield of lighter products, as C<sub>5</sub> and C<sub>6</sub>, especially over NiMoS/H-USY, which was slightly more selective towards cracked products at isoconversion

than NiMoS/H-Beta zeolite catalysts (Figure 4). C<sub>8</sub> and C<sub>9</sub> naphthenes did not undergo secondary cracking.

In spite of the observed shift of the product selectivity to cracking products (Figure 4) and the occurrence of over-cracking, the product distribution of sulfide catalysts is not radically different from Pt catalysts. C<sub>14</sub> isomers were abundant products of the sulfide catalysts at low conversions. This is in stark contrast with the hydrocracking of n-hexadecane. When n-hexadecane is converted on Pt/H-USY zeolite, i-C<sub>16</sub> isomers are the major products up to fairly high conversions, before cracking becomes dominating. With NiMoS/H-USY zeolite catalysts, however, cracking becomes the major reaction starting from very low conversion (unpublished results). The reason for the much lower tendency of octylcyclohexane to crack over sulfide catalysts (compared to n-hexadecane) is probably the difficulty of endocyclic cracking. In other words, the cracking selectivity of naphthenes seems to be less sensitive to the metal-acid balance than the cracking selectivity of alkanes.

#### *4.3. Comparison of the hydroconversion of perhydrophenanthrene vs octylcyclohexane and n-hexadecane*

Whereas the zeolite topology had a big influence on the distribution of intermediates and cracking products in the hydroconversion of perhydrophenanthrene, hydroconversion of octylcyclohexane (C<sub>14</sub>H<sub>28</sub>) over Pt and sulfide-catalysts was less controlled by shape selective effects. The conversion of the model molecule towards isomers revealed a similar distribution of these compounds on zeolite catalysts, with preferential formation of methylheptylcyclohexane, along with other di- or tribranched molecules. Over ASA-supported catalyst, the distribution of isomers was shifted in favor of multibranched compounds.

Opening of the unique ring of octylcyclohexane was a minor reaction and it only took place on ASA-catalysts. Cracking of the isomers led to the preferential formation of C<sub>7</sub> compounds on Pt-supported catalysts and an otherwise flat distribution of C<sub>4</sub> to C<sub>10</sub> products. In contrast, hydrocracking of perhydrophenanthrene gave different distributions according to the acid phase tested. USY-supported catalysts generated a broad distribution of cracked

products, while Pt/H-Beta and Pt/ASA bifunctional catalysts resulted in a central cracking to C<sub>7</sub> compounds.

The catalytic activity per catalyst mass estimated through apparent first-order kinetic constants for hydroconversion of perhydrophenanthrene and octylcyclohexane over Pt and sulfide bifunctional catalysts, as a function of the acid phase and zeolite loading in the alumina binder (except for ASA catalysts), is summarized in Table 3. The catalytic activity in hydroconversion of perhydrophenanthrene at 280°C decreased from USY to Beta, followed by ASA-based catalysts, regardless of zeolite content. Activity was roughly proportional to zeolite loading in Pt/zeolites catalysts, although USY zeolites gave a greater ratio zeolite content/activity (3.4 vs 2.3 on Beta zeolite).

Interestingly, in the hydroconversion of octylcyclohexane at 300°C, Beta catalysts were more active than USY zeolites, which were much more active than amorphous catalysts. There was a clear impact of the hydrogenating phase on activity of sulfide catalysts in hydroconversion of octylcyclohexane. The catalytic performance of sulfide catalysts was inferior to Pt ones, because of the poor equilibrium between metallic and acid phases of these bifunctional catalysts.

The inversion on activity of zeolite catalysts with respect to the model molecules suggests the hypothesis that USY-based catalysts converted more efficiently bulky molecules, thanks to their larger pores and supercages, while linear structures are preferentially converted on Beta-zeolites. This is also in line with the observation that Beta was more active than USY in the hydroconversion of n-hexadecane (see supporting information and [35]).

Table 3. Catalytic activity of Pt and sulfide bifunctional catalysts on hydroconversion of perhydrophenanthrene and octylcyclohexane as a function of acid phase.

$k_{app}, h^{-1}$										
Metallic phase		Pt catalysts			Sulfide catalysts					
Acid phase		USY		BETA		ASA	USY		BETA	ASA
Zeolite loading (wt.%)		1	3	1	3	-	1	1	-	
Perhydrophenanthrene (280°C)		8.8	29.6	5.6	13.1	6.5	-	-	-	
Octylcyclohexane (300°C)		21.3	-	47.3	-	7.4	9.1	10.2	1.1	

Monocyclic naphthenes containing a long alkyl-chain substituent seem to behave as acyclic compounds. The naphthenic ring provides the branchings (through ring-contraction isomerization) that will be shifted towards the side chains, to improve cracking.

## 5. Conclusions

Hydroisomerization and hydrocracking of octylcyclohexane were evaluated on Pt- and NiMoS-supported bifunctional catalysts. Two large-pore zeolites (USY and Beta), along with an amorphous silica-alumina, were used as acid function. A pre-catalyst Pt or NiMoS/Al<sub>2</sub>O<sub>3</sub> was employed to guarantee a complete hydrogenation of the parent aromatic compound, phenyloctane, towards the naphthenic model molecule. Octylcyclohexane was then isomerized and cracked afterwards over the bifunctional catalysts.

Reaction products were carefully analyzed in order to verify if hydrocracking pathways were changed according to the hydrogenated phase tested. It was confirmed that the same reaction intermediates, which were assigned as isomerization products, were observed on Pt and sulfide catalysts. The distribution of isomerization products, though, changed according to the acid phase tested. Despite of that, the distribution of cracked products was independent of the acid function. Similar profiles were observed over USY and Beta zeolite catalysts.



Reaction pathways observed on hydroconversion of octylcyclohexane over Pt/zeolites were also applicable to NiMoS/zeolite bifunctional catalysts, with secondary cracking being observed on sulfide catalysts. The amorphous silica-alumina behaved differently, because it produced light products as methane, ethane and propane through hydrogenolysis.

Sulfide catalysts are less well equilibrated than Pt-supported ones. As a consequence, secondary cracking took place over the former, and their carbon atoms distribution was shifted mainly towards the formation of C<sub>4</sub>, C<sub>5</sub>, C<sub>6</sub>, C<sub>8</sub> and C<sub>9</sub> cracked products. In contrast, Pt-based catalysts gave a more homogeneous distribution in terms of carbon atoms, with a preferential central cracking to C<sub>7</sub> compounds. Another indication of secondary cracking on sulfide catalysts is related to higher yields of cracked products obtained on these solids, compared to Pt-catalysts at isoconversion.

The activity of Pt and sulfide catalysts were compared in the hydroconversion of perhydrophenanthrene and octylcyclohexane. ASA was the least active among the solids tested. Pt/H-USY was more active than Pt/H-Beta in the hydroconversion of perhydrophenanthrene, but less active in the hydroconversion of octylcyclohexane and also of n-hexadecane. These results altogether indicate a preferential conversion of linear compounds over Beta catalysts, whereas large-pore USY zeolite is more active in the conversion of bulky polycyclic naphthenes.

## REFERENCES

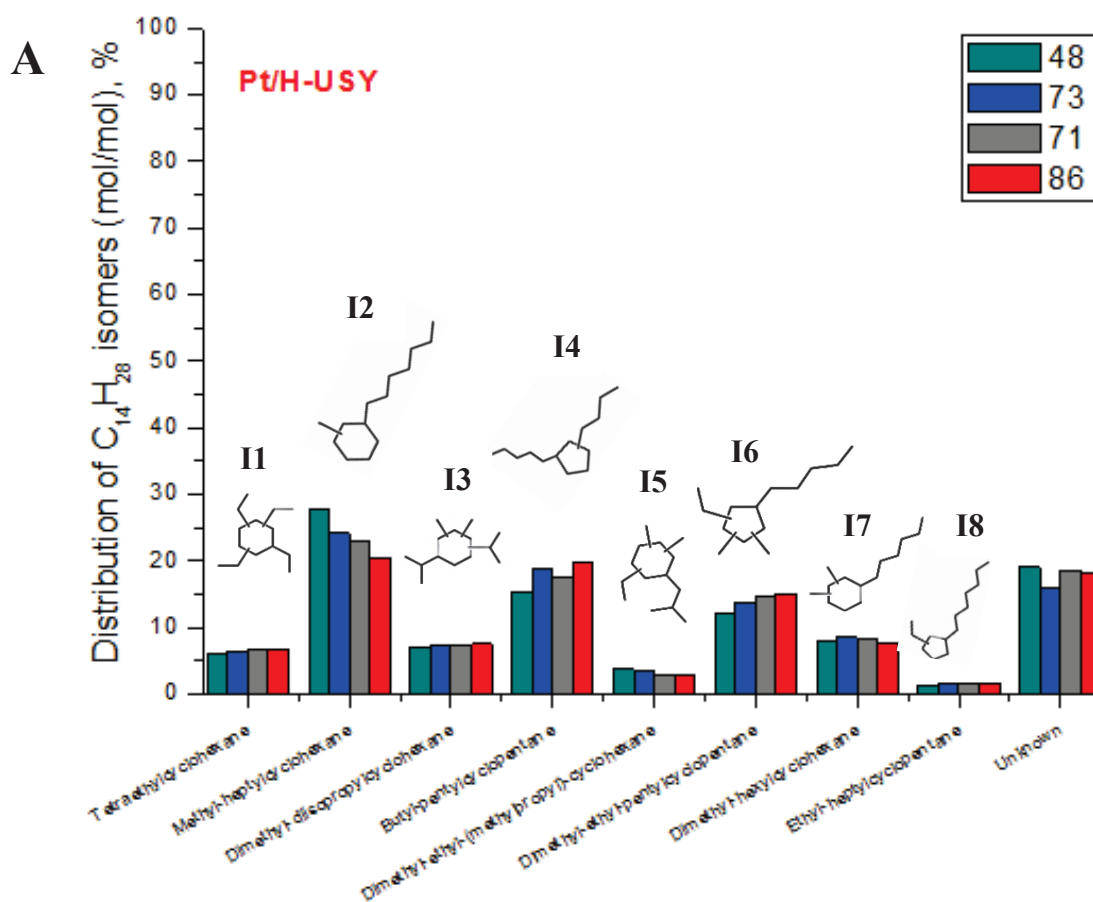
- [1] J.W. Ward, Design And Preparation Of Hydrocracking Catalysts, in: G. Poncelet, P. Grange, P.A. Jacobs (Eds.), Preparation of Catalysts III, Elsevier, 1983, pp. 587–618.
- [2] M.A. Ali, T. Tatsumi, T. Masuda, Development of heavy oil hydrocracking catalysts using amorphous silica-alumina and zeolites as catalyst supports, Appl Catal a-Gen 233 (2002) 77–90.
- [3] K. Ben Tayeb, C. Lamonier, C. Lancelot, M. Fournier, E. Payen, A. Bonduelle, F. Bertoncini, Study of the active phase of NiW hydrocracking sulfided catalysts obtained from an innovative heteropolyanion based preparation, Catalysis Today 150 (2010) 207–212.

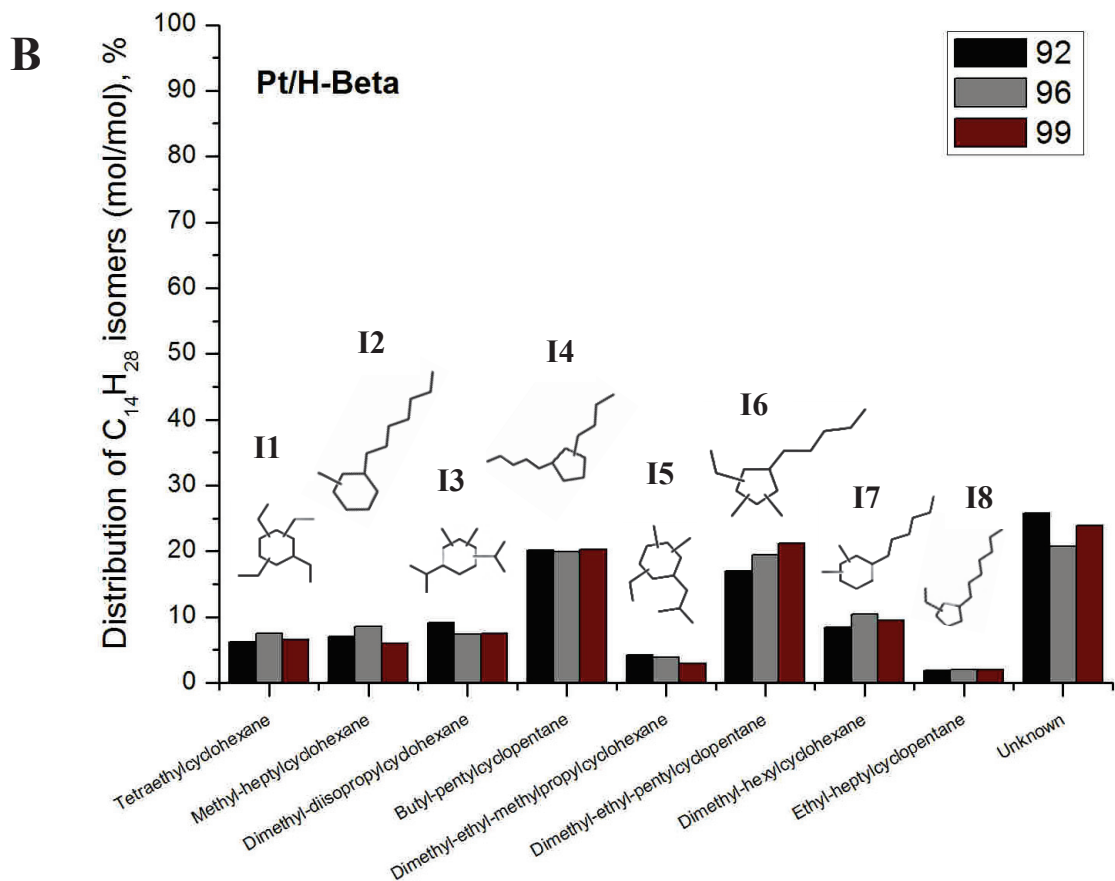
- [4] E.T.C. Vogt, G.T. Whiting, A. Dutta Chowdhury, B.M. Weckhuysen, Zeolites and Zeotypes for Oil and Gas Conversion, in: F.C. Jentoft (Ed.), *Advances in catalysis*, Academic Press, Amsterdam, 2015, pp. 143–314.
- [5] V. Calemme, S. Peratello, C. Perego, Hydroisomerization and hydrocracking of long chain n-alkanes on Pt/amorphous SiO<sub>2</sub>-Al<sub>2</sub>O<sub>3</sub> catalyst, *Applied Catalysis A: General* 190 (2000) 207–218.
- [6] F. Regali, M. Boutonnet, S. Järås, Hydrocracking of n-hexadecane on noble metal/silica-alumina catalysts, *Catalysis Today* 214 (2013) 12–18.
- [7] C. Marcilly, Evolution of refining and petrochemicals: what is the place of zeolites.
- [8] A. Primo, H. Garcia, Zeolites as catalysts in oil refining, *Chemical Society reviews* 43 (2014) 7548–7561.
- [9] J.W. Ward, *Applied Industrial Catalysis*, Academic Press, San Diego, 1984.
- [10] C. Augusto, J. Zotin, Faro, ArnaldodaCosta, Jr., Effect of Sulfur or Nitrogen Poisoning on the Activity and Selectivity of Y-Zeolite-Supported Pt-Pd Catalysts in the Hydrogenation of Tetralin, *Catal. Lett.* 75 (2001) 37–43.
- [11] F. Alvarez, G. Giannetto, A. Montes, F. Ribeiro, G. Perot, M. Guisnet, Catalytic Properties of PtH Zeolites, in: A. Galarneau, F. Fajula F. Di Renzo, J. Vedrine (Eds.), *Studies in Surface Science and Catalysis*, Elsevier, 2001, pp. 479–486.
- [12] P. Gallezot, The State and Catalytic Properties of Platinum and Palladium in Faujasite-type Zeolites, *Catalysis Reviews* 20 (1979) 121–154.
- [13] A. Elkilani, M. Fahim, Maximizing diesel production from Vacuum Gas Oil using a two-stage hydrocracker, *Petroleum Science and Technology* 32 (2014) 2303–2311.
- [14] K.H. Kang, G.T. Kim, S. Park, P.W. Seo, H. Seo, C.W. Lee, A review on the Mo-precursors for catalytic hydroconversion of heavy oil, *Journal of Industrial and Engineering Chemistry* 76 (2019) 1–16.
- [15] M. Breyse, E. Furimsky, S. Kasztelan, M. Lacroix, G. Perot, Hydrogen activation by transition metal sulfides, *Catalysis Reviews* 44 (2002) 651–735.
- [16] N. Guernalec, T. Cseri, P. Raybaud, C. Geantet, M. Vrinat, Influence of H<sub>2</sub>S on the hydrogenation activity of relevant transition metal sulfides, *Catal Today* 98 (2004) 61–66.
- [17] Camblor, M. A., et al., Mild Hydrocracking of Vacuum Gasoil over NiMo-Beta Zeolite Catalysts: The Role of the Location of the NiMo Phases and the Crystallite Size of the Zeolite, *Journal of Catalysis* 179 (1998) 537–547.
- [18] M. Guisnet, “Ideal” bifunctional catalysis over Pt-acid zeolites, *Catalysis Today* 218-219 (2013) 123–134.

- [19] Joris W. Thybaut, †, C. S. Laxmi Narasimhan, Joeri F. Denayer, ‡, Gino V. Baron, Pierre A. Jacobs, §, J. A. Martens, § and, and Guy B. Marin\*, Acid–Metal Balance of a Hydrocracking Catalyst: Ideal versus Nonideal Behavior.
- [20] P.S.F. Mendes, J.M. Silva, M.F. Ribeiro, P. Duchêne, A. Daudin, C. Bouchy, Quantification of metal-acid balance in hydroisomerization catalysts, *AIChE J* 63 (2017) 2864–2875.
- [21] N. Batalha, L. Pinard, C. Bouchy, E. Guillon, M. Guisnet, n-Hexadecane hydroisomerization over Pt-HBEA catalysts. Quantification and effect of the intimacy between metal and protonic sites, *Journal of Catalysis* 307 (2013) 122–131.
- [22] J. Zečević, G. Vanbutsele, de Jong, Krijn P, J.A. Martens, Nanoscale intimacy in bifunctional catalysts for selective conversion of hydrocarbons, *Nature* 528 (2015) 245–248.
- [23] E. Gutierrez-Acebo, C. Leroux, C. Chizallet, Y. Schuurman, C. Bouchy, Metal/Acid Bifunctional Catalysis and Intimacy Criterion for Ethylcyclohexane Hydroconversion, *ACS Catal.* 8 (2018) 6035–6046.
- [24] T. Degnan, The implications of the fundamentals of shape selectivity for the development of catalysts for the petroleum and petrochemical industries, *Journal of Catalysis* 216 (2003) 32–46.
- [25] H. Toulhoat, P. Raybaud, E. Benazzi, Effect of confinement on the selectivity of hydrocracking, *Journal of Catalysis* 221 (2004) 500–509.
- [26] E. Benazzi, L. Leite, N. Marchal-George, H. Toulhoat, P. Raybaud, New insights into parameters controlling the selectivity in hydrocracking reactions, *Journal of Catalysis* 217 (2003) 376–387.
- [27] H.B. Mostad, T.U. Riis, O.H. Ellestad, Shape selectivity in Y-zeolites, *Applied Catalysis* 58 (1990) 105–117.
- [28] R. Kenmogne, A. Finiels, C. Cammarano, V. Hulea, F. Fajula, Hydroconversion of n-hexadecane over bifunctional microporous and mesoporous model catalysts. Influence of pore architecture on selectivity, *Journal of Catalysis* 329 (2015) 348–354.
- [29] W. Zhang, P.G. Smirniotis, Effect of Zeolite Structure and Acidity on the Product Selectivity and Reaction Mechanism for n-Octane Hydroisomerization and Hydrocracking, *Journal of Catalysis* 182 (1999) 400–416.
- [30] Christian R. Marcilly, Where and how shape selectivity of molecular sieves operates in refining and petrochemistry catalytic processes, *Topics in Catalysis* 13 (2000) 357–366.
- [31] P.S.F. Mendes, J.M. Silva, M.F. Ribeiro, A. Daudin, C. Bouchy, From powder to extrudate zeolite-based bifunctional hydroisomerization catalysts, *Journal of Industrial and Engineering Chemistry* 62 (2018) 72–83.

- [32] Edmond de Hoffmann and Vincent Stroobant, *Mass Spectrometry Principles and Applications*, 3rd ed., Wiley.
- [33] *Interpretation of Mass Spectra*, 4th ed. (McLafferty, Fred W; Turecek, Frantisek), <https://pubs.acs.org/doi/abs/10.1021/ed071pA54.5> (accessed 1.08.2019).
- [34] D.M. Brouwer, H. Hogeveen, *Recl. Trav. Chim. Pays-Bas* 89 (1970) 211–224.
- [35] Pedro Mendes, *Hydroconversion catalysts based on zeolite mixtures, from ideality to reality*, 2017.

### Supporting information





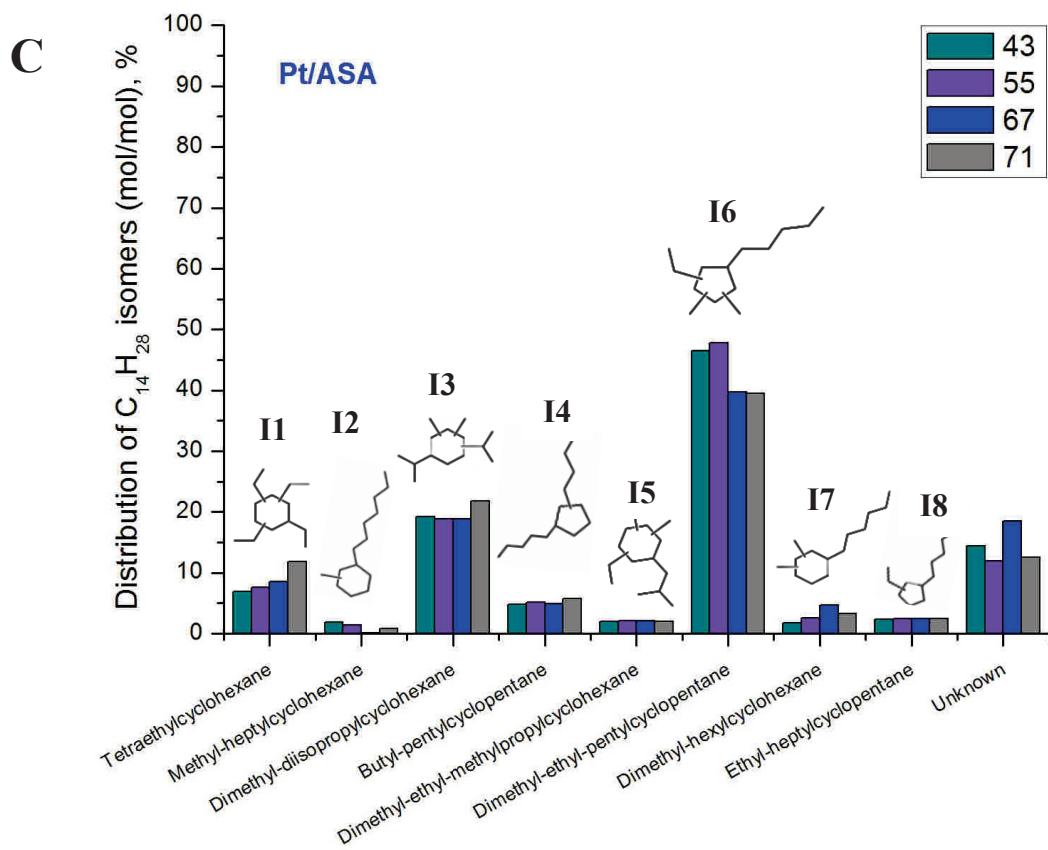


Figure S 1. Distribution of positional and ring-contraction isomers of octylcyclohexane over A) Pt/H-USY, B) Pt/H-Beta and C) Pt/ASA bifunctional catalysts.

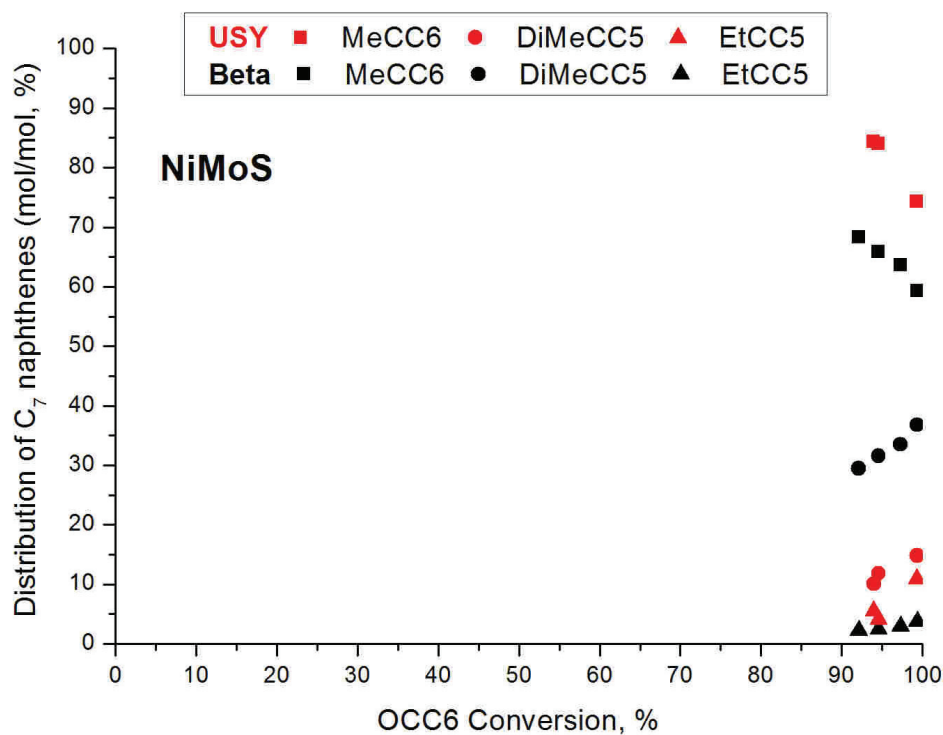


Figure S 2. Distribution of C<sub>7</sub> naphthenes as a function of octylcyclohexane conversion over bifunctional NiMoS/H-USY and NiMoS/H-Beta zeolite catalysts.

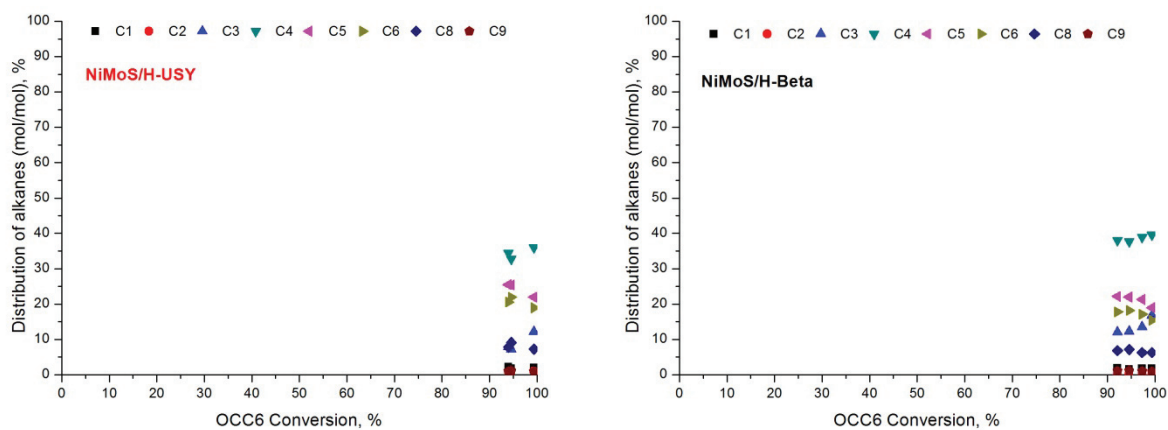


Figure S 3. Distribution of alkanes as a function of octylcyclohexane conversion over bifunctional NiMoS/H-USY and NiMoS/H-Beta zeolite catalysts.

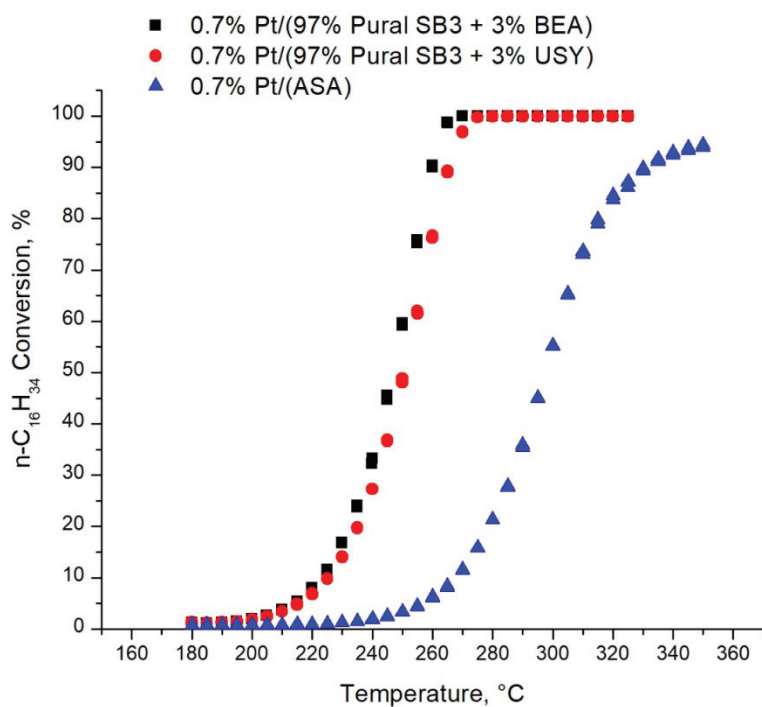


Figure S 4. Conversion of n-hexadecane as a function of temperature over Pt/H-USY, Pt/H-Beta and Pt/ASA bifunctional catalysts.





## CHAPTER VI: GENERAL DISCUSSION

---

This work investigated hydroisomerization and hydrocracking of perhydrophenanthrene, a 3-cycle naphthene (Chapters 2 and 3), and octylcyclohexane, a substituted monocyclic naphthene (Chapters 4 and 5), over large-pore zeolites and amorphous silica-alumina supported catalysts. The main objectives of this study were to rationalize the reactivity of (poly)cyclic compounds and comprehend the bifunctionality of catalysts employed in hydrocracking of heavy oil cuts in order to propose reaction pathways on hydroconversion of naphthenes. The impact of the acid phase as well as the balance between metallic and acid functions on reaction pathways were also evaluated. This chapter aims to highlight the key points discussed throughout this work and cross the information obtained on hydroconversion of both model molecules.

Conversion of perhydrophenanthrene (PHP) was carried out over Pt-supported bifunctional catalysts (Pt/H-USY, Pt/H-Beta and Pt/ASA) in order to understand the reactivity of polycyclic naphthenes (14 carbon atoms, 3 cycles) and the impact of the acid phase on the distribution of carbon atoms. Reaction products were lumped into groups, according to carbon number and chemical family. We focused our study and discussion on reaction intermediates resulting from isomerization, ring-opening and cracking of perhydrophenanthrene over the aforementioned bifunctional catalysts.

It was shown that isomerization compounds ( $C_{14}H_{24}$ ) were formed in a primary route over all Pt-supported catalysts, followed by ring-opening and cracking reactions. USY and ASA supported catalysts were the most selective to isomerization and, at isoconversion, had almost equivalent selectivities towards these products. Beta zeolites were slightly more selective to cracking.

This order of selectivity was similar to that proposed by Leite *et al.* on hydrocracking of perhydrophenanthrene over Pt/zeolite and Pt/ASA bifunctional catalysts, although this

study resulted in ASA as the most selective catalyst to isomerization products [1,2]. According to Leite and coworkers, the selectivity to cracking products over Pt/zeolites is related to the pore structure of these catalysts, based on calculations developed by Fraissard [3]. In this case, a higher number of interactions between the acid sites and molecules should be found with zeolite-based catalysts, because of their more strained pores network, compared to the mesopores of ASA.

In our work, perhydrophenanthrene isomers were classified as skeletal PHP isomers and alkyladamantanes. The former comprised ring-contraction and ring-shift tricyclic molecules, as perhydroanthracene stereoisomers and methylperhydrophenalene, and underwent further isomerization to produce alkyladamantanes. Comparing different catalysts, a preferential formation of linear skeletal isomers such as perhydroanthracene was revealed over Beta zeolites, whereas bulky molecules resulting from ring-contraction of perhydrophenanthrene were mainly processed over USY zeolite and ASA. Molecular Monte Carlo (MC) simulation demonstrated that the BEA structure led indeed to a higher adsorption selectivity to perhydroanthracene stereoisomers than the FAU structure. This was attributed to the bigger pore size and supercages of USY zeolites, which can accommodate large molecules. These shape selectivity effects were the first hints to better appreciate the role of the acid phase on hydroconversion of polycyclic naphthenes.

Alkyladamantanes, bridged perhydrophenanthrene isomers, were secondary isomerization products and resisted hydrocracking due to their high stability, except for a small fraction that was converted to C<sub>10</sub> adamantanes and isobutane. They were strongly favored over USY zeolites at high PHP conversion, in contrast to Beta and ASA-supported catalysts. MC simulations indicated that the adsorption of adamantanes was hindered on both types of zeolites, compared to skeletal perhydrophenanthrene isomers. In literature, the high selectivity to alkyladamantanes on USY zeolites was attributed to their large-pore size and supercages [4,5]. However, our simulation results strongly suggest that substituted adamantanes are not produced on the pores of either USY or Beta zeolites, but at the pore-mouth of these solids. USY zeolite was more selective to these isomers because of the easiness to process methylperhydrophenalenes, bulky precursors of alkyladamantanes, compared to Beta and ASA catalysts. In spite of their mesopores of 70Å, ASA catalysts were the least selective towards the bridged isomers. On the other hand, Pt/ASA was also the least acidic

catalyst among the solids tested. Our interpretation infers that the production of alkyladamantanes is a function of both pore-size and acidity.

The formation of alkyladamantanes over an aluminum bromide sludge catalyst, initially proposed by Schneider and coworkers [6], is based on multiple rearrangements of tricyclic naphthenes, starting from perhydrophenanthrene, which isomerizes into perhydroanthracene and methylperhydrophenalene, before acquiring the armchair conformation leading to the bridged isomer. This reaction pathway was also valid for all Pt-catalysts tested in our work. In addition, the reaction intermediates necessary to synthesize C<sub>14</sub> adamantanes were successfully identified among isomerization products. Precursors of alkyladamantanes have also been distinguished among reaction products in other works available in literature.

Substituted adamantanes are rarely reported in literature of bifunctional reaction pathways, although some few works certified the efficiency of large-pore zeolites of processing it [2,4,5]. Previous study on hydroconversion of perhydrophenanthrene on Pt-supported bifunctional catalysts revealed the presence of such naphthenes among reaction products, even if they could not be separated from other isomerized compounds [2,7]. More recently, alkyladamantanes resulted from hydroisomerization of fluorene, and USY zeolite was also the most selective catalyst to the bridged isomers, which did not undergo hydrocracking [4]. Our work confirms these results, providing a detailed description of isomerization of perhydrophenanthrene on Pt-supported catalysts and shedding light on the characterization of substituted adamantanes. Even if they are not easily cracked, these molecules are particularly interesting because of their high cetane number, and could be employed in the production of high-quality diesel fuels [8].

Ring-opening products (C<sub>14</sub>H<sub>26</sub>) were obtained after scission of one cycle of ring-contraction and ring-shift perhydrophenanthrene isomers. Opening of two cycles of PHP skeletal isomers did not occur, because opening of a ring is a strained reaction and its rate decreases with the number of remaining cycles of the molecule. This was verified through hydroconversion of octylcyclohexane, where the unique cycle of the naphthene was preserved throughout the reaction. USY zeolite and ASA gave similar ring-opening intermediates, with preferential cleavage of the central cycle of skeletal perhydrophenanthrene isomers. The preferred production of such ring-opening intermediates is probably related to a high adsorption selectivity towards these molecules on FAU topology. Beta zeolites were selective towards

formation of butyldecalin and more branched ring-opening intermediates. MC simulations indicated, however, a more balanced selectivity to different ring-opening products, but a fast cracking of substituted cyclohexane ROP explains why this intermediate was not perceived at high PHP conversion over Beta catalysts.

Previous work on hydroconversion of perhydrophenanthrene established that primary products on USY and ASA-supported catalysts consisted of ring-contraction PHP isomers, whereas Beta zeolites privileged the formation of ring-opening molecules in a primary route [7]. Isomerization and ring-opening compounds were then lumped into the same family of reaction products. In contrast, thanks to a thorough molecular characterization, our work allowed to distinguish different families of reaction intermediates, expanding the knowledge on the types of reactions taking place in hydroconversion of polycyclic naphthenes.

Cracking took place after ring-opening of skeletal perhydrophenanthrene isomers. Cracked products were essentially constituted of naphthenes over all catalysts. The yield of cracked products on Pt/H-USY zeolite catalyst resulted in a broad distribution of carbon atoms, while Beta and ASA catalysts privileged cracking to C<sub>7</sub> products. Conversely, Leite and coworkers found the same distribution of cracked products centered at C<sub>7</sub> naphthenes over all Pt-supported bifunctional catalysts tested, irrespective of the reaction intermediates formed on each solid. The large distribution of carbon atoms on Pt/H-USY was deeply rationalized through hydrocracking pathways of ring-opening intermediates observed among reaction products. The preferential cracking to C<sub>7</sub> products over Beta resulted from conversion of substituted bicyclohexyl- intermediates through fast tertiary-tertiary beta-scission, whereas reaction intermediates on USY catalysts led to more possibilities for fast cleavage to a broad number of cracked products. ASA-catalysts also cracked mainly to C<sub>7</sub>, but only to a small extent, given the poor acidity of these catalysts. The global reaction pathway for hydroconversion of perhydrophenanthrene on Pt-supported catalysts is illustrated in Figure 1.

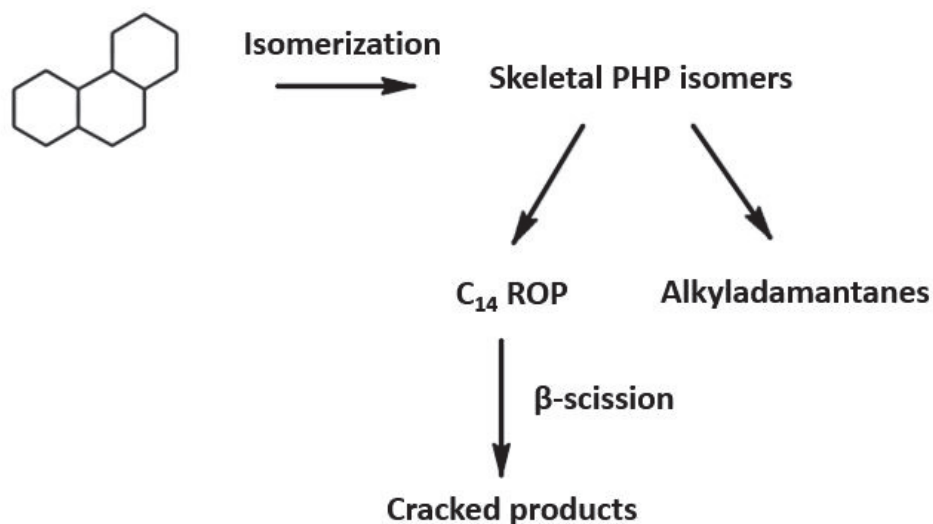


Figure 1. Global reaction scheme for hydroisomerization and hydrocracking of perhydrophenanthrene over Pt/H-USY, Pt/H-Beta and Pt/ASA bifunctional catalysts (see further details in Chapters II and III).

The activity of bifunctional Pt-supported catalysts on hydroisomerization and hydrocracking of perhydrophenanthrene followed the order USY > Beta >> ASA, independent of the zeolite loading in alumina binder. The study of Leite and coworkers on hydroconversion of perhydrophenanthrene revealed that Beta zeolites were the most active among the catalysts tested, followed by USY, which were much more active than ASA [7]. Conversely, our simulations indicated that PHP reactant is poorly adsorbed on BEA topology, which correlates well with the higher activity of USY-based catalysts. It is likely that, in our work, a better separation between reaction products and PHP reactant led to an opposite order of activities compared to the work of Leite and coauthors.

Families of products resulting from octylcyclohexane conversion (chapters 4 and 5), as for hydroconversion of perhydrophenanthrene, were divided into substituted cyclopentane and substituted cyclohexane isomers (C<sub>14</sub>H<sub>28</sub>), ring-opening resulting in isoalkanes (C<sub>14</sub>H<sub>30</sub>) and cracked products containing less than 14 carbon atoms. Formation of isoalkanes through opening of the unique ring of octylcyclohexane was a minor reaction, as expected in literature for monocyclic naphthenes [9]. The activity of Pt and NiMoS-supported catalysts followed an opposite trend to that on hydroconversion of perhydrophenanthrene: Beta was the most active catalyst, followed by USY zeolite. ASA was significantly less active than both zeolites.

Isomerization products were meticulously analyzed over Pt-based bifunctional catalysts. A similar distribution of isomerization products over Pt/H-USY and Pt/H-Beta zeolite catalysts was obtained at close octylcyclohexane conversion, although a smaller proportion of methylheptylcyclohexane, the primary isomerization product, was found over the latter. In contrast, the distribution of isomers over Pt/ASA bifunctional catalyst led to a preferential formation of multibranched compounds because of its high selectivity towards isomerization products and the poor cracking activity of these catalysts. At isoconversion, Pt/ASA was more selective to isomerization than Pt/USY zeolite catalyst. Among zeolites, USY was slightly more selective towards cracking, which was also valid for sulfide-based zeolite catalysts.

Few works in literature dealt with hydroconversion of long-chain substituted monocyclic naphthenes [10,11]. Souverijns *et al.* investigated the isomerization of octylcyclohexane over Pt/H-USY bifunctional catalyst. Major isomerization products comprised dibranched structures that were mainly substituted at positions close to the ring. This indicates that branching was originated by the cycle through ring-contraction, migrating afterwards to the side chain. In our work, isomerization products presented different degrees of branching, with preferential alkyl-substitution around the cycle, in agreement with Souverijns and coauthors.

Cracking of octylcyclohexane took place rapidly after isomerization. Cracked products were mainly comprised of naphthenes and alkanes over Pt and sulfide catalysts. Hydrocracking pathways leading to major cracked products were also evaluated and were similar in both systems of catalysts, as well as the number of slow steps, i.e. type B isomerization, required to achieve a configuration allowing fast beta-scission. A comparison between the degree of branching of isomers and major cracked products allowed determining which isomer structure could easily undergo hydrocracking. However, even if a given molecule requires a small number of type B rearrangements to be cracked because of their superior number of tertiary carbon atoms (multibranched isomers), the most suitable structures to undergo hydrocracking seem to be less branched compounds, because of the easiness to process these isomers. This could explain why multibranched molecules accumulate within the isomers fraction, but the competition between isomerization and cracking pathways is difficult to elucidate.

Both Pt/H-USY and Pt/H-Beta zeolite catalysts resulted in similar and homogeneous distribution of cracked carbon atoms, with a major cracking to C<sub>7</sub> compounds. Zeolite-based

sulfide catalysts, in contrast, gave a distribution with maxima at 4, 6 and 8 carbon atoms. Yields higher than 200 mol per 100 mol of cracked products indicated that secondary cracking took place on sulfide catalysts, with subsequent formation of lighter compounds. In effect, sulfide catalysts are less well equilibrated than Pt ones, because molybdenum sulfides are not a strong hydrogenating as platinum. Therefore, the metallic phase of sulfide catalysts are not able to saturate cracked olefins produced on the acidic sites of zeolites fast enough in order to avoid secondary cracking. Besides over-cracking, the reaction pathways for hydroconversion of octylcyclohexane on Pt-supported catalysts were also valid for bifunctional sulfide-supported catalysts. The reaction pathway for hydroconversion of octylcyclohexane over bifunctional Pt and NiMoS-supported catalysts is depicted in Figure 2.

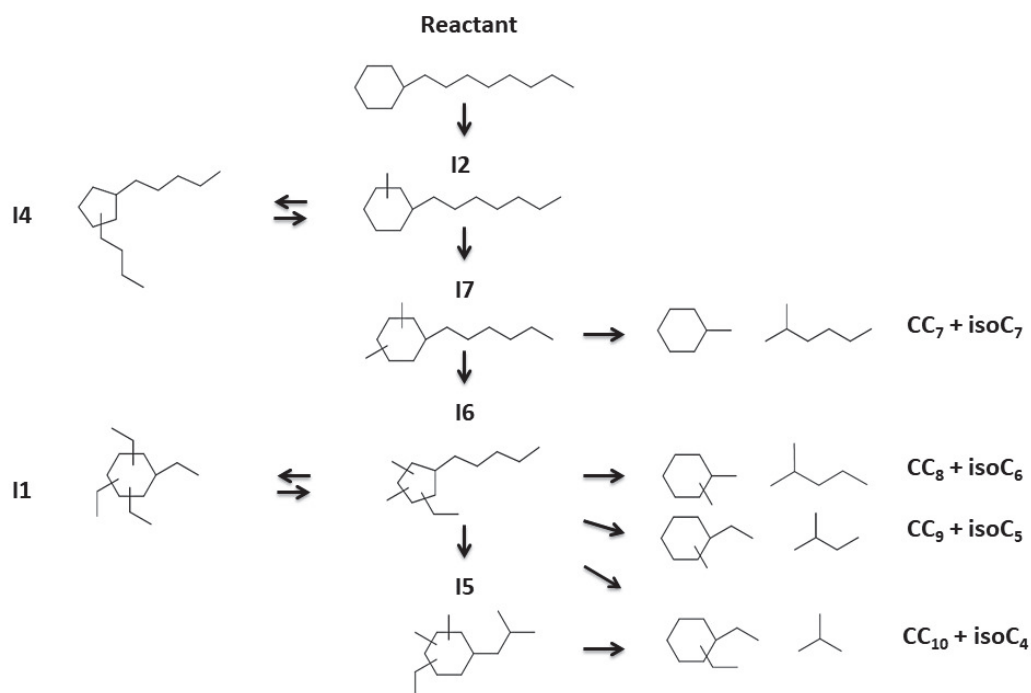


Figure 2. Reaction pathways for hydroconversion of octylcyclohexane over Pt and NiMoS-supported catalysts. Over-cracking over NiMoS catalysts is not represented.

From what has been previously discussed, it is clear that there are more reaction possibilities, from a mechanistic point of view, on hydroconversion of polycyclic naphthenes. The presence of two or three cycles in a molecule creates a new route which goes from isomerization of the cycle until its opening prior to cracking. In addition to ring-opening, shape selectivity effects may also play an important role on the final distribution of carbon atoms, as it was



evidenced in the formation of PHP isomers. Octylcyclohexane was less subject to shape selectivity because of its linearity and less bulky structure.

Hydroconversion of monocyclic naphthenes are globally easier to predict, because ring-opening is only observed to a small extent, thus a straightforward reaction pathway consists of isomerization leading to cracking. With respect to octylcyclohexane, the key point in this case is to investigate the influence of a long alkyl-substituent on reaction pathways and the reactivity of this molecule vs. perhydrophenanthrene.

In hydroconversion of perhydrophenanthrene, Pt/H-USY and Pt/ASA catalysts were more selective to isomerization products, whereas Pt/H-Beta zeolite catalyst privileged cracking. USY-based catalysts were the most active among the solids tested, followed by Beta and ASA. Hydroconversion of octylcyclohexane, in contrast, indicated an inverse trend, and Pt and sulfide catalysts supported over shaped Beta zeolites were more selective towards isomerization compounds. The study of selectivities at isoconversion according to metallic phase and catalyst tested allows comparing the evolution of both model molecules towards isomerization, ring-opening and cracking pathways (Tables 1-3). On USY and ASA catalysts, cracking of octylcyclohexane was favored over Pt and NiMoS, whereas PHP underwent isomerization and ring-opening, subsequent steps necessary to crack polycyclic naphthenes. These results clearly illustrate the high selectivity towards cracking of sulfide catalysts, compared to Pt/zeolites and Pt/ASA on hydroconversion of octylcyclohexane (see supporting information for full selectivity profiles).

Table 1. Selectivity towards isomerization, ring-opening and cracking products on hydroconversion of perhydrophenanthrene and octylcyclohexane over USY-supported catalysts.

USY	Selectivity (mol C/mol C reaction products, %) over Pt catalysts							Selectivity (mol C/mol C reaction products, %) over NiMoS catalysts
	PHP				OCC6			OCC6
Conversion	94	83	68	47	86	71	48	94
Isomerization	32	51	64	85	31	51	71	6
ROP	4	9	10	7	1	1	1	-
Cracking	64	40	26	8	68	48	28	94

Table 2. Selectivity towards isomerization, ring-opening and cracking products on hydroconversion of perhydrophenanthrene and octylcyclohexane over Beta-supported catalysts.

Beta	Selectivity (mol C/mol C reaction products, %) over Pt catalysts		Selectivity (mol C/mol C reaction products, %) over NiMoS catalysts	
	PHP		OCC6	
Conversion	71	56	76	56
Isomerization	58	66	42	54
ROP	14	10	-	-
Cracking	28	24	58	46

Table 3. Selectivity towards isomerization, ring-opening and cracking products on hydroconversion of perhydrophenanthrene and octylcyclohexane over ASA-supported catalysts.

ASA	Selectivity (mol C/mol C reaction products, %) over Pt catalysts					Selectivity (mol C/mol C reaction products, %) over NiMoS catalysts	
	PHP			OCC6		OCC6	
Conversion	45	37	30	50	38	38	26
Isomerization	82	86	86	69	74	80	87
ROP	10	8	7	10	7	-	-
Cracking	8	6	7	21	19	20	13

Pt catalysts were also evaluated on hydroconversion of n-hexadecane ( $C_{16}H_{34}$ ). Pt/H-Beta zeolite catalyst was slightly more effective to process the alkane molecule than Pt/H-USY and Pt/ASA. The amorphous catalyst was the least active among the solids tested. These results are in agreement with previous study carried out in hydroconversion of n-hexadecane [12]. Together with the activity of Pt and sulfide catalysts on octylcyclohexane conversion, these trends confirm the preferential cracking of linear structures over Beta zeolite based catalysts, as it was evidenced in hydrocracking of perhydrophenanthrene. We may assume that octylcyclohexane reacted in a similar way as n-hexadecane, and the cycle provided the branchings in order to promote cracking of the cyclic molecule. The flat carbon distribution obtained in hydrocracking of octylcyclohexane (spite of major cracking to  $C_7$  products) is another common point with hydroconversion of long-chain alkanes.

In conclusion we can make a parallel between the molecules studied with respect to cracked products resulting from their hydroconversion. The yield of cracked products generated from hydroconversion of perhydrophenanthrene over Pt-supported catalysts indicated minima at  $C_9$  naphthenes and  $C_5$  isoalkanes. The reaction pathways leading to these compounds go through the opening of a second ring of perhydrophenanthrene, which produces a di- or

tetrabranched monocyclic C<sub>14</sub> naphthene. These structures corresponded to similar molecules identified as isomers of octylcyclohexane (C<sub>14</sub>H<sub>28</sub>) generated from hydroisomerization of the monocyclic naphthene over the solids tested. The same C<sub>9</sub> and C<sub>5</sub> compounds were produced after hydrocracking of both model molecules. This confirms that opening of a second cycle of perhydrophenanthrene would lead to similar reaction pathways as observed for hydroconversion of octylcyclohexane. However, as the distribution of cracked products demonstrated, this second ring-opening was not the preferential route on hydrocracking of the polycyclic model molecule. Instead, a tendency to preserve two out of three cycles of perhydrophenanthrene was noticed.

By looking forward to industrial hydrocracking of heavy molecules, in terms of distribution of carbon atoms, USY-supported catalyst would give a great range of cracked products, irrespective of the structure of the molecule (mono- or polycyclic naphthenes), which is interesting in terms of versatility of the process. Beta zeolites were more selective to cracking of polycyclic naphthenes and could be tuned to produce lighter products in hydrocracking of heavy VGO feedstocks. ASA catalysts were the most selective to isomerization products on hydroconversion of both model molecules, compared to zeolite catalysts. Therefore, ASA could be employed to limit over-cracking and increase the selectivity towards middle distillates, especially if the (de)hydrogenating function is represented by molybdenum sulfides.

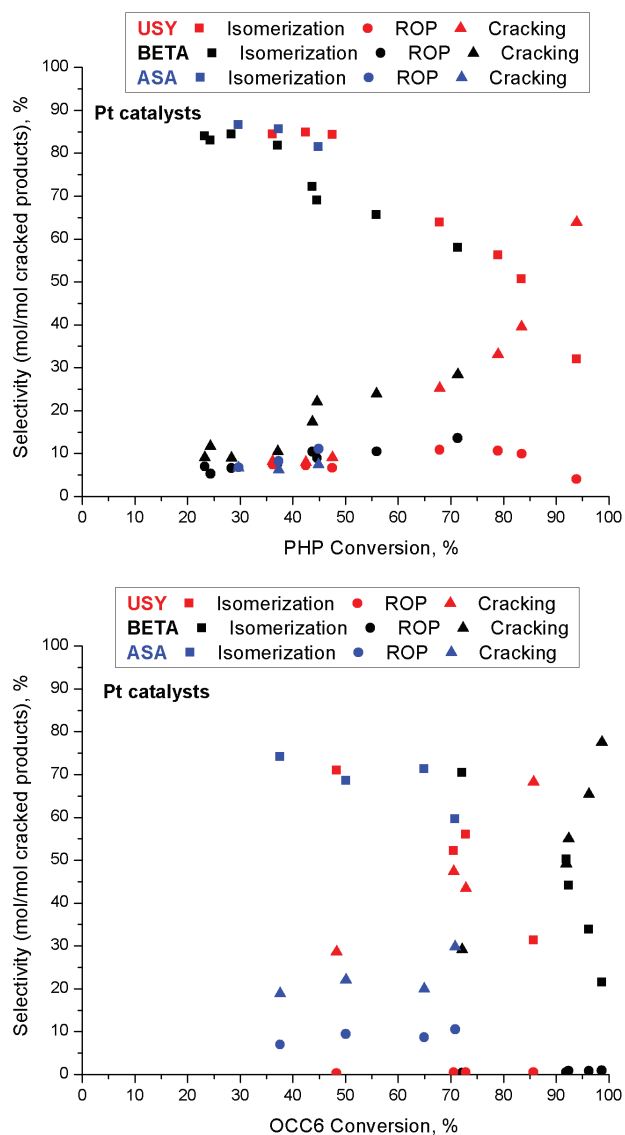
## REFERENCES

- [1] L. Leite, E. Benazzi, N. Marchal-George, H. Toulhoat, Hydrocracking of phenanthrene over Pt/SiO<sub>2</sub>-Al<sub>2</sub>O<sub>3</sub>, Pt/H-Y, Pt/H-β and Pt/H-ZSM-5 catalysts: Reaction pathway and products distribution, in: A. Corma (Ed.), 12th International Congress on Catalysis: Proceedings of the 12th ICC, Granada, Spain, July 9-14, 2000, 1st ed., Elsevier, Amsterdam, New York, 2000, pp. 2495–2500.
- [2] Lorraine Leite, Eric Benazzi, Nathalie Marchal-George, Hydrocracking of phenanthrene over bifunctional Pt catalysts, *Catalysis Today* 65 (2001) 241–247.
- [3] J. Fraissard, Why are HY Zeolites so Much More Active Than Amorphous Silica-Alumina, in: B. Imelik, C. Naccache, Y.B. Taarit, J.C. Vedrine, G. Coudurier, H. Praliaud (Eds.), *Catalysis by Zeolites*, Elsevier, 1980, pp. 343–350.

- 
- [4] L. Wang, Y. Chen, S. Jin, X. Chen, C. Liang, Selective Ring-Shift Isomerization in Hydroconversion of Fluorene over Supported Platinum Catalysts, *Energy Fuels* 30 (2016) 3403–3412.
- [5] L.D. Rollmann, L.A. Green, R.A. Bradway, H.K.C. Timken, Adamantanes from petroleum with zeolites, *Catalysis Today* 31 (1996) 163–169.
- [6] A. Schneider, R. W. Warren, and E. J. Janoski, Formation of Perhydrophenalenes and Polyalkyladamantanes by Isomerization of Tricyclic Perhydroaromatics, *J. Org. Chem* 31 (1966) 1617–1625.
- [7] L. Leite, Etude sur molecule modèle des paramètres régissant la sélectivité des catalyseurs d’hydrocraquage des charges lourdes, 2000.
- [8] B.G. Harvey, K.W. Harrison, M.C. Davis, A.P. Chafin, J. Baca, W.W. Merriman, Molecular Design and Characterization of High-Cetane Alkyl Diamondoid Fuels, *Energy Fuels* 30 (2016) 10171–10178.
- [9] G. McVicker, Selective Ring Opening of Naphthenic Molecules, *Journal of Catalysis* 210 (2002) 137–148.
- [10] J.A.M. Arroyo, J.W. Thybaut, G.B. Marin, P.A. Jacobs, J.A. Martens, G.V. Baron, Reaction Pathways of 1-Cyclohexyloctane in Admixture with Dodecane on Pt/H-ZSM-22 Zeolite in Three-Phase Hydroconversion, *Journal of Catalysis* 198 (2001) 29–40.
- [11] W. Souverijns, R. Parton, J.A. Martens, G.F. Froment, P.A. Jacobs, Mechanism of the paring reaction of naphthenes, *Catal Lett* 37 (1996) 207–212.
- [12] Pedro Mendes, Hydroconversion catalysts based on zeolite mixtures, from ideality to reality, 2017.

## Supporting Information

Figure S1



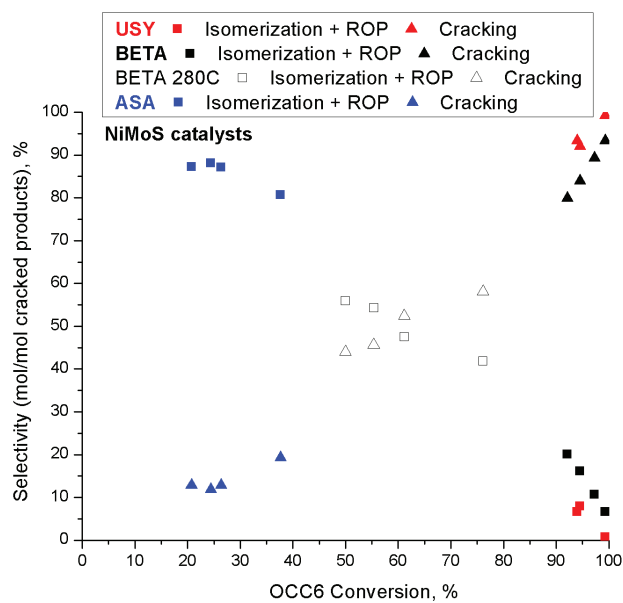


Figure S1. Selectivity towards isomerization, ring-opening and cracking according to model molecule and catalysts tested. A) Hydroconversion of perhydrophenanthrene over Pt-supported catalysts. Hydroconversion of octylcyclohexane over B) Pt-supported and C) NiMoS-supported catalysts.





The main objective of this work was to elucidate reaction pathways on hydroconversion of (poly)cyclic naphthenes, major constituents of heavy oil fractions, e.g. Vacuum Gas Oil (VGO). Bifunctional Pt and NiMoS-supported catalysts, containing different acid phases represented by large-pore zeolites and silica-alumina, were employed for hydroisomerization and hydrocracking of two  $C_{14}$  cyclic molecules. Perhydrophenanthrene, a polycyclic naphthene, and octylcyclohexane, a long alkyl-chain substituted monocyclic naphthene, were chosen as model molecules in order to evaluate the reactivity of different cyclic structures in bifunctional pathways. Their hydroconversion followed the rules of carbocation chemistry and generated hundreds of products, which were exhaustively identified and quantified with GCxGC-FID/MS. The thorough characterization of reaction products allowed a detailed study of reaction pathways and the identification of families of compounds that are rarely reported in literature.

Hydroisomerization and hydrocracking of perhydrophenanthrene (PHP,  $C_{14}H_{24}$ ) were performed over Pt/H-USY, Pt/H-Beta and Pt/ASA bifunctional catalysts. A global pathway for all catalysts consisted of isomerization of the three-cycle naphthene, followed by ring-opening of extreme or central cycle of PHP, prior to cracking. The formation of skeletal isomers of PHP and ring-opening products were controlled by shape-selectivity, leading to different distribution of carbon atoms. While USY-supported catalysts gave a broad distribution of cracked products, Beta and ASA bifunctional catalysts privileged cracking to  $C_7$  naphthenes. Another isomerization route of perhydrophenanthrene resulted in the production of  $C_{14}$  substituted adamantanes, bridged and stable compounds that almost did not undergo hydrocracking. Alkyladamantanes are scarcely documented in literature of bifunctional catalysis, given the difficulties to properly separate and identify these compounds among reaction products. In our work, the formation of alkyladamantanes was granted to pore-mouth catalysis and it was favored at high PHP conversion over Pt/H-USY zeolite catalyst. Shape-selectivity effects and pore-mouth catalysis were also rationalized with the contribution of molecular simulation by taking important reaction intermediates as probe molecules. USY zeolites were more active in hydroconversion of perhydrophenanthrene,

---

followed by Beta and, at a lower degree, ASA catalysts. The higher activity of Pt/H-USY in the conversion of the polycyclic naphthene is related to the favored adsorption of PHP reactant on FAU topology, as demonstrated by simulations.

Hydroconversion of octylcyclohexane ( $C_{14}H_{28}$ ) was carried out over Pt- and NiMoS-supported catalysts, under the same operating conditions as catalytic tests with perhydrophenanthrene. The reaction pathway, valid for Pt- and sulfide-supported catalysts, started from isomerization of the model molecule, before achieving a conformation enabling fast beta-scission. Ring-opening was a minor reaction, as expected for monocyclic naphthenes. The distribution of isomers was equivalent over zeolite catalysts, whereas ASA formed preferentially multibranched structures, related to the poor cracking activity of the silica-alumina phase. As previously reported in literature, the consecutive branching of isomers started at the cycle, migrating afterwards to the side-chain. Pt-catalysts resulted in similar distribution of carbon atoms, with preferential cracking to  $C_7$  compounds in addition to a homogeneous distribution of the remaining carbon atoms. NiMoS bifunctional catalysts were less well equilibrated than the noble ones and resulted in formation of lighter cracked products, due to over-cracking. We tried to rationalize the competition between isomerization and cracking pathways by comparing the degree of branching of molecules representative of these two families. In spite of a lower number of tertiary carbon atoms, di- or tribranched isomers cracked preferentially over multibranched isomers, because of the higher number of slow type B isomerization required to produce the latter. The order of activity in hydroconversion of octylcyclohexane was opposite to that obtained with perhydrophenanthrene. Beta zeolites were more active than USY catalysts, and ASA was the least active of the solids tested, irrespective of the metallic phase composing the bifunctional catalyst.

Pt-supported catalysts were also evaluated in hydroconversion of a long chain alkane, n-hexadecane ( $n-C_{16}H_{34}$ ). As for octylcyclohexane, Beta catalysts were more effective in converting the alkane, followed by USY zeolites. Again, ASA catalyst was the least active among the solids tested. These results, together with shape-selectivity effects observed on hydroisomerization of perhydrophenanthrene, confirm the preferential conversion of linear structures on Beta zeolites. We may also infer that octylcyclohexane, a monocyclic

---

naphthene containing a long alkyl-substituent, reacted similarly as n-hexadecane, with the cycle providing the branchings to improve beta-scission.

This work provides a deep characterization of reaction intermediates and pathways that are useful to understand the distribution of cracked products in noble and base bifunctional catalysts. It is clear that polycyclic and monocyclic naphthenes react in different ways, and the complexity of reaction pathways increases with the number of cycles of the molecule. The data provided herein may contribute to rationalize the behavior of more complex feedstocks in a molecular level, and adapt textural and acidic properties of bifunctional catalysts accordingly.

For future work, it could be particularly interesting to test reaction intermediates resulting from isomerization or ring-opening of perhydrophenanthrene or octylcyclohexane, in order to build a more complex reaction network. Another possibility is to convert different types of molecules typically present in a VGO fraction, i.e. alkanes, naphthenes and aromatics, to investigate the reactivity of these compounds in a more realistic feedstock. In addition, a kinetic study could be carried out to elucidate isomerization, ring-opening and cracking rates, thus determining more precisely the competition between different reaction routes.

Due to lack of time, hydroconversion of perhydrophenanthrene was not performed over NiMoS-supported catalysts. We would like to address the impact of the balance between metallic and acid phases on hydroisomerization and hydrocracking of perhydrophenanthrene. As aforementioned, the conversion of this molecule resulted in a large number of reaction products, with shape selectivity effects playing an important role in the distribution of carbon atoms, which makes this molecule attractive from a mechanistic point of view. In addition, NiMoS catalysts are commonly used in industrial environments, thus they could be evaluated in more severe operating conditions, expanding the knowledge on hydrocracking of cyclic molecules.

